ELECTRONIC TRANSPORT IN SEMICONDUCTORS

by

T.H.H. Vuong

A thesis submitted for the degree of

Doctor of Philosophy

St Anne's College
Hilary Term 1985



Tặng ba má

(To my parents)



A heterojunction sample mounted for thermopower measurements.

ELECTRONIC TRANSPORT IN SEMICONDUCTORS

by

T.H.H. Vuong

A thesis submitted for the degree of
Doctor of Philosophy

St Anne's College
Hilary Term 1985

ABSTRACT

The first part of this thesis is a study of thermally activated conduction, Hall effect, and Far-Infrared absorption in n-InP. Accurate measurements of threshold energies are deduced from the temperature dependence of these effects, after correction for Fermi level variations, and it is shown that the threshold for electrical conduction is higher than for Hall effect, or cyclotron resonance. An explanation is given in terms of the long range impurity potential fluctuations.

The second part of this thesis presents measurements of the thermopower in heterostructures for the GaInAs - InP, GaInAs - InAlAs, and GaAs - GaAlAs systems, with and without magnetic field, for temperature varying from 2K to 10K. In high magnetic fields, strong oscillations of the thermopower are seen, with the same phase as the Shubnikov - de Haas oscillations in the resistivity, in accordance with theory. The magnitude and temperature dependence of the thermopower are mostly as predicted for the superlattice but those of the heterojunctions disagree with the predictions. A discussion of the cause of this disagreement is given.

In the final part, the value of the relative energy shift between different valleys of the conduction band of a thin film of PbTe grown on BaF_2 is obtained. This will be used to obtain the deformation potential of PbTe.

Acknowledgements

I would like to express my thanks to Professor E.W.J. Mitchell for allowing me the use of the facilities in the Clarendon Laboratory.

I am indebted to my supervisor Dr R.J. Nicholas for his constant, generous help throughout this work.

I would like to thank all my colleagues for their help and encouragement, especially Mark Brummell and John Singleton for many stimulating discussions.

Special thanks are due to all the staff and workshops of the Clarendon Laboratory, and in particular the high-field support group.

The writing of this thesis was made possible by the Bursary awarded me by St Anne's College, which also provided generous travel grants enabling me to attend conferences. My thanks are particularly due to the former Principal, Mrs M.S. Trenaman, for her encouragement.

My thanks are also due to the Scott Fund, the C. Barber Trust Fund, and the Graduate Committee of Oxford University for travel funds and to the Scott Fund for a further support grant.

I would like to thank Fernando, Ilse, Jorunn, Susan, and Robert for much help given.

Contents

Abstract

Acknowledgements

Chapter 1 Introduction

1•1	Scope of the thesis	1 - 2
1•2	Magnetic field facility	3
1•3	Experimental technique for magneto-optical measurements	4

Chapter 2 The theory of activated conduction

2•1	Introduction	5
2•2	The difference in the activation energy for the resistivity and for the Hall effect	6 - 7
2•3	The variation of the Fermi level with temperature	8 - 11
2•4	Some points on the effect of a magnetic field on the conduction band	12 - 14
2•5	The temperature dependence of the cyclotron resonance linewidth	15 - 19

Chaper 3 A study of activated conduction in n - InP

3·1 Introduction 20

3·2 Experimental procedure

(a) Sample characteristics 21 - 24

(b) Experimental conditions 24 - 27

3·3 Experimental results 28 - 40

3·4 Estimates of the Fermi-level variation with temperature 41 - 43

3·5 Analysis 44 - 57

3·6 Conclusion 58

Chapter 4 An introduction to the two-dimensional electron gas

4·1 Introduction 59 - 64

4·2 Subband levels of the heterojunction 65 - 68

4·3 Effect of a strong magnetic field 69 - 73

Chapter 5 Thermopower measurements of heterostructures

5·1 Introduction 74

5·2 Experimental apparatus 75 - 84

5·3 Sample characteristics 85 - 89

5·4 Thermopower measurements in zero magnetic field 90 - 102

5·5 Thermopower measurements in a strong magnetic field 103 - 125

Chapter 6 The theory of thermopower in heterostructures

6·1 Introduction 126

6·2 The theory of thermopower in the 2DEG

(a) Thermopower in zero magnetic field 127 - 132

(b) Thermopower in a quantising magnetic field 133 - 141

6·3 Thermopower in heterostructures 142 - 153

6·4 Conclusion 154 - 155

Chapter 7 A study of the thermally induced stress in thin film PbTe

7·1 Introduction 156 - 159

7·2 Effect of stress on the band structure of PbTe 160 - 164

7·3 Shubnikov - de Haas measurements 165 - 171

7·4 F.I.R. magneto-optic experiment

(a) Experimental results 172 - 184

(b) Theoretical model 185 - 191

(c) Results of fits to experimental data 191 - 194

7·5 Conclusion 195

References 196 - 202

CHAPTER 1

Introduction

1·1 Scope of the thesis

This thesis has two main parts, and a small section on Lead Telluride. The first part is concerned with conduction in a semiconductor at doping levels below the Metal-Insulator transition, and the problem of the different values observed for the activation energy from the Hall effect and from the resistivity. Several previous experimental studies have noted this difference in various semiconductor systems. In this thesis, n-type Indium Phosphide has been chosen for study as a typical III-V compound semiconductor. In addition to the D.C. transport studies, magneto-optical measurements on the Indium Phosphide samples were also made. These proved to be important and led to a new interpretation of the old problem of the different activation energy values. This work is presented in chapters 2 and 3.

The second part of this thesis presents measurements of the thermopower in three different heterostructure systems, both with and without a magnetic field. These systems are GaInAs - InP, GaInAs - InAlAs, and GaAs - GaAlAs. In recent years, many theoretical studies have appeared which calculate the thermopower behaviour of two-dimensional degenerate carrier systems in a magnetic field. There are, however, few experimental studies to compare with the theory. This thesis reports measurements both on a superlattice and on heterojunctions. Results for the superlattice agree, for the most part, with the theory for a two-dimensional electron gas. For the heterojunctions, however, there are serious disagreements between the experimental results and the theory. A discussion of the possible causes for these disagreements is given. The thermopower study is presented in chapters 4, 5 and 6.

Finally, chapter 7 is concerned with obtaining the value of the energy shift between different conduction band valleys in a thin film of Lead Telluride grown on Barium Fluoride. Similar magneto-optical and transport studies to those used on the InP and the 2-D systems were used to measure the free carrier populations, and so deduce the energy offsets. The energy shift is caused by thermally-induced stress in the thin film. The value of the shift will be used together with X-ray measurements of the strain in the same sample to deduce the deformation potential for Lead Telluride.

Some experimental details which are general to the whole work are given in this chapter.

1·2 Magnetic field facility

The magnetic field employed for the experiments reported in this thesis was provided by water-cooled solenoid magnets at the Clarendon Laboratory. These magnets have a 2" bore, in which the cryostat is centred, and are all powered by a 2 MW generator. For some of the thermopower measurements, a polyhelix type magnet was used which gave a maximum field to 10T. This magnet is described by Hudson et al. (1984). The other measurements employed Tsai magnets (Hudson 1972) whose maximum fields are 9T for the magnet used for cyclotron resonance studies and 9·5T for the transport studies. The maximum sweep time is 0·5 minute from zero to full field. Sweep times normally employed are 2 to 5 minutes.

The current supplied to the magnets is stable to 1 part in 10^5 and is measured to an accuracy of better than 0·1%. The magnetic field is calibrated by measuring the N.M.R. signal of protons in wax. By this method the field is found to be homogeneous within a sphere of ~ 2 cm diameter around the centre.

1·3 Experimental technique for magneto-optical measurements

The radiation source is one of several molecular gas discharge lasers. The strongest laser wavelengths available from each laser are: 337 μm (HCN laser), 192 μm (DCN laser), 172 μm (D_2O laser), and 119 μm (H_2O laser).

The sample is mounted in a cold-finger cryostat at the end of a long stainless steel tube which may be heated. The sample's temperature can be varied from 17K to ~ 100K. The cryostat is placed to position the sample at the magnetic field centre.

The laser radiation is mechanically chopped and led to the cryostat through light pipes and an electroformed copper reducing cone. The light transmitted by the sample is detected by a photoconducting Germanium detector heat sunk to 4·2K. The signal from the detector is amplified, fed to a PSD, then taken to an X-Y chart recorder.

CHAPTER 2

The theory of activated conduction

2·1 Introduction

The first part of this thesis is a detailed investigation of some simple transport and optical properties for one type of activated conduction, the conduction by electrons thermally activated to the conduction band. Measurements were made of the resistivity, the low-field Hall effect, and the cyclotron resonance of the free carriers. Even though these effects are amongst the most basic, and are used as tools in the characterisation of samples, fundamental questions about the nature of the conduction involved remain. This work concentrates on the problem of the difference in the values of the activation energy for the electrons as measured by the resistivity and by the Hall effect. Two central results emerged: firstly, it is necessary in the activated conduction regime to take the temperature variation of the Fermi level into account when calculating the activation energies, or indeed any other quantities, from the temperature dependence of the properties of the material. This is particularly important for more heavily compensated material. In this work, the variation of the Fermi level was properly included in the calculations of the activation energies for d.c. conduction and for the Hall effect. These activation energy values taken together with the information yielded by the optical experiments lead to a novel explanation of the discrepancy between Hall effect and conductivity. This is the second and main result.

This chapter presents briefly the theory relevant to this work. The subsequent chapter describes the experiments and results, the analysis made, and the final conclusion drawn.

2·2 The difference in the activation energy for the resistivity and for the Hall effect

In the case of impurity conduction in semi-conductors, the conductivity σ can in general be written as (see, e.g. Davis and Compton 1965)

$$\sigma = \sum_{i=1}^{3} \sigma_i \exp\left[-\varepsilon_i/kT\right] \qquad (2\cdot1)$$

where ε_i is the activation energy of the i^{th} conduction process and σ_i can be temperature dependent, with

$$\sigma_1 > \sigma_2 > \sigma_3 \quad \text{and} \quad \varepsilon_1 > \varepsilon_2 > \varepsilon_3.$$

The following discussion is confined to n-type samples where the conduction is dominated by the presence of the donor impurities. The first contribution to σ, the ε_1 process, is the conduction by electrons thermally excited to the conduction band from the donor 1s level. The ε_1 process is observed for all donor concentrations at high temperatures, if one includes the case of $\varepsilon_1 = 0$ observed in highly doped samples which show metallic behaviour and for which the 1s level has broadened to merge with the conduction band. The second contribution, the ε_2 process, occurs in specimens with so-called 'intermediate' impurity contribution, and involves conduction within the impurity band. Electrons are thermally excited from the donor ground state to mobile-electron states within the impurity band. The third conduction process is due to the hopping of electrons between the ground states. It is only observed for either low impurity concentrations, and/or at low temperatures.

Discrepancies between results inferred from the resistivity and from the Hall effect have been reported by many authors working on different semiconductors. Davis and Compton (1965) observed that in the ε_1 regime, the fits to the temperature dependences of the Hall

effect and of the resistivity in n-Ge give distinctly different activation energy values. Mansfield and Ahmad (1970) studied the magnetic freeze-out of n-InSb and obtained different values of the donor ionisation energy from the magnetic field dependence of the Hall effect and from the values of the electric field for the resistance breakdown. In the ε_2 regime, Fritzsche (1978) pointed out a similar difference in the values of ε_2 from the two transport processes. This is followed up by Narita and Kobayashi (1980) as part of their optical far-infrared (F.I.R.) study on heavily doped n-Ge. Their work is of particular interest here because, similar to this work, it combines results from the measurements of both the transport and optical properties (though their results come from separate studies). Their analysis will be referred to in a later section.

In this work samples of n-InP with low impurity concentrations were used. Therefore, the ε_2 conduction process was not observed. The ε_1 process dominates at high temperatures ($T \gtrsim 10K$) and the ε_3 process at low temperatures in these samples. This study concentrates on the temperature range in which ε_1 is dominant. The results show that the activation energy ε_1 as deduced from the Hall effect and the resistivity are different in all samples.

In addition to the measurements of resistivity and Hall effect, the F.I.R. transmission of the samples in a varying magnetic field was also examined. The combination of the optical and electrical measurements proved to be crucial in the understanding of the mechnisms involved in the two transport processes.

2·3 The variation of the Fermi level with temperature

As predicted by simple statistics (Blakemore 1962), in the range of temperature where the ε_1 conduction process is observed in this work ($10K \lesssim T \lesssim 80K$), the Fermi level E_F decreases rapidly with increasing temperature. At the limit of the temperature range concerned (~ 80K), E_F has fallen below the donor level by approximately one effective Rydberg, Ry^*. Therefore, it is certainly invalid to assume E_F to be constant and equal to the donor level. However, it is not possible to predict E_F (T) for the samples under study as this function depends strongly on the compensation ratio K of the sample concerned (Blakemore 1962), and K cannot be calculated with much accuracy in this work. The normal method of eliminating the temperature dependence of E_F is to fit n (T), the electron concentration, to the expression

$$\frac{n\,(n + N_A)}{(N_D - N_A - n)} = \beta^{-1} N_c \exp\,(- E_c/kT) \qquad (2\cdot2)$$

where N_A and N_D are the total concentration of acceptors and shallow donors, $\beta = 2$ is the degeneracy of the donor 1s level, E_c is the critical energy ('mobility edge') for conduction/Hall effect/cyclotron resonance, and

$$N_c = 2\left(\frac{2\pi m^* kT}{h^2}\right)^{3/2}$$

(Blakemore 1962, p. 138).

The above expression for N_c was obtained assuming a conduction band density of states $g(E) \propto E^{\frac{1}{2}}$. It is shown in the next chapter that the observed temperature dependence of the cyclotron resonance linewidth of the samples studied indicates that the conduction bands in these samples are broadened by impurity scattering. This means that, particularly near to the bottom of the conduction band, the density of states differs widely from the $E^{\frac{1}{2}}$ dependence. Therefore, another

expression for N_c would have to be used. Equation (2·5) gives a reasonable model for the density of states in the tail of the band $g_t(E)$ which can be used to find a new expression for N_c. However, $g_t(E)$ involves an unknown parameter A(E), and since N_A, N_D, and E_c are also unknown values, this would give four variable parameters in fitting n(T). For this reason, the temperature dependence of E_F has been eliminated by using the measurements from the optical experiment in the manner described below. This method leaves only the single variable parameter E_c by utilising additional information from the optical measurements.

From optical measurements, the concentration of neutral donors N_{Dn} can be calculated. This is related simply to the Fermi level

$$N_{Dn}(T) = \frac{N_D}{1 + \beta^{-1} \exp(-E_F/kT)} \qquad (2\cdot3)$$

where the zero of energy is taken at the 1s level. Since the samples studied were heavily compensated, the Fermi level falls quickly below the impurity 1s level for $T > 0K$, and $N_{Dn} \ll N_D$ in the temperature range of the experiment. Therefore, equation (2·3) can be approximated by

$$N_{Dn}(T) \simeq 2 N_D \exp(E_F/k\ T). \qquad (2\cdot4)$$

In order to use this in the analysis of the activated behaviour of the electrons, the statistics for the conduction band electron concentration, n (T), is required. In the transport processes studied in this work, the primary contributions come from electronic states in the tail of the impurity broadened conduction band. A reasonable model for the density of states in the tail g_t (E) would be a simple exponential, of the form:

$$g_t(E) \propto \exp\left(-E/A(E)\right) \qquad (2\cdot5)$$

where A (E) is in general not constant in all parts of the tail.

The electron concentration n (T) is given by

$$n\ (T) \;=\; \int_{E=E_c}^{\infty} g\ (E)\ \ f\ (E)\ dE \qquad (2\cdot6)$$

where f (E) is the Fermi-Dirac function

$$f\ (E) \;=\; \left[1 + \exp\left((E - E_F)/kT\right)\right]^{-1}. \qquad (2\cdot7)$$

Assuming that in the temperature range of interest only the electronic states in the tail make significant contribution to n (T), then

$$n\ (T) \;=\; \int_{E=E_c}^{\infty} g_t\ (E)\ f\ (E)\ dE. \qquad (2\cdot8)$$

Using the density of states given in equation (2·5) this gives n (T) as

$$n\ (T) \;\propto\; \frac{1}{1/A(E) + 1/kT}\ \ \exp\left(-(E_c - E_F)/kT\right). \qquad (2\cdot9)$$

In the temperature region of interest A (E) and kT are comparable (see section 2·4), so that a good approximation is to take a simple activated behaviour of the form

$$n\ (T) \;\propto\; \exp\left(-(E_c - E_F)/kT\right). \qquad (2\cdot10)$$

Combining equations (2·4) and (2·10), it is then possible to eliminate the unknown Fermi energy:

$$\frac{n\ (T)}{N_{Dn}\ (T)} \;\propto\; \exp\ (-E_c/kT). \qquad (2\cdot11)$$

It can therefore be concluded that by ratioing n (T) with the density of neutral donors N_{Dn} (T), the activation plot of these <u>ratioed</u> data (i.e. the plot of $\ln\left[\frac{n\ (T)}{N_{Dn}\ (T)}\right]$ vs $^1/_T$) will yield unambiguously the threshold energy E_c as the value of the slope.

This procedure of ratioing with N_{Dn} (T) may be equally well applied to the electron concentrations deduced from either the resistivity, the Hall coefficient, or the cyclotron resonance absorption, in order to

remove the influence of the temperature dependent Fermi energy. In the next chapter, the effect of this ratioing procedure is clearly shown in the plots of the data before and after the ratioing, and the importance of this correction for the Fermi level variation is demonstrated.

2·4 Some points on the effect of a magnetic field on the conduction band

Much of the basic theory on the effect of a magnetic field on conduction band electrons, which can be found in standard texts (e.g. Nag (1980), Kubo et al. (1965)), is not repeated here. This section is primarily concerned with the derivation of the density of states of the conduction band when an external magnetic field is applied, for the case of an unbroadened conduction band, and then for a conduction band broadened by impurity scattering.

Indium Phosphide, the semiconductor used in this work, is a direct gap semiconductor, with the lowest energy conduction band at the Γ point of the Brillouin zone which is spherical. Thus, the effective mass of its conduction band, m^*, is a scalar quantity. Therefore, the following discussion can be limited to the case of a scalar m^*.

For the ideal case of no electron scattering, the conduction band electron energy is given by

$$E(\underline{k}) = \frac{\hbar^2 k^2}{2m^*} \qquad (2\cdot12)$$

where $\underline{k}$ is the electron wavevector. In the presence of an applied magnetic field $\underline{B}$, this becomes

$$E = \left(n + \tfrac{1}{2}\right)\hbar\omega_c + \frac{\hbar^2 k_B^2}{2m^*} \qquad (2\cdot13)$$

where n is any integer ≥ 0, $\omega_c = eB/m^*$ is the cyclotron resonance frequency, and k_B is the electron wavevector parallel to $\underline{B}$. Different n corresponds to different Landau levels. An electron can absorb a photon of energy equal to $\hbar\omega_c$ and be excited from the n^{th} to $(n+1)^{th}$ Landau level. This is the cyclotron resonance absorption. The density of states corresponding to the Landau levels given by equation (2.13) is

$$g_{co}(E) = \frac{1}{(2\pi L)^2} \left(\frac{2m^*}{\hbar^2}\right)^{\frac{1}{2}} \sum_n \left[E - (n+\tfrac{1}{2})\,\hbar\omega_c\right]^{-\frac{1}{2}} \qquad (2\cdot14)$$

where $L = \sqrt{\frac{\hbar}{m^*\omega_c}}$ is the Larmor radius, and the subscript o denotes that the density of states is applicable for the case of unbroadened levels.

When there is strong electron scattering, equations (2·12) - (2·14) are modified. In the following, the particular case of a strongly compensated semiconductor is considered, since this applies to the samples studied. For such substances, the carrier concentration n is much smaller than the ionised impurity concentration N_i. Therefore, even when n is small, scattering due to ionised impurities can be important. This is the dominant scattering mechanism at low temperature and, more importantly for this work, it alters the density of states of the conduction band at B = 0, and of the Landau levels. The works of Kane (1963) and Dyakonov et al. (1969) show that the electrons experience a fluctuating local potential V due to the ionised impurities, which has a Gaussian probability distribution of the form

$$P(V) = \frac{1}{\sqrt{\pi}\,\gamma} \exp\left[-V^2/\gamma^2\right] \qquad (2\cdot15)$$

where γ is defined as the average depth of the potential due to the ionised impurities. (These models are expanded on in section 3·5.)

The expression for γ depends on which assumption is made about the spatial distribution of the impurities. If it is assumed to be random (Kane 1963) then

$$\gamma = (e^2/\varepsilon)\,(4\pi\, N/K_D)^{\frac{1}{2}} \qquad (2\cdot16)$$

where ε is the dielectric constant, N the density of impurities, and K_D is the reciprocal screening length given by the Thomas-Fermi model ($K_D = 2\,N^{1/6}\,(3/\pi)^{1/6}\,a_o^{*-\frac{1}{2}}$, where a_o^* is the effective Bohr radius). On the other hand, Dyakonov et al. (1969) followed the work of Keldysh

and Proshko (1964) and assumed that there is a correlation between the impurity positions during the growth process which is 'frozen in' afterwards. This gives

$$\gamma = (e^2/\varepsilon) \ (4\pi N r_0)^{\frac{1}{2}} \qquad (2\cdot17)$$

where r_0 is the screening radius, 'set' at the formation of the sample. r_0 is given by

$$r_0 = (\varepsilon T_0 / 4\pi Ne^2)^{\frac{1}{2}} \qquad (2\cdot18)$$

and T_0 is the temperature of growth for the sample. Comparing (2·16) and (2·17), it is seen that the two equations for γ differ only in the screening radius taken.

With the important assumption that V is slowly varying in space, so that a <u>local</u> density of states can be defined for a given value of V which is the same as the density of states for an infinite volume, the total density of states can be easily written down (although not solved algebraically). When there is no applied magnetic field, the density of states for the conduction band is

$$g_c(x) \propto \int_{-\infty}^{x} (x - \xi)^{\frac{1}{2}} \exp(-\xi^2) \, d\xi \qquad (2\cdot19)$$

where x is the reduced energy, $x = E/\gamma$.

In the presence of an applied magnetic field, the density of states for each of the impurity-broadened Landau levels would have the form

$$g_c(x_n) \propto \int_{-\infty}^{x} (x_n - \xi)^{-\frac{1}{2}} \exp(-\xi^2) \, d\xi \qquad (2\cdot20)$$

where $x_n = \left(E - (\frac{1}{2} + n)\hbar\omega_c\right)/\gamma$.

2·5 The temperature dependence of the cyclotron resonance linewidth

Theoretical predictions for the temperature dependence of the cyclotron resonance linewidth Γ differ considerably, depending on whether the Landau levels are taken to be collision-broadened or not. At low temperatures, a model which is based on unbroadened Landau levels would yield, approximately, a $T^{-\frac{1}{2}}$ dependence for Γ, that is, a rapid increase in the linewidth as the temperature is lowered (Kawamura et al. 1964, Fujita and Lodder 1976, Srinivas et al. 1981, Arora and Spector 1979). On the other hand, when collision-broadened Landau levels are considered, Γ is predicted to decrease with decreasing temperature for the low temperature range. There are different experimental studies which support either model . In the present work, it was observed that Γ decreases with decreasing T, in accordance with the second model based on broadened Landau levels. This model has also been borne out by other experimental studies both on elemental semiconductors (Bagguley et al. 1961) and on III-V and II-VI compound semiconductors (Chamberlain and Stradling 1969, Mears and Stradling 1969, Kaufman and Neuringer 1970, Nicholas and Sarkar 1982). The work of Nicholas and Sarkar (1982) in particular is used a great deal in this section, and will be referred to from now on as NS.

The purpose of this section is to give a brief outline of the theory predicting $\Gamma(T)$ based on both a broadened and an unbroadened density of states. From this, it is shown that experimental data of $\Gamma(T)$ at low temperatures can be used to indicate whether the conduction band is broadened by impurity scattering and, if so, to yield a value for the broadening parameter Υ (see previous section for the definition of Υ).

The high frequency conductivity is given by

$$\sigma(\omega) \propto \int \frac{\tau f(E_z)\, g(E_z)}{1 + (\omega - \omega_c)^2 \tau^2}\, dE_z \qquad (2\cdot21)$$

where $f(E_z)$ is the Fermi-Dirac function, E_z is the energy due to motion parallel to the magnetic field, $g(E_z)$ the appropriate density of states, and τ^{-1} is the scattering rate.

Assuming that

$$\tau^{-1} = A\, g(E_z) \qquad (2\cdot22)$$

where A contains the details of the scattering mechanisms, and is assumed to be independent of E_z, then (2·21) can be rewritten as

$$\sigma(\omega) \propto \int \frac{A^{-1} f(E_z)}{1 + A^{-2} (\omega - \omega_c)^2 g^{-2}(E_z)}\, dE_z. \qquad (2\cdot23)$$

In fact, more detailed theoretical calculations (for unbroadened Landau levels) show that (2·22) is true when E_z is small and $k_z \ll 1/k_z$ (Fujita and Lodder 1976, Srinivas et al. 1981).

The cyclotron resonance linewidth Γ can be obtained from the definition

$$\sigma(\omega_c \pm \Gamma) = \tfrac{1}{2}\, \sigma(\omega_c). \qquad (2\cdot24)$$

For the case of unbroadened Landau levels, substitution of the density of states $g_{co}(E)$ given in equation (2·14) leads to

$$\Gamma = CA^{-1} (kT)^{\frac{1}{2}} \qquad (2\cdot25)$$

where C is a numerical factor, given by

$$\int \frac{f(x)\, dx}{1 + C^2 x} = \tfrac{1}{2} \int f(x)\, dx \qquad (2\cdot26)$$

For the case of broadened Landau levels, putting the density of states g_c of equation (2·20) into equation (2·23), $\Gamma(T)$ is not given by a simple analytical solution. The numerical solution is easily

obtained, however. The function $\Gamma\left(T/(\Upsilon/k)\right)$ for each model is shown in figure 2·1.

In contrast to NS, it is assumed here that all the states in the tail of the broadened Landau levels contribute to the cyclotron resonance (i.e. the mobility edge ε_c in NS is set to zero). Since the density of states g_c was calculated with the assumption that the impurity potential V is slowly varying in space with respect to the electron's wavefunction (see previous section 2·4), it follows that each 'pocket' of constant V should be of dimensions >> L (B_{min}), where L is the Larmor radius, and B_{min} is the magnetic field which is sufficiently strong to cause observable cyclotron resonance absorption. For this case, electronic states arising from these potential 'pockets', i.e. states in the tail of the Landau level, can effect cyclotron motion and exhibit cyclotron resonance.

From figure 2·1, it can be seen that for the high temperature range ($kT > 5\Upsilon$) both models give the same temperature dependence, $T^{-\frac{1}{2}}$, since in this high temperature limit the main contribution to $\sigma(\omega)$ in equation (2·26) comes from the high energy electronic states for which $g_{co}(E) \sim g_c(E) \propto E^{-\frac{1}{2}}$. On the other hand, the difference between the two models for $kT < 3\Upsilon$ is striking. It has been calculated from experimental data that Υ lies between 2 to 4 meV (NS, Vuong and Nicholas 1985) for some samples of CdTe and InP. Thus, from the temperature dependence of the cyclotron resonance linewidth for $T \lesssim 35K$, a temperature range easily reached in practice, it should be possible to deduce whether or not the Landau levels are broadened. Furthermore, a quantitative fit of the universal function $\Gamma\left(T/(\Upsilon/k)\right)$ to experimental values of $\Gamma(T)$ should yield a value for Υ, the broadening parameter. This is done in the next chapter.

As has been pointed out by NS, Υ may be dependent on temperature, in addition to the temperature dependence of the concentration of

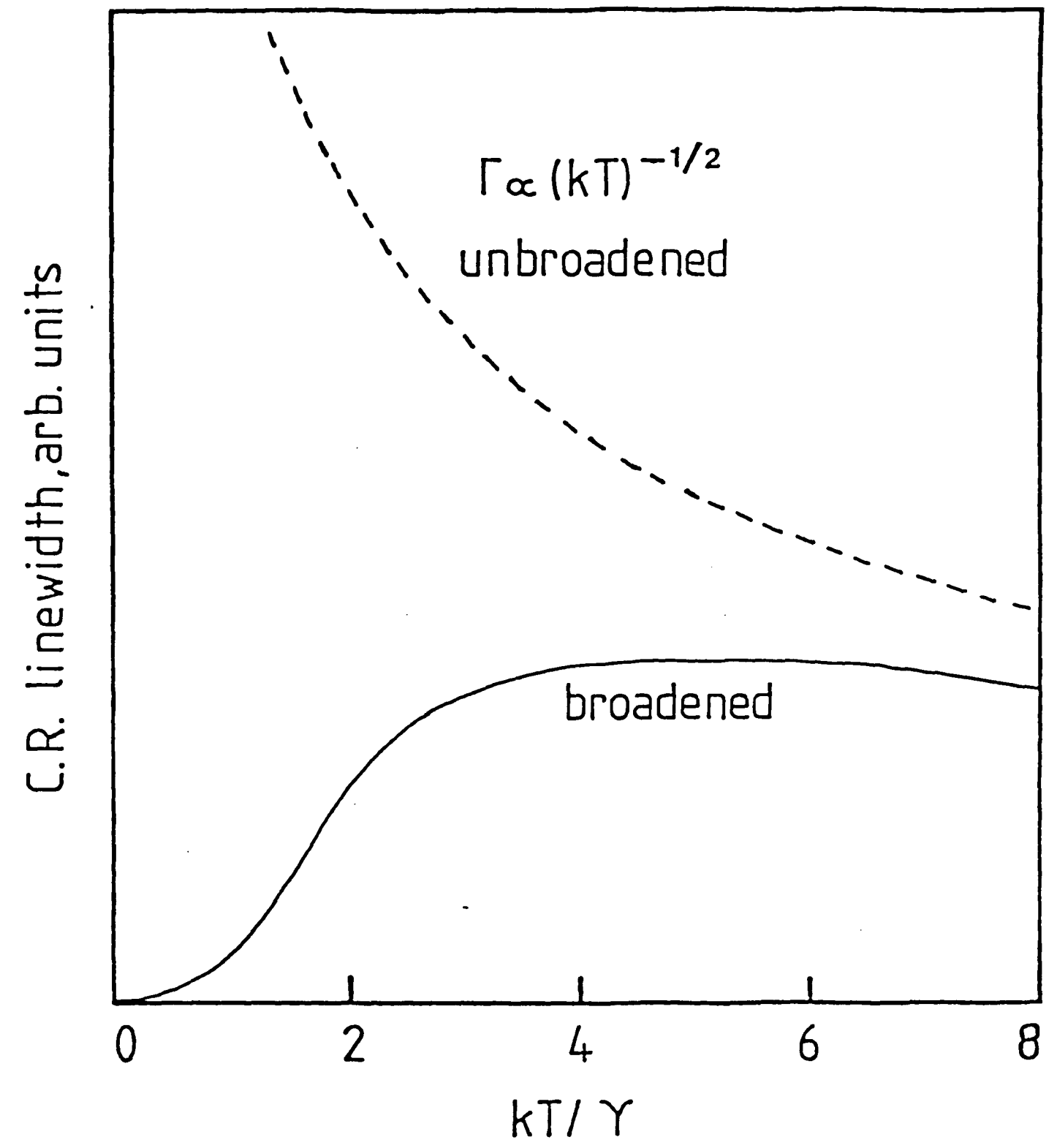


Figure 2·1

Theoretical predictions of the cyclotron resonance linewidth as a function of kT/γ for the case of unbroadened Landau levels (dash line) and for broadened Landau levels (solid line).

ionised impurity scatterers itself which enters into the proportionality constant A (equation (2·22)). These temperature dependences have been ignored in this work, as their effect is expected to be small for the highly compensated samples which are used in the present study. The good fits of $\Gamma(T)$ in the next chapter show that the assumptions of temperature-independent γ and A are justified.

CHAPTER 3

A study of activated conduction in n - InP

3·1 Introduction

This chapter describes the experimental work, carried out on several samples of n-type Indium Phosphide, to investigate the difference in the activation energies of various transport processes. The analysis of the data, using the theory outlined in chapter 2, is then presented. Several possible interpretations of the values of the activation energies and their differences are given. Of these, only one explains all the experimental observations. The conclusion is that the differences between the temperature dependence of the Hall effect, the d.c. conductivity, and the cyclotron resonance occur because they have different threshold energies in the conduction band. These can be thought of as different mobility edges for the two transport processes. A physical insight into the presence of such threshold levels is given, which also explains why they are not coincident. This is based both on an effective medium model, and on the manner in which localisation explains the Hall effect and resistivity results in 2-D systems.

3·2 Experimental procedure

(a) Sample characteristics

The samples used were epitaxial layers of n-type Indium Phosphide, grown on semi-insulating substrates. These samples have good boundaries between the epitaxial layer and the substrate as shown by Auger profiles where available. In fact some samples, which are not mentioned further in this work, were discarded when the Hall coefficient showed a broad peak in its temperature dependence at around 77 K. This feature has been identified by other workers as due to imperfect boundaries. All the samples were wedged on the substrate side to inhibit interference effects in the optical experiments which could be caused by light multiply-reflecting within the samples. The characteristics of the samples are given in table 3·1. The data given under 'n at 300 K' and 'μ_{max}' were calculated using the values of the Hall coefficients and appropriate values of the geometrical factor, f. This factor converts the measured Hall coefficient of the actual sample into that of an infinitely long, thin bar. To calculate f, it was assumed that all samples have a room-temperature Hall mobility of 4900 $cm^2\ V^{-1}\ s^{-1}$, and f is then the ratio of this value to the measured room temperature Hall mobility. The chosen value of 4900 $cm^2\ V^{-1}\ s^{-1}$ is a typical value of Indium Phosphide grown epitaxially in recent years, and is representative of the values quoted for the samples used in this work where such information was available. f was calculated to be between 0·8 and 2·1 for these samples. The carrier concentration n at 300 K is then given by

$$n\ (300\ K) = \frac{1}{|e|\ f\ R_H(300\ K)}\ , \qquad (3\cdot1)$$

assuming the Hall factor to be equal to 1. The maximum Hall mobility, μ_{max}, is given by:

Table 3·1

Sample Characteristics

Sample	Thickness /μm	n at 300 K /cm^{-3}	μ_{max} /$cm^2\ V^{-1}\ s^{-1}$	Compensation Ratio $K = N_A/N_D$
PR 181	4·3	$1·3 \times 10^{15}$	44 400	0·4
R 294	3·9	$1·8 \times 10^{15}$	42 300	0·4
PR 182	4·3	$6·5 \times 10^{14}$	27 200	0·5
NAG 365A	12	$6·8 \times 10^{14}$	38 300	0·9
NAG 365B	11	$6·8 \times 10^{14}$	28 400	0·9

$$\mu_{max} = f\left(\frac{R_H(T)}{\rho(T)}\right)_{max} . \qquad (3\cdot2)$$

The temperature at which the Hall mobility reaches its maximum value is between 55 K and 85 K for the various samples.

The values of the compensation ratios, K, given in table 3·1 are deduced from the 77 K Hall mobility, and the Brooks-Herring formula as used with the approximations made by Chattopadhya and Queisser (1981). This work gives the drift mobility as

$$\mu_{BH} = \frac{128\sqrt{2\pi}\,\varepsilon^2 (kT)^{3/2}}{\sqrt{m^*}\,N_I Z^2 e^3}\left[\ln\left(\frac{24m^*\varepsilon(kT)^2}{n\,e^2\,\hbar^2}\right)\right]^{-1} \qquad (3\cdot3)$$

where N_I is the concentration of ionised impurities, Z is the charge on the impurity in units of e taken as 1 in this case, ε is the static permittivity of the semiconductor, and the other symbols have their usual meanings.

However, electron-electron scattering in the low carrier concentration limit reduces the mobility. Taking this into account, Appel (1961) finds the mobility to be

$$\mu_{e-e} = 0\cdot58\ \mu_{BH} \qquad (3\cdot4)$$

Using equations (3·3) and (3·4), and assuming the measured Hall mobility (at 77 K) to be the same as the drift mobility (an approximation), values of N_I at 77 K were calculated taking $m^* = 0\cdot08\ m_o$, $\varepsilon = 14\ \varepsilon_o$, and n given by the Hall coefficient.

Using the calculated values of N_I and n, the compensation ratios were calculated with the further assumption that at 77 K, all the uncompensated donors are thermally excited. Thus, at 77 K, $n = N_D - N_A$, and $N_I = N_D + N_A$, where N_D and N_A are the concentrations of the donors and acceptors respectively. Because of the assumptions made, the values of K given are rather inaccurate and meant as a rough guide only.

As well as the samples whose characteristics are given in table 3·1, experiments were also carried out on a bulk sample of n - In P, V201. This sample has comparable values of n and μ to those of the epitaxial samples used. The thickness of the bulk sample makes it impossible to record good F.I.R. transmission data. These optical measurements turned out to be necessary to the final analysis of the data. Therefore, results from V201 have not been included here. However, the transport data gave the same activation energies as the epitaxial samples and, in particular, the same difference between the Hall effect and the d.c. conductivity. This shows that this difference is a property of n-Indium Phosphide and not an effect of the samples being epitaxial layers.

(b) Experimental conditions

The low field Hall coefficient and resistivity were measured simultaneously for temperatures from 4·2 K to room temperature. For the Hall effect, the magnetic field was swept between 0 T and 0·2 T. Within this range, the Hall voltage varied linearly with field. The small magnetoresistance component was eliminated by reversing the direction of the magnetic field for each measurement and taking the average of the magnitude of the Hall voltage for the two field directions. The current used was kept as low as possible, well within the Ohmic region to avoid hot-electron effects, e.g. the maximum voltage applied across samples of 6 mm length was kept below 10 mV at low temperatures. The resistivity (at B = 0) was measured at the same current as the Hall effect by the 4-contact method (van der Pauw 1958).

Transmission traces for F.I.R. radiation of wavelengths 172 μm (D_2O laser) and 337 μm (HCN laser) were recorded for magnetic fields up to 9 T and for temperatures from 17 K to 60 K. Typical traces are shown in figures 3·1a and 3·1b. The transmission traces for 337 μm radiation

show the cyclotron resonance (C.R.) absorption, while the traces for 172 μm show in addition the impurity absorption due mainly to the $1s - 2p^+$ transition. The C.R. lines observed in all traces gave the band-edge effective mass value of 0·08 ± 2%, in good agreement with the accepted value for Indium Phosphide (Lawaetz 1971, Rochon and Fortin 1975, Chamberlain et al. 1972). The corrections for non-parabolicity for C.R. masses at the wavelengths used were in fact small compared with the experimental errors: 0·5% for the 337 μm line and 1% for the 172 μm line. These corrections were calculated using expressions for the energies of the Landau levels derived from a 3 band $\underline{k}.\underline{p}$ model (Palik et al. 1961a,b) which has been shown to be adequate for InP (Shantharama et al. 1984). It is assumed that only the lowest Landau level, n = 0, was populated, that the spin-orbit splitting of the valence band $\Delta \to \infty$, and that $k_z \cong 0$ (z is the direction of the magnetic field). This gives

$$\frac{m^*_{CR}}{m^*_{BE}} = 1 + \left(1 - \frac{m^*_{BE}}{m_o}\right)^2 \cdot \frac{2\hbar\omega_c}{Eg} \qquad (3·5)$$

where m^*_{CR} and m^*_{BE} are the C.R. and the band edge effective masses respectively, and Eg is the band gap which is taken to be 1·42 eV for Indium Phosphide.

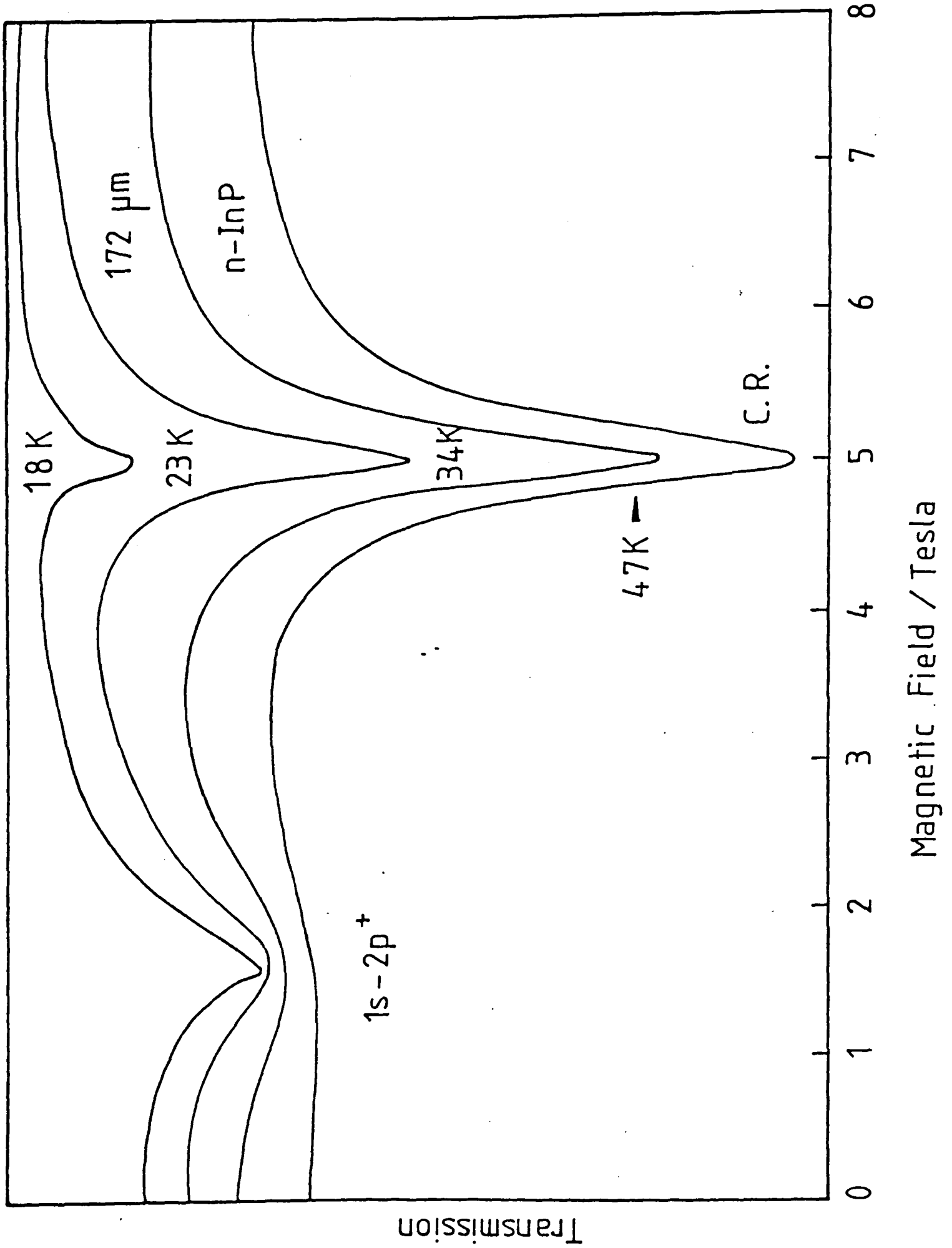


Figure 3·1a

Typical transmission traces of 172 μm for sample R294 at various temperatures.

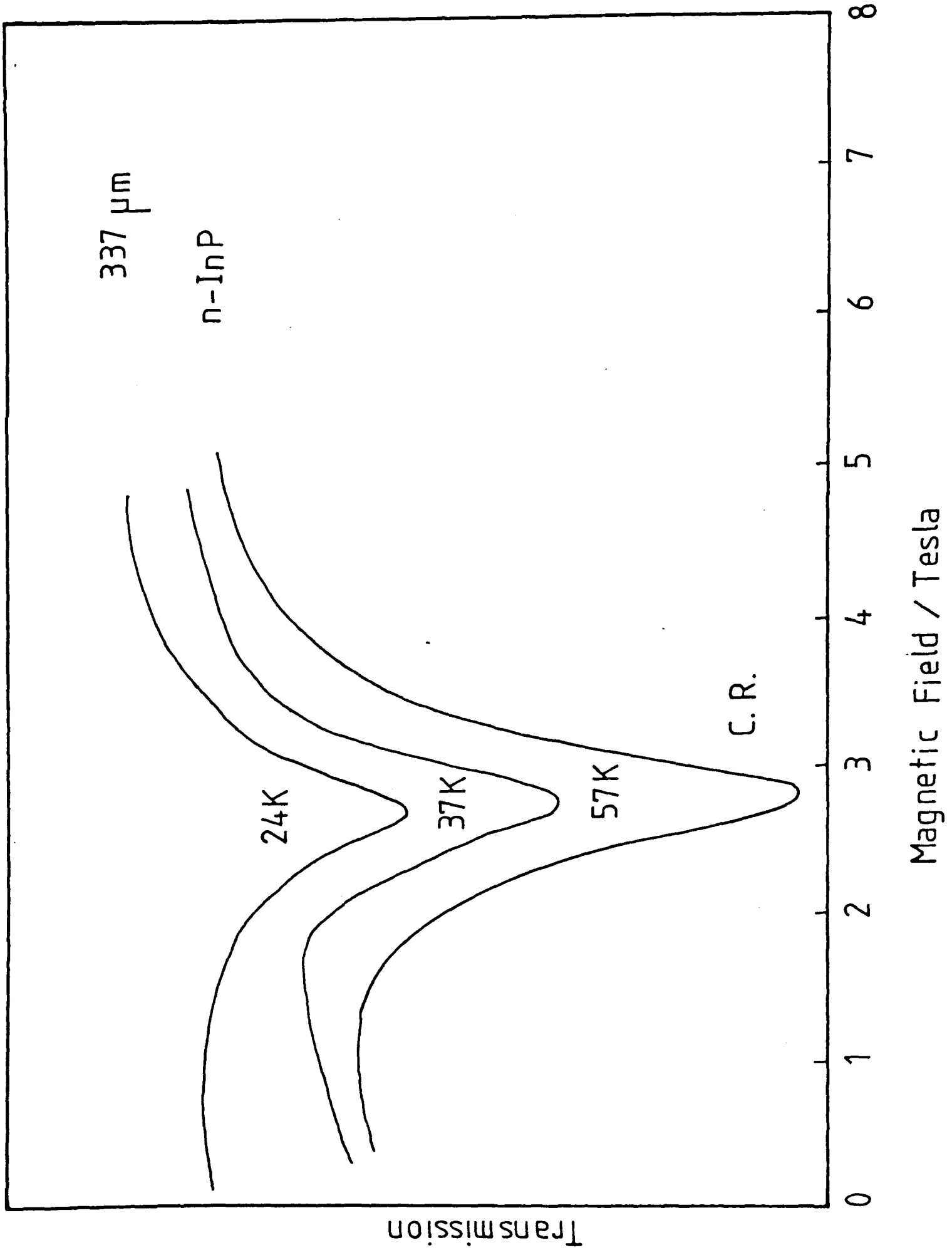


Figure 3·1b

Typical transmission traces of 337 μm for sample R294 at various temperatures.

3·3 Experimental results

Measurements of resistivity ρ and of the Hall coefficient R_H are shown for the five samples studied in figures 3·2 and 3·3, as $\ell n\ \rho$ and $\ell n\ R_H$ against 1/T respectively. This type of plot is known as an activation plot. In the temperature range in which the exponential, 'activated' behaviour of the electron concentration n dominates other temperature dependences, so that

$$n\ (T) \ \propto \ \exp\ \left(-(E_c - E_F)/kT\right) \qquad (3\cdot6)$$

such an activation plot should be linear with a gradient equal to the activation energy $(E_c - E_F)$, assuming that the Fermi level E_F remains constant. It may be seen from figures 3·2 and 3·3 that most of the plots for ρ and R_H show distinct breaks in their linear dependence, leading to two different gradients in the activated conduction regime. This is an effect of the variation of the Fermi level E_F with temperature and will be discussed later. The activation energies for the two transport processes are different in both regimes; the activation energies for the Hall effect are smaller in both regimes, and a simple combination of the values of ρ and R_H would lead to the deduction of a thermally activated value of the d.c. mobility, falling to values of order 800 $cm^2\ V^{-1}\ s^{-1}$ at 10 K. Below this temperature hopping conduction starts.

Measurements of the temperature dependences of the transmission of 337 μm and 172 μm radiation as a function of the applied magnetic field lead to three important deductions. Firstly, it can be seen from figures 3·1a and b that the cyclotron resonance width Γ is narrowing with decreasing temperature. Since Γ is inversely proportional to the mobility of the cyclotron motion, this shows that the a.c. mobility increases as the temperature falls, in complete contrast to the apparent d.c. behaviour. According to the theoretical predictions

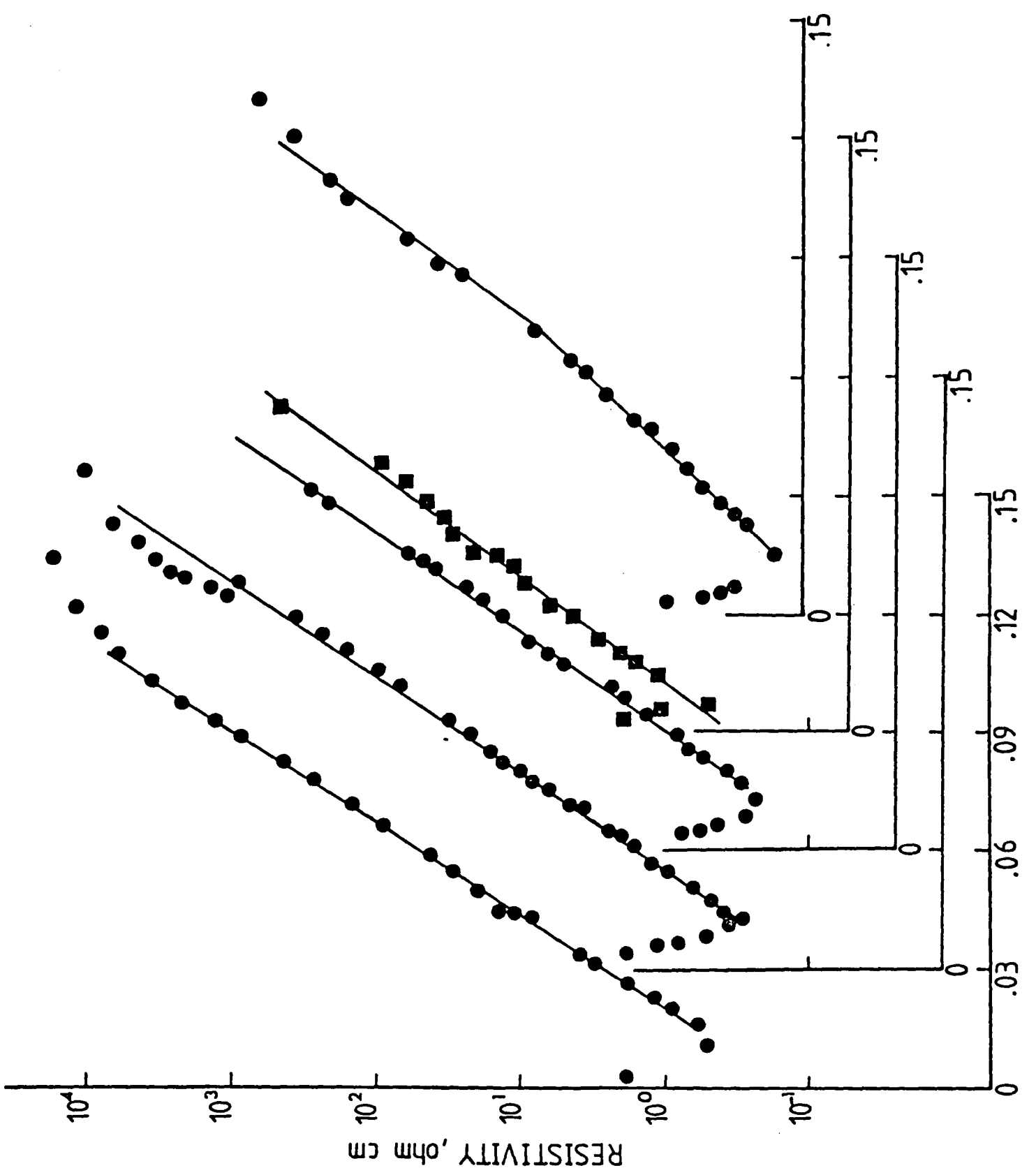


Figure 3·2

Logarithmic plot of the resistivity vs 1/temperature.

For the purposes of clarity, the x-axis is displaced by 0·03 for each sample. The y-axis is common to all five samples, which are, from left to right, NAG 365B, NAG 365A, PR 181, PR 182, R 294.

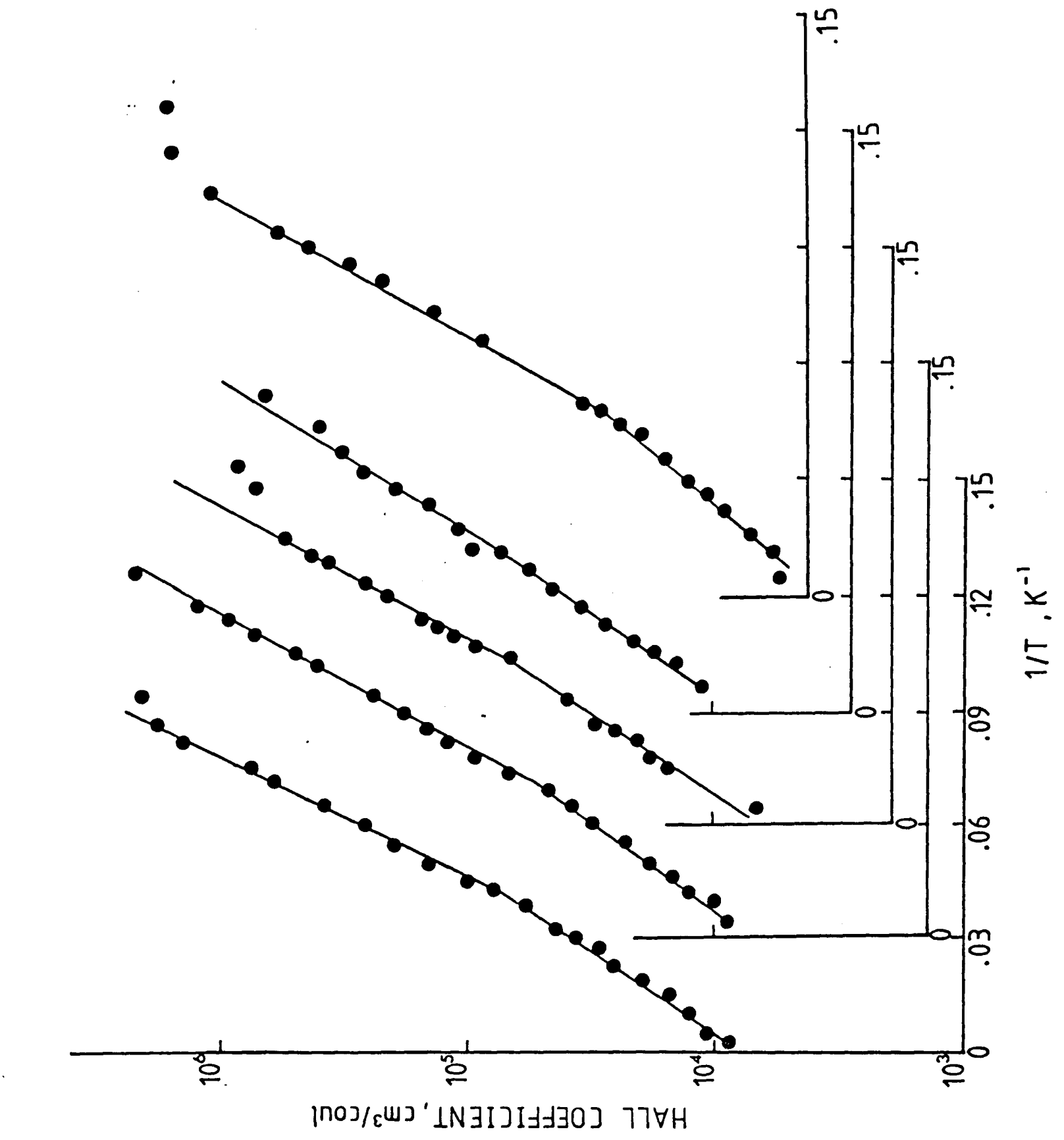


Figure 3·3

Logarithmic plot of the Hall coefficient vs 1/temperature.

For the purposes of clarity, the x-axis is displaced by 0·03 for each sample. The y-axis is common to all five samples, which are, from left to right, NAG 365B, NAG 365A, PR 181, PR 182, R 294.

discussed in section 2·5, this decrease of Γ with temperature at low temperatures indicates that the Landau levels' density of states is broadened. Quantitatively, the dependence of Γ on T measured for all samples was fitted to the predicted $\Gamma(T/(\gamma/k))$ which was shown in figure 2·1. Figure 3·4 shows a typical fit for values of Γ measured from the C.R. of sample R294 with line 172 μm. The agreement of the experiment and the theoretical predictions is good, and gives values of γ in the range 3-4 meV for the samples under study. This is in good agreement with similar measurements by Nicholas and Sarkar (1982) on InP and CdTe which gave γ = 2 meV. Based on a similar model of long range potential fluctuations, Pistoulet et al. (1985) calculated γ from values of $\sigma_{a.c.}(\omega, T)$ and $\sigma_{d.c.}(T)$. They obtained values of 4·06 meV and 7·85 meV for X-Si. Considering that γ depends on the conditions of growth and doping, this also is in fair agreement with the present results.

The second set of information to be obtained from the transmission curves is the concentration n of free electrons. In the present case, n is directly proportional to the area under the absoption curve, A_{CR}, of the cyclotron resonance. This direct proportionality depends on certain approximations which are discussed below. Firstly, the F.I.R. is polarised so that the total transmittivity observed is

$$T(\omega) = x\,T^{+}(\omega) + (1 - x)\,T^{-}(\omega) \qquad (3\cdot7)$$

where $T^{+}(\omega)$ and $T^{-}(\omega)$ are the transmittivities of the sample for the cyclotron resonance active (C.R.A.) and inactive (C.R.I.) polarized light respectively, and x is the ratio of their intensities and is called the polarization ratio.

On reversing the direction of the magnetic field, the new transmittivity observed is

$$T'(\omega) = (1 - x)\,T^{+}(\omega) + x\,T^{-}(\omega) \qquad (3\cdot8)$$

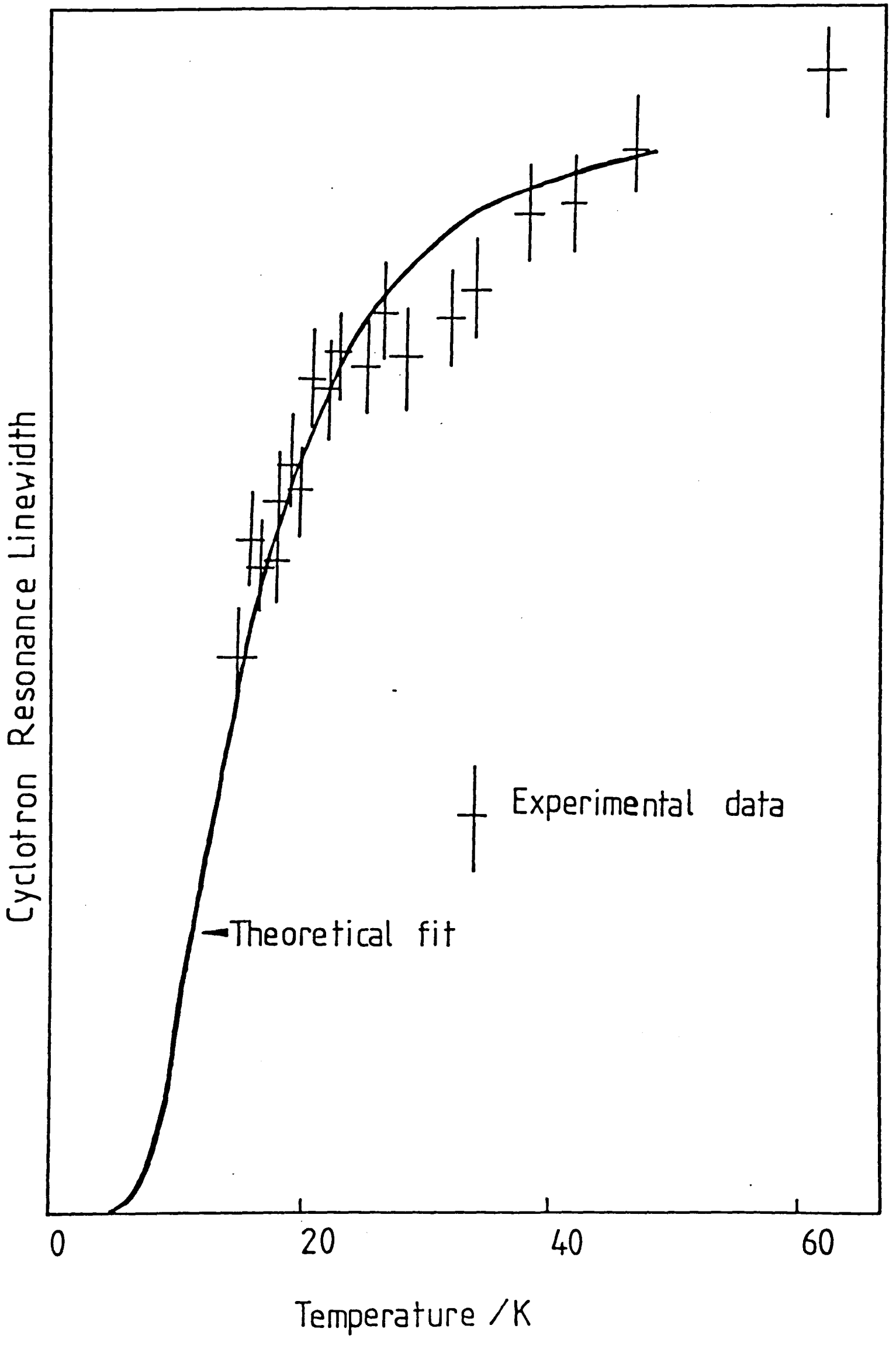


Figure 3·4

Plot of cyclotron resonance linewidth vs temperature for the 172 μm resonance for sample R 294. The theoretical fit is shown as the continuous curve.

In the limit of $\omega_c \tau >> 1$, $T^-(\omega) = 1$. This approximation can be made in the present case, where typically $\omega_c\tau \sim 6$ for the 337 μm and ~ 20 for the 172 μm line. Using this approximation for $T^-(\omega)$ and combining equations (35) and (36), the polarisation ratio is given as:

$$x = \frac{1-T(\omega)}{[1-T(\omega)] + [1-T'(\omega)]}, \qquad (3\cdot9)$$

which can be measured experimentally.

x was measured to be between 0·6 and 0·65 during the optical experiments made, showing that the F.I.R. was nearly linearly polarized. More importantly, the value of x did not change appreciably during a run. Thus, in summary, $T(\omega)$ can be written as

$$T(\omega) = x\, T^+(\omega) + (1-x) \qquad (3\cdot10)$$

where x can be treated as a constant. The transmittivities $T^{\pm}(\omega)$ are given as (Palik and Furdyna 1970)

$$T^{\pm}(\omega) \propto \exp\left[-\alpha'\, \sigma^{\pm}(\omega)/\sigma_0\right] \qquad (3\cdot11)$$

where

$$\alpha' = \frac{\sigma_0 d}{cn'\varepsilon_0} = \frac{ne^2\tau d}{cn'\varepsilon_0 m^*} \qquad (3\cdot12)$$

with τ^{-1} being the absolute linewidth, d the sample thickness, n' the refractive index and the other symbols have their usual meanings. For the ideal case, $\sigma^{\pm}(\omega)$ has a Lorentzian shape:

$$\frac{\sigma^{\pm}(\omega)}{\sigma_0} = \left[1 + (\omega \mp \omega_c)^2\, \tau^2\right]^{-1} \qquad (3\cdot13)$$

For this case, the carrier density n can be calculated simply from

$$n \propto -\frac{\ell n\, [T^+(\omega_c)]}{\tau} \qquad (3\cdot14)$$

However, the resonances obtained are not of this ideal shape; instead they are asymmetrical. Since the samples have been wedged to suppress interference effects, and since values of $\omega_c\tau$ are quite large, these two usual causes of non-ideal lineshape cannot be, here, the main

reason for deviations from equation (3·13). The most probable cause is failure in the assumption of an energy-independent mean free time τ in equation (3·13); as discussed later on, it is believed that cyclotron resonance in these samples involves states in the tail of broadened Landau levels, for which states many classical assumptions are inapplicable. Therefore, instead of using equation (3·14), it is assumed that $\alpha' << 1$, i.e. that the absorption is small, which is the present case. This gives:

$$T^+(\omega) \propto \exp\left[-\alpha' \frac{\sigma^+(\omega)}{\sigma_0}\right] \simeq 1 - \alpha' \frac{\sigma^+(\omega)}{\sigma_0} \qquad (3\cdot15)$$

The area of absorption of the cyclotron resonance, A_{CR}, is obtained by integrating the absorption over ω:

$$A_{CR} = \int_0^\infty (1-T(\omega))d\omega \qquad (3\cdot16)$$

Using equation (3·10) to substitute for $T(\omega)$

$$A_{CR} = \int_0^\infty \left[1 - \left(xT^+(\omega) + (1-x)\right)\right] d\omega$$

$$= x \int_0^\infty \left[1 - T^+(\omega)\right] d\omega. \qquad (3\cdot17)$$

Using equation (3·15) for $T^+(\omega)$,

$$A_{CR} \propto \alpha' \propto n. \qquad (3\cdot18)$$

Thus from $A_{CR}(T)$ we have a very direct measurement of the temperature dependence of the free electron concentration, with a 'free electron' defined as one which takes part in the cyclotron resonance with an effective mass of 0·08 m_0, the typical conduction band edge mass for InP. Figures 3·5a and b show an activation plot of n determined by

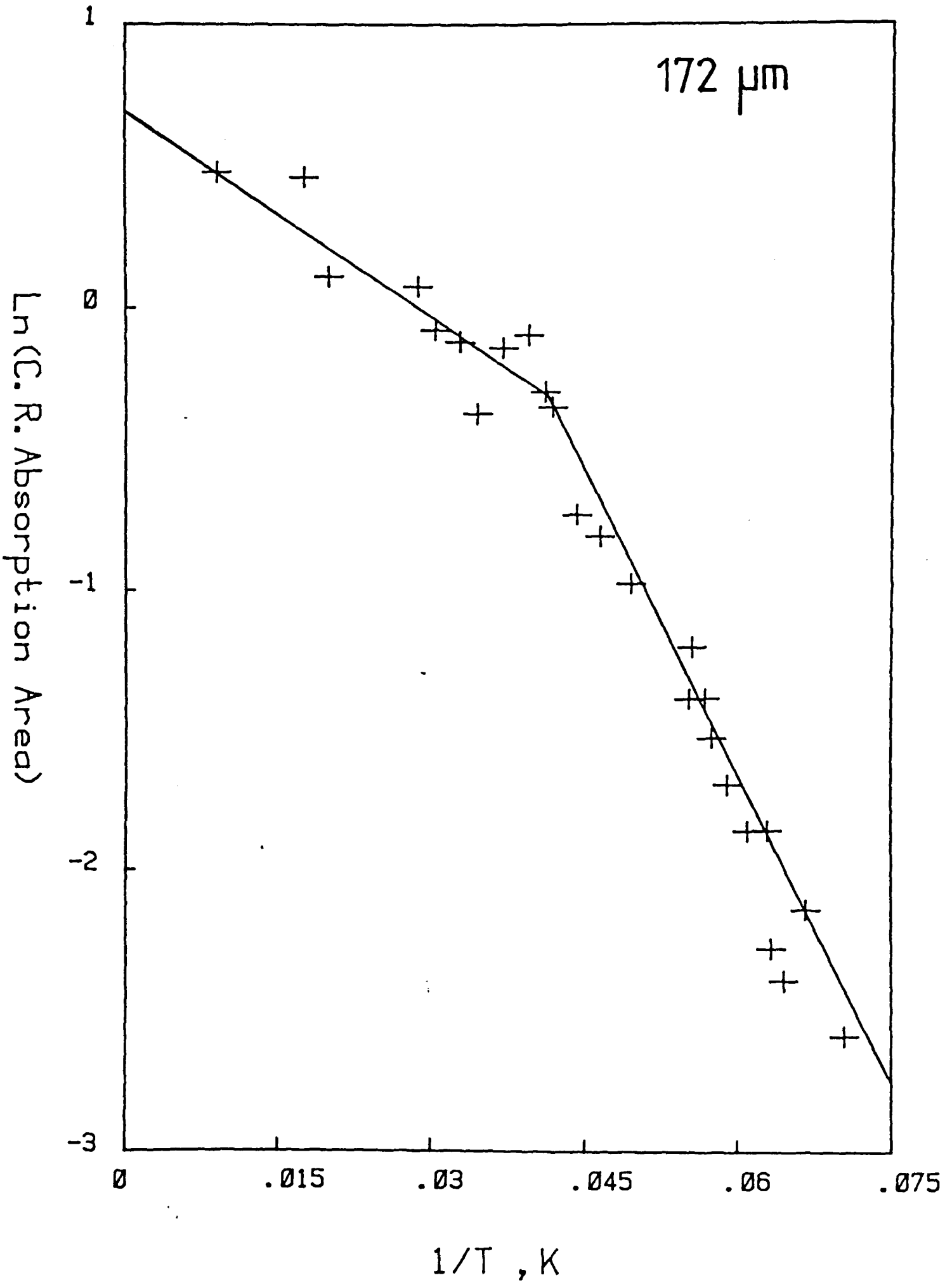


Figure 3·5a

Logarithmic plot of the C.R. absorption area vs 1/temperature for sample R 294, for wavelength 172 µm.

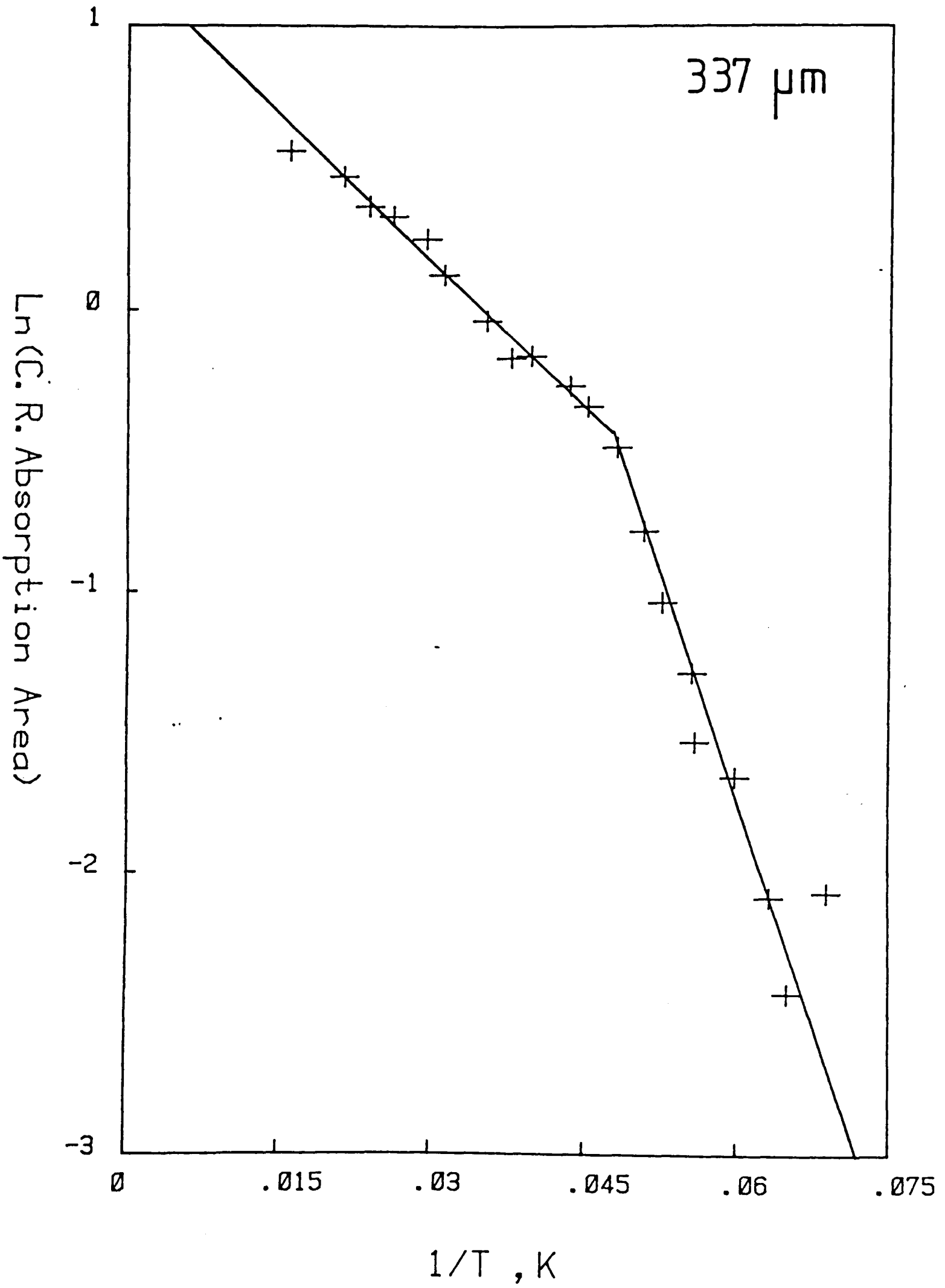


Figure 3·5b

Logarithmic plot of the C.R. absorption area vs 1/temperature for sample R 294, for wavelength 337 µm.

this method for one of the samples. This shows a break in slope very similar to that found for both ρ and R_H, proving that this feature is indeed caused by the temperature dependence of n(T) in all three types of measurements.

The third and final deduction which can be made from the F.I.R. transmission measurements is the population of the 1s donor impurity state, which give information on the position of the Fermi energy. At low magnetic fields, the transmission of the 172 μm radiation shows an impurity absorption, due mainly to the $1s - 2p^+$ transition (figure 3·1a). The strength of this feature is proportional to the number of electrons in the donor 1s level, which is equal to the concentration of neutral donors, N_{Dn}. As discussed in 2·3, the ratio $n(T)/N_{Dn}(T)$ should be independent of $E_F(T)$, and the activation plot of this ratio should be linear, giving the threshold energy E_c as the gradient. This is indeed the case. Figure 3·6 shows activation plots of the cyclotron resonance area A_{CR} both direct and after ratioing by N_{Dn}. The unratioed plot again shows the distinct break in slope which was seen in the plots for ρ and R_H. However, the ratioed points give an excellent straight line, with an activation energy rather lower than would be deduced from the direct plot. An exactly similar behaviour is shown by ρ and R_H when ratioed against N_{Dn}. One disadvantage of this procedure is that there is a relatively large experimental error in the area of the $1s - 2p^+$ absorption, and this is therefore carried through to all of the other measurements.

Thus by ratioing against N_{Dn}, unambiguous activation energies are obtained for the three different measures of the electron concentration n: Hall effect, resistivity and cyclotron absorption. The values deduced for the various samples studied are given in table 3·2. In the

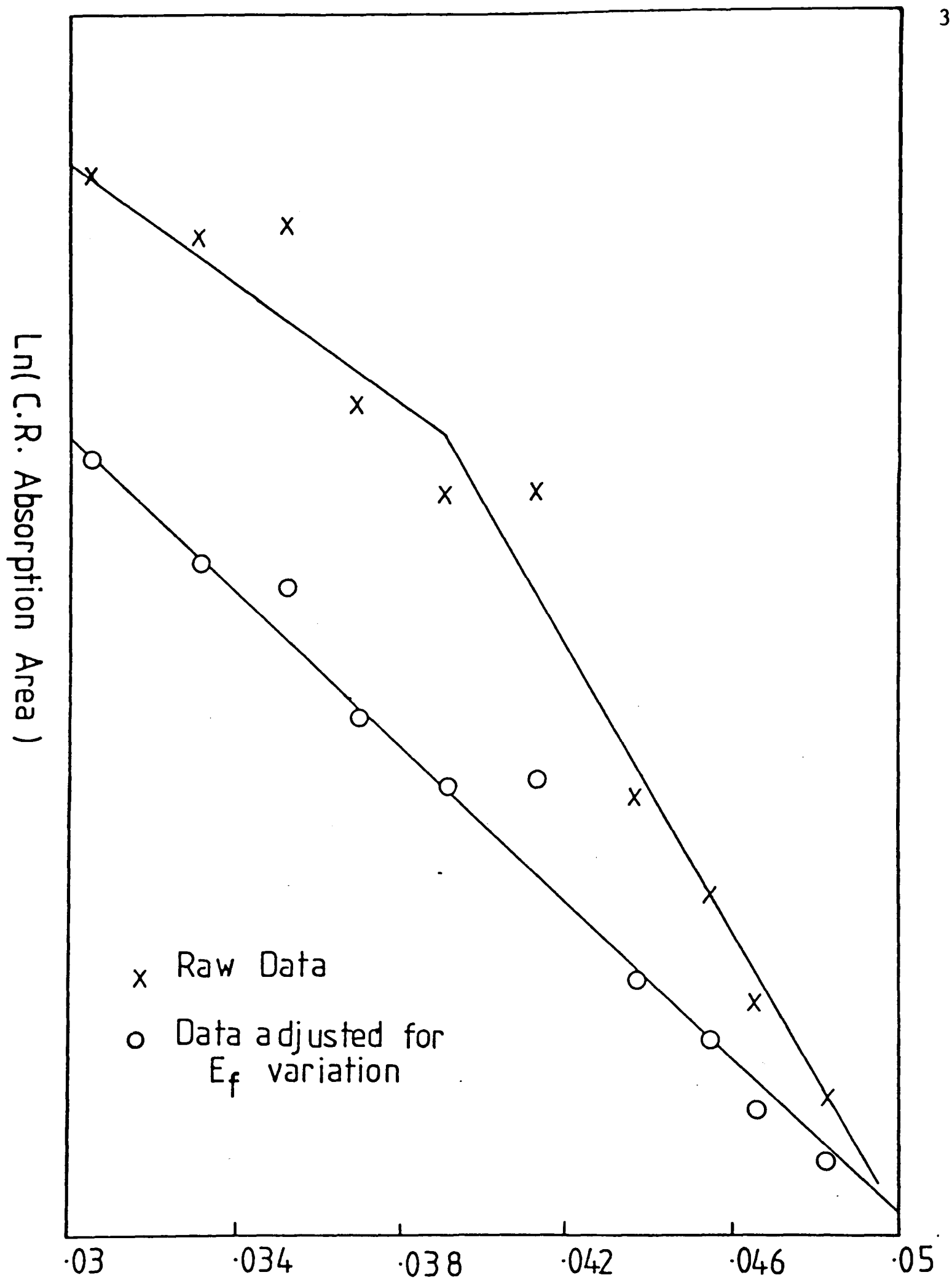


Figure 3·6

Plot of ℓn (C.R. absorption area) vs 1/temperature before and after adjustment for the variations of the Fermi level. It can be seen that the 'kink' in the raw (i.e. unratioed) data is absent in the adjusted (i.e. ratioed) data, giving one single activation energy for the whole temperature range as expected.

Table 3·2

The activation energies E_c in Kelvins

Sample	K	Resistivity $(E_c)_{RE}$	Hall effect $(E_c)_{Hall}$	Cyclotron Resonance $(E_c)_{CR}$ 172 μm	Cyclotron Resonance (a) 337 μm	$\frac{E_{c_{RE}} \approx E_{c_{Hall}}}{(\gamma/2)}$
PR 181	0·4	52 ± 10	36 ± 10	-	-	16/18·5
R 294	0·4	57 ± 10	47 ± 10	49 ± 10	39 ± 15	10/13·5
PR 182	0·5	63 ± 10	46 ± 10	48 ± 10	41 ± 15	17/15
NAG 365A	0·9	78 ± 11	46 ± 10	61 ± 10	-	32/15
NAG 365B	0·9	76 ± 18	44 ± 18	43 ± 10	45 ± 15	32/20·5

(a) To compare the activation energy of cyclotron resonance with those obtained at B = 0, the additional magnetic contribution to the binding energy E_M has been subtracted. E_M is estimated using the calculations of Lee et al. (1973). E_M is calculated to be 33 K for the 172 μm resonance and 19 K for 337 μm.

activation plots of n/N_{Dn} obtained from the Hall coefficient R_H, the temperature dependence of the Hall ratio r was neglected. This is justifiable since r has been calculated to vary from 1·15 to 1·2 in the range of temperature of the experiment (Lee et al. 1980) while R_H was found to vary over three orders of magnitudes for the samples studied. A more serious approximation was to ignore the temperature dependence of the mobility in taking n to be inversely proportional to the resistivity. This approximation is discussed in section 3·5. Finally, n is taken to be directly proportional to A_{CR} as has been discussed earlier.

3·4 Estimates of the Fermi-level variation with temperature

In the above calculations, only the temperature dependence of E_F is required, not the actual value of E_F. To obtain the former, very few approximations were made (see 2·3). However, it was felt that an estimate of the actual values of the Fermi level would be of interest. This estimate was made, using equation (2·4) and some further assumptions and estimates not needed in the general body of this work.

Since

$$N_{Dn}(T=0K) = N_D - N_A \qquad (3·19)$$

where N_A is the concentration of acceptors,

$$N_{Dn}(T=0K) = N_D(1-K) \qquad (3·20)$$

where K is the compensation ratio of the sample, $K = N_A/N_D$. Therefore, equation (2·4) can be re-written as follows:

$$N_{Dn}(T) = 2 \frac{N_{Dn}(T=0K)}{1-K} \exp(E_F/kT) \qquad (3·21)$$

If $A_i(T)$ is the area of impurity absorption, then since $A_i(T) \propto N_{Dn}(T)$, equation (3·21) can be re-written as

$$A_i(T) = 2 \frac{A_i(T=0K)}{1-K} \exp(E_F/kT) \qquad (3·22)$$

Therefore, to evaluate E_F from the experimental values of $A_i(T)$, the rather inaccurate values for K, which was deduced from the 77K mobility and the Brooks-Herring formula, were used together with the assumption that $A_i(T=0K) \approx A_i(T=10K)$ - 10K being the lowest temperature for which absorption data are available. The resultant variation of the Fermi level with temperature for the four samples is shown in figure 3·7. It can be seen that there is a change in the temperature dependence of E_F around 20K. This is the origin of the break in the activation plots of

ρ, R_H and A_{cr}. Secondly, the temperature dependence is greater for larger values of the compensation ratio, K. This is in agreement with theoretical predictions (Blakemore 1962). The difference between the curves for the two samples with K nominally equal to 0·9 is probably due to the large errors in estimating the values of the compensation ratio K.

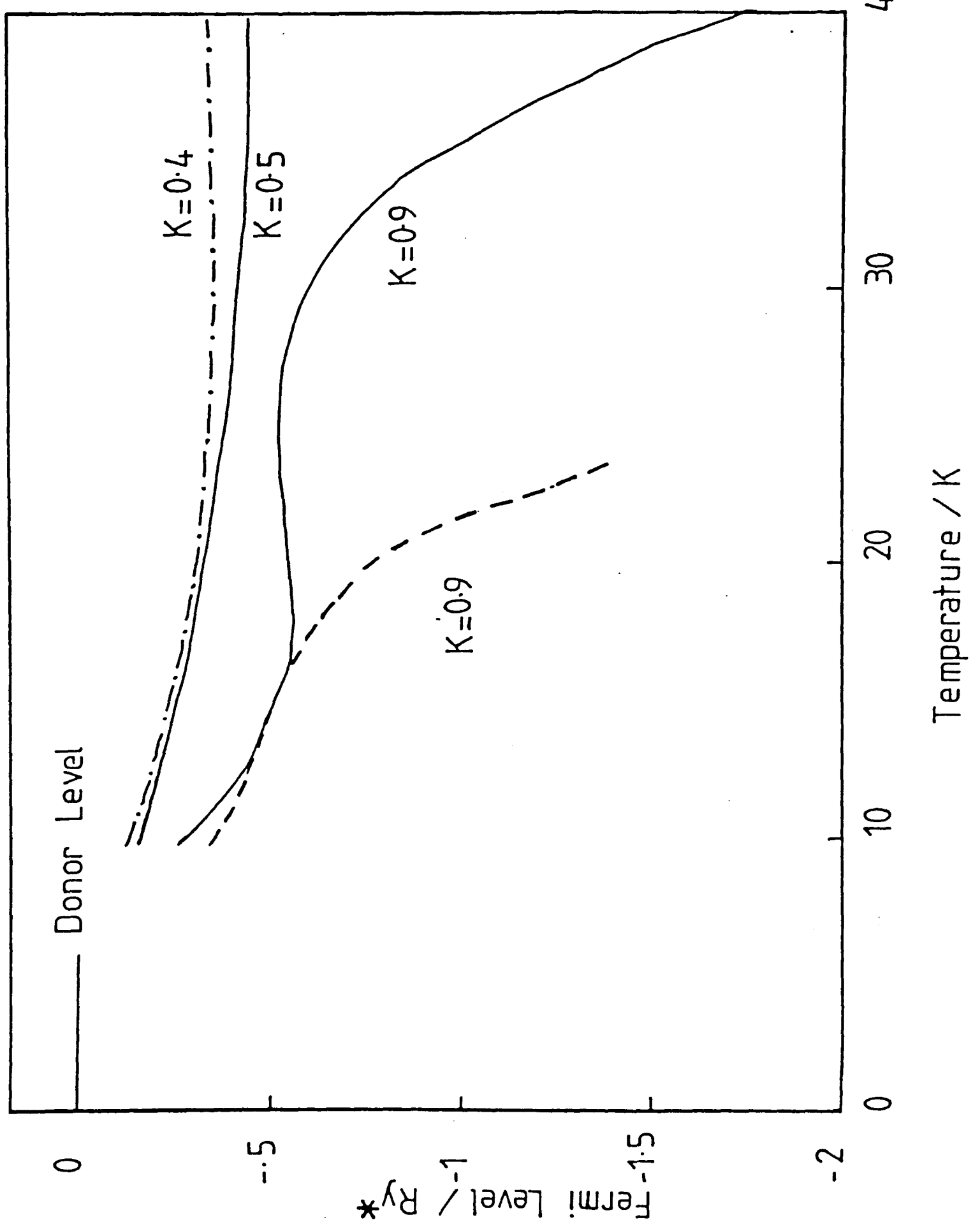


Figure 3·7

Temperature dependence of the Fermi level, obtained experimentally, for samples with estimated compensation ratios of K = 0·4, 0·5, 0·9 and 0·9.

3·5 Analysis

The Hall mobility μ_H, which is equal to $(R_H\ \sigma)$, is anomalously activated for all five samples. The values of μ_H are ~ 800 $cm^2\ V^{-1}\ s^{-1}$ at 10K, the temperature just above the start of hopping conduction. This is approximately 50 times smaller than the value at 77K. In complete contrast to this behaviour, the scattering time for a.c. conduction as observed in the cyclotron resonance linewidth increases by a factor ~ 2 for the same drop in temperature. This suggests that the scattering time $\tau_{d.c.}$ involved in d.c. conduction is unlikely to decrease greatly as the sample is cooled over the same range of temperature. Thus, the activated behaviour of the Hall mobility must be due to causes other than the temperature dependence of $\tau_{d.c.}$.

There are two alternative ways of treating the question of the activated Hall mobility, whose differences in the end reduce to differences in the definitions involved. In this work, we have chosen to define the d.c. conductivity mobility $\mu_{d.c.}$ as proportional to $\tau_{d.c.}$ in the usual manner. From the above discussion $\mu_{d.c.}$ should therefore be only weakly dependent on the temperature T. It is difficult to calculate this weak temperature dependence because simple scattering theories use densities of states varying as $E^{\frac{1}{2}}$, which is appropriate to free electron-like behaviour. In these samples however, the impurity broadening of the conduction band, as characterised by the parameter γ, is large compared with kT. The $E^{\frac{1}{2}}$ density of states is thus inapplicable. In the following discussion, it is assumed for simplicity that the d.c. mobility is approximately independent of temperature in comparison with the exponential temperature dependence of n. Hence, the activation energy of the resistivity can be equated with that of the concentration of electrons involved in d.c. conduction, i.e. it is assumed that $\rho(T) \propto \left(n(T)\right)^{-1}$. The values of the

activation energy $(E_c)_{RE}$ shown in table 3·2 were calculated with this assumption. This gives $(E_c)_{RE} > (E_c)_{Hall}$ for all five samples studied. Since the Hall mobility is given by

$$\mu_H = \frac{|R_H|}{\rho} = \frac{(n_{Hall}\, e)^{-1}}{(n_{RE}\, e\, \mu_{d.c.})^{-1}}$$

$$= \mu_{d.c.} \times \frac{n_{RE}}{n_{Hall}}$$

$$\simeq \mu_{d.c.} \times \frac{\exp\left(\frac{-[(E_c)_{RE} - E_F]}{kT}\right)}{\exp\left(\frac{-[(E_c)_{Hall} - E_F]}{kT}\right)} . \qquad (3\cdot23)$$

Thus, $\mu_H(T)$ is approximately proportional to

$$\exp\left(\frac{(E_c)_{Hall} - (E_c)_{RE}}{kT}\right),$$

and its activated behaviour is therefore due to $(E_c)_{Hall}$ being smaller than $(E_c)_{RE}$. The conclusion is that the threshold level for resistivity is <u>higher</u> in energy than the threshold level for the Hall effect, the difference between them being given approximately by $(E_c)_{RE} - (E_c)_{Hall}$.

The second, alternative approach to the problem of the activated Hall mobility is to define the concentration of electrons taking part in the d.c. conduction as $n'_{RE} \equiv n_{Hall}$. (The prime distinguishes quantities defined in this approach from those used in the rest of this work.) Thus $\mu_{Hall}(T) = r\mu'_{d.c.}(T)$ where r is the Hall ratio which is approximately temperature-independent, and $\mu'_{d.c.}$ is therefore activated following μ_H. This can occur if the mobility of the n'_{RE} electrons is a strong function of the electron's energy. $\mu'_{d.c.}$ is then the average over energy of the mobility, $\mu'_{d.c.}(T) = \int \mu'_{d.c.}(E) f(E,T) dE$. If $\mu'_{d.c.}(E)$ decreases rapidly with E, then $\mu'_{d.c.}(T)$ decreases rapidly with

temperature for activated conduction. The previous approach is equivalent to assuming a step function for $\mu'_{d.c.}(E)$

$$\mu'_{d.c.}(E) = \mu_{d.c.} \quad , \quad E \geq (E_c)_{RE}$$
$$\mu'_{d.c.}(E) = 0 \quad , \quad E < (E_c)_{RE} \qquad (3\cdot24)$$

To sum up, the difference between the two approaches is that the first defines the concentration of the electrons involved in d.c. conduction as those with a large (macroscopic) mobility, $\mu_{d.c.}$, which varies weakly with temperature. On the other hand, the second approach includes all electrons which are involved in the Hall effect, whatever their mobility, so that their <u>effective</u> mobility, $\mu'_{d.c.}$, is thermally activated. It is shown below that the explanation which fits all the observed data results in $\mu'_{d.c.}(E)$ being close to the step function given in (3·24), so that the two approaches are nearly equivalent. At the same time the explanation accounts for the existence of states capable of showing the Hall effect which yet do not contribute to d.c. conduction, which is in apparent contradiction with simple transport theories. These states are called Hall states hereafter for brevity. It is the first set of definitions which is chosen here as it is thought that this gives a more physical picture. Furthermore, this approach enables one to examine the possibility that the Hall states are not part of the conduction band.

Table 3·2 shows that within the experimental errors, the activation energies of the cyclotron resonance $(E_c)_{CR}$ at both 337 μm and 172 μm are the same as for the Hall effect. Thus the Hall states are the same, within the experimental errors, as the threshold states for the cyclotron resonance of <u>free</u> electrons. There are several candidates for the Hall states.

(i) D^- or D_n^- bands

D^- level electrons have been identified in many works (e.g. Narita and Kobayashi 1980, Larsen 1979, Norton 1976, Narita et al. 1982, Ichiguchi et al. 1983, Armistead et al. 1984). The work of Narita and Kobayashi (1980) on Sb-doped Germanium is of particular interest here. The samples studied were more highly doped than those used here, so that they studied conduction in impurity bands rather than thermally activated conduction in the conduction band as in this work. By comparing with Fritzsche's results (Fritzsche 1958, 1978) which show the same sort of discrepancy between the two transport processes as found here (but for impurity band conduction) Narita and Kobayashi assigned the lower edge of the D^- band to the Hall process.

In the present work on Indium Phosphide, calculations based on the effective mass approximations would give the binding energy of a D^- electron as 3·1K (= 0·27 meV). This is too small to account for the difference between $(E_c)_{Hall}$ and the effective Rydberg, which varies between 38K (3·27 meV) and 47K (4·05 meV). Therefore the Hall states cannot be identified with the D^- band in this work.

Electronic states of clusters of n-donors, for example the D_n^- level formed from the D^- levels of n donors, have negligible probability of existing in these samples. Bhatt and Rice (1980) show that for fractional donor concentrations smaller than 10^{-4}, isolated donor features dominate. The most highly doped sample used here gives a value for c of only 10^{-7}.

(ii) 2p band

An impurity band formed from donor 2p levels can exist at the impurity concentration of the samples studied here. In addition, the energy level of the 2p band of 67K (Chamberlain et al. 1971) above the 1s level, although still larger than the value of $(E_c)_{Hall}$ obtained, is

much closer than the D^- level would be. However, if the Hall states were 2p states, they would not be able to take part in the cyclotron resonance (although the levels $2p^+$ and $2p^-$ are separated by $\hbar\omega_c$ in magnetic field, the transition between these levels is forbidden). The identification of the Hall states leads one to choose instead the third possibility.

(iii) Edge states of the broadened conduction band

Impurities in semiconductors are irregularly distributed and this may affect the properties of the semiconductors in some cases. This may arise simply from statistical fluctuations due to the distribution being random. On the other hand, it has been suggested that clusters of impurities are likely to be formed during the growth process of the crystal. Weisberg (1962) observed that compound semiconductors of groups III-V and II-VI are more likely to form impurity clusters than elemental semiconductors because the former's constituent elements form a wide range of compounds with other elements. They can also act as solid solutions for clusters of other elements. Lastly, local deviations from the stoichiometry are more likely to occur due to compositional fluctuations during growth. Dakhno et al. (1979) explained their measurements on n - InP in the temperature range of 78K - 300K as due to the presence of clusters of acceptors which act as large insulating inclusions. Their samples were prepared by the zone-melting method, however, so that their results are not expected to be directly applicable to the MBE-grown samples used in this work.

Whether due to randomness or clustering, the non-uniform distribution of the impurities leads to inhomogeneity in the crystal. In the following, four types of semi-classical calculations are briefly reviewed. These work out the effect of the inhomogeneities on the transport properties of semiconductors, and are usually called

effective medium calculations. A comparison is then made between their predictions and the results obtained here. Finally, developments of one of the models are presented which are suggested by the sum of all the observations of the present study on n - InP.

(a) Impurity scattering

Weisberg (1962) treated the inhomogeneities simply as large scatterers of the carriers. They are large because a space - charge region is formed around the actual inhomogeneity to provide electrical neutrality. To a first approximation, the carriers cannot penetrate into the space - charge regions but are scattered by them. The mobility μ_S which is due to this scattering is given by

$$\mu_S = e\,[N_S\,(2m^*kT)^{\frac{1}{2}}A]^{-1} \qquad (3\cdot25)$$

where N_S is the concentration of the space - charge regions, and A is the effective scattering area of the space - charge region.

For low carrier concentrations, A varies with temperature as $(T/n)^{1/3}$ where n is the carrier concentration, for both spherical and cylindrical space - charge regions. Thus, the temperature dependence of μ_S is

$$\mu_S \sim n^{1/3}\,T^{-5/6} \qquad (3\cdot26)$$

(b) Inclusions with sharp boundaries

This model, like the two following, is a version of the effective medium approximation. In this model, the inhomogeneities are treated as inclusions with abrupt boundaries. They have conductivity σ_1 which is much smaller than σ_0, the conductivity of the host material. These inclusions are assumed to occur randomly, with a volume probability of (1-C). The macroscopic transport properties of such a mixed material can be described by the properties of an effective medium with conductivity σ and Hall coefficient R_H. Cohen and Jortner (1973)

calculated, for the general case of variable $x = \sigma_1/\sigma_0$ and variable $y = \mu_1/\mu_0$ where the μ's are Hall mobilities, that

$$R_H = h(R_H)_0 \qquad (3\cdot27)$$

$$\sigma = f\,\sigma_0 \qquad (3\cdot28)$$

where

$$fh = f^{-1}\left[1 - \frac{(2f+1)^2\,(1-C)\,(1-xy)}{(2f+1)^2\,(1-C) + (2f+x)^2 C}\right] \qquad (3\cdot29)$$

These results agree with earlier works by Juretschke et al. (1956), which examined the case of $x = 0$ only, in the limit of $(1-C) \ll 1$.

(c) Continuously variable fluctuations

Herring (1960) treated the case of weak, continuously variable fluctuations in the electrical properties of the material. His formulae are subsequently shown to be a good approximation also for most cases of large fluctuations. The results of greatest relevance to this work are that the low field Hall coefficient and the d.c. conductivity are reduced by the same factor. For both R_H and σ, the only effect of the fluctuations is in substituting $\langle n \rangle$ for n, if the fluctuations are in carrier concentration n but not in mobility.

(d) Broadening of the impurity band and of the conduction band edge

In all the three models above, whenever the screening of the inhomogeneities is explicitly mentioned it is the Debye screening which is used (Gossick 1959, Weisberg 1962, Dakhno 1979). Shklovskii and Efros (1971, 1980, 1984) considered the case of weakly doped samples with large compensation ratios $(1-K \ll 1)$, for which the Debye screening is not effective at low temperatures where the concentration of free carriers is very small. Instead, the screening is due to the redistribution of the electrons over the donors. The assumption of weak doping is appropriate in this study, since the samples' doping

gives $N_{imp}a^{*3} \sim 10^{-2}-10^{-3}$, where N_{imp} is the total impurity concentration, and a^* is the effective radius, $a^* = 86\text{Å}$ for InP. The criterion of weak doping ensures that in the interaction between the impurities only classical effects are important. This interaction can be regarded as the sum (Shklovskii and Efros 1984) of short range interactions between nearest-neighbour impurities, and of long-range interactions with the rest of the impurities. Both these types of interactions lead to a lowering of the Fermi level from the level appropriate to the single donor, e.g. in the case of large compensation, at T = 0 the Fermi level is below the isolated donor level because some electrons have been transferred to the acceptors. In addition, the long-range interactions lead to long-range fluctuations in the potential, which produce a classical shift in the energy levels. The crystal may be thought of as a collection of domains which are macroscopic in the sense that each contains many impurity complexes. Electrons within each domain have energy levels which are shifted by a constant amount $-e\phi(\underline{r})$, where $\underline{r}$ specifies any point in the domain. The long-range spatial fluctuations in the impurity levels are duplicated by the bottom of the conduction band, because the donor level E_D is still unchanged. Therefore, one effect of the inhomogeneous distribution of the impurities is the smearing of the impurity levels and of the bottom of the conduction band, i.e. it gives rise to the broadening of the conduction band tail evident in the temperature dependence of the cyclotron resonance linewidth.

For this model to be valid, an important parameter is the spatial extent of the domains. This needs to be macroscopic in two senses. Firstly, for electrons confined in a domain of low potential energy - a 'well' - the separation of the quantised levels arising from the confinement must be negligible with respect to the well's depth. Secondly, the wells must be sufficiently separated so that no strong

tunnelling occurs between the wells, and electrons are not able classically to jump over the wells' barriers. In the samples studied, the average distance between impurities is ~ 600 Å. Hence, the extent of the domains and the wells' separation are $\gtrsim 10^3$ Å and satisfy easily the conditions to be isolated and classical.

Shklovskii and Efros (1971) used the fact that the electrons would distribute themselves amongst the donors to minimise their potential energy to calculate the broadening of the impurity band. They found that this is of order μ_o where μ_o is given by

$$\mu_o = \frac{e^2}{\varepsilon} \frac{N_D^{2/3}}{n_t^{1/3}} \qquad (3\cdot30)$$

where n_t is the concentration of excess electrons, $n_t = N_D + N_A$.

Furthermore, since the bottom of the conduction band duplicates the large-scale fluctuations of the impurity level, there exists a threshold level <u>above</u> the bottom of the broadened conduction band which corresponds to the percolation level. At this level ε_p, there is a continuous path across the sample whose potential energy at each point is smaller than ε_p. In analogy with the problem of flow of a liquid through a random labyrinth this threshold level is

$$\varepsilon_p = \beta \mu_o , \qquad (3\cdot31)$$

measuring from the bottom of the original conduction band. Shklovskii and Efros predicted that β is probably negative, and should be constant for all cases for which the model is valid.

(e) <u>Comparison of the models with experimental results</u>

From the temperature dependence of the cyclotron resonance linewidth, a significant broadening of the bottom of the conduction band has been deduced. Therefore, the following analysis is based on

the model proposed by Shklovskii and Efros (1971), which can explain such broadening. This work is referred to as SE hereafter.

It has been proposed previously in this work that the Hall states are different from the states contributing to the conductivity, based on the argument that if they were the same states then this would lead to an improbable temperature dependence of the d.c. mobility $\mu_{d.c.}$. As a further justification for this proposal, the first three models of inhomogeneous media are examined to determine whether they would give rise to such an experimental dependence of $\mu_{d.c.}$. This is done before developments of the model of SE are proposed.

The impurity scattering model predicts $\mu_S(T)$ as given by equation (3·26). Using values of n(T) which were calculated from the cyclotron resonance absorption, the most direct of the methods of measurements used here, μ_S (77K) is calculated to be $4x\mu_S$ (10K). Therefore, this model cannot explain the reduction by 50 of the value of (R_H σ) between 77K and 10K which was measured.

The inclusion model predicts (equations (3·27) - (3·29)) that the original values of R_H and σ are changed. The ratios by which these values are altered differ from each other, and depend on the fractional volume of the inclusions, (1-C). This is temperature-dependent because of the temperature dependence of the space-charge region. However, (1-C) cannot be calculated for the present samples because even at intermediate temperatures the low electron concentration means that the Debye screening is ineffective. (A quick calculation would give (1-C) >> 1, which does not make sense.) Thus, a comparison cannot be made in this case.

The variable-fluctuations model (which does not take broadening into account) predicts that R_H and ρ vary in a similar way, so that the inhomogeneities have no special effect on the Hall mobility, which

ought therefore to vary as $T^{3/2}$ when impurity scattering dominates. Thus, this model cannot explain the observed temperature dependence.

In summary, previous works on inhomogeneous media based on Debye screening do not explain the present observed temperature dependences of the transport properties, especially when the Hall mobility is compared with the observed a.c. value.

The model which is based on broadening of the impurity and conduction bands suggests that a threshold energy ε_p exists above the bottom of the (broadened) conduction band, similar to a percolation threshold. We propose that this is the threshold for the Hall effect, $(E_c)_{Hall}$. The mobility of this level would be small. It is only at an energy significantly higher than this, which must be above the majority of the potential wells of the sample, that the electrons' mobility is unaffected by the presence of the inhomogeneities, and equals that defined by the local d.c. scattering rate, $\mu_{d.c.}$. This higher level corresponds to the d.c. conduction threshold $(E_c)_{RE}$. On the other hand, cyclotron motion should be possible for an electron classically confined to a potential well because the domains are of macroscopic extent. Therefore, cyclotron resonance, which is a local transition, should be possible in states at or slightly below $(E_c)_{Hall}$. Thus, one would expect $(E_c)_{CR} \leq (E_c)_{Hall}$, as was observed. The difference between $(E_c)_{Hall}$ and $(E_c)_{RE}$ can be expressed algebraically in the following manner.

The Hall coefficient R_H is defined for a magnetic field B in the z-direction and current j_x passing in the x-direction as

$$R_H = E_y / (j_x B) \qquad (3\cdot32)$$

The actual quantities measured are B, V_y, and I_x so that in practice the value of R_H for a long thin bar is taken as

$$R_H = \frac{1}{B} \times \frac{V_y}{I_x} \times t \qquad (3\cdot33)$$

where t is the sample thickness.

Similarly, the resistivity ρ is

$$\rho = \frac{V_x}{I_x} \times \frac{tw}{\ell} \qquad (3\cdot34)$$

where ℓ and w are the length and width of the sample.

The quantities measured are V_y/I_x and V_x/I_x. If the width of the sample, w, is reduced, the former ratio is not affected but the latter, which is the resistance of the sample, is increased. This reduction in the width can effectively occur if the conduction band electrons are localised in certain regions of the sample by the macroscopic fluctuations in the impurity potential. Therefore, the effective width of the (conducting) sample is reduced from the value of the physical width for electrons in the low-energy edge states, which are localised by these fluctuations. Since measurements of the Hall effect are independent of the width (equation (3·33)), these edge states should show the Hall effect as normal.

Physically, this occurs because the Hall voltage is essentially independent of the microscopic current distribution, at least in a planar geometry, for which we may write

$$\begin{aligned} V_y &= B\, R_H \int j_x \, dy \\ &= B\, R_H\, I_x \end{aligned} \qquad (3\cdot35)$$

In contrast, the resistivity depends very strongly upon the current distribution, tending to infinity if the current is confined to a narrow strip. The insulating regions need only maintain a constant potential in order to communicate the Hall field from one side of the

sample to the other, whereas in order for conduction to occur there must be a nett transfer of charge. In three dimensions, the exact results depend upon the geometry and proportion of the inhomogeneous regions, as has been calculated by Wolfe and Stillman (1971), although the same general conclusions are reached.

This train of reasoning is essentially the same as the phenomenological explanation of the quantum Hall effect in 2-D systems (Tsui and Allen 1981, see also section 4·3), which is based on the idea that localised states in Landau level tails do not affect the Hall voltage. Electrons occupying these states are localised in certain regions of the sample. These regions can be represented by holes in the sample across which the Hall voltage can still be established, while the conducting regions carry extra current lines to offset the effect of the 'holes'. Thus, in both 3-D and 2-D systems, the effective width, w_{eff}, of the sample is reduced from its actual width, w. However, as equation (3·33) shows, this does not affect the value of R_H.

In summary, if the Hall states are identified with the edge states of the conduction band, the similarity between the activation energies for the cyclotron resonance and the Hall effect is explained at the same time as the much larger activation energy for resistivity. This explanation is also borne out quantitatively, allowing for the simplicity of the theory as follows. In all five samples examined, $(E_c)_{cr}$ and $(E_c)_{Hall}$ are ~ 40K, while γ, the broadening parameter calculated from the temperature dependence of the C.R. linewidth, is ~ 40K. Thus

$$(E_c)_{CR} \approx (E_c)_{Hall} \approx Ry^* - \gamma \qquad (3·36)$$

where Ry^*, the effective Rydberg for Indium Phosphide is 83K.

Since the unbroadened conduction band edge is at 1 Ry^* above the donor level and γ is approximately the amount by which the conduction

band edge is lowered by the broadening (Dyakonov et al. 1969), equation (3·36) confirms that the identification of the Hall states with the states in the tail of the broadened conduction band is reasonable. The parameter γ is also, by definition, the average of the variation of the impurity potential (Nicholas and Sarkar 1982, Dyakonov et al. 1969). Therefore, γ is also the average depth of the 'pockets' caused by the variation. Since the d.c. conduction threshold occurs at a level higher than the majority of the potential wells, and should therefore be near to the unbroadened band edge, this should be some constant multiple of γ above the percolation threshold identified as $(E_c)_{Hall}$. Choosing $\frac{1}{2}$ arbitrarily as this multiple, so that

$$(E_c)_{RE} - (E_c)_{Hall} \sim \gamma/2 \qquad (3\cdot37)$$

this seems to be in fair agreement with the measured values of the two activation energies, as shown in table 3·2.

Comparing (3·36) with the SE model, and noting that the μ_o of SE plays the same role as γ in the present work, it is seen that β in equation (3·31) is here set to -1 by equation (3·36). The negative value of β (showing that the threshold level is below the unbroadened band) and the fact that it is roughly constant for all the samples studied agree with the predictions made by SE. Thus, based on a similar model to SE, this work has predicted the behaviour of the Hall effect and cyclotron resonance, and the expanded theory is found to explain all the results obtained.

3·6 Conclusion

In conclusion, this work shows that the differences between measurements of thermally activated d.c. conductivity and Hall effect are due to the different way localisation at the bottom of the broadened conduction band affects these properties, and that with regard to showing the presence of electrons in the conduction band, the Hall effect gives the truer picture. The explanation given is similar to the way localisation in 2-D systems is used to explain the existence of Hall plateau where conductivity goes to zero. It is also an expansion of the theory of effective media for 3-D. This predicts that the Hall coefficient and resistivity values would be changed by different amounts by such a reduction in the effective width of the sample due to impurity scattering. In this work, the experimental results show that different states are involved in the two effects, leading to differing activation energies.

This work also shows the importance of taking into account the variation of the Fermi level with temperature, particularly for compensated materials. When the correction for this variation is omitted, low temperature measurements, for example, would give activation energy values which differ from the true values by as much as 25%.

CHAPTER 4

An introduction to the two-dimensional electron gas

4·1 Introduction

This part of the thesis presents the measurements of the temperature and magnetic field dependence of the thermopower for several types of heterojunctions and for a superlattice. The measurements are, in the first place, concerned with the two-dimensional electron gas (2DEG is the usual acronym) present in these systems. This chapter aims to give a simple theoretical description of the 2DEG. In sections 4·2 and 4·3 the band structure of the 2DEG without and with magnetic field is described. This first section aims only to give an extended introduction to the terminology subsequently used, rather than to give a survey of the large amount of work on heterostructures. Chapter 5 presents the experimental results of the thermopower measurements and chapter 6 compares these with present theories and the experimental work of other authors.

In recent years, advances in the growth technique of semiconductors have made possible the production of high mobility electron systems which are confined to two or even one dimension. The properties of such artificial systems may be greatly varied by controlling the factors which give rise to the reduction in their dimensionality, as well as the more usual factors such as impurity doping. This controlled variability makes low dimensional systems of great interest, both in their application and in the study of their physics. The first of these systems to be studied, and then utilised was the Metal - Oxide - Semiconductor (M.O.S.) structure consisting of the semiconductor silicon and the oxide silicon dioxide. Large concentrations of surface charges can be induced at the oxide - semiconductor interface by the application of an electric field across the M.O.S. structure, and these carriers approximate closely to a two-dimensional electron or hole gas. There is a recent review paper

which concentrates on this system, by Ando, Fowler and Stern (1982). The second type of structure which may give rise to 2DEG systems is the semiconductor heterostructure. This consists of several layers of different crystalline semiconductors grown epitaxially, so that the crystalline structure is preserved across the interface and the number of interface trap states is kept low. The semiconductors in the heterostructure have different values of the band gap E_G and of the electron affinity χ, so that the conduction and valence band edges have sharp discontinuities at the interface. Figure 4·1 shows the two types of heterostructure for the simple combination of a thin layer of semiconductor A grown between two layers of semiconductor B.

This work is concerned only with type I heterostructures, for which the conduction band minimum and valence band maximum lie in the same semiconductor. Furthermore, only systems which are n-doped in a way which produces a 2DEG were studied. Therefore, the following discussion is limited to electrons in type I heterostructure.

Referring to figure 4·1(a), electrons initially in the conduction band of semiconductor B would transfer to the conduction band of A which is lower in energy. The growth techniques such as Molecular Beam Epitaxy (MBE) and Metal Organic Chemical Vapour Deposition (MOCVD) can produce layers of A thin enough so that electrons confined in A by the sandwich structure shown in figure 4·1(a) exhibit 2-D motion and form a 2DEG. Furthermore, the donor level in B is usually higher than the conduction band of semiconductor A, so that if B is strongly doped n-type, the donors' electrons will transfer to A and give rise to a large concentration of electrons in A. The importance of this is that these electrons are spatially separated from the large number of ionised donors which provide them, so that ionised impurity scattering which normally dominates at low temperatures is considerably reduced. In addition, the large value of the electron concentration in A

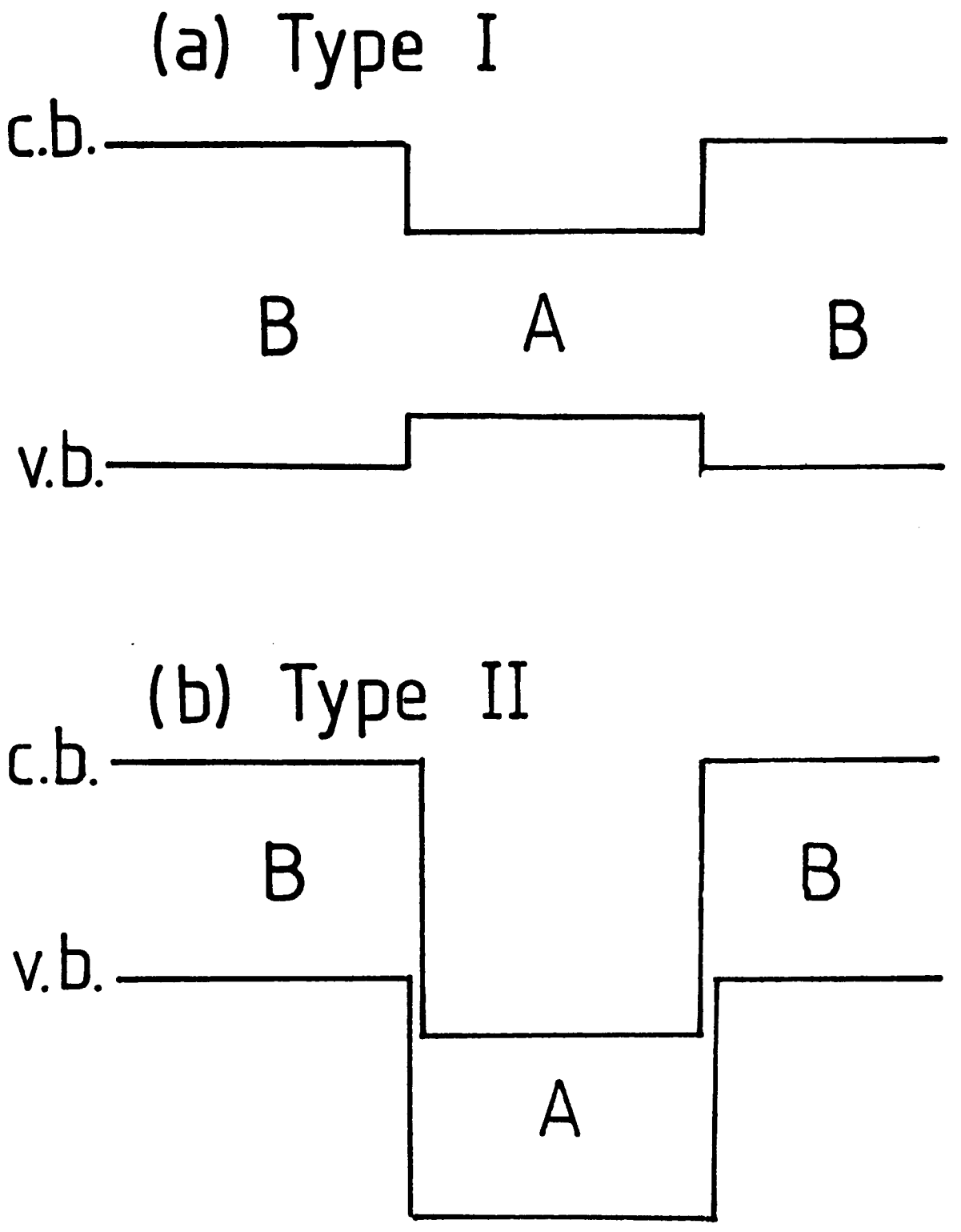


Figure 4·1

Schematic representation of the band structure of a quantum well of

(a) type I and

(b) type II.

enhances their mobility because this enhances the screening of the ionised impurity potential, as well as reducing the phase-space available for scattering by a given wavevector $\underline{q}$. This doping technique is called modulation doping and represents a major advance in the growth of the heterostructures. A mobility of $2{\cdot}1 \times 10^6$ cm^2 V^{-1} s^{-1} have been observed with MBE growth (Hiyamiza et al. 1983) and of $1{\cdot}6 \times 10^5$ cm^2 V^{-1} s^{-1} with MOCVD growth (Hersee et al. 1982) for GaAs - $Ga_{.7}Al_{.3}As$. For these high mobility samples, a so-called spacer layer of the high conduction band material (GaAlAs in this case), which is nominally undoped, is grown at the interface between the doped GaAlAs and the undoped GaAs. This provides a further spatial separation between the 2DEG and their ionised impurities. There is, however, an optimum value for the thickness of the spacer layer as a thick layer decreases the carrier density. This is 50 - 200 Å depending on temperature and carrier concentration (Delescluse et al. 1981, Drummond et al. 1981, Ando 1982b) for GaAs - GaAlAs. One important effect of the transfer of large numbers of carriers in a modulation-doped structure is the resultant large bending of the bands of both semiconductors due to the potential of the excess charges on both sides (ionised donors on one side and free electron gas on the other). Figure 4·2 shows the case for a single junction between two n-doped semiconductors. This represents the situation for many samples studied in this work. The semiconductor with the higher energy conduction band is heavily doped n$^+$-type, while the semiconductor with the low-lying conduction band has residual impurities which make it n-type also. This band bending is present whenever there is charge transfer but modulation doping exaggerates the effect.

Figure 4·2 can be taken either as the detailed diagram of the edge of the quantum well structure shown in figure 4·1(a), or as the whole

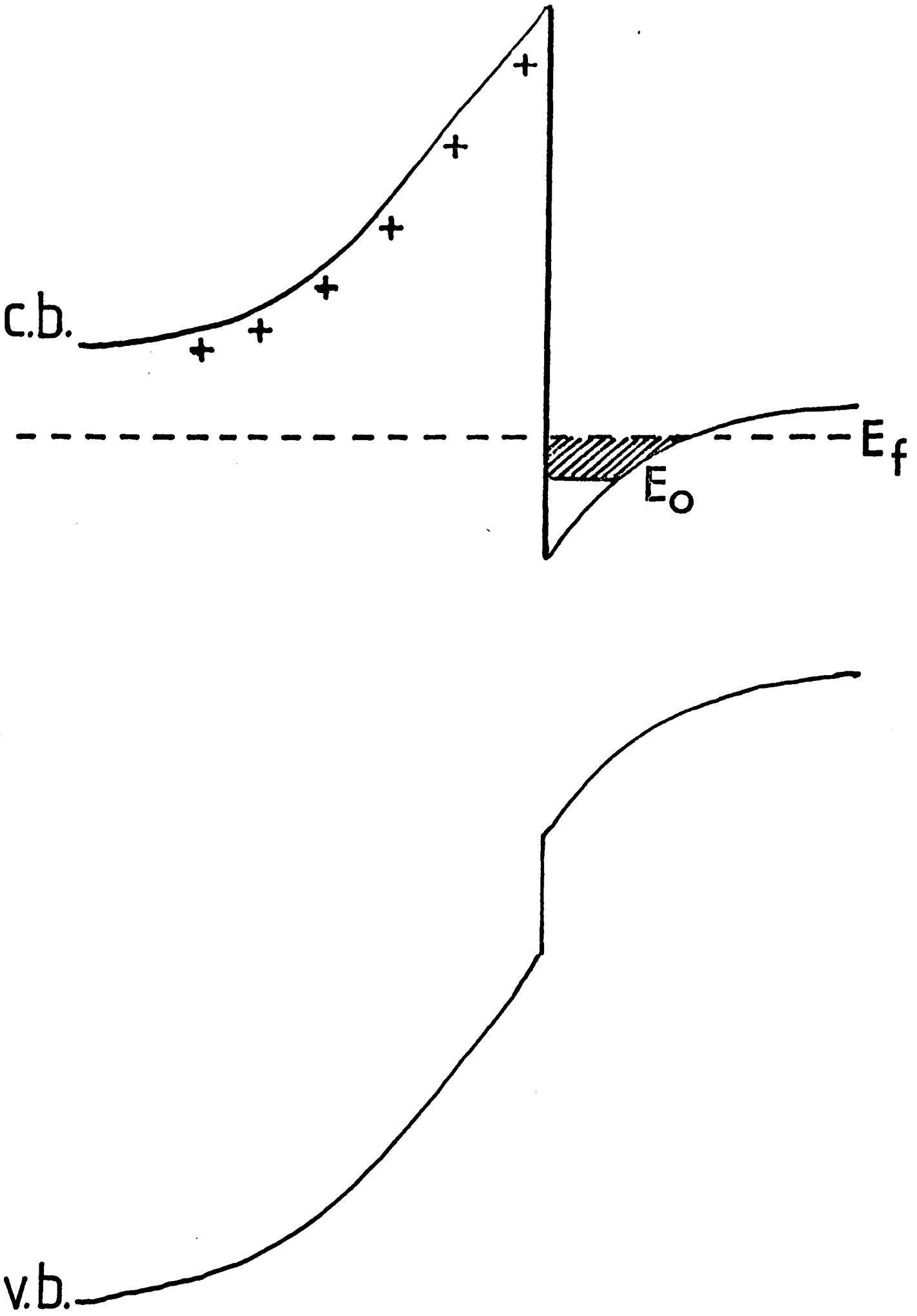


Figure 4·2

Band bending in a type I heterojunction which is modulation doped. The shaded area represents the 2DEG.

diagram of a simple heterojunction. For a sufficiently large band bending, electrons are confined near to the interface between the semiconductors, and the heterojunction alone can provide a 2DEG system, rather than a quantum well structure.

The heterojunction and quantum well are the building blocks for other heterostructures. An example is a long series of alternating layers of two semiconductors. Strictly speaking, depending on whether or not the quantum wells are close enough for the confined electrons to interact, the structure is called a superlattice or a multiple quantum well (MQW). However, 'superlattice' is often used in both cases. In this study, sample MB44 is strictly speaking a MQW. The other samples for which the thermopower is measured are heterojunctions.

4·2 Subband levels of the heterojunction

Confinement of electrons in a heterojunction in the direction perpendicular to the interface, normally taken as the z-direction, gives rise to quantised energy levels E_i for the z-direction. The electrons are still free to move in the x-y plane, so motion in this plane gives rise to a continuum of energy levels. Each level E_i is therefore the bottom of a continuum of levels, called a subband. In order to calculate the energy values of the subbands, four equations need to be solved: the coupled Schrödinger and Poisson equations which give the relationship between E_i and n_i (n_i is the electron concentration in the i^{th} subband), and the electrical neutrality and constant chemical potential conditions which determine the relationship between the concentrations of ionised impurities and the n_i's. It is usual to assume that the penetration of the n_i electrons into the semiconductor with the higher conduction band, often referred to as the barrier side, is so small that it does not influence at least the energy of the lowest subband. With this assumption, the first two equations may be solved separately from the last two (Bastard 1983).

Of the many theoretical studies, the results of Stern's variational calculations (Stern 1972) are the most easily applicable because they give algebraic expressions for the values of the subband energy and of the average distance of the carriers from the interface. These equations have been used in many works on heterojunctions as a first approximation. However, Stern's calculations were applied to the 2DEG of silicon inversion layers, and important differences exist between this and the heterojunction system. There are two main differences. The first is that the conduction band discontinuity at the $Si-SiO_2$ interface is ~ 3 eV whereas for GaAs - $Ga_{.7}Al_{.3}As$ and $Ga_{.47}In_{.53}As$ - InP it is ~ 0·3 eV. Therefore, Stern's assumption that there is no

penetration of the subband carriers into the barrier side is valid for the former but not for the latter. Secondly, for modulation doped heterojunctions, the carrier concentration of the 2DEG is much larger than the concentration of the ionised (residual) impurities in the semiconductor with the lower conduction band, called the channel side. This is in contrast with the silicon inversion system, where the depletion charge is large in the silicon layer. As a consequence, it is often acceptable to ignore the channel side's fixed charges when applying Stern's expresssions to heterojunctions.

In the following, Stern's variational calculations are described as these will be used later on in this work. Reference will then be made to other theoretical works more appropriate to the heterojunctions studied.

In the effective mass approximation, the Schrödinger equation for the 2DEG is

$$[T - e\phi(z) - E]\ \psi = 0 \qquad (4\cdot1)$$

where T is the kinetic-energy operator, and for an isotropic effective mass m^* T has the simple form

$$T = \sum_i \frac{1}{2m^*} \left(-i\hbar \frac{\partial}{\partial x_i}\right)^2$$

and ϕ is the electrostatic potential. Since this is a function of z alone, ψ has the form

$$\psi\ (x,y,z) = \xi_i(z)\ \exp\ (ik_1x + ik_2y)$$

Putting this into equation (4·1) gives

$$E = E_i + \frac{\hbar^2(k_1^2 + k_2^2)}{2m^*}$$

where E_i and $\xi_i(z)$ satisfy equation

$$\frac{d^2\xi_i}{dz^2} + \frac{2m^*}{\hbar^2}\ [E_i + e\ \phi(z)]\ \xi_i(z) = 0 \qquad (4\cdot2)$$

Equation (4·2) is solved self-consistently with the Poisson's equation for $\phi(z)$

$$\frac{d^2\phi}{dz^2} = -\left[\rho_{depl}(z) - e \sum_i n_i \xi_i^2(z)\right] / \varepsilon\varepsilon_0 \qquad (4\cdot3)$$

where ε is the dielectric constant and ρ_{depl} is the charge density of the depletion layer for the channel layer.

When only the lowest subband is occupied, the variational approach is valid. Using the Fang-Howard trial eigenfunction

$$\xi_0(z) = \begin{cases} (\frac{1}{2}b^3)^{\frac{1}{2}} z\, e^{-bz/2} & z \geq 0 \\ 0 & \text{elsewhere} \end{cases}$$

and choosing b to minimize the total energy, Stern obtained the lowest subband energy E_0

$$E_0 = \left(\frac{3}{2}\right)^{5/3} \left(\frac{e^2\hbar}{m^{*\frac{1}{2}}\varepsilon\varepsilon_0}\right)^{2/3} \frac{N_{depl} + \frac{55}{96} n_0}{\left(N_{depl} + \frac{11}{32} n_0\right)^{1/3}} \qquad (4\cdot4)$$

where n_0 is the lowest subband electron density (which is equal to the total density by assumption) and N_{depl} is the areal density of depletion charge.

Bastard (1983, 1984) also used self-consistent variational calculations but included penetration of the electrons into the barrier side by using the envelope function

$$\chi_1(z) = \begin{cases} M_1 \exp(K_1 z/2) & z < 0 \\ N_1(z+z_0) \exp(-b_1 z/2) & z > 0 \end{cases} \qquad (4\cdot5)$$

This penetration couples the Schrödinger and Poisson equations to the condition of constant E_F via $\chi_1(z)$

$$E_F = E_0 + \frac{\pi\hbar^2 n_0}{m_c} = \Delta E_c - R_b - \frac{2\pi e^2}{\varepsilon_b} N_d \ell_d^2 - \frac{4\pi e^2}{\varepsilon_b} \int_{-\infty}^{0} z\, \chi_1^2(z)\, dz \qquad (4\cdot6)$$

where R_b is the effective Rydberg and ε_b the dielectric constant in the barrier side. Equation (4·6) needs to be solved together with the

condition of electrical neutrality

$$n_o + N_a \ell_a = N_d \ell_d, \tag{4.7}$$

where the ionised impurity concentrations have position dependence

$$N_d(z) = \begin{cases} N_d & -\ell_d < z < 0 \\ 0 & \text{elsewhere} \end{cases}$$

and

$$N_a(z) = \begin{cases} N_a & 0 < z < \ell_a \\ 0 & \text{elsewhere} \end{cases}$$

where ℓ_d and ℓ_a are the donor and acceptor depletion lengths.

Bastard's results show that by taking into account the finite value of ΔE_c, this leads only to a small probability density of penetration, e.g. ~ 1% for $n_s = 4 \times 10^{11}$ cm^{-2} and $\Delta E_c = 0{\cdot}3$ eV, whereas the effect on E_o is a large reduction of its value, by ~ 15% for the same parameters. His calculations were applied to the GaInAs - InP system, which is studied in this work, so that they are of relevance here. Bastard's results are also in good agreement with the more accurate numerical work of Ando (1982a), who presented results for the GaAs - $Ga_{.7}Al_{.3}As$ heterojunction.

4·3 Effect of a strong magnetic field

Since the Landau level spacing for practicable values of magnetic field is small compared with the subband spacing which arises from V(z), an approximate derivation of the Landau levels for the 2DEG may be simply obtained by using the same z-component of the eigenfunction as for the case of B = 0. Following the work of Stern and Howard (1967), the energy eigenvalues for the 2DEG in a strong magnetic field are

$$E(i,n) = E_i + (n+\tfrac{1}{2})\frac{\hbar e|B_z|}{m^*c} + \frac{1}{2m^*}\left((z^2)_{av} - (z_{av})^2\right)\left(B_x^2+B_y^2\right) \qquad (4\cdot8)$$

The first point of note in equation (4·8) is that the eigenvalues are discrete, and the density of states (D.O.S.) consists of a series of delta functions corresponding to the Landau levels for each subband. This is shown schematically in figure 4·3a. Thus, as the Fermi level is varied with respect to the Landau levels, either by changing the magnetic field or by varying the electron concentration, dramatic changes of the 2DEG's properties which depend on the D.O.S. are expected. An example is the sample's resistivity. Large Shubnikov de - Haas oscillations can be observed directly for the 2-D system, whereas in the bulk case the signal often needs to be differentiated for the oscillations to be accurately recorded.

The second point of note is that the Landau level spacing depends only on the z-component of the magnetic field. Indeed, one of the methods of verifying that a specimen does exhibit 2-D motion is to record the Shubnikov de - Haas oscillations as the angle θ between $\underline{B}$ and the perpendicular to the interface is varied. The oscillations ought to follow $|B|\cos\theta$ exactly.

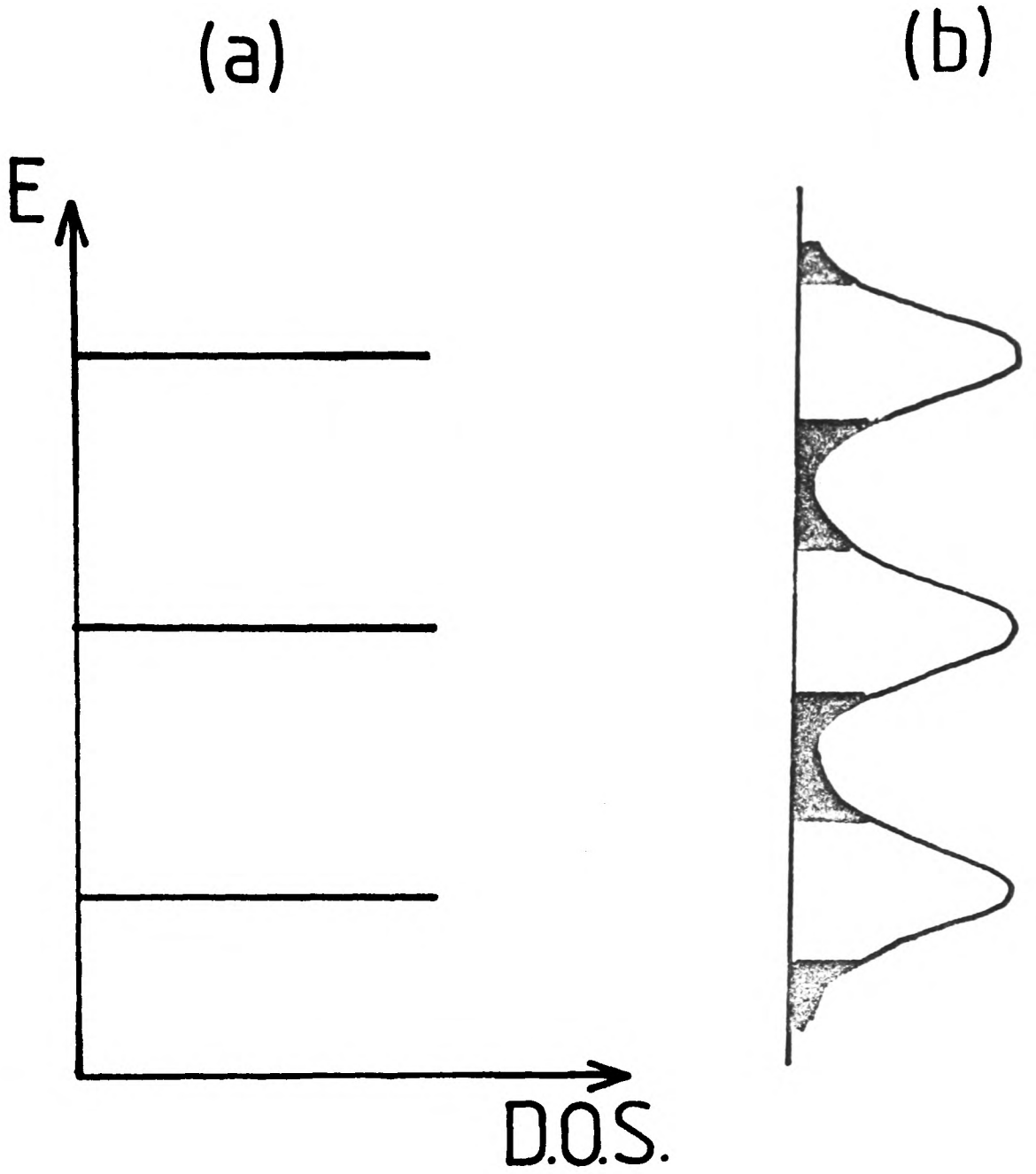


Figure 4•3

Landau levels of one subband for the case of

(a) no scattering and

(b) with broadening caused by scattering.

In deriving (4·8), the spin splitting has been ignored. This is a rather complex matter, with the spin g value taking large values in the 2DEG due to many-body effects (see, e.g., the review paper by Ando, Fowler and Stern 1982). The spin splitting can be distinguished from the Landau level spacing because the former depends on the magnitude of the total magnetic field, and not just the z-component. In fact, accurate measurements of the enhanced g-factor have been made by choosing θ so that the spin splitting is some exact fraction of the Landau level splitting. This so-called tilted field method was first employed by Fang and Stiles (1968) for measurements on n-type silicon. Nicholas et al. (1983) used the same method and obtained enhanced g-values of up to ~15 for a $Ga_{.47}In_{.53}As$ - $Al_{.48}In_{.52}As$ heterojunction, which is one of the systems studied here.

In practice, scattering will broaden the Landau level delta functions into a band of states, as shown in figure 4·3b. States in the tails of these Landau subbands, shaded in the diagram, are now agreed to be localised by the potential fluctuations (although they retain some short range correlation) for typical values of electron concentration in heterostructure and practicable temperatures. When the Fermi level E_F lies in the middle of one of the Landau subbands, the system acts as a good conductor. On the other hand, when E_F lies in the localised states' region, $\sigma_{xx} \to 0$ for $T \to 0$. In contrast, the Hall conductivity $\sigma_{xy} = ne/B = i\ e^2/h$ when E_F lies between Landau subbands i and (i+1). This remarkable quantisation of σ_{xy} was first observed by von Klitzing, Dorda and Pepper in 1980 in a Si MOSFET, and subsequently seen in heterostructures, where the exactness of the quantisation was verified to a high degree of accuracy (von Klitzing and Ebert 1984, and references therein). Some of the theories which explain the quantum Hall effect are referred to in a summary by Thouless (1984). There is also a simple argument proposed by Tsui and

Allen (1981) which is of interest here because it relates back to the argument used in this work on bulk InP in chapter 3. In their picture the localised states carry no current. When E_F lies in the localised range of the D.O.S., the localised (spatial) regions do not contribute to the Hall voltage but the conducting regions carry an extra current to offset this. In 2-D, this offset exactly balances out to give the quantised Hall resistances because the non-localised regions of the sample can be taken as perfect and filled with an integral number of Landau levels. Tsui and Allen's argument is explicitly based on effective medium calculations, modified for the reduced dimensionality.

To recapitulate, when E_F lies in the localised range of the D.O.S., $\sigma_{xx} \to 0$ for $T \to 0$ while σ_{xy} is a finite value which is an integral multiple of e^2/h. Since

$$\rho_{xx} = \frac{\sigma_{xx}}{\sigma_{xx}^2 + \sigma_{xy}^2} , \qquad (4\cdot9)$$

when E_F is in the localised range and $\sigma_{xx} \ll \sigma_{xy}$, then ρ_{xx} is

$$\rho_{xx} = \frac{\sigma_{xx}}{\sigma_{xy}^2} \qquad (4\cdot10)$$

$$\rho_{xx} \to 0 \qquad \text{as} \qquad T \to 0$$

At a finite temperature, variable range hopping will lead to a small, finite value for σ_{xx}, and hence ρ_{xx} which is proportional to σ_{xx} in this region (see, e.g., Ebert et al. 1983 and Tsui et al. 1982 for the GaAs - GaAlAs system, and Briggs et al. 1983 for the GaInAs - InP system). The finite value of ρ_{xx} due to this hopping conduction is very small, e.g., $\rho_{xx} \leq 5\times10^{-7}$ Ω/□ at 1·2K for the n = 1 minima. However, in many samples, the measured $(\rho_{xx})_{min}$ is much larger than this. Such a deviation is due to a small amount of conduction in the bulk

semiconductors forming the heterojunctions, which is enhanced by the Hall resistance. From (4·10)

$$\rho_{xx} \simeq \sigma_{xx} \rho_{xy}^2$$

$$\simeq \rho_{xy}^2 \left[(\sigma_{xx})_{bulk} t_{bulk} + (\sigma_{xx})_{2D}\right] \qquad (4\cdot11)$$

$$\simeq \rho_{xy}^2 (\sigma_{xx})_{bulk} t_{bulk}$$

The last approximation is valid when there is appreciable deviation of ρ_{xx} from zero. Equation (4·11) provides a quick and sensitive method of calculating $(\sigma_{xx})_{bulk}$, since the bulk contribution is multiplied by the relatively large Hall resistance ρ_{xy}.

CHAPTER 5

Thermopower measurements of heterostructures

5·1 Introduction

Recently, there has been a great deal of theoretical interest in the thermo-electric properties of the two-dimensional electron gas (Girvin and Jonson 1982, Jonson and Girvin 1984, Oji 1984a, b and c, Streda 1983 and 1984, Streda and Oji 1984, Ting et al. 1982, Zawadzki and Lassnig 1984, Zelenin et al. 1982). On the other hand, there are only to date three reports of experimental measurements in GaAs - GaAlAs heterojunctions (Obloh et al. 1984) and in silicon MOSFETs (Gibbings and Pepper 1985, Smith et al. 1984). This work reports measurements made on GaInAs - InP, GaInAs - InAlAs, and GaAs - GaAlAs heterojunctions (Nicholas et al. 1985) and a GaAs - GaAlAs superlattice, both with and without the application of a high magnetic field. The results show in almost all cases a clear disagreement with the established theory and other works reported on other 2DEG systems. Both the magnitude and the temperature dependence of the thermopower in the helium temperature range are significantly different. For this reason, descriptions of the experimental apparatus and procedure are given in some detail in this chapter in addition to the experimental results, so as to confirm the conclusions which are drawn. In the next chapter, comparison of the present results with the established theory and other experimental work is made, and suggested reasons for the disagreement are given.

5·2 Experimental apparatus

A special cryogenic insert, shown in figures 5·1 and 5·2, was used for the thermopower measurements. The aim of the design was to enable:

(a) the establishment of a well-defined thermal gradient,

(b) accurate measurements of the thermoelectric voltage V, typically a few μV's, and

(c) accurate measurements of the thermal difference induced, typically $0{\cdot}1\ K \leq \Delta T \leq 10\ K$ across the sample.

The design of the insert, and figures 5·1 and 5·2 are by M. A. Brummell.

A length of cotton-wrapped resistance wire acts as the heater. This insulated wire is wound around a thick copper post which is thermally insulated from the insert by a PTFE block. Heat is conducted to the sample by a thick wire which is silver painted to this copper post at one end, and to an edge of the sample at the other. The heater is thus isolated from the rest of the insert, and in particular from the sample. The heat sink is the large copper block which is also the main support of the insert. A short length of wire which is screwed to the block is silver painted to the other end of the sample. Apart from these defined thermal links, the sample is kept thermally isolated by both the PTFE sample mount and by the copper radiation shield beneath the mount which screens thermal radiation from the heater. The whole sample can is evacuated with a rotary pump to ~ 0·1 Torr so that there is no convection heating to the sample. By these means, a well-defined thermal gradient was achieved.

To measure the thermovoltage V, there are short contact wires which are soldered to the sample itself, usually by alloying in a blob of

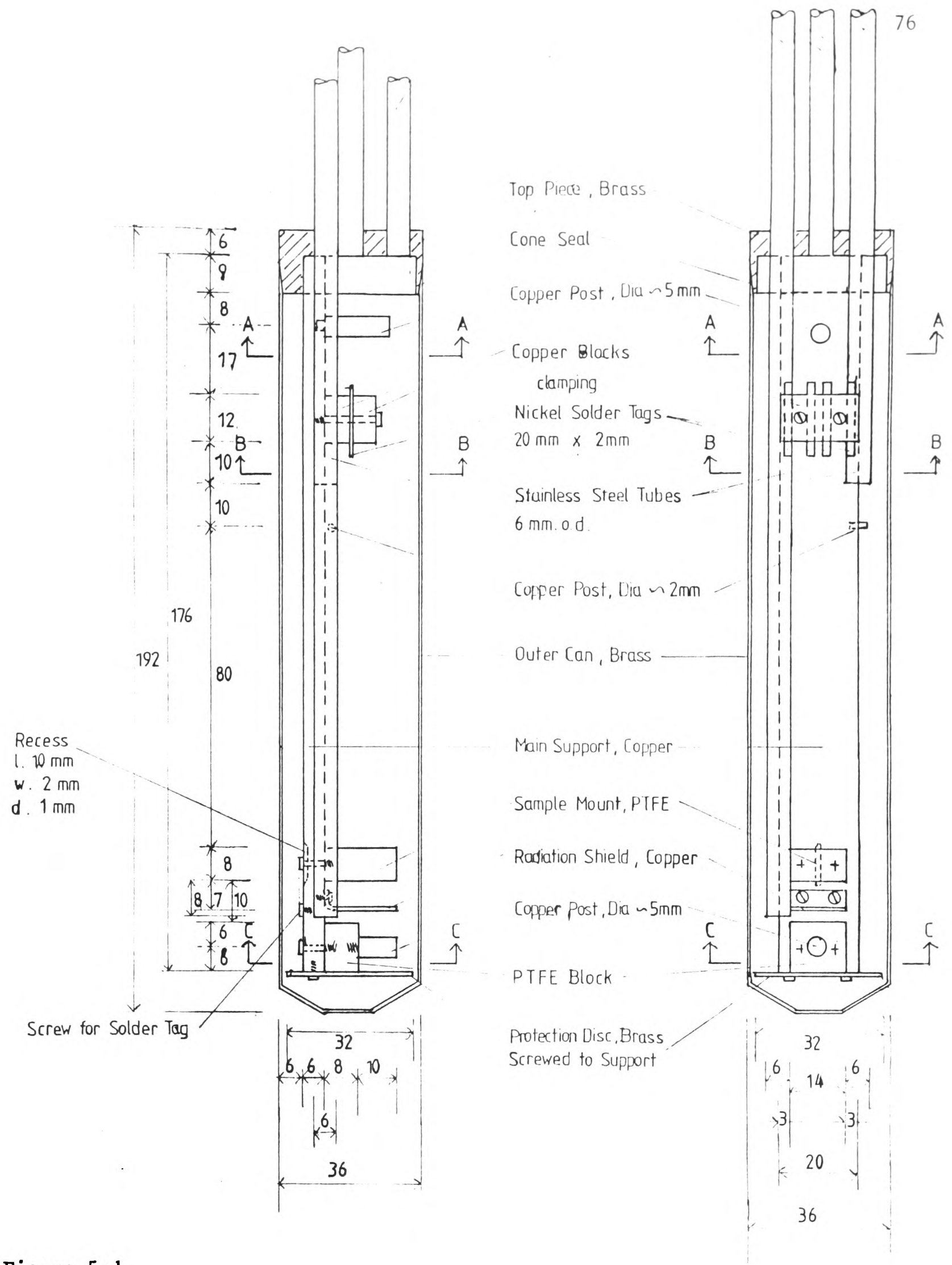


Figure 5·1

The main, lower part of the thermopower insert.

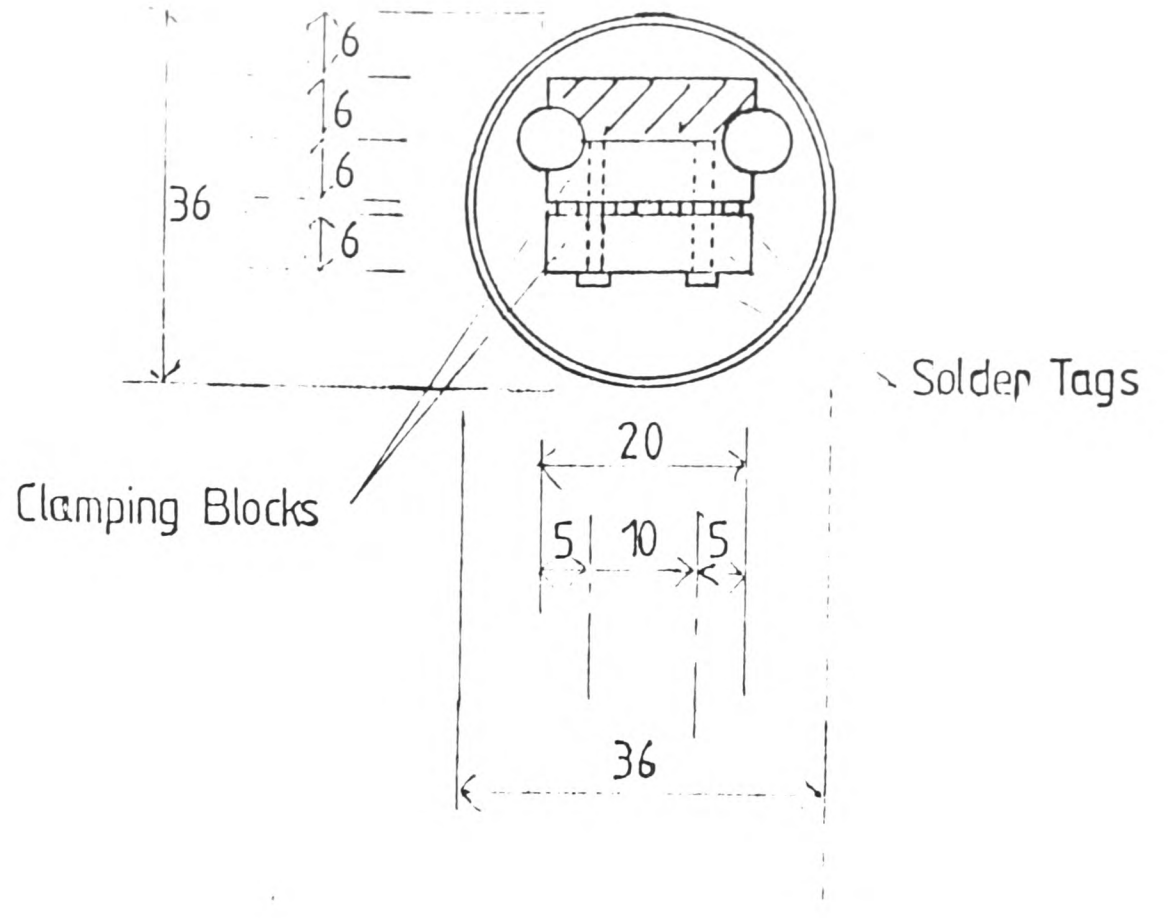


Figure 5·2

Top: section B-B of insert, showing the copper clamping blocks for the wires.

Bottom: section C-C of insert, showing sample mount and main support, which also acts as a heat bath for the cold end.

Indium solder (see figure 5·3). These are soldered at the other end (again by Indium solder) to long lengths of copper wire which are continuous along the whole insert. Continuous wires emerge out of the insert via vacuum seals. The purpose of this is to minimise the number of contacts across which spurious thermovoltages may be induced. These copper wires go through copper clamping blocks (figure 5·2, section B-B) before reaching the sample, so that they are at the bath temperature and do not provide extra heating from the outside. At the other end, the wires are screwed into copper blocks to make electrical contacts with the voltmeter leads, which end in copper slides. This ensures that there is no thermovoltage at the final contacts.

The temperature difference ΔT was measured using a Au(Fe) - Cu thermocouple attached to the sample with GE varnish which is a good thermal conductor but is electrically insulating (figure 5·3). A long length of the Au(Fe) wire (~ 30 mm) is used, so that there is no thermal shorting between the ends. This gold wire is wound around the PTFE sample mount, while the two copper wires at the two ends are heat sunk and then taken up the insert and out though vacuum seals, with the same precautions against spurious thermal voltages as for the contact wires.

A second Au(Fe) - Cu thermocouple measures T_a, the difference between the mean temperature of the sample and the big copper block. Typically, T_a is ~ $2\Delta T$. The temperature of the copper block, T_D, is measured by the resistance of a calibrated diode, which is attached by GE varnish to the block. The temperature of the sample is taken to be $T_m = T_a + T_D$.

The thermocouples were made by spot-welding the copper and gold wires together with gold. The gold wire is atomically pure gold with 0·03% Fe added. The thermopower of the Au(Fe) - Cu thermocouple for $T < 10$ K is taken to be that of the Au(Fe) wire, the copper being

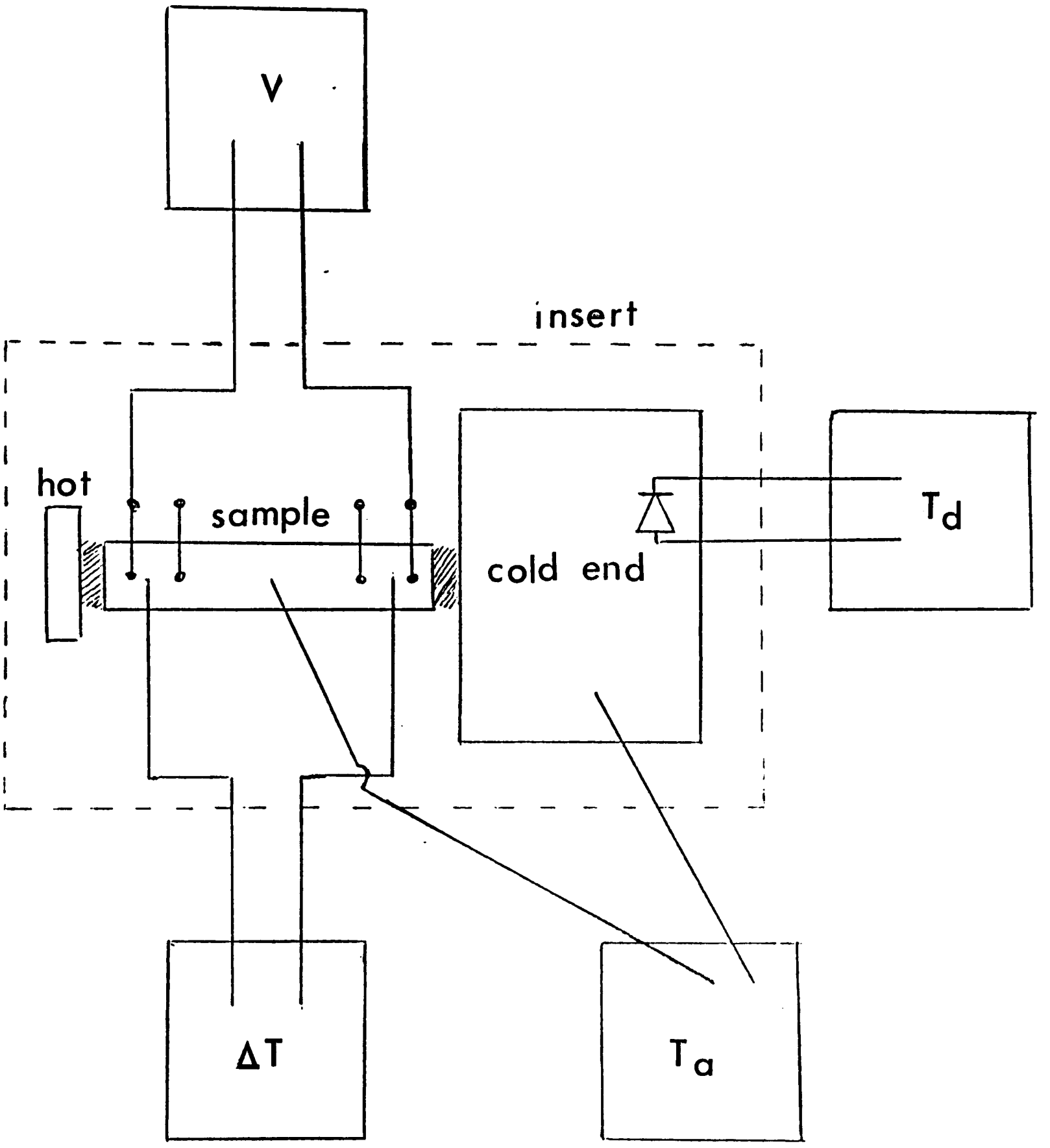


Figure 5·3

Schematic diagram of the experimental set up for thermopower measurements. The shaded regions are the silver paint thermal links. The gold wires connecting the two probes of each of the thermocouples are not shown for reasons of clarity.

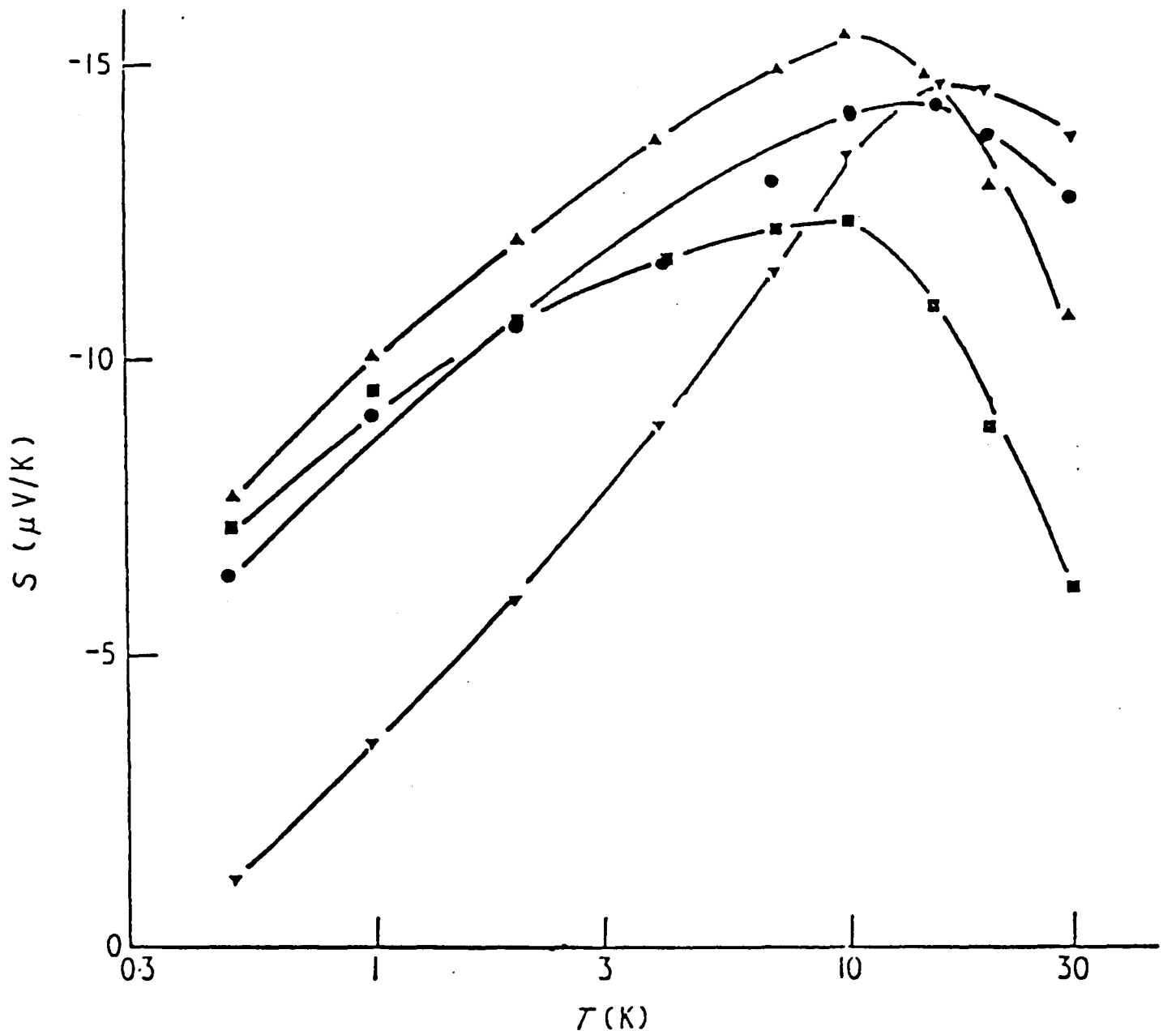
practically inert in this range. The calibration is taken from the results of Berman and Kopp (1971), and is shown in figure 5·4. For T > 10 K, the thermocouple was calibrated by measuring the voltage produced when one end is in liquid N_2, at 77 K, and the other is at a variable temperature, in an Oxford Instruments continuous-flow cryostat. The thermovoltage measured is shown in figure 5·5. The temperature inside the cryostat was itself measured by a calibrated thermocouple. The calibration for T > 10 K was obtained by taking the gradient of the curve shown in figure 5·5, and is given in table 5·1. This particular type of thermocouple, the Au(Fe) - Cu combination, was chosen here because of the large thermovoltages it produces for T ≦ 10 K, the range of temperature of greatest interest.

The voltmeters used were two Keithley 148 Nanovoltmeters to measure the thermocouple voltages, and a Keithley 150B microvolt ammeter to measure the sample thermovoltage V. The latter has an output which is amplified to 1 V full scale which serves as the input to the chart recorder for measurements with a varying magnetic field.

The inputs to the voltmeters were kept floating to reduce earth loops. In addition, appliances using a mains supply, such as pumps, were kept electrically isolated from the cryostat. It was observed that earth loops can cause spurious signals of several millivolts in the measurement of the thermovoltage V.

The experiments were performed with the (evacuated) insert in contact with liquid Helium at 4·2 K and pumped Helium at 1·65 K. These temperatures will be referred to in what follows as the base temperatures.

The temperature dependence of the thermopower could thus be measured either by variation of the heater current, in which case both the absolute temperature and the gradient are changed at the same time, or by making measurements at different base temperatures. The two



The thermoelectric power of Au-Fe alloys for various Fe concentrations. ■ 110 ppm; ▲ 300 ppm; ● 1100 ppm; ▼ 1900 ppm.

Figure 5·4

Calibration of the thermocouple for the low temperature range, taken from Berman and Kopp (1971).

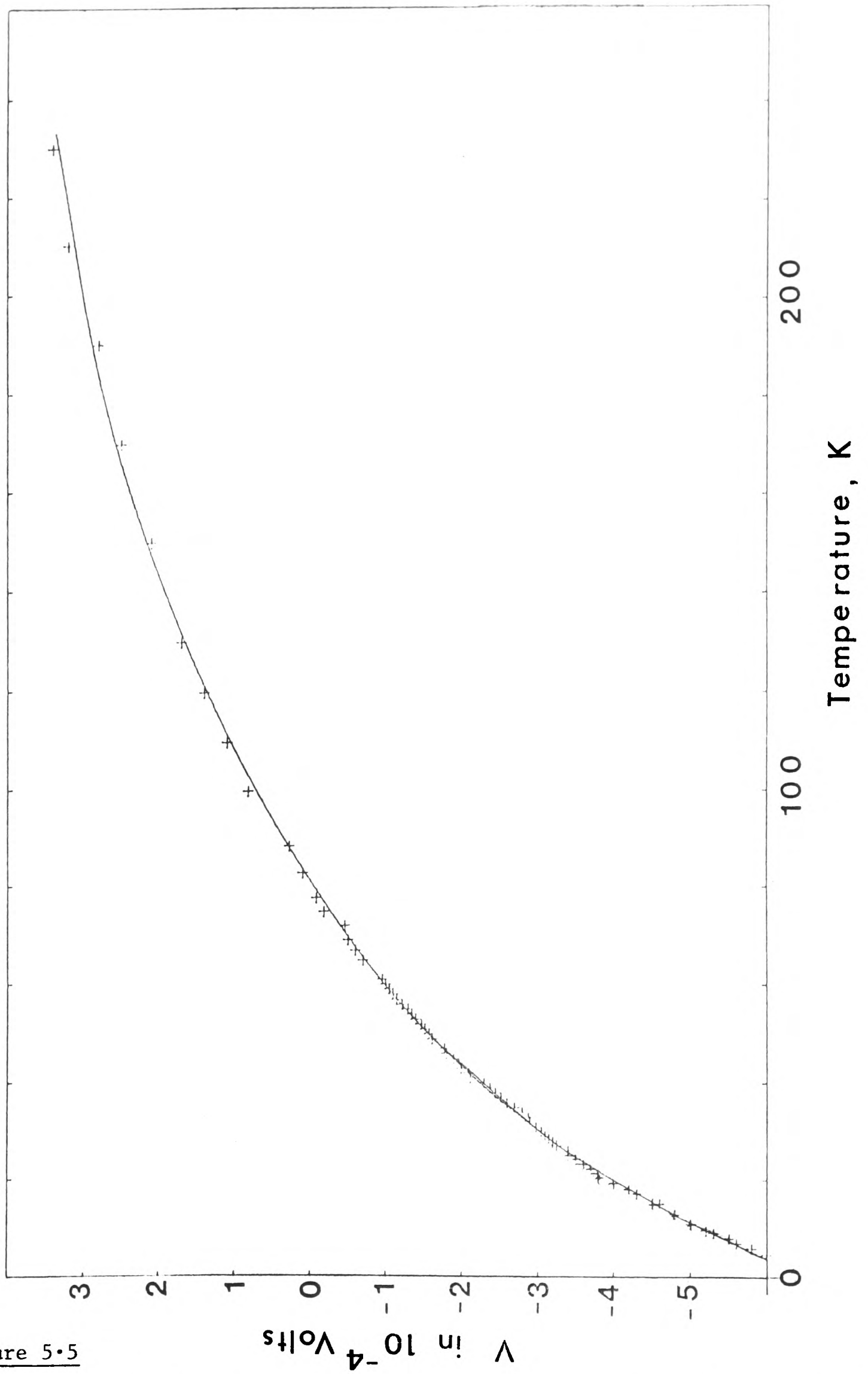


Figure 5·5

A plot of the voltage generated by a Au(Fe) - Cu thermocouple as a function of the temperature of one of its ends. The other end is kept at 77K.

Table 5·1

Thermocouple calibration for T > 10K

Calibration of Au(Fe) - Cu thermocouple

Temperature/K	Calibration in microvolts/K
10	14·0
15	12·0
20	10·5
25	9·26
30	8·32
35	7·59
40	7·02
45	6·56
50	6·19
55	5·87
60	5·58
65	5·32
70	5·06
75	4·80
80	4·55
85	4·29
90	4·03
95	3·77
100	3·51

methods usually gave agreement to within ~ 10%, which was taken as an indication that the thermopower was linear ($V = \alpha_{xx}\Delta T$), and that possible systematic errors were small. Such errors would include thermocouple and diode calibrations, possible thermal shorting or extraneous heating (the same amount of thermal offset would affect the results in different proportions), and errors in zeroing the voltmeters. The zeroing is effected by waiting for the system to reach thermal equilibrium at the beginning of each run, with the heater still off. The voltage readings of the thermocouples and of the sample contacts when there is no heating generally differ from the meters' absolute zeroes by less than 1 μV. The magnetic field measurements described below indicate that any residual temperature gradient when the heater is off is of the order of 10 mK or less. This could be corrected for by measuring the amplitude of the oscillatory structure in α_{xx} with the heater off.

The magnetic system used is described in chapter 1.

5·3 Sample characteristics

Three types of semiconductor heterostructures were studied:

- $Ga_{.47}In_{.53}As$ - InP heterojunctions
- a $Ga_{.47}In_{.53}As$ - $Al_{.48}In_{.52}As$ heterojunction with two subbands occupied
- GaAs - $Ga_{.7}Al_{.3}As$ heterojunction and superlattice

The characteristics of these samples are shown in tables 5·2a, b and c.

Measurements of thermopower were made for all these samples. In addition, Shubnikov - de Haas oscillations were recorded for comparison. Whenever Hall contacts were available, the Hall effect was also measured.

For the GaAs - $Ga_{.7}Al_{.3}As$ heterojunction, sample 6311, the persistent photoconductivity effect was used to change the carrier concentrations by illuminating the sample at helium temperatures with a light emitting diode. 6311a represents the original sample, while 6311b and c are the sample after successive bursts of illumination. The illumination increases the bulk conduction as well as the 2D carrier concentration, as can be deduced from the Shubnikov - de Haas oscillations, and a comparison between n_{Hall} and n_{S-dH}. Comparison between the thermopower data of 6311a and 6311c is therefore of great interest, because it indicates the extent of the direct contribution of the bulk semiconductors to the value of the thermopower measured for the whole heterojunction.

In this work, attempts were made to measure the thermopower of heterojunctions other than those listed in tables 5·2a, b, and c. However, results from these other samples were discarded because their electrical contacts were not sufficiently good for the purpose of

thermopower measurements. The criterion is that as the magnetic field is swept up or down, the contacts should produce no spurious signal greater than a microvolt in the absence of any applied thermal or electrical gradient.

Table 5·2a

$Ga_{.47}In_{.53}As$ - InP heterojunction

Sample	μ, $cm^2 V^{-1} s^{-1}$			n at 4·2K, 10^{11} cm^{-2}		Channel thickness, μm	Barrier thickness, μm
	300K	77K	4·2K	S-dH	Hall		
58	8900	32000	31500	3·8	-	0·9	0·075
68	9700	32150	32000	5·3*	-	1·0	0·075
135	8100	25000	23200	3·3*	-	0·7	0·1

Channel = $Ga_{.47}In_{.53}As$

Barrier = InP

* from thermopower oscillations in B-field.

Table 5·2b

$Ga_{.47}In_{.53}As$ - $Al_{.58}In_{.52}As$ heterojunction

Sample	μ, $cm^2 V^{-1} s^{-1}$			n at 4·2K, 10^{11} cm^{-2}		Channel thickness, μm	Barrier thickness, μm
	300K	77K	10K	S-dH	Hall		
168	8600	58490	88100	n_0=6·0 n_1=0·9	-	1·5	0·15

Channel = $Ga_{.47}In_{.53}As$

Barrier = $Al_{.48}In_{.52}As$

Table 5·2c

$GaAs - Ga_{.7}Al_{.3}As$ heterojunctions and superlattice

Sample	μ, $cm^2 V^{-1} s^{-1}$			n at 4·2K, 10^{11} cm^{-2}		Channel thickness, μm	Barrier thickness, μm
	300K	77K	4·2K	S-dH	Hall		
Hetero-junction							
6311a	7540	144300	364600	3·0	3·4	7	0·05
6311b	-	-	500000	3·6	4·2	7	0·05
6311c	-	-	-*	4·1	5·05	7	0·05
super-lattice							
MB44	-	-	19000	14·17	18·2	0·015 x 50 layers	-

Channel = GaAs

Barrier = $Ga_{.7}Al_{.3}As$

* Mixed conduction in 2DEG and n-GaAlAs layers

5·4 Thermopower measurements in zero magnetic field

Using the experimental set-up which has been described in section 5·2, the thermovoltage V between one pair of contacts is measured as a function of heater power. This varies the thermal difference between the contacts ΔT, and also the mean temperature T_m of the sample. In this way, a series of values of α (B=0) versus T_m is obtained, where α (B=0) = $V/\Delta T$.

The noise in the voltages is typically of order ± 0·02 μV for the thermocouple readings, which corresponds to ± 0·001 K, and ± 0·1 μV for the thermovoltage reading. The main sources of error are, firstly, spurious heating which can cause errors in the estimate of the true zeroes for all three of the voltage readings, and which can only be estimated approximately from the magnetic field measurements. Secondly, there is the problem of spurious contact potentials, which are difficult to detect in absolute terms. Finally, there is substantial geometrical inaccuracy in positioning the thermocouple probes at the same points on the sample as the electrical probes. This is corrected by estimating the ratio of the distances between the pair of thermal probes and the pair of electrical probes, and assuming a uniform thermal gradient along the sample. This assumption was shown to be reasonable by the observation that the thermovoltages measured for different pairs of contacts scale with the distance. The errors due to the spurious heating are important for readings taken with a small gradient, but should be negligible otherwise. This is shown by the agreement between the data taken for base temperatures of 1·65 K and 4·2 K, for all data points except those very near to 4·2 K. The geometrical error in measuring the separation of the electrical and thermal probes is of order ± 10%, due to the large size of the probes (of order 0·5 - 1 mm) compared with their separation (~ 5 mm). Since

this only influences the absolute magnitude of α_{xx}, it does not affect measurements of the temperature dependence of α_{xx}.

Figures 5·6a to 5·6h show plots of α_{xx} versus the mean temperature T_m in zero magnetic field. Figures 5·6a to 5·6c are results for the GaInAs ≡ InP heterojunctions, 5·6d is for the GaInAs - InAlAs heterojunction, and 5·6e to 5·6h are results for the GaAs ≐ GaAlAs system. In these plots, the white squares show results obtained with base temperature 4·2 K, the black triangles are those obtained with the base temperature 1·65 K. The error bars shown in figures 5·6a to 5·6h are typical values of the estimated errors due to random fluctuations and zeroing errors, but for the sake of clarity do not include the geometrical factor. The combined errors are given in table 5·3 which gives the values of α_{xx} obtained for T_m = 3 K and T_m = 10 K. These are near to the maximum and minimum values, respectively, of α_{xx} in the range of T_m used.

Lastly, figure 5·7 shows plots of log (α_{xx}) versus log (T_m) for the GaInAs - InP and GaInAs - InAlAs heterojunctions, for 3 K ≦ T_m ≦ 10 K. Below 3 K, the values of α_{xx} are unreliable. Above 10 K, the values tend towards a constant value in this low temperature range, as can be seen in figures 5·6a to 5·6h. These plots are approximately linear, indicating a power law relationship of the form α_{xx} vs $(T_m)^c$. The values of c are listed in table 5·3, and are found to lie in the range ≒0·8 to -1·0. In contrast, it can be seen from figures 5·6e to 5·6h that the thermopower for the GaAs - GaAlAs system is independent of temperature, within the experimental errors. The absolute magnitude of α in the superlattice is however about an order of magnitude larger than for any of the heterojunctions. All of this behaviour is

inconsistent with existing theory, which predicts a T^{+1} dependence for degenerate carrier systems, and with experimental work on Si inversion layer (Gibbings and Pepper 1985). These results are discussed in the next chapter.

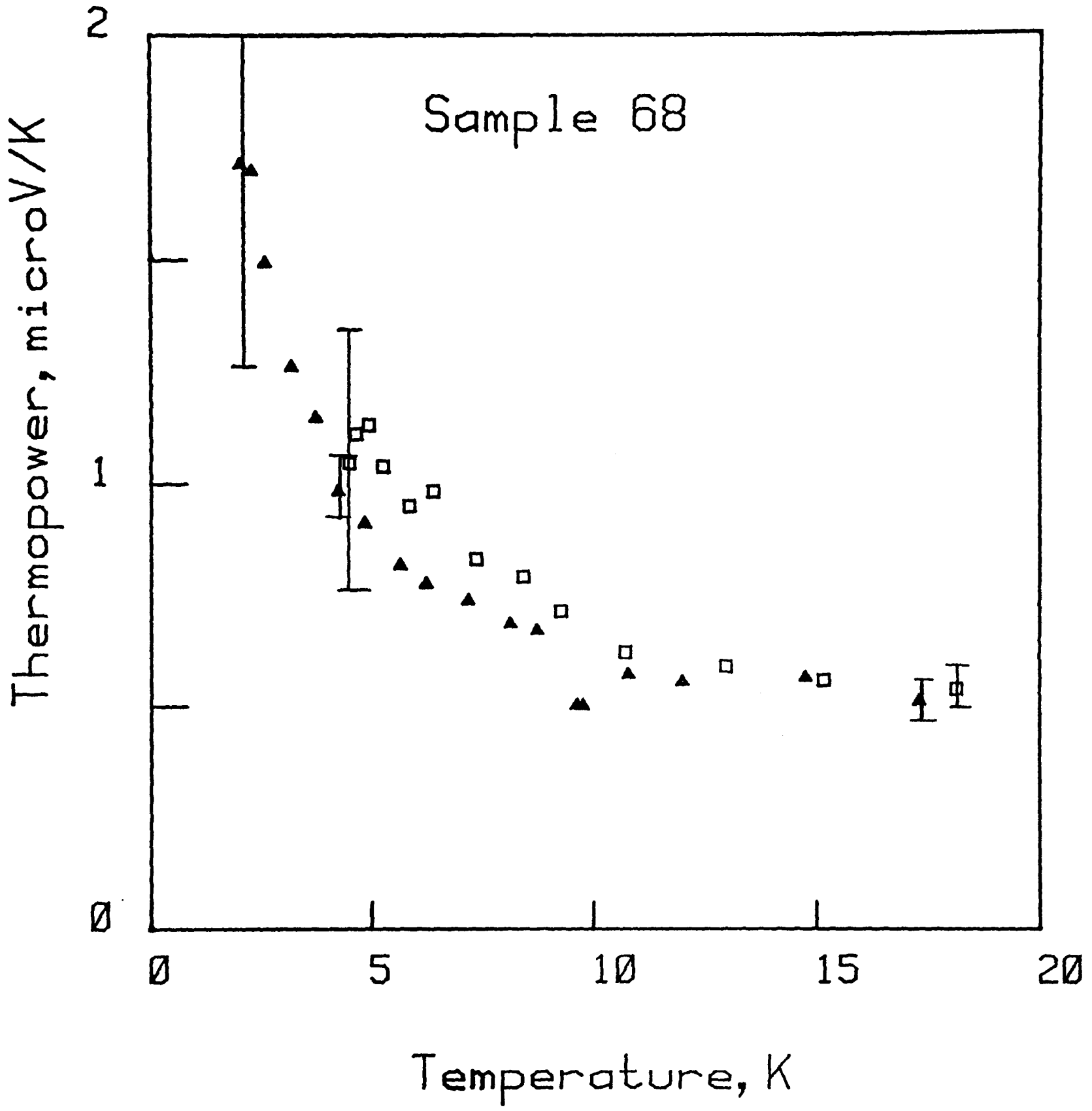


Figure 5·6a

Thermopower α for B = 0 as a function of the mean temperature T_m for sample 68. Typical errors are indicated.

▲ Base temperature of 1·65K

□ Base temperature of 4·2K.

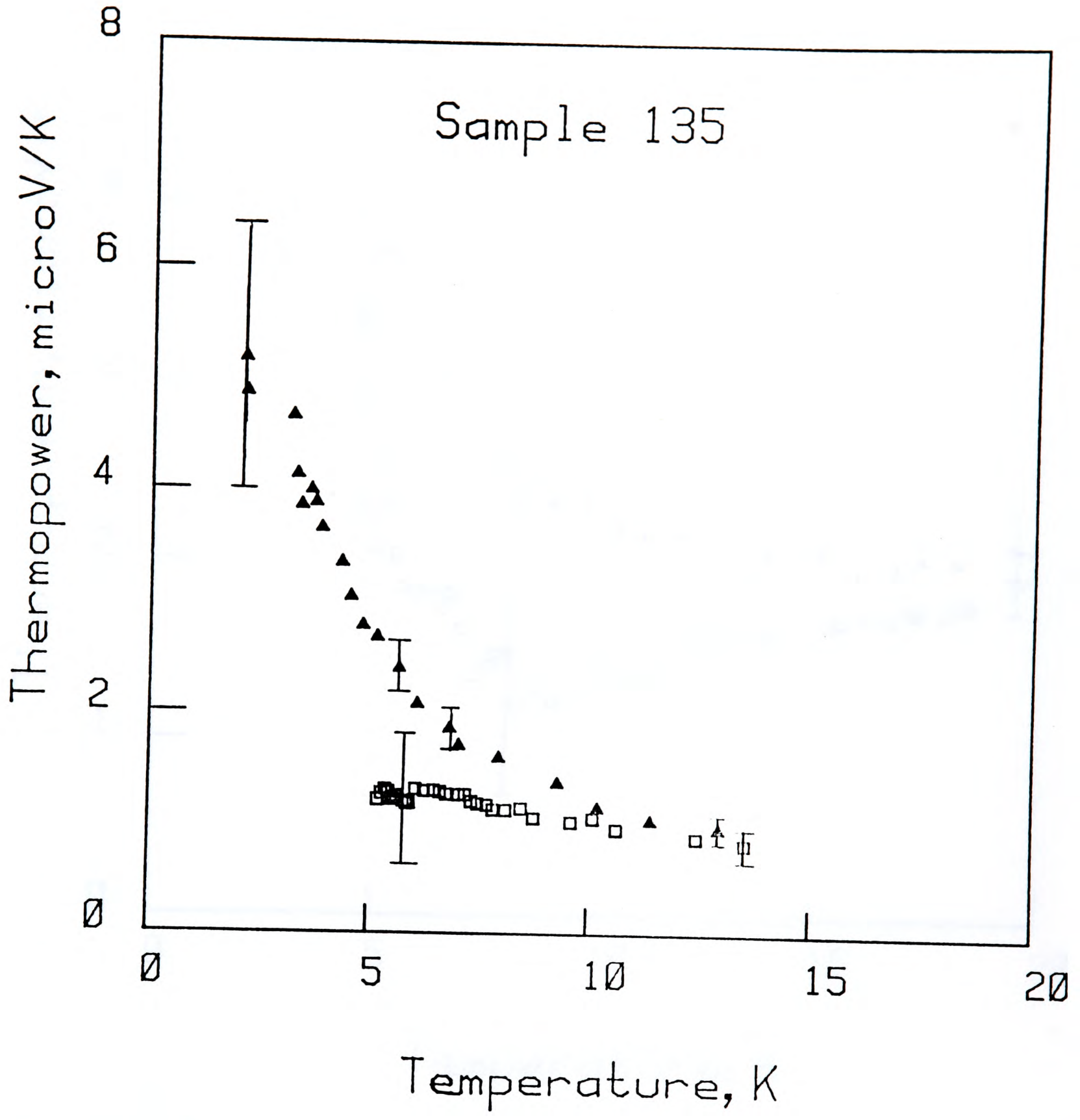


Figure 5·6b

α versus T_m for sample 135.

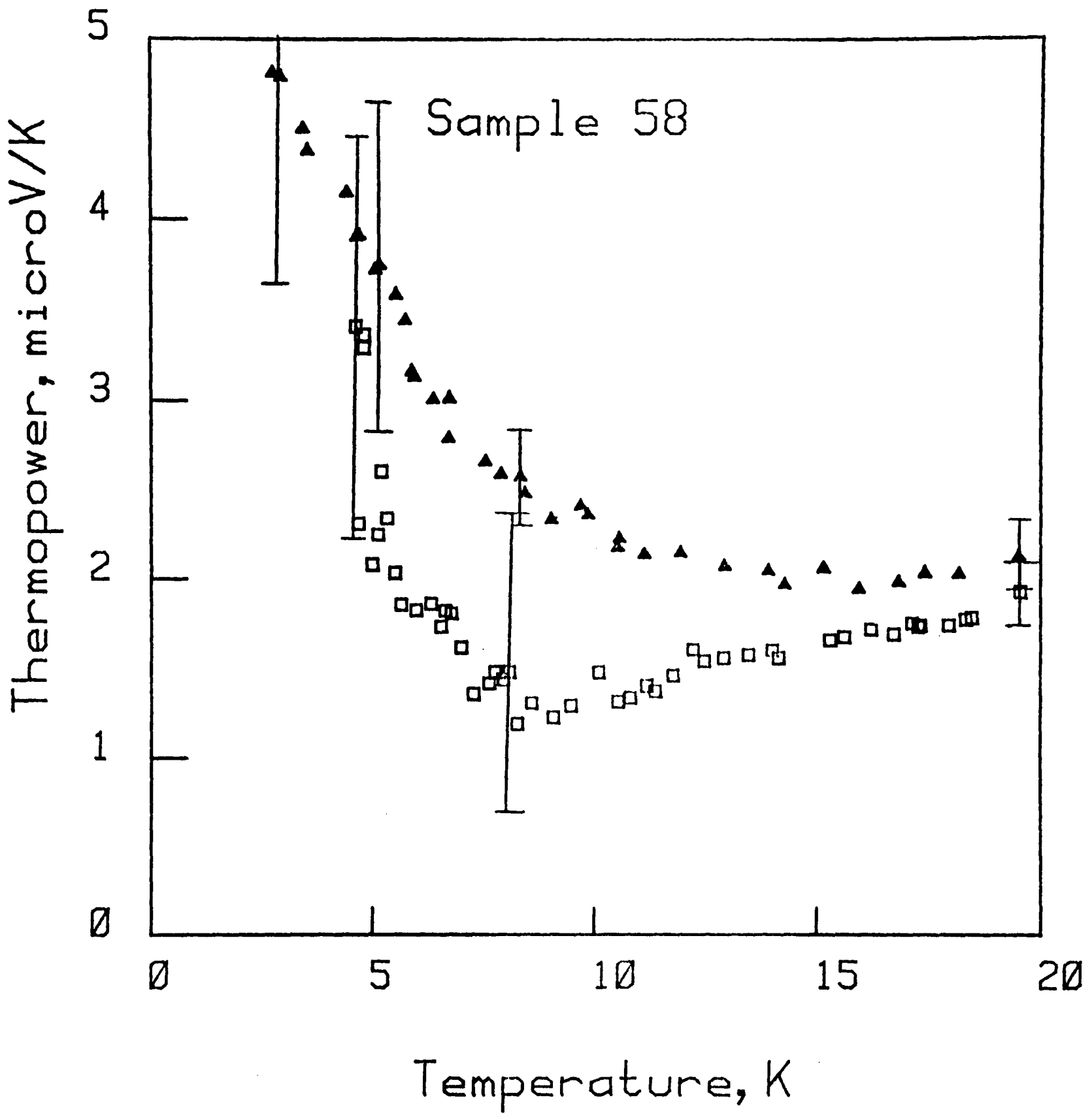


Figure 5·6c

α versus T_m for sample 58.

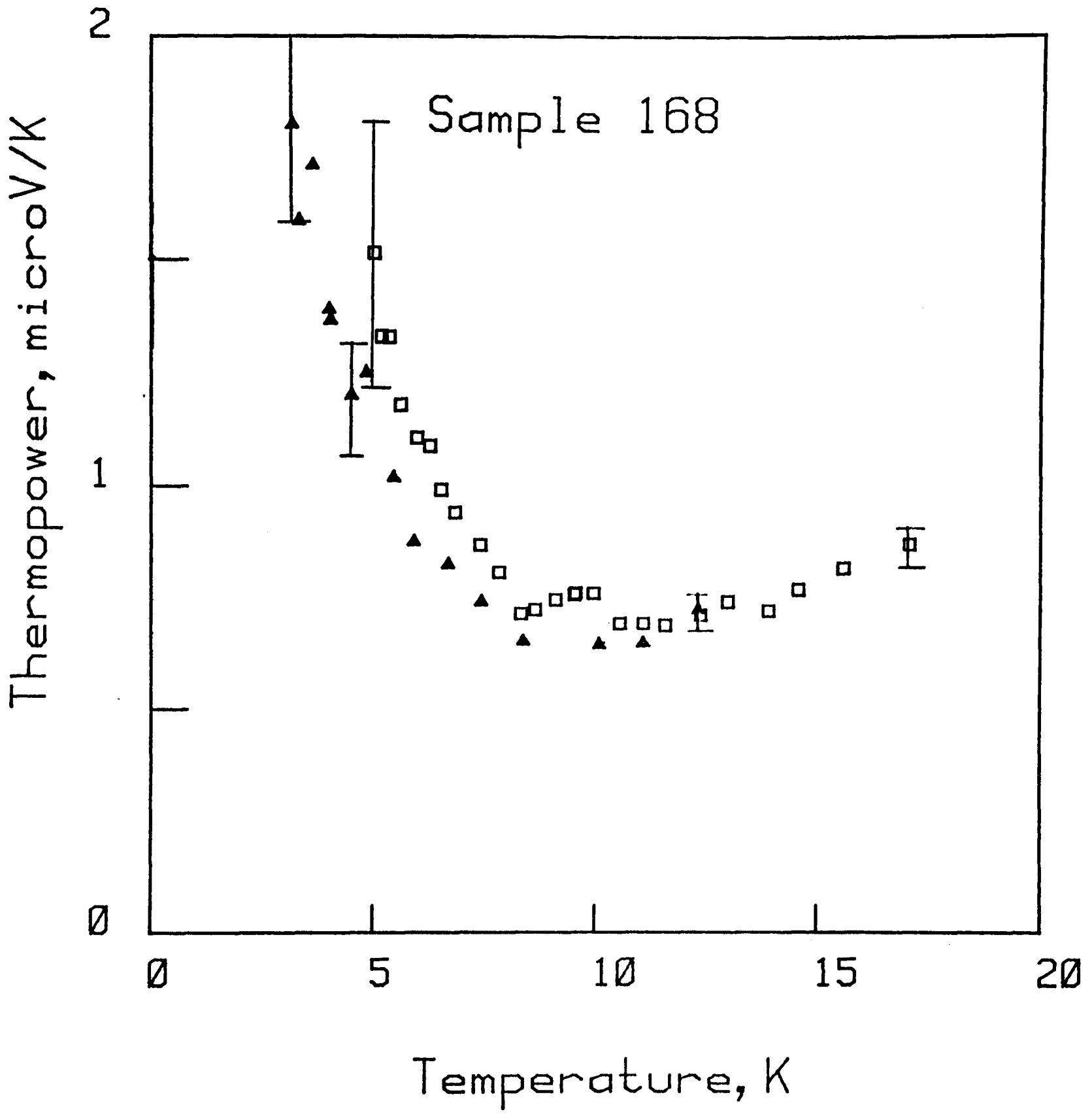


Figure 5·6d

α versus T_m for sample 168.

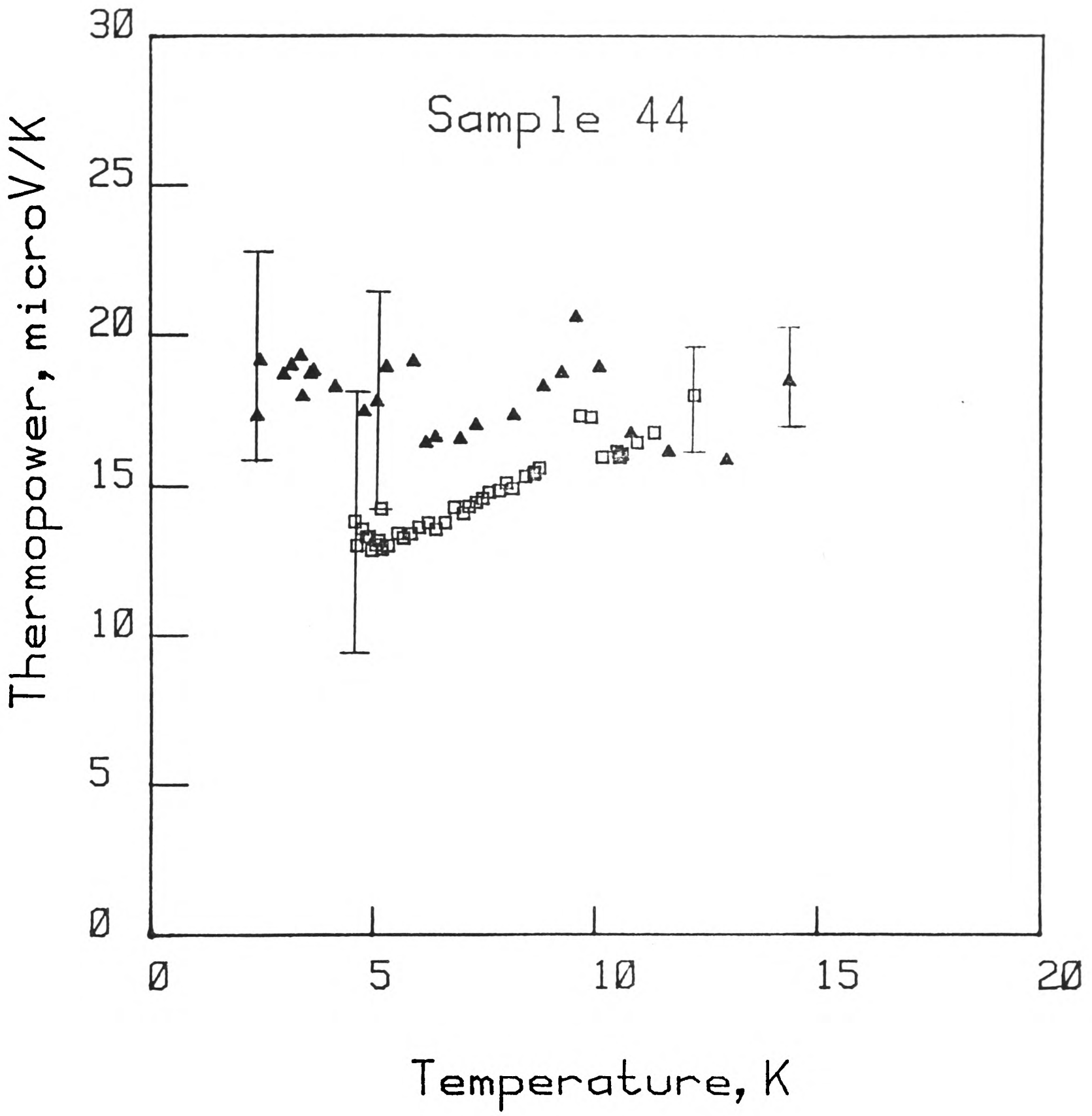


Figure 5·6e

α versus T_m for sample MB44.

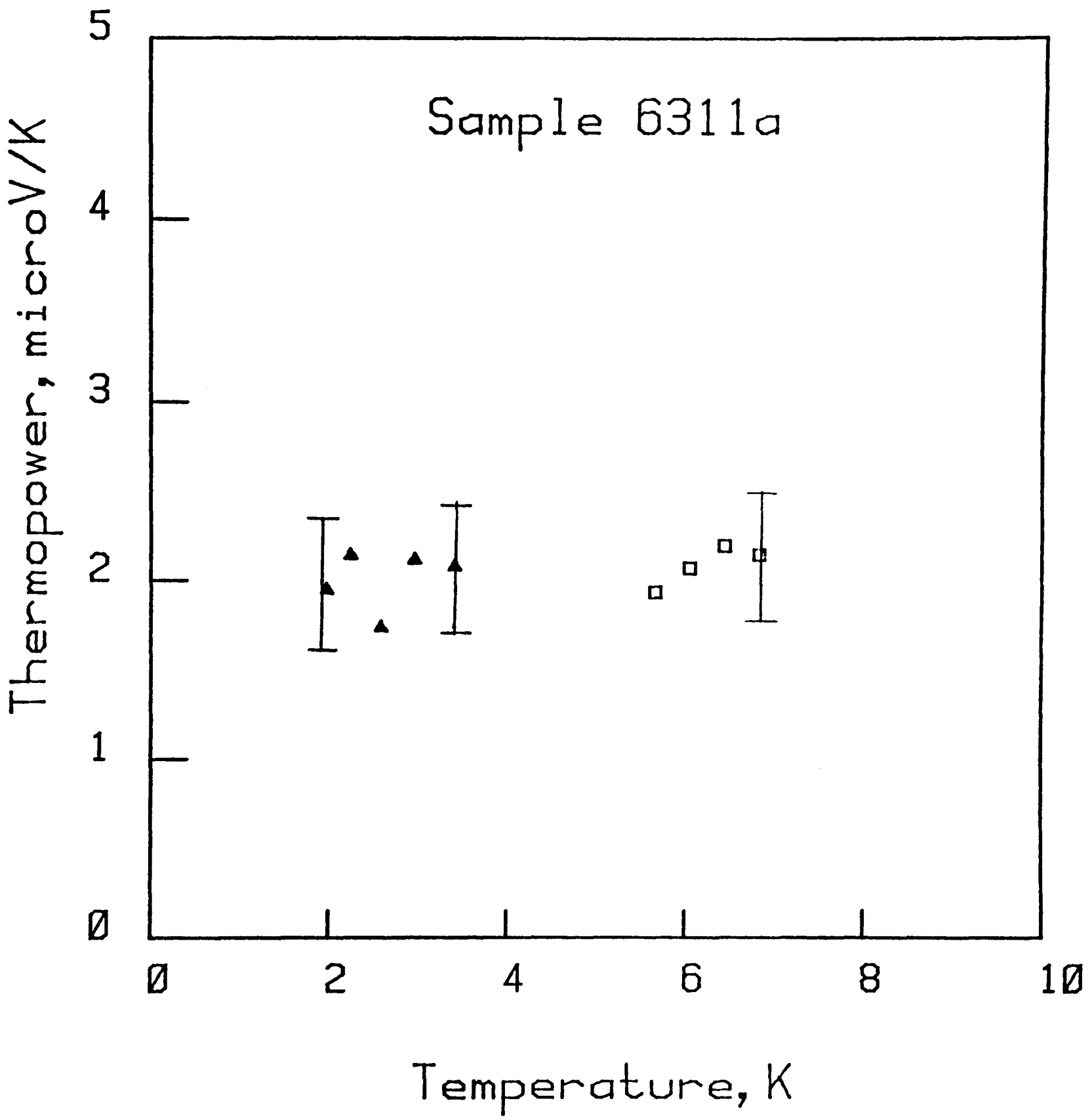


Figure 5·6f

α versus T_m for sample 6311a.

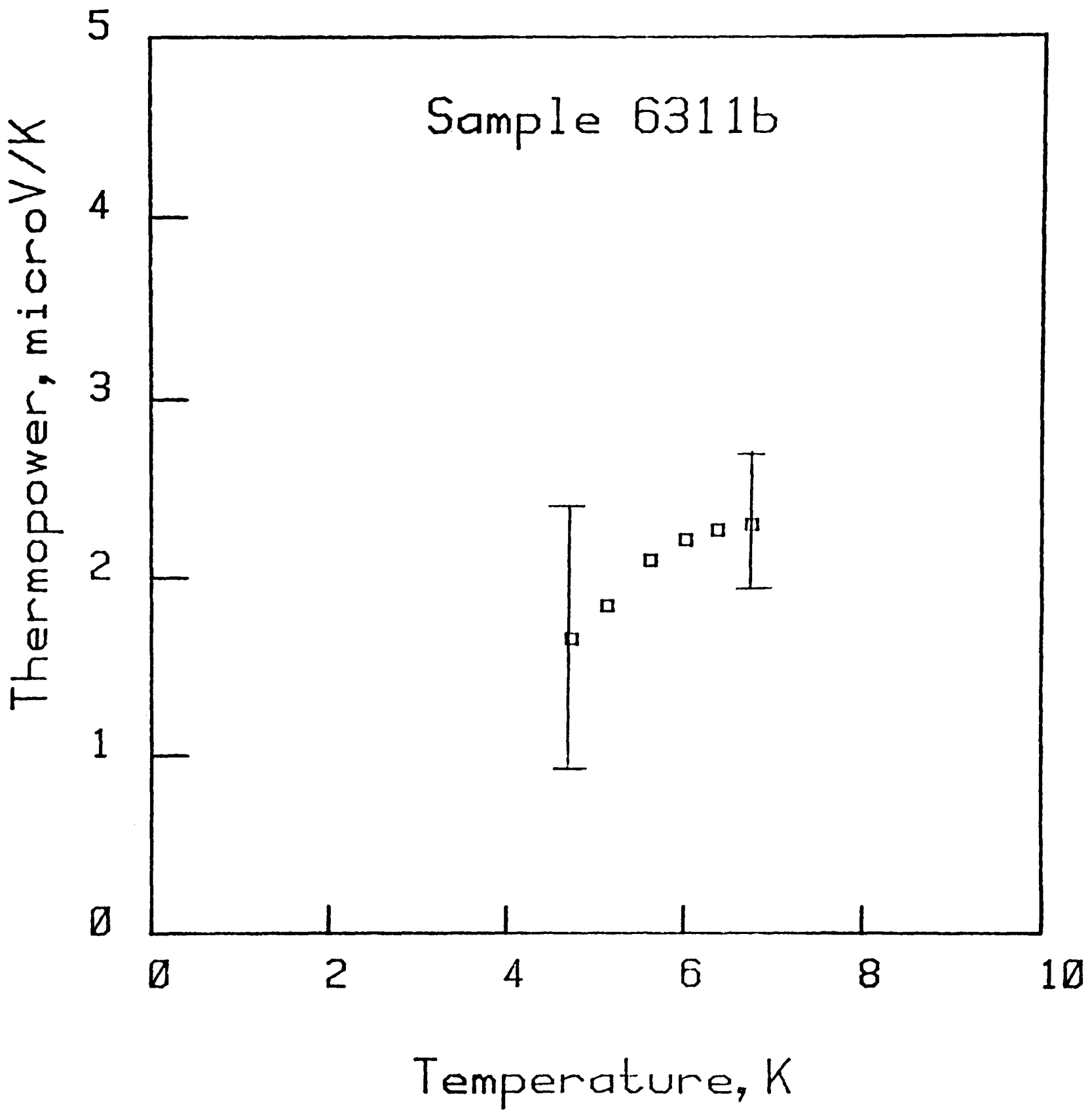


Figure 5·6g

α versus T_m for sample 6311b.

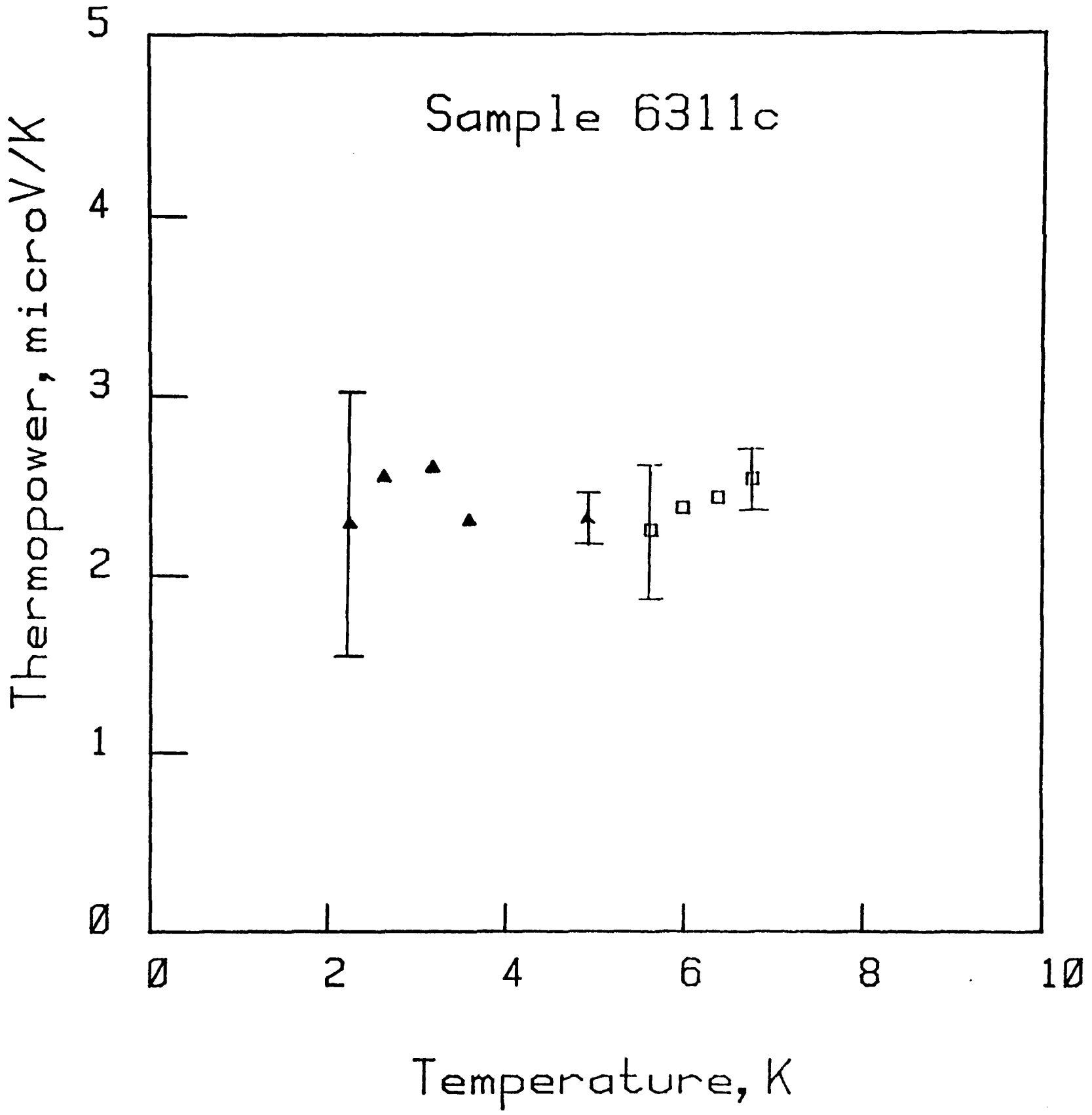


Figure 5·6h

α versus T_m for sample 6311c.

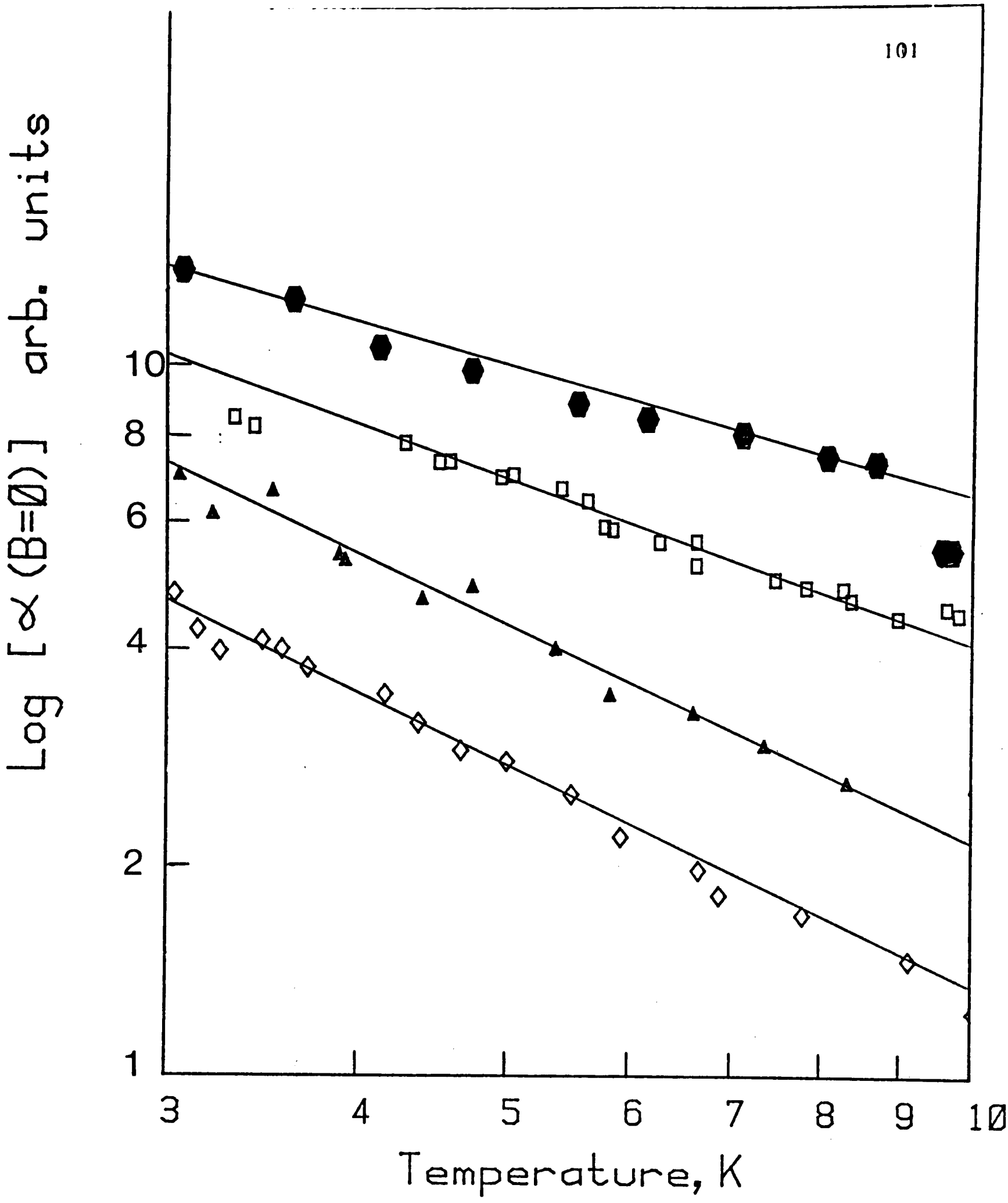


Figure 5·7

Log α versus log T_m for the GaInAs - InP and GaInAs - InAlAs systems.

The x-axis is common to all the curves; the y-axis is displaced for each curve, to show clearly their linear behaviour. Table 5·3 gives the values of the data points, and gradients of the curves.

From top to bottom, the results are for samples 68, 58, 168 and 135.

Table 5·3

Thermopower in zero mangetic field

Sample	Experimental α, in μV/K		Predicted α, in μV/K		c ± 10%
	T_m = 3K	T_m = 10K	T_m = 3K	T_m = 10K	
68	1·3 ± 0·3	0·6 ± 0·05	7·1	24·0	≈ 0·76
135	4·3 ± 2	1·2 ± 0·3	10·8	35·4	≈ 1·0
58	4·0 ± 1·3	2·4 ± 0·5	6·7	22·5	≈ 0·78
168	1·25 ± 0·25	0·66 ± 0·1	11·7	39·2	≈ 1·0
MB44	18·6 ± 6	18·6 ± 4	4·0	13·5	0
6311a	2·1 ± 0·6	2·1 ± 0·5	18	59·5	0
6311b	-	2·3 ± 0·6	12·75	42·5	0
6311c	2·4 ± 1	2·4 ± 0·5	10·6	35·5	0

5·5 Thermopower measurements in a strong magnetic field

Measurements were made of the thermovoltage V for fixed values of thermal difference ΔT and mean sample temperature T_m as a function of magnetic field up to 10T. The sweep time is typically 2 minutes. In all cases, there is a constant induced voltage of a few microvolts, proportional to the sweep rate, caused by the loops in the sample wire. This voltage remains constant during the sweep, and is subtracted from V to give the thermopower signal. For comparison, the Shubnikov - de Haas oscillations are also recorded.

Up to the present, only the diagonal component of the thermopower tensor in a magnetic field, α_{xx}, has been measured. The reason is that few of the samples studied have a geometry allowing Hall contacts to be deposited. For the samples where measurements of σ_{xy} are possible, the signals were too small to be detected above the noise, even for the largest temperature difference.

Typical experimental recordings of α_{xx} at two values of T_m and of the Shubnikov - de Haas oscillations for some of the samples studied are shown in figures 5·8a to 5·8h. The main points to note from these diagrams are, firstly, that the variation of α_{xx} with field is exactly in phase with the Shubnikov - de Haas oscillations. This agrees with theoretical predictions and other experimental studies on the GaAs - GaAlAs (Obloh et al. 1984) system. This study is the first such report (Nicholas et al. 1985) on the GaInAs - InP and GaInAs - InAlAs heterojunctions. In addition, this is the first observation of α_{xx} to show clearly a spin split minimum (samples 6311a and 6311c in figures 5·8f and 5·8h) as well as the complex oscillations characteristic of two-subband occupation (sample 168, figure 5·8d). In an earlier work, Portal et al. (1982) gave an analysis of the positions of the minima and maxima in the Shubnikov - de Haas oscillations for the same sample

168 in terms of the subband separation and of the magnetic depopulation of the higher energy subband at large magnetic field. In summary, for all cases studied, α_{xx} is in phase with the Shubnikov ⁻ de Haas oscillations, whether these oscillations have a single fundamental frequency, or whether they show a spin-split behaviour, or two-subband occupation.

The second general feature of figures 5·8a to 5·8h is that the maxima of α_{xx} lie approximately in a straight line which extrapolates back near to zero at B = 0. This is in qualitative agreement with theory, which predicts that the maximum value of α_{xx} which occurs at a filling factor of $[N+\frac{1}{2}]$, where N is an integer, should obey the rule that $[\alpha_{xx}(N+\frac{1}{2})]$ x $[N+\frac{1}{2}]$ is a constant. Since the magnetic field at which the filling factor is $[N+\frac{1}{2}]$ has the value of $B_f/[N+\frac{1}{2}]$, where B_f is the fundamental field, the above rule leads to a direct proportionality between the maxima of α_{xx} and the value of the applied field. Deviations from this behaviour occur at high fields, once the spin splitting is resolved. However, theory predicts that the product $[\alpha_{xx}(N+\frac{1}{2})]$ x $[N+\frac{1}{2}]$ should tend towards a universal constant. This constant is $^{k}/_{e}$ ℓn2 which is ~ 60 μV/K. This is in contradiction with all the present experimental data, except for those of the GaAs - GaAlAs superlattice MB44. With this one exception, the experimental values of $[\alpha_{xx}(N+\frac{1}{2})]$ x $[N+\frac{1}{2}]$ are lower than the predicted 60 μV/K, even allowing for large erors in the absolute magnitude of α_{xx} due to the geometrical factor. A more obvious deviation from theory is that the values of α_{xx} $(N+\frac{1}{2})$ are strongly temperature-dependent for the GaInAs - InP and GaInAs - InAlAs heterojunctions. This can be observed from figures 5·8a to 5·8d. These show that for almost equal values of ΔT, the peak values of α_{xx} are markedly larger for the lower temperature trace. There is a similar temperature dependence for the GaAs - GaAlAs systems, but it is much weaker. This is discussed in

more detail below. The final point to note from the experimental recordings concerns the results from sample 6311c (figure 5·8h). As mentioned in section 5·3, this sample presents some conduction in the bulk semi-conductor. This is clear from the fact that the minima of the Shubnikov - de Haas oscillations deviate considerably from zero. Using equation (4·17), the bulk contribution to the conduction is calculated to be 5 x 10^{-5} of the total conduction. The remarkable feature is that the minima of the thermovoltage for sample 6311c are still close to zero. This shows that even when bulk conduction affects the Shubnikov - de Haas effect considerably, its effect on α_{xx} is still negligible.

The temperature dependences of the peak values of α_{xx} are shown in figures 5·9a to 5·9h. For each sample, the set of peaks shown in these figures is the one observed at the lowest filling factor $[N+\frac{1}{2}]$ obtainable in the experimental range of B, except when this shows spin-splitting because the spin-split effect is itself temperature dependent. The other sets of peaks which correspond to larger filling factors are not shown here. They are observed to have the same temperature dependence within experimental errors, which are correspondingly larger for these smaller peaks. Table 5·4 lists the values of the product $[\alpha(N+\frac{1}{2})] \times [N+\frac{1}{2}]$ at T_m = 3K and 8K for all of the samples.

As in the case of measurements in zero field, an empirical temperature dependence of the peak values of α_{xx} $(N+\frac{1}{2})$ of the form $(T_m)^c$ is assumed. The values of c are obtained from the log-log plots shown in figures 5·10a and 5·10b, and are given in table 5·4. For the GaInAs - InP and GaInAs - InAlAs heterojunctions, α_{xx} $(N+\frac{1}{2})$ vary as $T_m^{-1.4}$ to $T_m^{-1.8}$ for different samples. Results for the GaAs - GaAlAs superlattice can be fitted approximately to a $T_m^{-0.1}$ dependence, and for the heterojunctions to T^{-1}. It is interesting to note that ρ_{xx} is

practically temperature independent in the same range. The GaInAs ⊣ InAlAs sample 168, for example, shows ρ_{xx} increasing by 4% over the range of heating which causes α_{xx} to decrease by 32%.

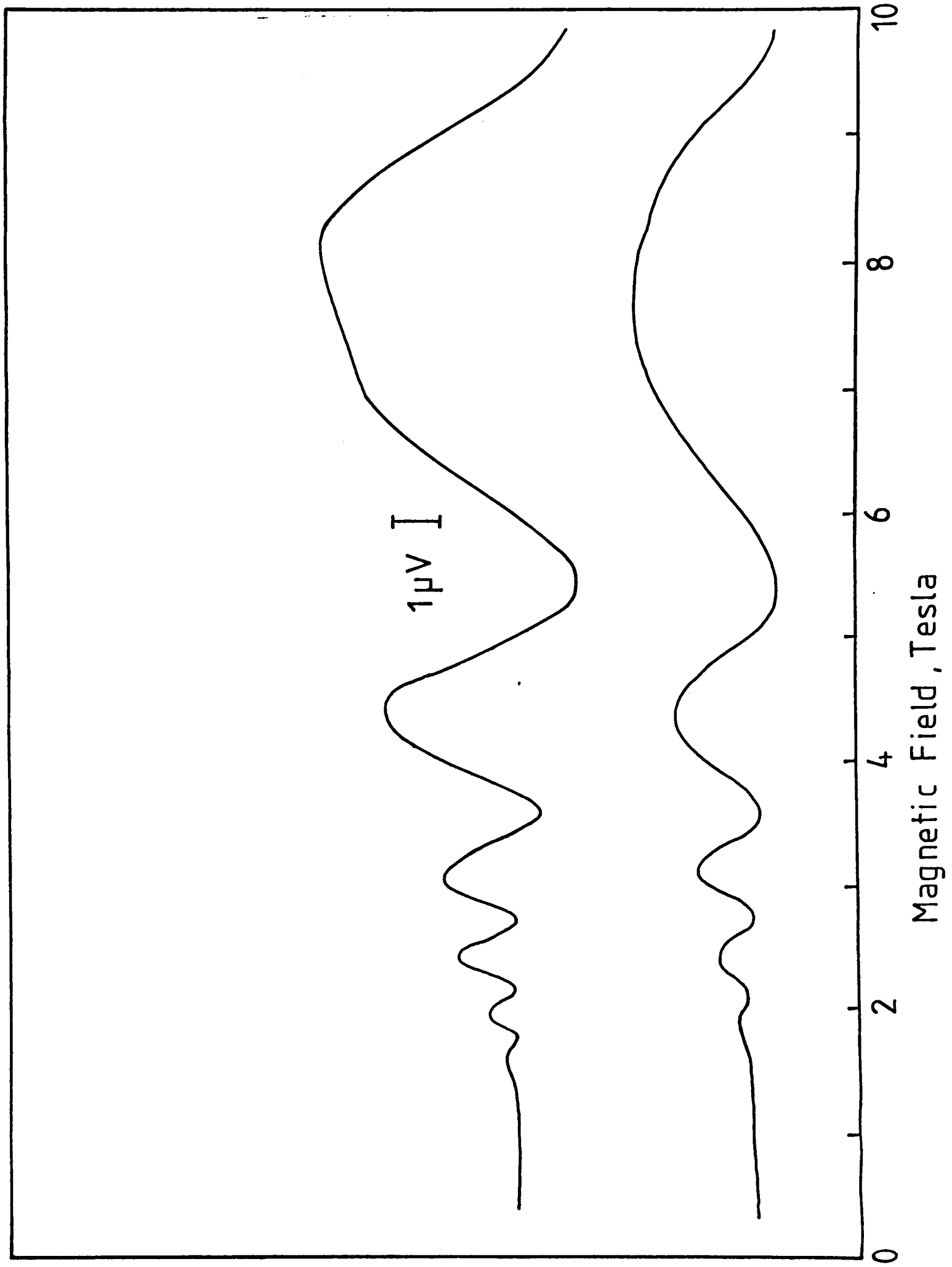


Figure 5·8a Sample 68

From top to bottom, the curves are:

- Thermovoltage V for $\Delta T = 1{\cdot}3K$ at $T_m = 3{\cdot}1K$
- Thermovoltage V for $\Delta T = 1{\cdot}3K$ at $T_m = 5{\cdot}3K$.

The thermovoltage curves have a common scale, as shown for 1 μV.

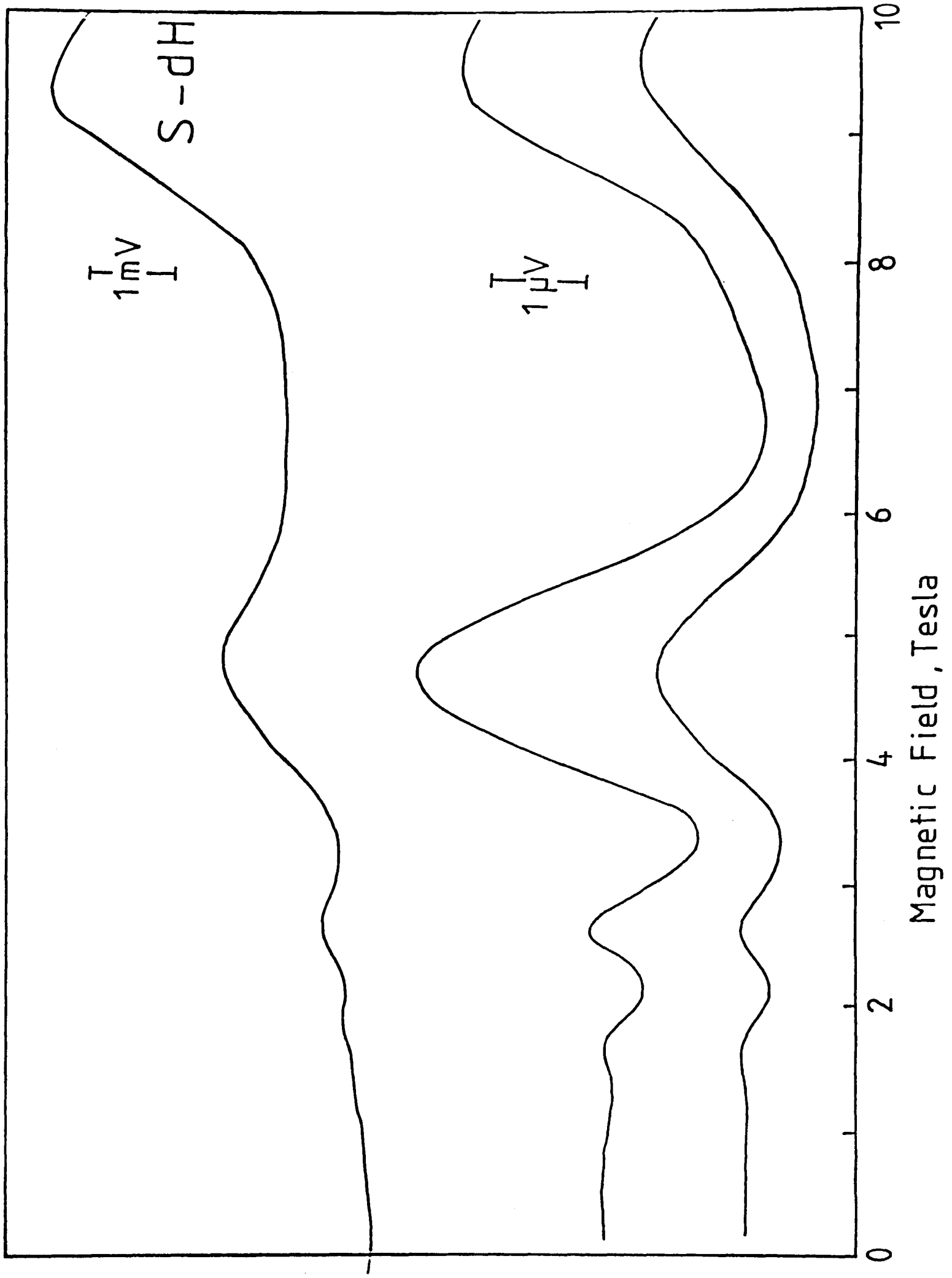


Figure 5·8b Sample 135

From top to bottom, the curves are:

- Shubnikov - de Haas oscillations at 1·65K for I = 1 μA, with the scale as shown for 1 mV.
- Thermovoltage V for ΔT = 0·8K at T_m = 3·7K
- Thermovoltage V for ΔT = 0·8K at T_m = 5·3K.

The thermovoltage curves have a common scale, as shown for 1 μV.

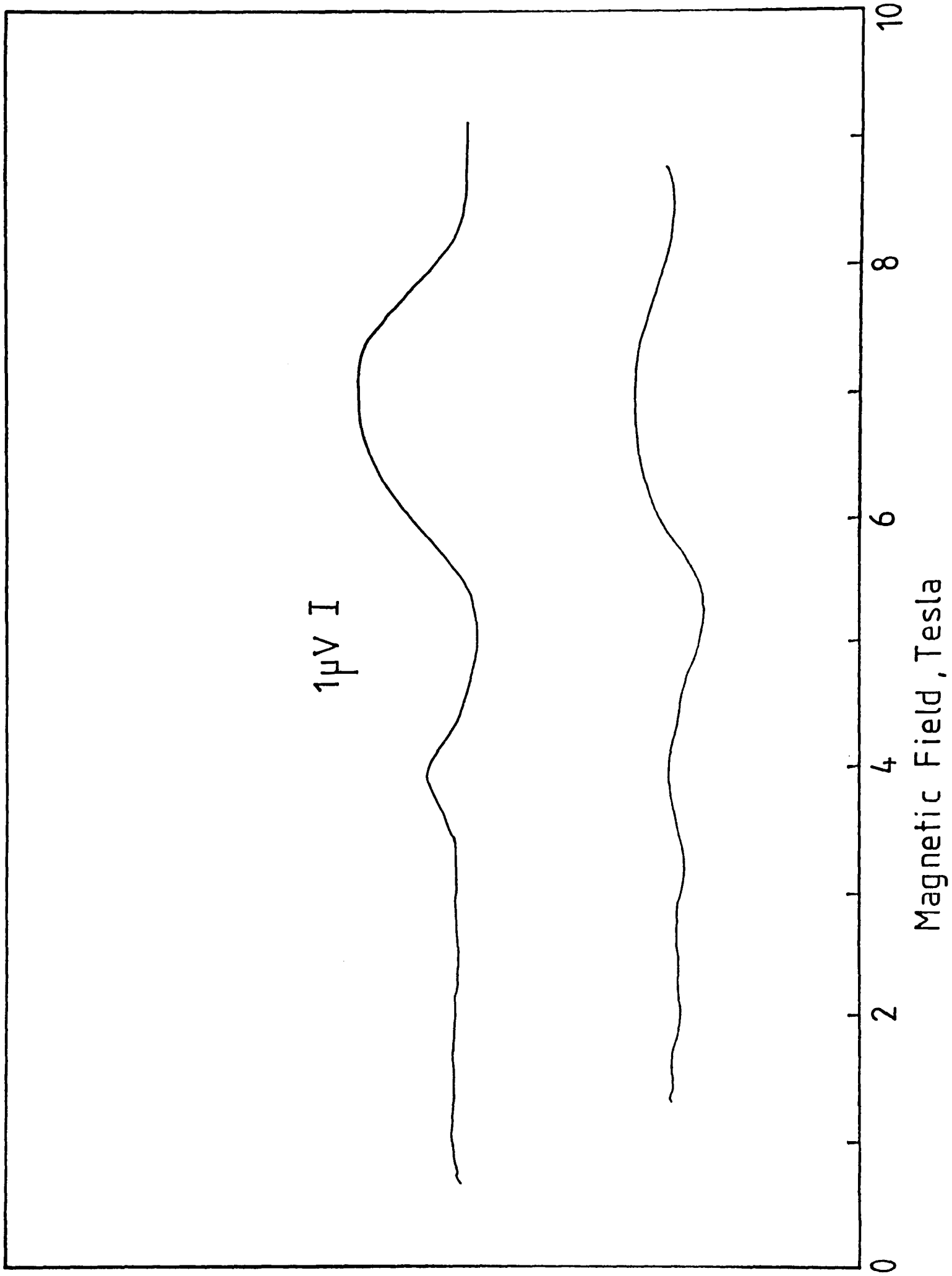


Figure 5·8c Sample 58

From top to bottom, the curves are:

- Thermovoltage V for $\Delta T = 1{\cdot}7K$ at $T_a = 3{\cdot}9K$
- Thermovoltage V for $\Delta T = 1{\cdot}75K$ at $T_a = 6{\cdot}1K$.

The thermovoltage curves have a common scale, as shown for 1 μV.

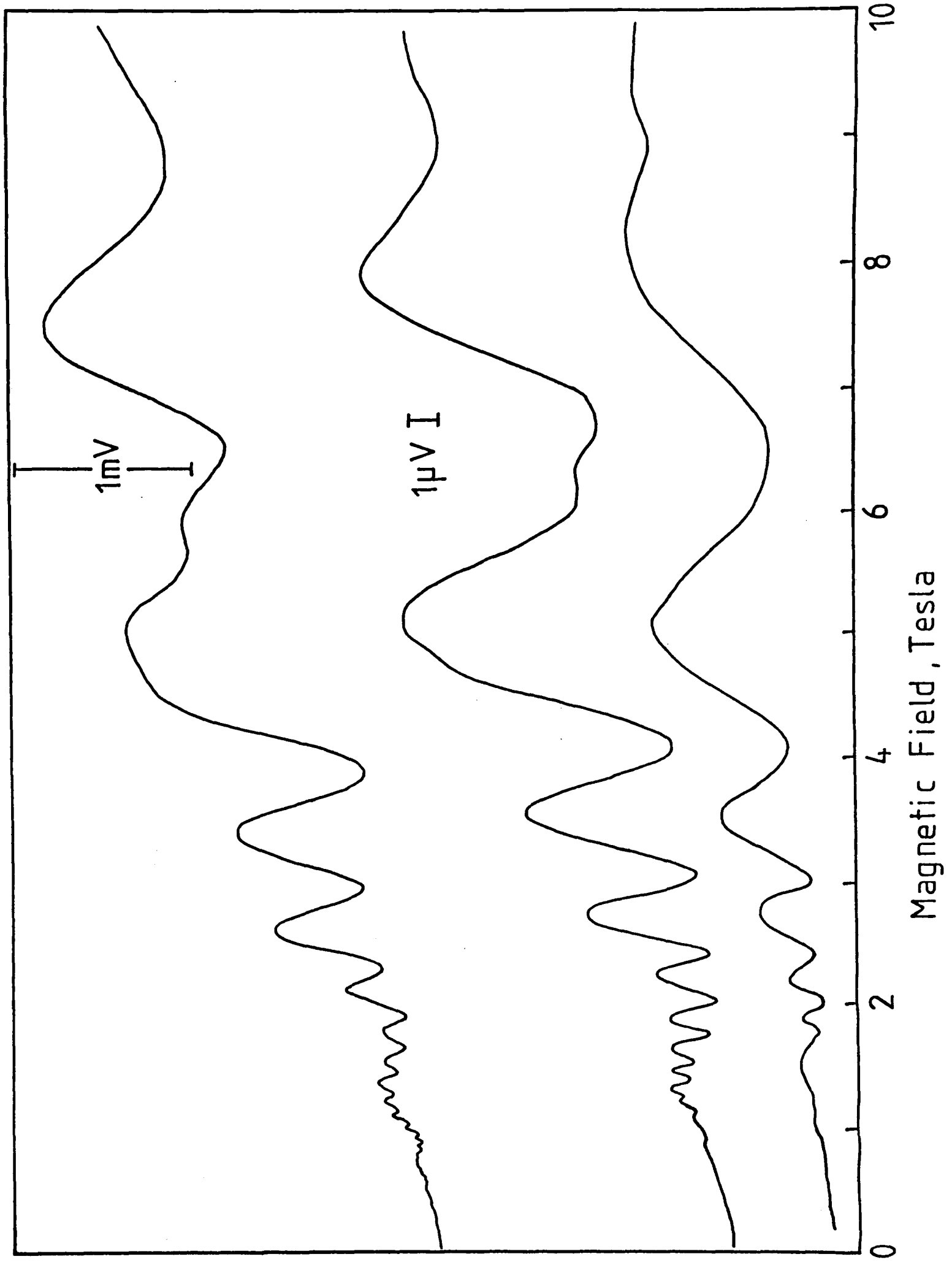


Figure 5·8d Sample 168, showing 2-subband occupation

From top to bottom, the curves are:

- Shubnikov - de Haas oscillations at 1·65K for I = 30 nA, with the scale as shown for 1 mV.
- Thermovoltage V for ΔT = 0·8K at T_m = 2·1K
- Thermovoltage V for ΔT = 0·9K at T_m = 5·5K.

The thermovoltage curves have a common scale, as shown for 1 μV.

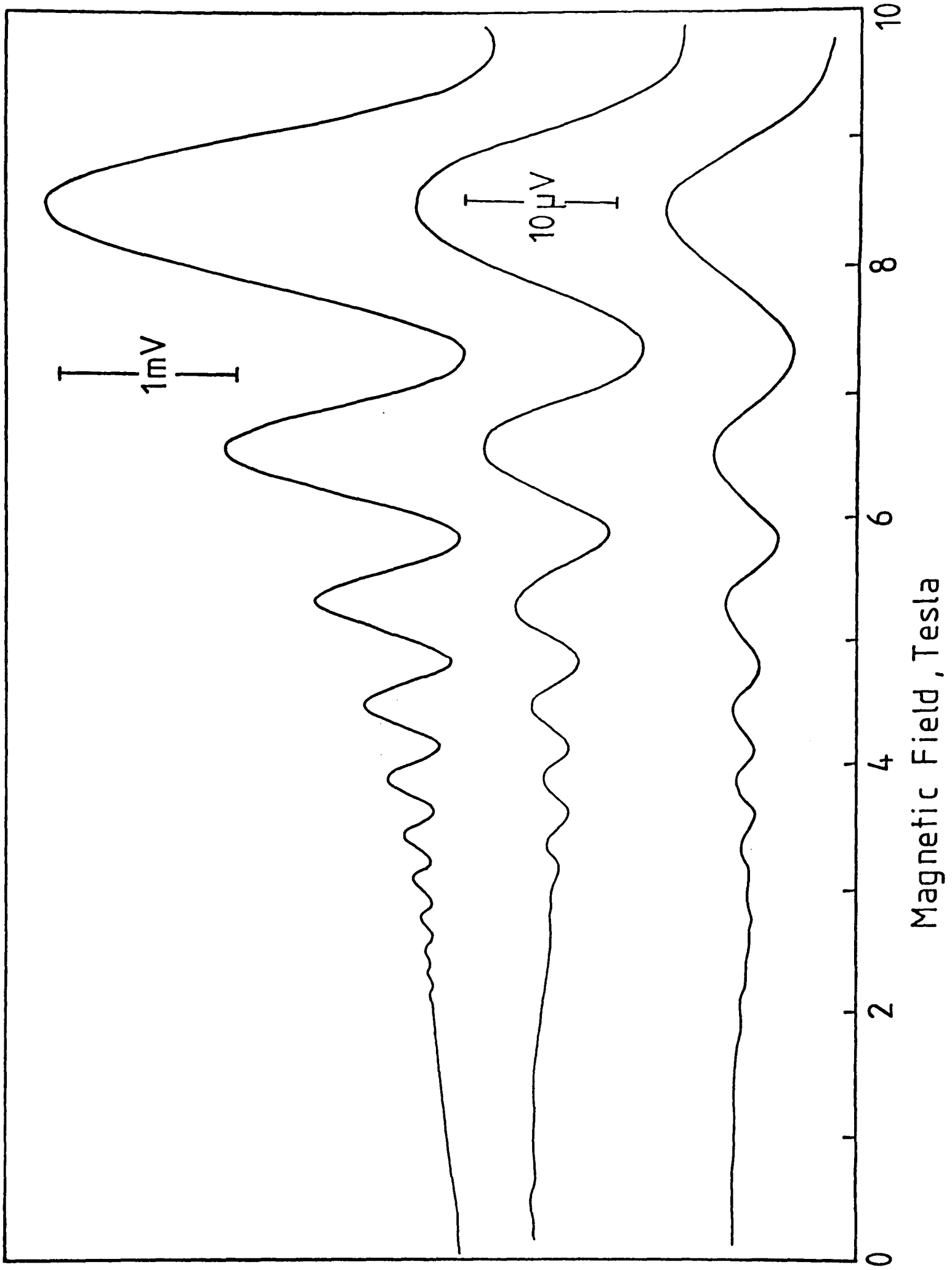


Figure 5·8e Sample MB44

From top to bottom, the curves are:

- Shubnikov - de Haas oscillations at 4.2K for I = 100 μA, with the scale as shown for 1 mV.
- Thermovoltage V for $\Delta T = 0{\cdot}8K$ at $T_m = 4{\cdot}6K$
- Thermovoltage V for $\Delta T = 0{\cdot}8K$ at $T_m = 5{\cdot}7K$.

The thermovoltage curves have a common scale, as shown for 10 μV.

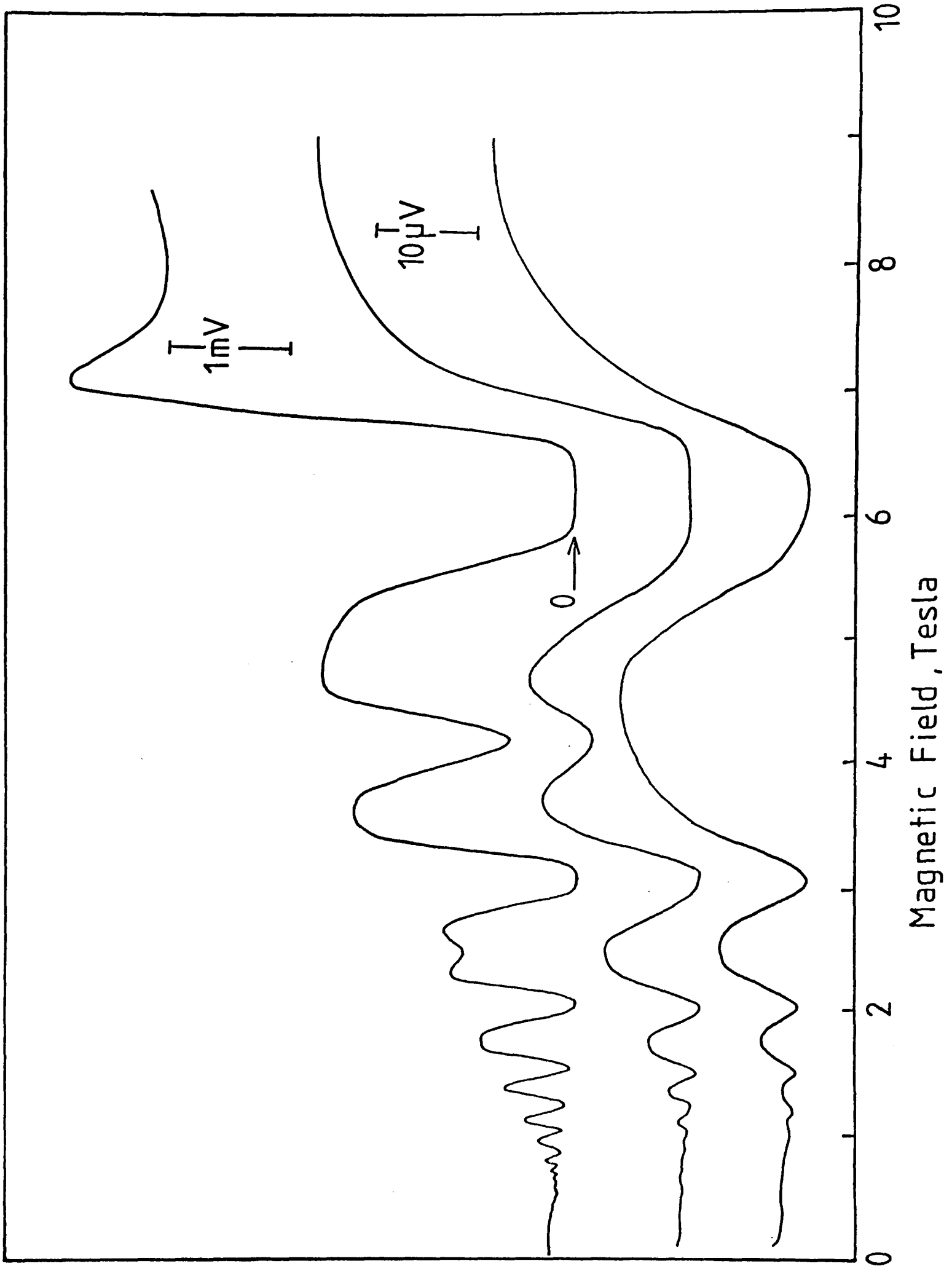


Figure 5·8f Sample 6311a, showing spin-split behaviour.

From top to bottom the curves are:

- Shubnikov - de Haas oscillations at 1·65K for I = 1 μA with the scale as shown for 1 mV.
- Thermovoltage V for $\Delta T = 0{\cdot}55K$ at $T_m = 2{\cdot}2K$
- Thermovoltage V for $\Delta T = 0{\cdot}45K$ at $T_m = 5{\cdot}2K$.

The thermovoltage curves have a common scale, as shown for 10 μV.

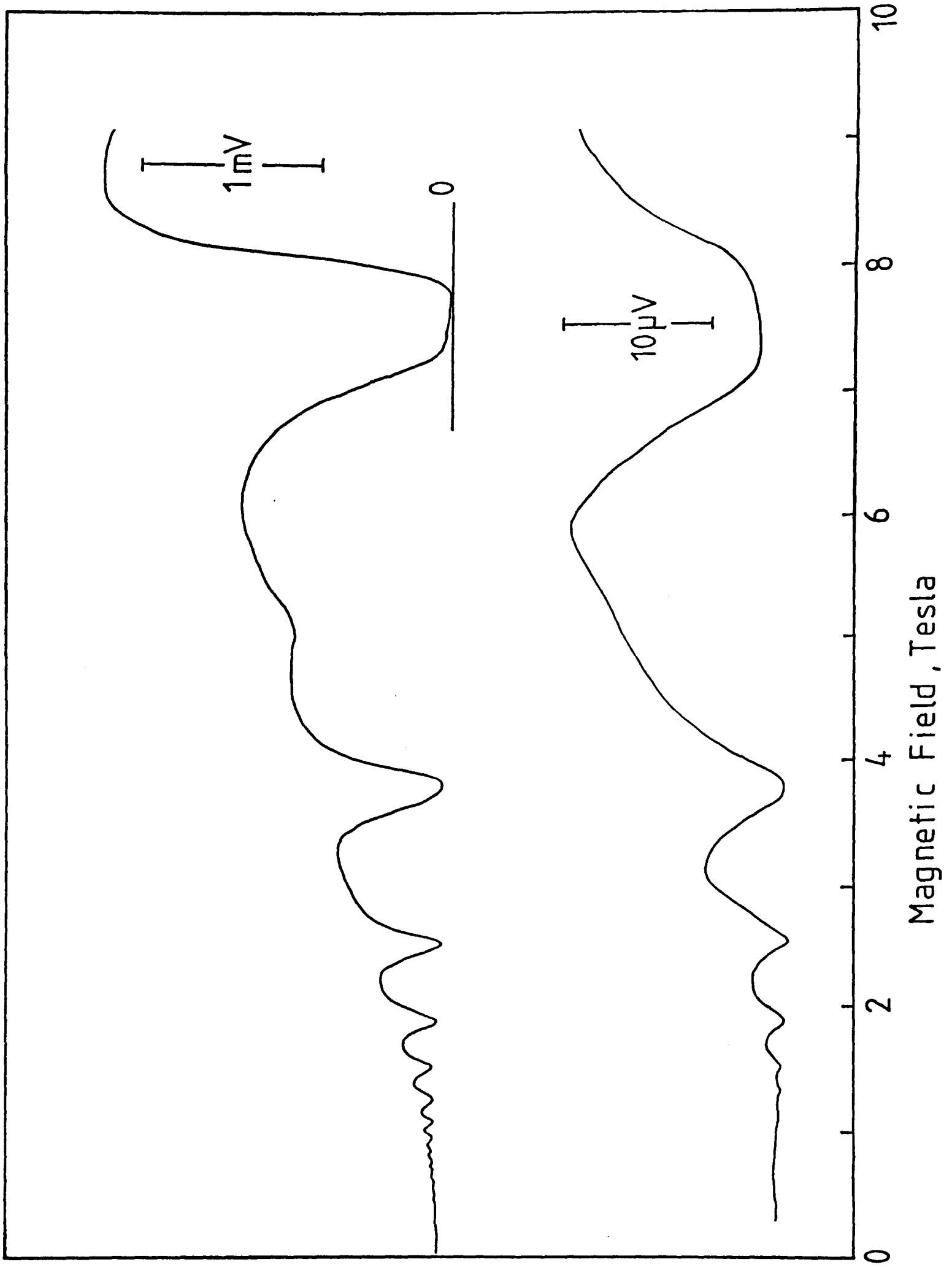


Figure 5·8g Sample 6311b

From top to bottom, the curves are:

- Shubnikov - de Haas oscillations at 4·2K for I = 1 μA, with the scale as shown for 1 mV.
- Thermovoltage V for $\Delta T = 0{\cdot}4K$ at $T_m = 4{\cdot}5K$, with the scale as shown for 10 μV.

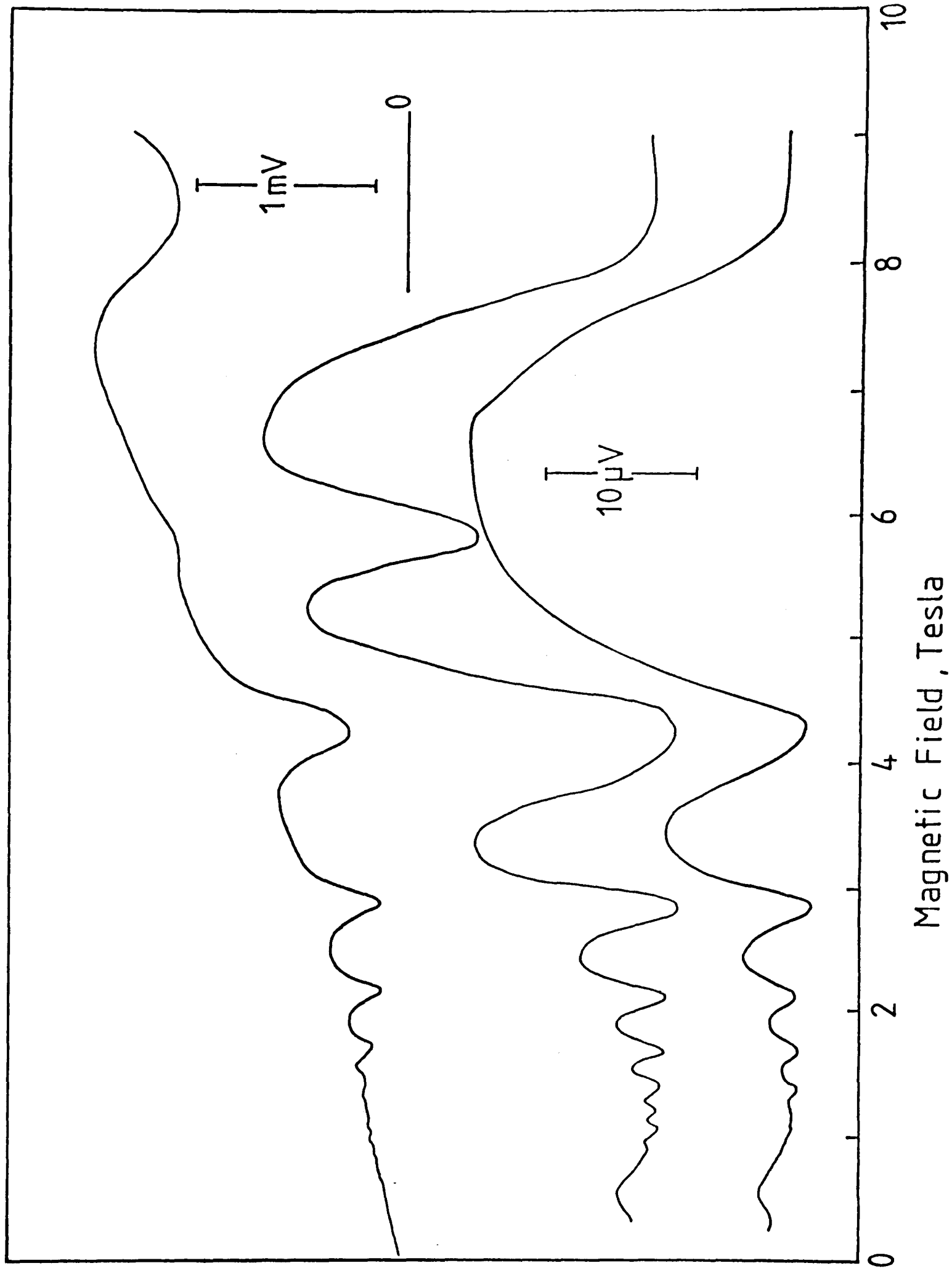


Figure 5·8h Sample 6311c, showing bulk conduction

From top to bottom, the curves are:

- Shubnikov - de Haas oscillations at 4·2K for I = 1 μA, with the scale as shown for 1 mV.
- Thermovoltage V for ΔT at 0·75K at T_m = 3·2K
- Thermovoltage V for ΔT at 0·8K at T_m = 4·9K.

The thermovoltage curves have a common scale as shown for 10 μV.

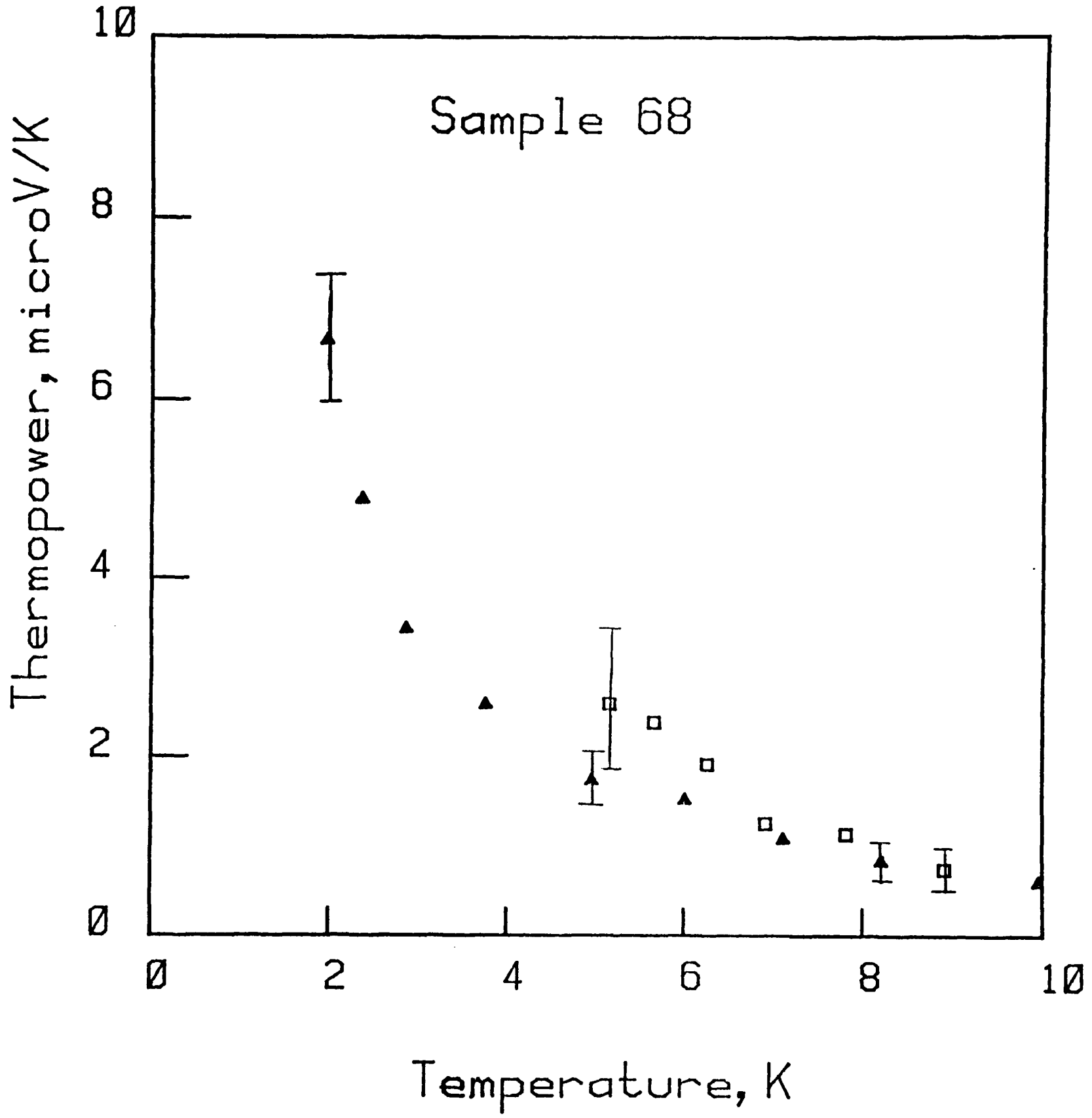


Figure 5·9a

Longitudinal thermopower α_{xx} as a function of the mean temperature T_m for sample 68, at filling factor of $2\frac{1}{2}$. Typical errors are indicated.

▲ Base temperature of 1·65K

□ Base temperature of 4·2K.

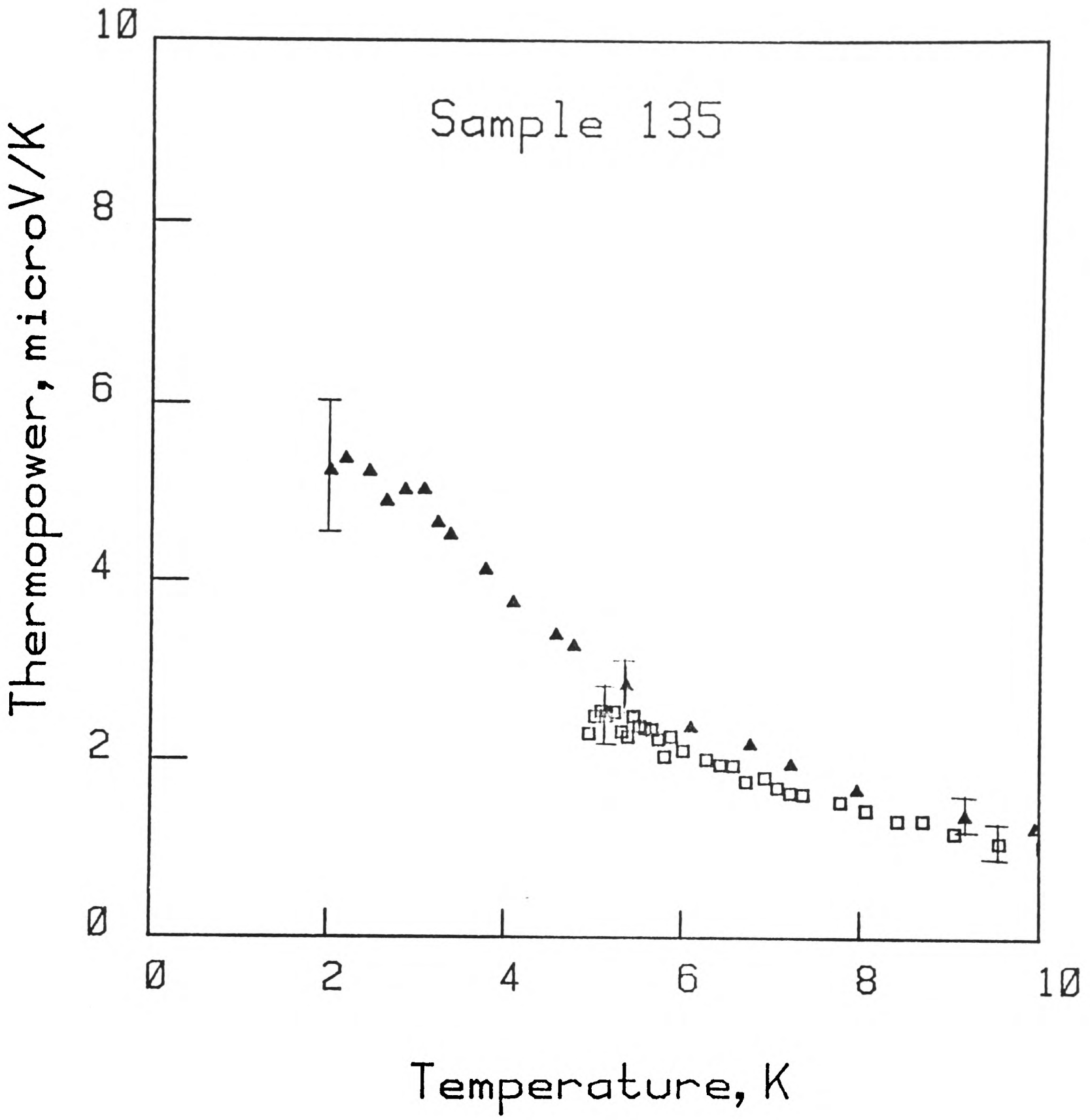


Figure 5·9b

α_{xx} versus T_m for sample 135, at filling factor $1\frac{1}{2}$.

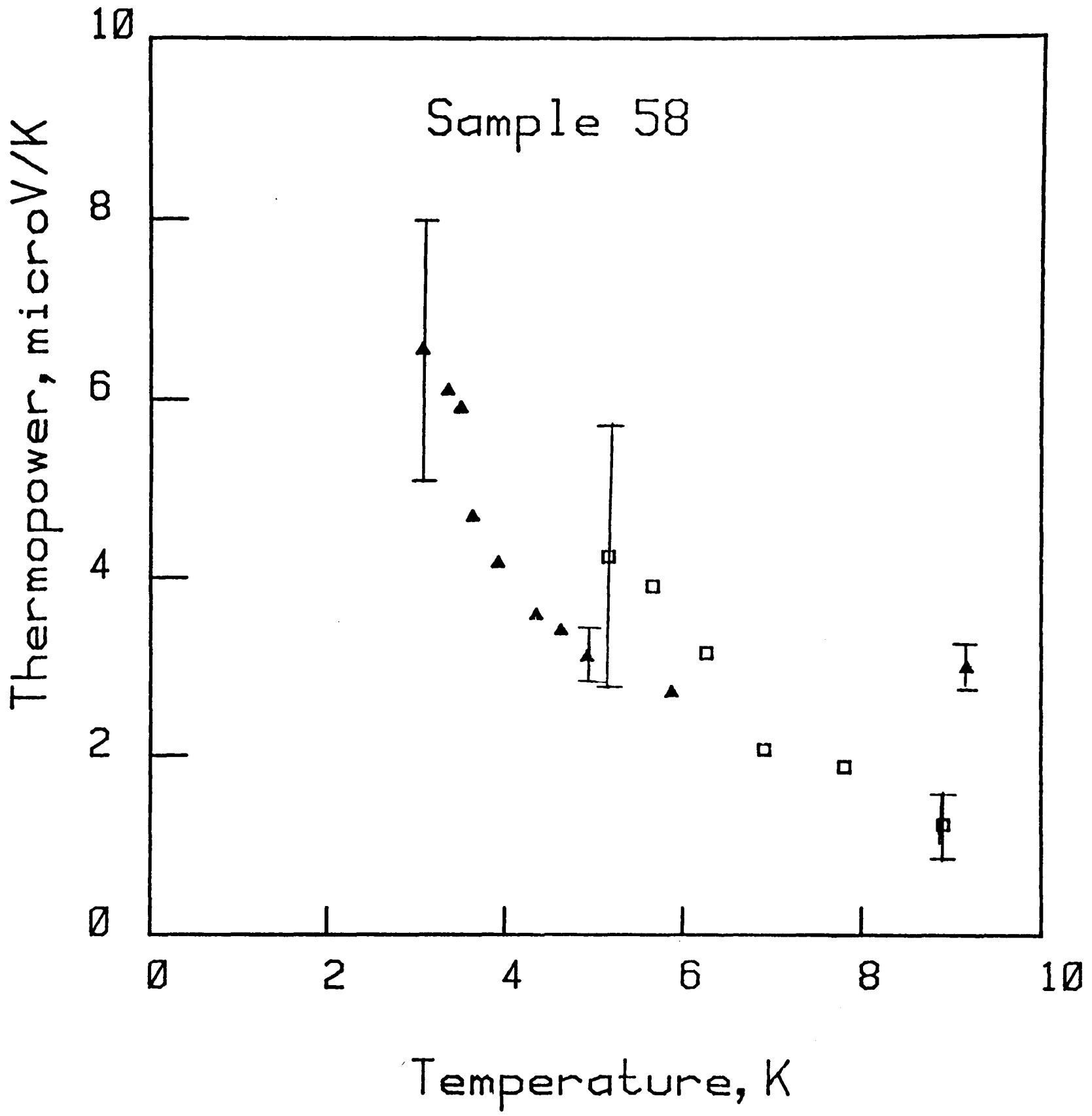


Figure 5·9c

α_{xx} versus T_m for sample 58, at filling factor $1\frac{1}{2}$.

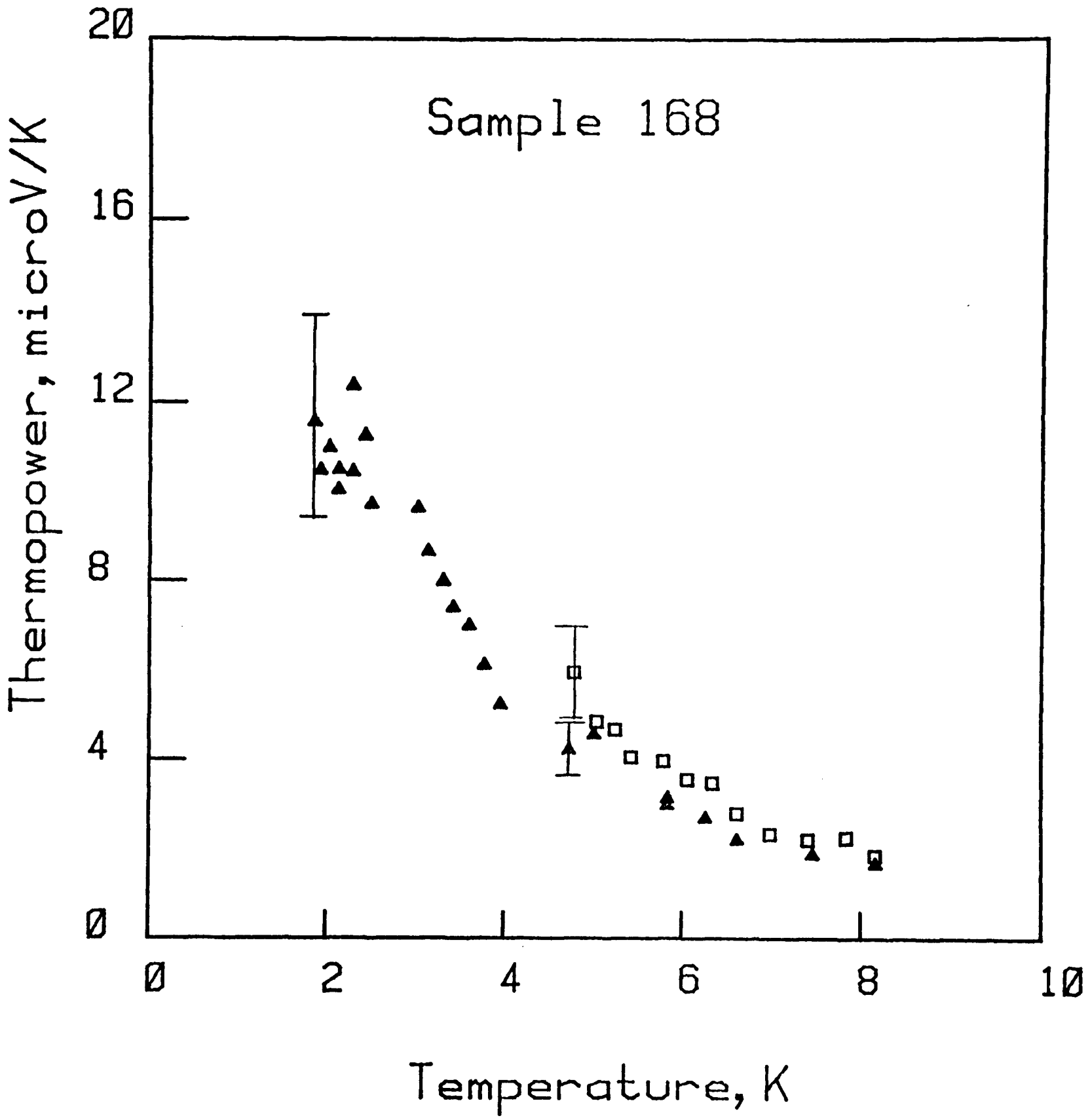


Figure 5·9d

α_{xx} versus T_m for sample 168, at filling factor $2\frac{1}{2}$.

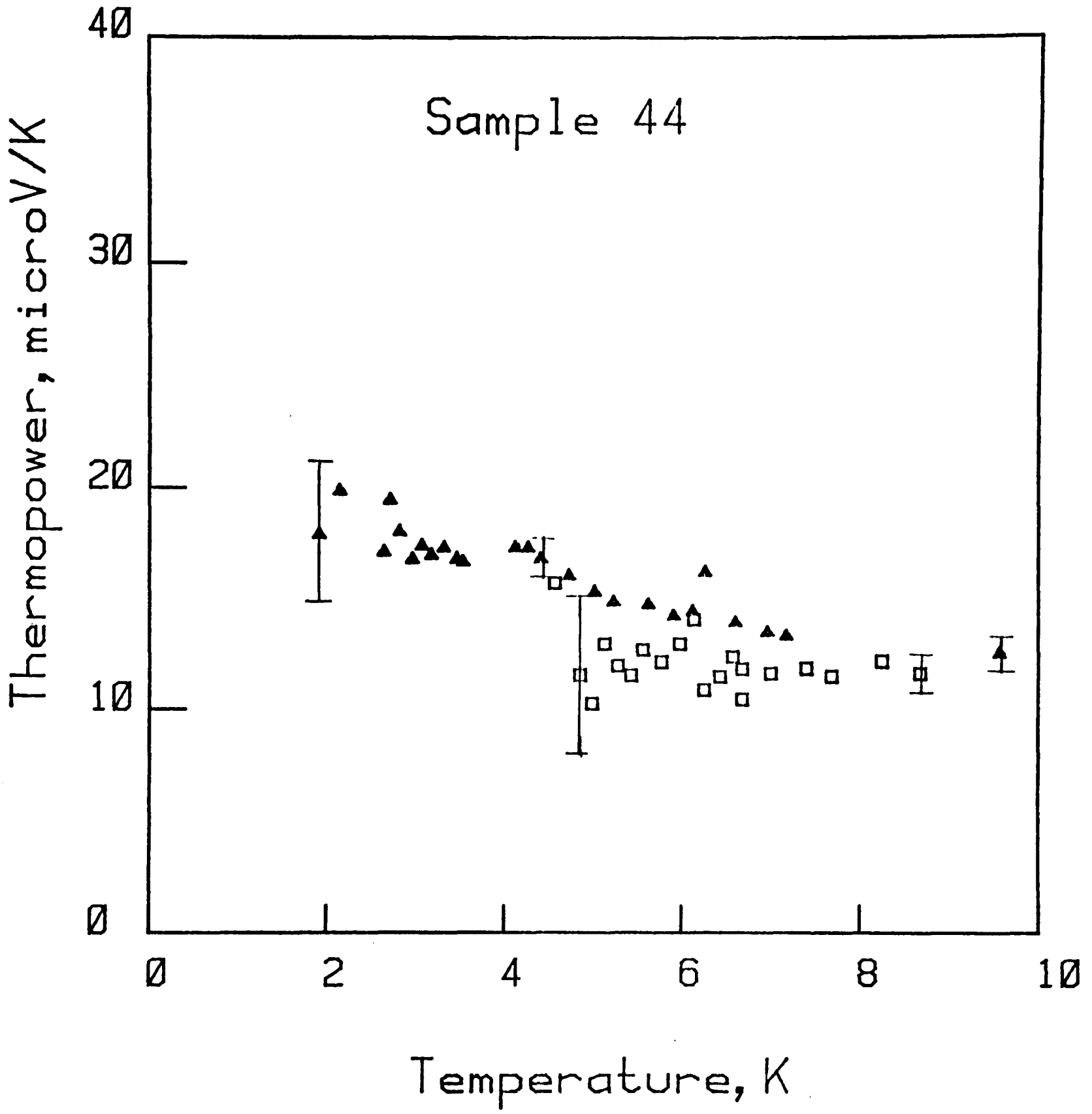


Figure 5·9e

α_{xx} versus T_m for sample MB44, at filling factor $3\frac{1}{2}$.

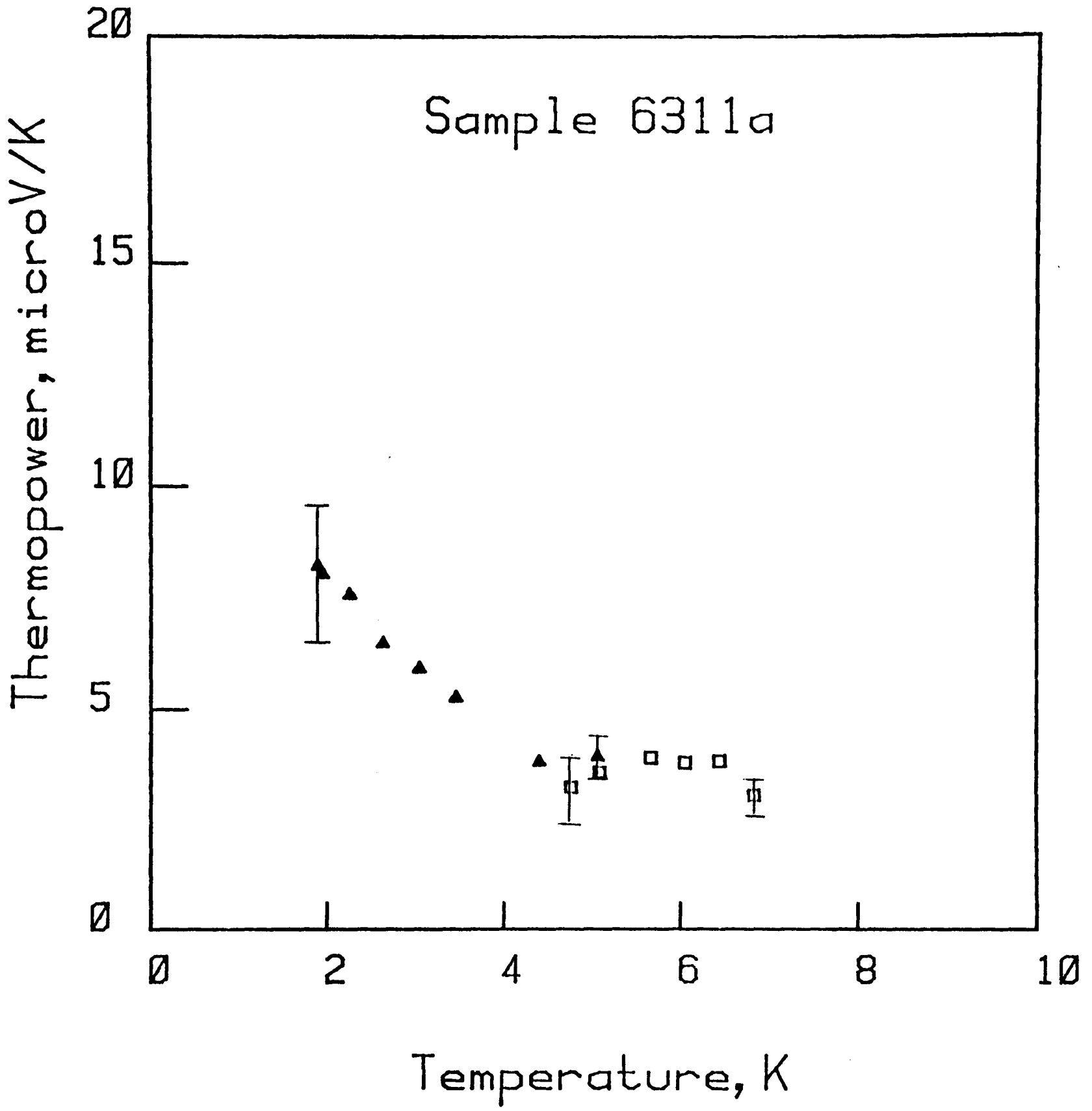


Figure 5·9f

α_{xx} versus T_m for sample 6311a, at filling factor $2\frac{1}{2}$.

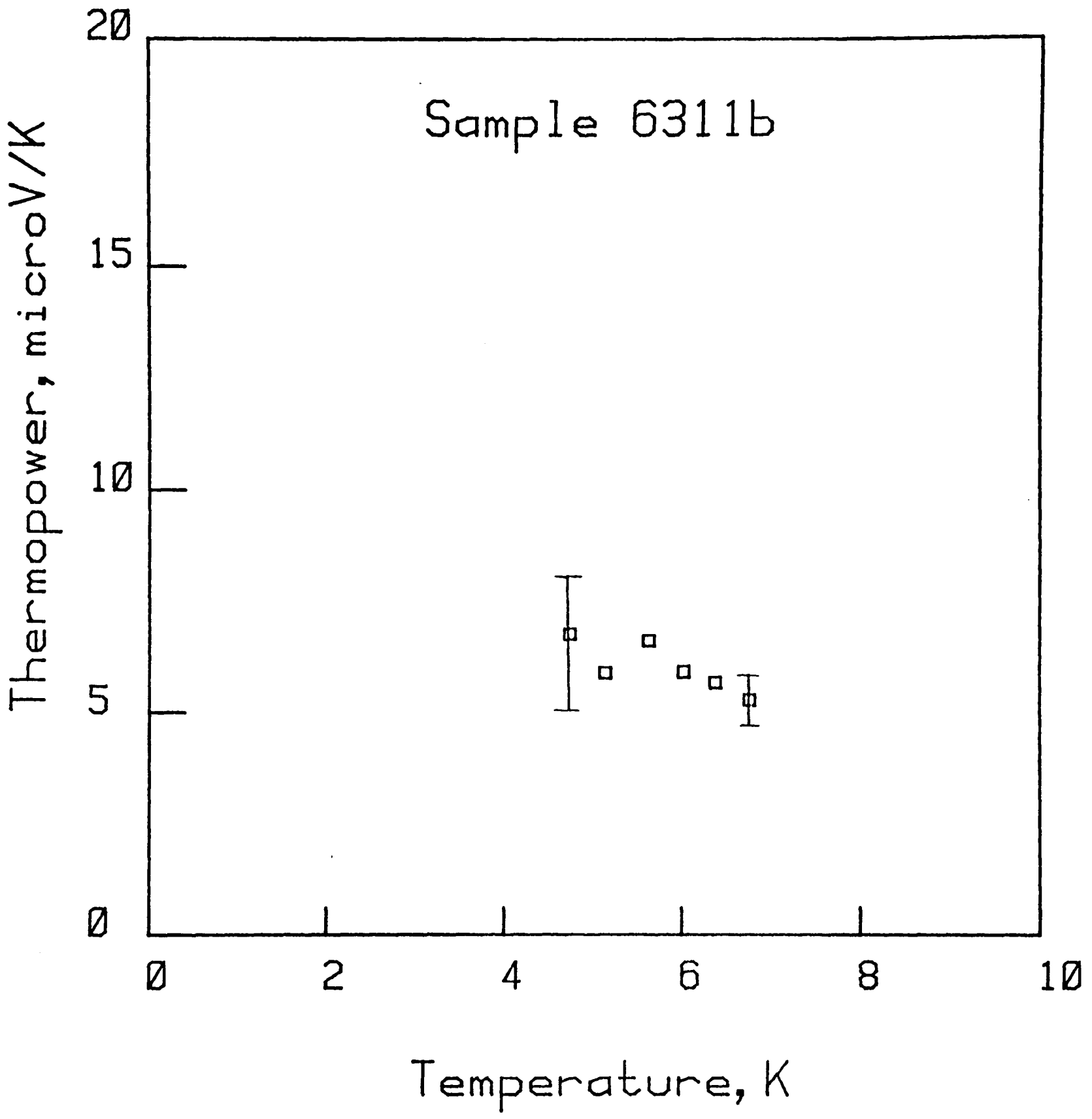


Figure 5·9g

α_{xx} versus T_m for sample 6311b, at filling factor $2\frac{1}{2}$.

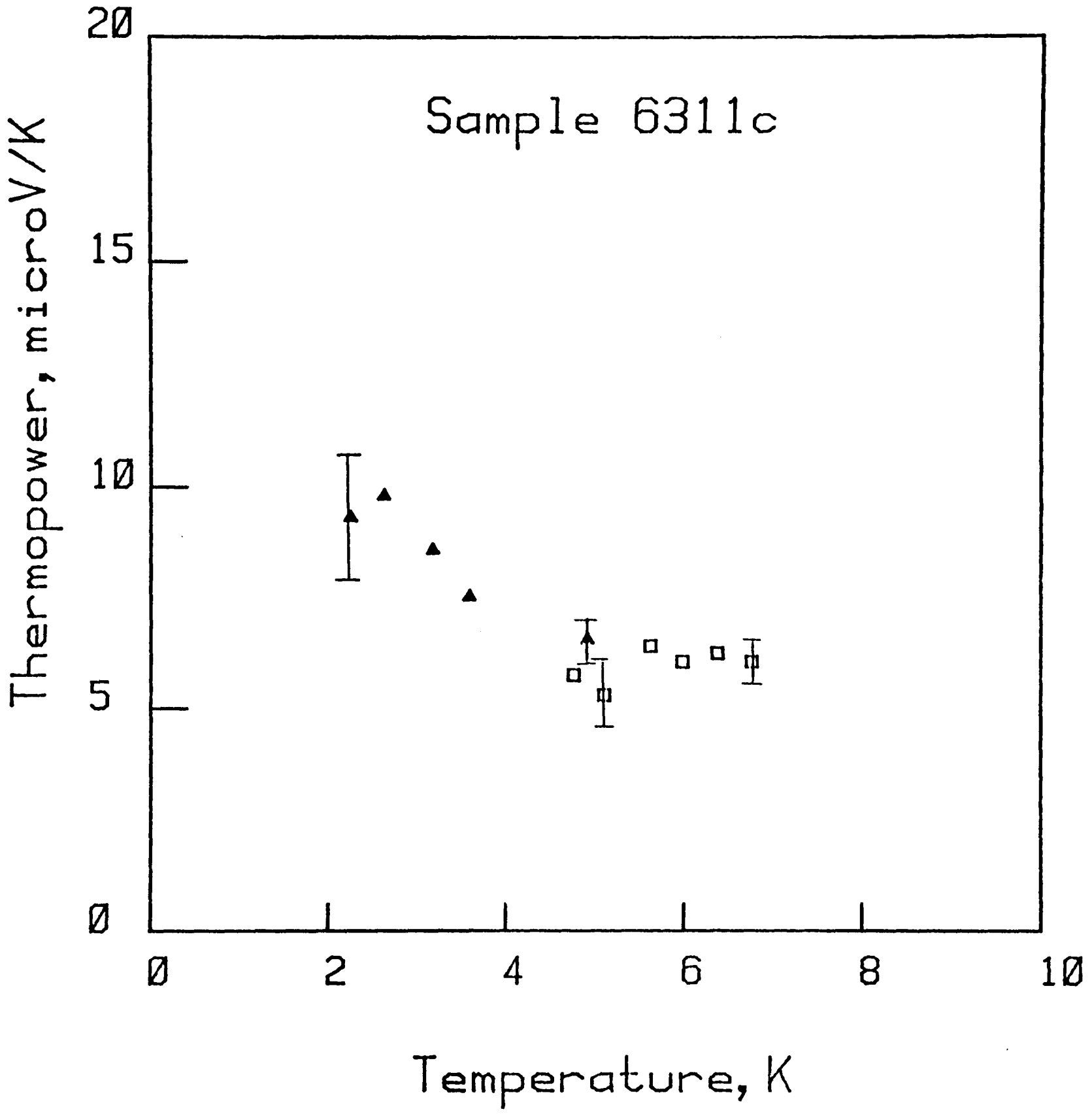


Figure 5·9h

α_{xx} versus T_m for sample 6311c, at filling factor $2\frac{1}{2}$.

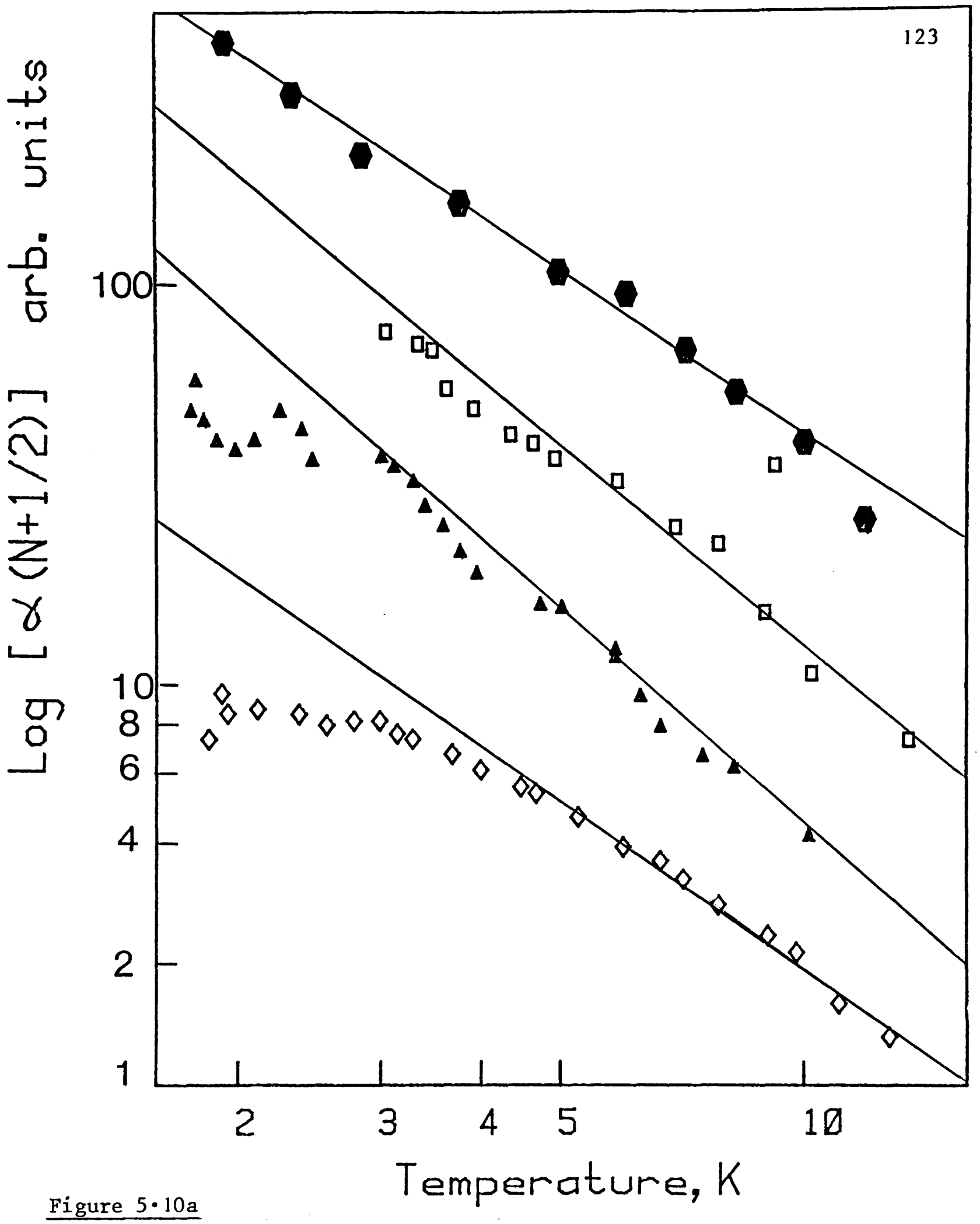


Figure 5·10a

Log $[\alpha_{xx}(N+\frac{1}{2})]$ versus log T_m for the GaInAs - InP and GaInAs - InAlAs systems.

The x-axis is common to all the curves; the y-axis is displaced for each curve. Table 5·4 gives the values of the data points and gradients of the curves.

From top to bottom, the results are for samples 68, 58, 168 and 135.

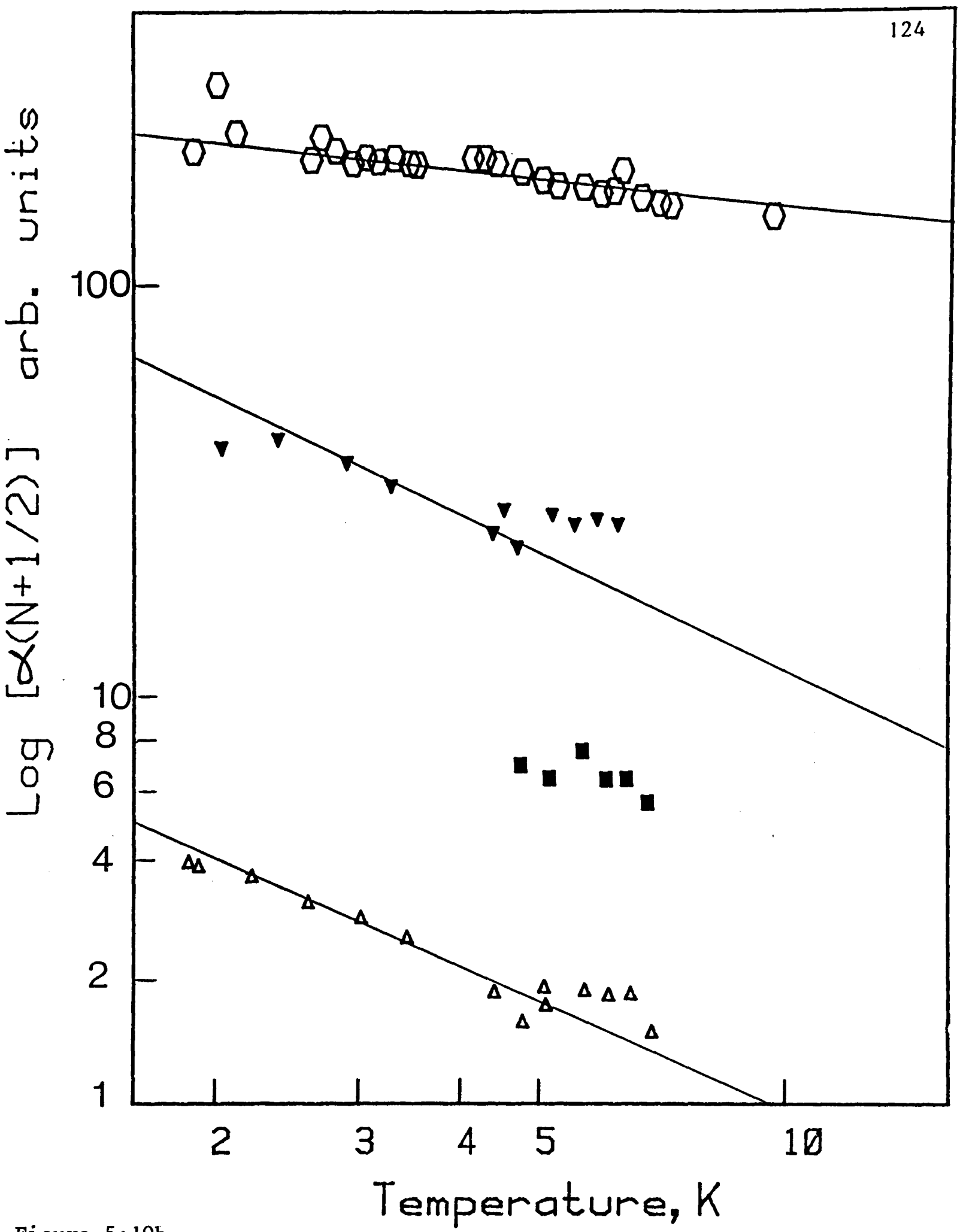


Figure 5·10b

Log $[\alpha_{xx}(N+\frac{1}{2})]$ versus log T_m for the GaAs - GaAlAs systems.

The x-axis is common to all curves; the y-axis is displaced for each curve, and has the same range as for figure 5·10a.

From top to bottom, the results are for samples MB44, 6311c, 6311b and 6311a.

Table 5·4

Peak values of thermopower in magnetic field

Sample	$N+\frac{1}{2}$	$[\alpha_{xx}(N+\frac{1}{2})] \times [N+\frac{1}{2}]$ in μV/K		c
		T_m = 3K	T_m = 8K	
68	$2\frac{1}{2}$	8·6 ± 1	2·4 ± 0·5	-1·38 ± 0·1
135	$1\frac{1}{2}$	7·2 ± 1·5	2·3 ± 0·5	-1·54 ± 0·1
58	$1\frac{1}{2}$	10 ± 3	3·6 ± 1·5	-1·7 ± 0·2
168	$2\frac{1}{2}$	22 ± 5	5·0 ± 0·5	-1·78 ± 0·2
MB44	$3\frac{1}{2}$	61 ± 15	50 ± 5	-0·1 ± 0·1
6311a	$2\frac{1}{2}$	15·5 ± 5	8·5 ± 2	-0·9 ± 0·2
6311b	$2\frac{1}{2}$	*	15 ± 3	*
6311c	$2\frac{1}{2}$	23 ± 6	16 ± 3	-1·0 ± 0·2

* no data in low temperature range

CHAPTER 6

The theory of thermopower in heterostructures

6·1 Introduction

The thermopower measurements on heterostructures, which were presented in chapter 5, are analysed in this chapter. Section 6·2 (a) presents the derivation of the expression for the thermopower of a degenerate carrier system in zero magnetic field, with special attention being paid to the assumptions normally made in this derivation. Comparisons are then given between the theory and the present results and other experimental works. Section 6·2 (b) briefly reviews the group of recent theoretical studies on the thermopower of the 2DEG in a magnetic field. These works predict peak values in the thermopower which approach a universal constant. Comparisons of these theories and experimental works are then made.

Many disagreements between the theoretical predictions and the present results are noted, both for the zero-field results and for the magnetic field results. These two types of measurements have quite different origins: the zero-field results are predicted by classical theory and depend on electron concentration, scattering rate etc., while the magnetic field results are predicted to be quantised, showing universal values. Therefore, in order to suggest reasons for the disagreement with the theories, the two types of measurements are examined together in section 6·3. The main discussion of the results is reserved for this part. The conclusion of this study of the thermopower is given in section 6·4.

6·2 The theory of the thermopower in the 2DEG

6·2a Thermopower in zero magnetic field

The thermopower α in zero magnetic field may be obtained from expressions of the transport coefficients σ and β, which can be derived from the Boltzmann equation. These coefficients are related by the phenomenological equation

$$\underline{j} = \sigma \underline{E} + \beta \underline{\nabla} T, \qquad (6\cdot1)$$

and the definition of the thermopower

$$\underline{E} = \alpha \underline{\nabla} T \quad ; \quad \underline{j} = 0 \ . \qquad (6\cdot2)$$

Thus

$$\alpha = -\beta/\sigma \qquad (6\cdot3)$$

In this treatment, isotropy is assumed.

The derivation of α for a degenerate carrier system may be found in standard texts. However, one contribution to α which is normally ignored is found to be important in this work. In the following, an outline of the derivation of α is given which follows the method given by Abrikosov (1972), but highlights this extra contribution and other assumptions used.

Assuming isotropy and elastic scattering, the Boltzmann equation can be written as:

$$\frac{\partial f}{\partial t} + \underline{v} \cdot \frac{\partial f}{\partial \underline{r}} + e\underline{E} \cdot \frac{\partial f}{\partial \underline{p}} = -\frac{f-f_0}{\tau} \qquad (6\cdot4)$$

where $f(\underline{p},\underline{r},t)$ is the distribution function and f_0 is its equilibrium value, and the other symbols have their usual meaning.

Assuming that the applied electric field $\underline{E}$ and thermal gradient $\underline{\nabla} T$ are small, so that

$$f = f_0 + f_1 \qquad \text{and} \qquad f_1 \ll f_0, \qquad (6\cdot5)$$

equation (6·4) can be rewritten for the steady-state condition as

$$\frac{\partial f_o}{\partial T} \underline{v} \nabla T \cdot \underline{v} + e \underline{E} \cdot \underline{v} \frac{\partial f_o}{\partial \xi} = - \frac{f_1}{\tau} \qquad (6\cdot6)$$

where $\xi = E \cong E_F$.

The term $\frac{\partial f_o}{\partial T}$ may be easily calculated from the Fermi-Dirac distribution f_o, giving

$$\frac{\partial f_o}{\partial T} = \cong \frac{\partial f_o}{\partial \xi} \left(\frac{\xi}{T} + \frac{dE_F}{dT} \right) \qquad (6\cdot7)$$

Normally, the second term in the brackets, $\frac{dE_F}{dT}$, is ignored. It is kept in this work, and gives rise to the extra contribution to α mentioned above.

The electric current is

$$\underline{j} = 2e \int \underline{v} f_1 \, d\xi \qquad (6\cdot8)$$

Substituting in equations (6·6) and (6·7) gives

$$\underline{j} = - e^2 C_D E \int v^2 \tau g(E) \frac{\partial f_o}{\partial \xi} d\xi + e C_D \nabla T \int v^2 \tau g(E) \left[\frac{\xi}{T} + \frac{dE_F}{dT} \right] \frac{\partial f_o}{\partial \xi} d\xi \qquad (6\cdot9)$$

where g(E) is the density of states, and C_D is a constant coming from the integration over all angles, $C_D = {}^1/_3$ for 3-D systems and $C_D = {}^1/_2$ for 2-D systems.

For a degenerate carrier system, $\frac{\partial f_o}{\partial \xi}$ is non-zero only near to $\xi = 0$. Therefore, assuming that the other functions in the integrands are slowly varying with respect to $\frac{\partial f_o}{\partial \xi}$ near to $\xi = 0$, and by comparing equation (6·9) with equation (6·1), one obtains

$$\sigma = C_D e^2 (v^2 \tau g)_{E_F} \qquad (6\cdot10)$$

and

$$\beta = - C_D \left[\frac{\pi^2}{3} e T \frac{d}{dE_F} (v^2 \tau g)_{E_F} + e \frac{dE_F}{dT} (v^2 \tau g)_{E_F} \right] \qquad (6\cdot11)$$

Therefore, the thermopower for a degenerate carrier system in 2D or in 3D is

$$\alpha = -\beta/\sigma$$

$$= \frac{\pi^2}{3}\frac{T}{e}\frac{d}{dE_F}\left[\ell n\ \sigma\right]_{E_F} + \frac{1}{e}\frac{dE_F}{dT} \quad . \qquad (6\cdot12)$$

The first term in equation (6·12) is the expression normally quoted for α, for a metallic system. The second term has a simple physical interpretation. It arises from the temperature dependence of the Fermi level, which is normally ignored. A change in the Fermi level ΔE_F would give rise to a voltage $\Delta E_F/e$ and hence a thermopower of $\frac{1}{e}\frac{\Delta E_F}{\Delta T}$. In the following, the first term in equation (6·12) is denoted by α_0 and the second α_1.

In order to predict values for α_0, the scattering rate is assumed to have energy dependence $\tau \propto (E - E_i)^p$ where E_i is the bottom of either the conduction band for the case of a metal, or of the subband for a heterostructure. Since in a 2-D degenerate system, $n(E) \propto (E - E_i)$,

$$\alpha_0 = \frac{\pi^2}{3}\frac{k^2T}{e}\frac{(p+1)}{E_F - E_i} \quad . \qquad (6\cdot13)$$

For the GaAs - GaAlAs system, it is probable that at low temperature remote ionised impurity scattering is the dominant scattering mechanism (Lin et al. 1984, who studied a heterojunction with comparable mobility to the one used here). This would give $p \approx 1\cdot5$ (Drummond et al. 1981). For the less studied systems of GaInAs - InP and GaInAs - InAlAs, it is not clear which scattering mechanisms dominate. In these systems, there is in addition to the impurity scattering mechanisms present in GaAs - GaAlAs alloy scattering in the channel material. Bastard (1984) calculated that

alloy scattering would give mobilities of $\gtrsim$ 150,000 $cm^2\ V^{-1}\ s^{-1}$, with a dependence on the electron concentration, and therefore on $(E - E_i)$ also, of $p \approx -0{\cdot}4$. However, the samples used here have mobilities ~ 30,000 $cm^2\ V^{-1}\ s^{-1}$ for the GaInAs - InP heterojunctions. These values are much lower than the values predicted for alloy scattering. In addition, the mobility of the samples studied increases with n, rather than decreasing as would be the case for alloy scattering. Thus, it seems likely that in these GaInAs - InP heterojunctions, alloy scattering is not dominant. The GaInAs - InAlAs heterojunction has a higher mobility of 88,000 $cm^2\ V^{-1}\ s^{-1}$. This is still about half of the value predicted by Bastard for alloy scattering for the concentration n involved. (The predicted values are calculated for the GaInAs - InP system, but should not be very different for the GaInAs - InAlAs system, since it is alloy scattering in the GaInAs which is considered). Therefore, for want of more accurate information, p is taken to be 1·5 for the GaInAs - InP and GaInAs - InAlAs, as well as for the GaAs - GaAlAs. This is in rough agreement with the observed values of n and μ for the two former systems.

The values of α_0 calculated with $p = 1{\cdot}5$ are given in table 5·3. As the above discussion indicates, the values of α_0 for the GaInAs - InP and GaInAs - AlInAs may be in error by ~ 50%, and are meant to be guidelines only.

Before comparing the calculated values of α_0 with the experimental results, it should be mentioned that the interaction effect and the localisation effect which give logarithmic corrections to σ for a 2DEG are negligible here. Ting et al. (1982) showed that for the thermopower, the interaction effect leads to a logarithmic correction but there is no correction due to the localisation effect. The former effect leads to a fractional correction to α which is $\leq 0{\cdot}02\ (1 - {}^3/_2\ F)$

for the samples studied, where F is between 0 and 1. This is smaller than the experimental errors and can therefore be ignored.

Table 5•3 shows that there are serious disagreements between the theoretical predictions for α_0 and the measured values. Firstly, even allowing for the uncertainty in the value of p and the experimental errors, the thermopower measured for all the heterojunctions is below the theoretical value. In contrast, the thermopower of sample MB44 which is a superlattice is larger than that predicted at low temperatures. Secondly, none of the heterostructures shows the T^{+1} dependence of α_0. Both the superlattice and the heterojunctions of the GaAs - GaAlAs system show a T^0 dependence, while the GaInAs - InP and GaInAs- InAlAs heterojunctions all show an approximate T^{-1} behaviour. Thus, the temperature dependence of α is observed to be common to all the samples of each system but to differ from one system to another. Therefore, it is probable that the present disagreement with theory is due to the inherent characteristics of the system studied, rather than a systematic experimental error or sample peculiarities. Lastly, the electron concentration dependence of α_0 is also in contradiction with the theory. Comparison between the samples 6311a, b and c shows this clearly. These are physically the same sample, but with the electron concentration n changed by the persistent photoconductivity effect. The illumination changes the value of n, by changing the ionisation in the barrier. For a constant energy dependence of the scattering rate, as found experimentally (Störmer et al. 1981), the thermopower α_0 scales with n^{-1}. This is in complete contrast with experimental observations of α, which increase with n. Before suggested reasons for these disagreements with theory are given, the theory and measurements in magnetic field are examined in section 6•3.

Measurements of α have also been carried out by Gibbings and Pepper (1985) on silicon inversion-layers. The electron concentration was

varied by means of the gate voltage so that the system passed from the metallic conduction regime of a 2DEG to activated conduction. In the metallic regime, their results agree with the expression for α_o. In the activated conduction regime, Gibbings and Pepper observed that α increases with decreasing T. This is consistent with the calculations of Cutler and Mott (1969) for activated conduction to mobility edge E_c

$$\alpha = \frac{k}{e}\left[\frac{E_c - E_F}{kT} + 1\right], \qquad (6\cdot14)$$

neglecting terms in $(kT\,\frac{d\ell n\sigma}{dE})$ inside the brackets, and assuming $kT << E_c - E_F$.

6·2b Thermopower in a quantising magnetic field

Following the discovery of the Quantum Hall Effect (QHE) and the theoretical works which explain this effect's precise quantisation, there have been recently many theoretical studies which predict the behaviour of the thermopower under the same conditions as those necessary for the observation of the QHE: that of strong magnetic field and of low temperature in a 2D degenerate carrier system. These thermopower studies have two main purposes. Firstly, because of the probability of the QHE being used as a standard resistance, calculations of the possible errors must be made. One source of error is a spurious thermovoltage, so that the magnitude of $\underline{\alpha}$ must be known. Secondly, within certain limits for small Landau level broadening, the thermopower should show quantised values of universal constants, similar to the behaviour of the QHE, because the thermopower depends only on the density of states. Thus, the behaviour of $\underline{\alpha}$ versus $(E_F/\hbar\omega_c)$ is intrinsically interesting.

The theoretical studies of the thermopower have all reached the same general conclusions. However, their different approaches give different physical insights to the problem. In the following, some of the recent theoretical works are referred to, together with the special points they raise.

The first works to predict the quantisation of α_{xx} were by Zelenin et al. (1982) and Girvin and Jonson (1982). Zelenin et al. started from the thermodynamic potential and calculated the thermopower component α_{xx} from

$$\alpha_{xx} = \frac{S}{eN} \qquad (6\cdot15)$$

where S and N are the local bulk entropy density and particle density. Equation (6·15) is valid whether the electron scattering is taken into

account or not, if $kT/\Gamma > 1$ where 2Γ is the width of the Landau level (Oji 1984c). Zelenin et al. found that for a size-quantised film, α_{xx} reaches a maximum when a level is half-filled i.e. when the filling factor ν is $N + \frac{1}{2}$ (Zelenin et al. assumed $\nu \approx N$ but the correct expression is $\nu = N + \frac{1}{2}$ for a half-filled band). This maximum is, for $\Gamma << kT << \hbar\omega_c$

$$\alpha_{xx} \approx \frac{k}{e} \ln 2 \frac{1}{N + \frac{1}{2}} , \qquad (6\cdot16)$$

the approximation is due to the level broadening having been ignored. Zelenin et al. pointed out that these peak values are much larger than the value for the thermopower of a bulk sample in the same B-field because, at low temperatures, a narrow energy subband is equivalent to a degenerate energy level, for which the entropy is independent of temperature. From this, we can deduce that inclusion of the broadening of the level would reduce α_{xx} from the value given in equation (6·16).

Girvin and Jonson (1982) used the concept of edge currents in skipping orbits to calculate the transport response functions, and obtained $\underline{\alpha}$ from the ratio of the transport coefficients (see equation (6·3)). They obtained peak values of α_{xx} as given in equation (6·16). In addition, they predicted that minima in α_{xx}, which occur when the chemical potential lies between two levels, are thermally activated with an activation energy of $\sim \hbar\omega_c$. Therefore, errors from thermovoltages should be exponentially small at the centre of the Hall step at low temperatures.

Streda (1984) supported the work of Girvin and Jonson (1982) by demonstrating that surface effects (i.e. edge currents) are the sole contributor to α_{xx}.

Jonson and Girvin (1984) derived $\underline{\alpha}$ in a more general way, by using the Kubo formalism. They made the point that the familiar expression

$$\bar{L}_{ij} = \text{Re} \lim_{w \to 0} \bar{L}_{ij} (w + i\delta), \qquad (6\cdot17)$$

where L_{ij}'s are the transport response functions, is inapplicable in the presence of a magnetic field for the purpose of calculating the thermal reponse tensor L_{12}. The reason is that an extra 'diathermal' current is set up, which is analogous to the diamagnetic currents, and this diathermal current has non-zero expectation value in the presence of a magnetic field.

Jonson and Girvin treated the effect of the level broadening quantitatively. They gave several plots of α_{xx} and α_{xy} as a function of the reduced chemical potential $\mu/\hbar\omega_c$, for various values of the disorder parameter σ. One of these plots is reproduced in figure 6·1. The main point of note here is that the peak values of α_{xx} fall to half of its disorder-free values given in equation (6·16) for $\hbar\sigma = 0{\cdot}15\ \hbar\omega_c$. For this degree of disorder, the peaks of α_{xx} develop an apparent splitting as a function of the reduced chemical potential, in place of the single peaks at filling factor $(N + \frac{1}{2})$ predicted in the case of small or no disorder. These splittings become relatively more pronounced the larger the filling factor. The second point of note is that the non-diagonal component α_{xy} increases with the disorder. This agrees with Streda (1984), who predicted that $\alpha_{xy} \propto \Gamma/kT$. Oji (1984b) also showed that when the disorder is taken into account fully, an asymmetry is developed between the positive and negative peaks of α_{xy}.

Zawadzki and Lassnig (1984) also considered the effect of the level broadening on α_{xx}. The density of states of the Landau levels, g(E), was taken to be a sum of Gaussian peaks

$$g(E) = \frac{2}{2\pi L^2} \sum_N \sqrt{\frac{2}{\pi}} \frac{1}{\Gamma} \exp\left[-2\left(\frac{E - (N+\frac{1}{2})\hbar\omega_c}{\Gamma}\right)^2\right] \qquad (6\cdot18)$$

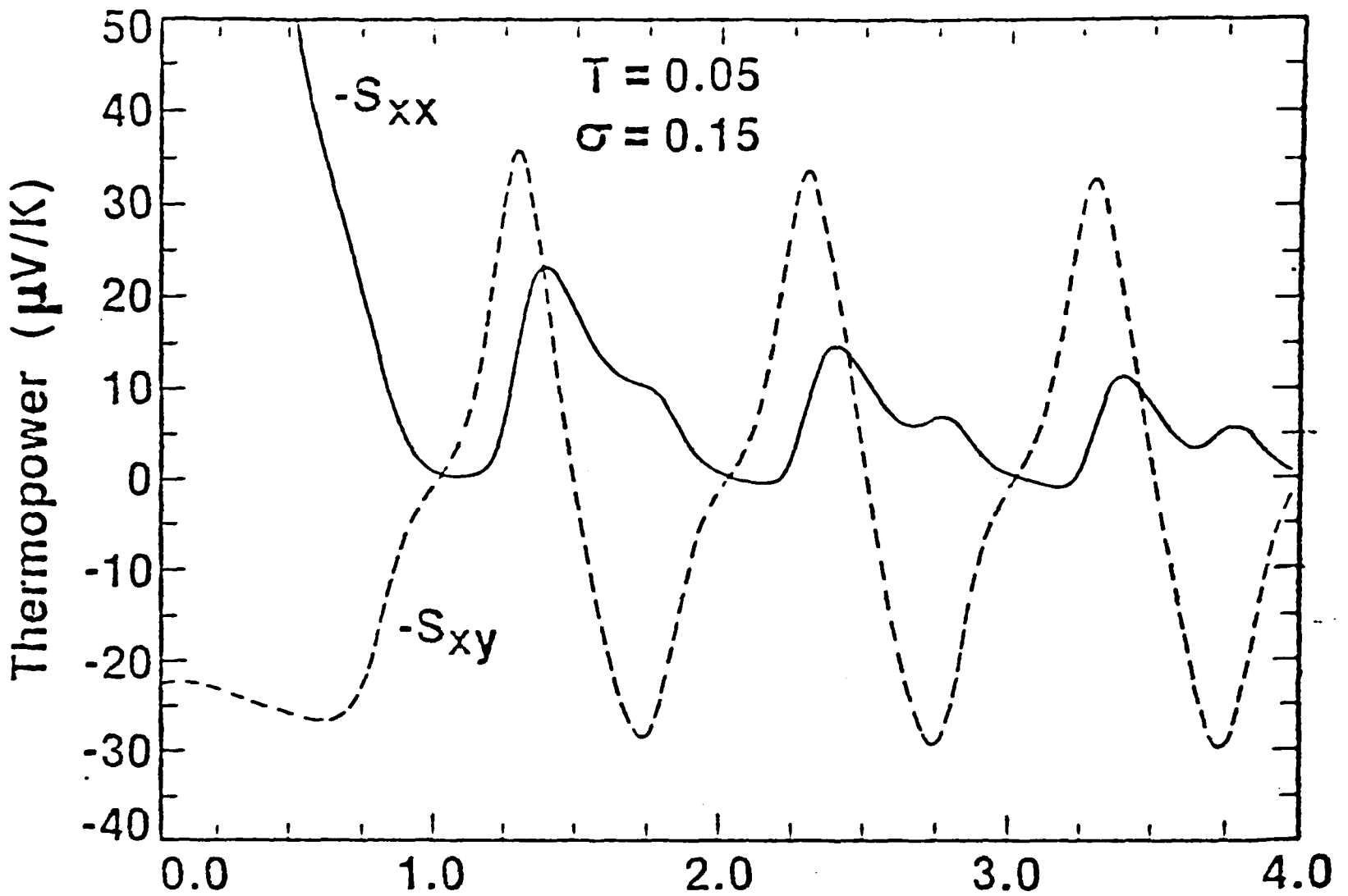


Figure 6·1

Diagonal and off-diagonal components of the thermopower tensor versus chemical potential in units where $\hbar\omega_c = 1$, $kT = 0{\cdot}05$ and $\hbar\sigma = 0{\cdot}15$.

Reproduced from Jonson and Girvin (1984).

where the broadening parameter Γ is assumed to be independent of the value of the magnetic field.

In the limit of high field ($\omega_c\tau >> 1$, $\hbar\omega_c >> kT$, and $\hbar\omega_c >> \Gamma$) α_{xx} was calculated to be zero for $\nu = N$, and to have peak values for $\nu = N + \frac{1}{2}$. These peak values are smaller than those predicted by equation (6·16) by a factor g_α which is a function of (kT/Γ). The plot of g_α versus (kT/Γ) is reproduced in figure 6·2. In the limit of $(kT/\Gamma) \to \infty$, $g_\alpha \to 1$. At weaker magnetic fields, if the temperature is not too low, inter-Landau-level transitions are possible. These cause the minima in α_{xx} at $\nu = N$ to deviate from zero.

Finally, Oji (1984a) considered the spin-splitting. In the limit of $\Gamma << kT << \hbar\omega_c$, the spin-split peaks tend to the universal values of

$$\alpha_{xx}\,(N + \tfrac{1}{2},\ \sigma) \;=\; \frac{k}{e}\,\ell n\ 2\,\frac{1}{2[N + \tfrac{1}{2}] + \sigma/2} \qquad (6\cdot19)$$

where $\sigma = \pm 1$ is the spin quantum number.

The experimental study of Obloh et al. (1984) on GaAs - GaAlAs heterostructures supports these theoretical predictions. The two samples studied by them with mobilities $\mu \geq 41{,}000\ cm^2\ V^{-1}\ s^{-1}$ give values of α_{xx} which are close to the predicted universal values for $1{\cdot}5K < T < 5K$. A third sample with mobility of $24{,}000\ cm^2\ V^{-1}\ s^{-1}$ shows a decrease of $\alpha_{xx}\,(1 + \frac{1}{2})$ with temperature, in qualitative agreement with the calculations of Zawadzki and Lassnig (1984). This lower mobility sample, which presumably has a larger level broadening, also shows α_{xy} with the oscillatory structure as predicted. On the other hand, some recent measurements by Obloh et al. have yielded values of α_{xx} of ~ 100 μV/K, rather than the predicted 40 μV/K. The cause for this is not known (von Klitzing, private communication).

As seen in section 5·5, measurements in this work show that the dependence of α_{xx} on the filling factor for all samples studied agree with the predictions of the above theories. Peaks in the value of α_{xx}

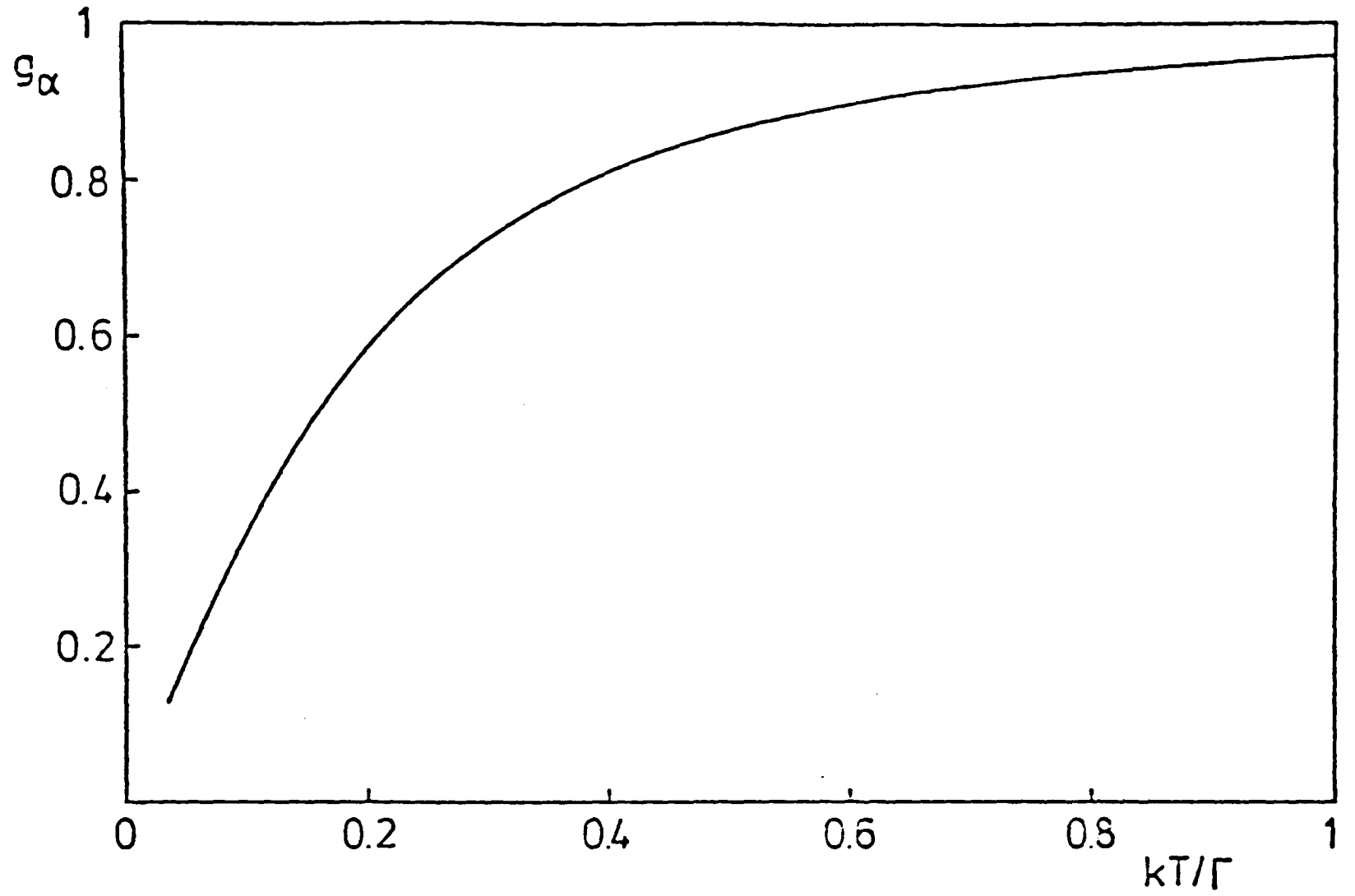


Figure 6·2

g_α plotted as a function of kT/Γ, where $g_\alpha = \alpha(N+\frac{1}{2}) \; / \; \{(k/e)\ell n2[N+\frac{1}{2}]^{-1}\}$.

Reproduced from Zawadzki and Lassnig (1984).

occur when the Landau levels are half-filled. This is observed even for the case of two-subband occupation and for the case of spin-split levels. At the centre of the Hall steps, α_{xx} falls to zero for large values of the magnetic field, as predicted. At weaker magnetic field, the minima of α_{xx} deviate from zero. This can be explained as being due to contribution from interlevel transitions (Jonson and Girvin 1984, Zawadzki and Lassnig 1984), and also because $\Gamma/\hbar\omega_c$ is large at low magnetic field. The peak values at different factors scale with $[N + \frac{1}{2}]^{-1}$, in qualitative agreement with equation (6·16).

Quantitatively, the results for the GaAs - GaAlAs superlattice, sample MB44, agree with equation (6·16) both in the magnitude of $\alpha_{xx}(N+\frac{1}{2})$ and in the fact that this values is, within experimental errors, constant with temperature. In contrast, the heterojunctions of all three systems studied give values of $\alpha_{xx}(N+\frac{1}{2})$ which are much lower than the values predicted by equation (6·16). Furthermore, $\alpha_{xx}(N+\frac{1}{2})$ for the heterojunctions increases with decreasing temperature, rather than remaining constant. Theory predicts that the product $[\alpha_{xx}(N+\frac{1}{2})] \times [N+\frac{1}{2}]$ would fall below the universal constant k/e ℓn 2 for large broadening Γ of the Landau level. From Cyclotron Resonance studies, Γ can be estimated. For the GaInAs - InAlAs heterojunction, Γ ~ 10K from C.R. at 4·35T (Portal et al. 1982). For the GaInAs - InP heterojunctions studied here, no C.R. results are available, but results on a number of similar GaInAs - InP heterojunctions grown in similar conditions also give Γ ~ 10K (Brummell et al. 1984). There are no C.R. results for the GaAs - GaAlAs sample, but measurements in comparable material (Schlesinger et al. 1984) indicate a value of Γ of order 1K. Thus, in the range of temperature of the recorded results, $3K \leq T \leq 10K$, the condition $0{\cdot}3 < kT/\Gamma \lesssim 10$ exists for the heterojunctions studied. From the work of Zawadzki and Lassnig (1984), referring to the plot reproduced in figure 6·2, the GaInAs - InP and

GaInAs - InAlAs heterojunctions are predicted to show values of $[\alpha_{xx}(N+\frac{1}{2})] \times [N+\frac{1}{2}]$ which are smaller than the universal constant by a factor g_α, where g_α is 0·96 at 10K and decreases with decreasing temperature to ~ 0·75 at 3K. For the GaAs = GaAlAs heterojunction, $g_\alpha(T)$ should be close to 1. Experimentally, g_α at 10K and at 3K is approximately 0·05 and 0·1 respectively for the GaInAs = InP heterojunctions, 0·08 and 0·4 for the GaInAs = InAlAs heterojunction, and 0·25 and 0·3 for the GaAs = GaAlAs heterojunctions. These values of the observed g_α are lower than those predicted by considering kT/Γ. Furthermore, the experimental values increase with decreasing temperature, rather than decreasing as would be expected from the theory of Zawadzki and Lassnig. It seems probable that there is a mechanism not yet considered which is responsible both for the low values of g_α and for its temperature dependence, which masks the dependence of g_α on kT/Γ. It is to be noted that the largest g_α's recorded are still smaller than the values estimated from the plot of Zawadzki and Lassnig, and thus it is possible that the dependence of g_α on kT/Γ is as predicted, although this dependence has been masked.

The predictions of Jonson and Girvin (1984) on the effect of disorder on α_{xx} are not borne out by the present observations. For a given amount of disorder σ, the ratio $\bar{n}\sigma/\bar{n}\omega_c$ is large for oscillations in α_{xx} at low magnetic field. Therefore, the theory predicts that the peaks in α_{xx} should split at low magnetic field (see figure 6·1). This was not observed. Instead, α_{xx} is seen to have simple peaks at $(N+\frac{1}{2})$ at low field (see figure 5·8d in particular) and to spin split at high field.

The spin-splittings shown by samples 6311a, b, and c at low temperatures (figures 5·8f, 5·8g, and 5·8h) agree qualitatively with Oji's prediction of equation (6·19): the $\sigma = -1$ peaks are indeed larger than the $\sigma = +1$ peaks. However, the differences between the

peak values are not as large as predicted. This is not surprising, as there is considerable overlap between the spin-split peaks observed experimentally, in contrast with the theoretical model.

6·3 Thermopower in heterostructures

For the GaInAs - InP and GaInAs - InAlAs heterojunctions, the approximately T^{-1} behaviour of $\alpha(B=0)$ is suggestive of activated conduction (equation (6·14)). This may take place in the bulk semiconductors. However, it can be quickly proved that activated conduction in the bulk is not directly responsible for this behaviour, as follows.

If one considers a system composed of parallel layers so that these layers experience a common thermal gradient, simple calculations give the total thermopower as

$$\alpha = \sum_i \sigma_i \alpha_i / \sum_i \sigma_i \qquad (6\cdot20)$$

where α_i and σ_i are the thermopower and electrical conductivity of the i^{th} layer. In practice, the parallel layers may be different groups of carriers,e.g. electrons and holes, or different subbands, or the combination of the 2DEG and the bulk semiconductors. The contribution from an α_i which is varying as T^{-1}, characteristic of activated conduction, would be weighted by $\sigma_i \propto \exp\left[\frac{E_c - E_F}{kT}\right]$, against the temperature-independent σ_{2D}. Therefore, such a contribution would <u>decrease</u> with decreasing temperature, approximately as $\exp\left[\frac{E_c - E_F}{kT}\right]$, rather than increasing as T^{-1}.

Furthermore, a quantitative examination of the temperature dependence of $\alpha(B=0)$ shows that the T^{-1} behaviour cannot be due to activated conduction from <u>any</u> source. Equation (6·14) shows that for activated conduction to mobility edge E_c, a plot of α against T^{-1} would give a gradient equal to $(E_c - E_F)/e$. The plots of α versus T^{-1} are resonably linear for the four GaInAs - InP and GaInAs - InAlAs heterojunctions. The gradients obtained range from 3 μV to 15 μV for

the different samples, which correspond to activation energies ($E_c - E_F$) between 0·04K and 0·2K. It is clearly unreasonable to have activated conduction with activation energies of ~ 0·1K in the range of temperature of the experiments, $2K \leq T_m \leq 10K$.

Effects from other subbands can also be dismissed as a possible cause of the observed temperature dependences. Experimentally, this is shown by the fact that results for the GaInAs - InAlAs sample 168, which shows two-subband occupation, do not differ qualitatively from results for the GaInAs - InP samples which have single-subband occupation. In theory, the thermopower of the two subbands can be calculated from equation (6·20). However, knowledge of $\sigma_i(E)$ for the two subbands is required for an explicit calculation. Provided that these do not change with temperature over the range concerned, a T^{+1} dependence is expected from the (weighted) sum of the two subbands' contributions.

For the special case of a heterostructure with an electron concentration, n, close to the threshold for occupation of the second subband, an anomalous temperature dependence of α might be expected, since a number of electrons proportional to kT/E_F can be thermally excited into the second subband. However, this is not likely to be the explanation for the results obtained here because for each heterostructure system the results have been studied over a range of electron concentration.

Finally, there may be a phonon drag contribution to α, which assumes a special form in the 2DEG system. This contribution can be estimated as follows.

At the low temperatures of the experiment, the probability of Umklapp electron-phonon scattering is negligible. From considerations of energy and momentum conservations, the normal electron-phonon scattering must involve phonons with wavevector of order k_F, the Fermi

wavevector. These long-wavelength phonons have energy ~ $\hbar(v_s k_F)$ where v_s is the sound velocity. Typical values of these quantities are:

$$v_s \sim 4{\cdot}7 \times 10^3 \text{ m s}^{-1} \text{ for GaAs}$$

(Landolt-Börnstein 1982, volume III/17a). The value of v_s for InAs is comparable to that of GaAs, so v_s in GaInAs should be similar to v_s in GaAs.

$$k_F = 1{\cdot}6 \times 10^8 \text{ m}^{-1} \text{ for } n = 4 \times 10^{11} \text{ cm}^{-2}$$

This gives $\hbar v_s k_F \sim 6K$. Therefore, the phonons which take part in the electron-phonon scattering can be described classically for $T \gtrsim 6K$. For these phonons, the drift velocity v_d in a thermal gradient ∇T is given by

$$v_d u' = K' \nabla T \qquad (6{\cdot}21)$$

where u' and K' are respectively the energy density and thermal conductivity. The prime denotes quantities appropriate to this section of the phonon distribution.

For these phonons

$$u' = c'T$$

and

$$K' = \tfrac{1}{3} c' \ell' v_s \qquad (6{\cdot}22)$$

where c' is the specific heat and ℓ' is the mean free path.

Combining equations (6·21) and (6·22) gives

$$v_d = \frac{\ell' v_s}{3T} \nabla T \qquad (6{\cdot}23)$$

Thus, in a frame which is moving with velocity v_d, the phonons are stationary, and the electrons have a drift velocity of magnitude v_d (in

the opposite direction to the phonon velocity). This drift velocity corresponds to an applied electric field E_{drag}, where

$$v_d = \mu_{ph} E_{drag} = \mu_{ph} \nabla V_{drag} \quad , \qquad (6\cdot24)$$

μ_{ph} is the phonon-limited mobility of the electrons, and V_{drag} is the phonon-drag contribution to the thermovoltage. Combining equations (6·23) and (6·24), the phonon-drag thermopower is

$$\alpha_{drag} = \frac{\nabla V_{drag}}{\nabla T} = \frac{\ell' v_s}{3T\mu_{ph}} \quad . \qquad (6\cdot25)$$

The mean free path ℓ' is likely to be limited by the boundaries at these temperatures. For the GaInAs - InP heterojunctions, the channel layer of GaInAs is grown between layers of InP. Therefore phonon scattering can occur at the boundaries of the channel, and ℓ' is of the order of the width of the channel, $\ell' \sim 1$ μm. For the GaInAs - InAlAs, the channel layer is sandwiched between layers of InAlAs and of InP, so that ℓ' is again of the order of the channel width, $\ell' \sim 1$ μm. For the GaAs - GaAlAs heterojunction, the channel layer of GaAs is grown between the barrier of GaAlAs and the substrate of GaAs. Thus, there should not be much phonon scattering at the channel-substrate interface. Furthermore, it is known that the barrier-channel interface in this system is of high quality. Since the velocity of sound is very similar in the GaAs and in the GaAlAs material, the barrier-channel interface should not give rise to much phonon scattering. Therefore, the phonon-scattering boundaries in this system are likely to be the surface of the GaAlAs barrier, and the layer of the 2DEG. This would give $\ell' \sim$ width of the barrier = 0·05 μm.

The phonon limited mobility, μ_{ph}, at low temperature is a combination of piezoelectric and deformation potential acoustic scattering. The values of μ_{ph} are $\sim 5 \times 10^6$ cm^2 V^{-1} s^{-1} for GaAs -

GaAlAs and ~ 10^7 cm^2 V^{-1} s^{-1} for GaInAs - InAlAs (Walukiewicz et al. 1984). These values for ℓ' and μ_{ph} give

$$\alpha_{drag} \cong \begin{cases} \frac{2}{T}\ \mu V/k & \text{for the GaIn As - InP and GaInAs - InAlAs heterojunctions} \\ \frac{0{\cdot}2}{T}\ \mu V/k & \text{for the GaAs - GaAlAs heterojunctions} \end{cases} \qquad (2{\cdot}26)$$

Equation (6·26) is only expected to give the corrrect order of magnitude for α_{drag}, because values of ℓ' and μ_{ph} are rough estimates. It also becomes invalid at very low temperature, where the phonon population is falling rapidly.

The phonon-drag thermopower, which has the same sign as the electron diffusion thermopower, is expected to show oscillations in the magnetic field which are in phase with the diffusion thermopower. This arises because the scattering rate is proportional to the number of final states available to the electrons. In the presence of a large magnetic field, for filling factor $\nu = N$ there are no empty states near to E_F and the phonon-drag thermopower should be zero. Conversely, when $\nu = N + \frac{1}{2}$ the phonon-drag should show a peak value. There are no calculations for the phonon-limited mobility, μ_{ph}, as a function of the filling factor in a strong magnetic field. However, it can be expected that the peak value of α_{drag} in a magnetic field increases with the field, since the Landau level density of states is proportional to the B-field.

From the experimental results, it is clear that the behaviour of the superlattice sample differs widely from the heterojunctions. The magnetic field results are considered first. The values of $\alpha_{xx}(N + \frac{1}{2})$ for the superlattice agree well with theory, while those of the heterojunctions have absolute values of α_{xx} which are too low. There are four obvious points of difference between the heterojunctions and the superlattice. Firstly, the small widths of the barriers and wells

in the superlattice ensure that these layers are completely depleted, so that there is no bulk conduction. A rough calculation for the heterojunctions shows that all the heterojunctions, excepting sample 6311c, have barrier layers which are nearly or completely depleted, and channel layers which could show some bulk conduction. For sample 6311c, bulk conduction is clearly observed in the Shubnikov & de Haas oscillations. This is probably occurring in the barrier layer, after the illumination from the diode has ionised the deep donors and changed the band-bending. Secondly, the electron gas in the superlattice is confined to two dimensions by the width of the well, whereas in the modulation-doped heterojunction the band-bending of the channel's conduction band is responsible for the confinement. The well width is a fixed quantity, in contrast to the band-bending which is dependent on the doping of the bulk semiconductors, their temperature-dependent ionisation, and the electron concentration. Thirdly, the physical structure of the superlattice, which is composed of fifty wells, can lead to differences from the heterojunctions over lattice properties such as thermal conductivity and the phonon dispersion curves. Finally, for the samples studied the electron concentration is much greater in the superlattice than in the heterojunctions. The possible effects of these differences are discussed below.

The fact that the heterojunctions have conducting bulk layers may lead to a contribution to the thermopower in two ways, but neither of these is expected to influence greatly $\alpha_{xx}(N + \frac{1}{2})$. Firstly, the direct contribution to α from bulk conduction has been discussed above, and found to be negligible. Secondly, the conducting bulk layers can influence α indirectly through the 2DEG. The reason for this is that the condition of constant chemical potential, which also involves the band bending, relates the bulk layers to the 2DEG. Thus, any temperature dependence of the Fermi level in the bulk would be

reflected in the Fermi level of the 2DEG, and thereby contribute to α via the term α_1 as shown in section 6·2. The term α_1 will be discussed in more detail in connection with the results at zero field. In a large magnetic field, however, this contribution should be negligible because the magnetic freeze-out effect pins the Fermi level in the bulk to the impurity level.

It is unlikely that the difference in the thermal conductivity of the superlattice and of the heterojunctions plays a part in the difference in their results. The silver paint thermal link at the edge of each sample ensures that the whole edge is at the same temperature, while the thermal gradient along the sample is known to be constant because the thermovoltage scales with the distance between the probes. These two facts mean that in the measurements of α there has been no change which is due to a variation in the thermal conductivity.

As discussed above, the phonon-drag can give a contribution to $a_{xx}(N + \frac{1}{2})$ which is in phase with the diffusion thermopweer, and also with the Shubnikov - de Haas oscillations. For the GaInAs - InP and the GaInAs - InAlAs heterojunctions, the increase of α_{xx} with decreasing temperature may be due in part to the phonon-drag term. Equation (6·26) gives values of α_{drag} wich are lower than the observed values of α_{xx} by ~ 10. This may indicate that the phonon-drag is not the only contribution to α_{xx}. On the other hand, equation (6·26) gives only rough estimates, and was calculated with the value of μ_{ph} at zero field. For the GaAs - GaAlAs heterojunctions, the observed α_{xx} does not have a simple power-law dependence on temperature. It is probable that α_{drag} is negligible for the GaAs - GaAlAs heterojunctions. As equation (6·26) shows, α_{drag} is an order of magnitude lower in the heterojunctions of this system compared with its value in the other two systems.

The phonon-drag contribution may be very different in the superlattice. In the direction perpendicular to the interfaces, the phonon dispersion curve of the superlattice is a set of minibands, whose Brillouin zone boundary is close to the value of the Fermi wavevector. This may affect the electron-phonon interaction and changes α_{drag} considerably.

In the above discussion, some possible contributions to α_{xx} other than the diffusion thermopower were considered. These should normally be dominated by the large diffusion thermopower, which is predicted to have peak values of $\sim 60[N + \frac{1}{2}]^{\pm 1}$ μV/k. However, this large thermopower has not been observed in the heterojunctions, and none of the above effects can explain its suppression. It is observed experimentally that the values of α_{xx} for the GaAs - GaAlAs system increases with the electron concentration, n. The comparison of the results for samples 6311a, 6311b and 6311c is particularly significant because these are physically the same sample. The only differences are the electron concentration n, and the amount of bulk conduction. The value of the ratio $[\alpha_{xx}(N + \frac{1}{2})] \times [N + \frac{1}{2}]/n$, denoted by F, is found to be approximately constant for all three samples,

$$F = \frac{[\alpha_{xx}(N+\frac{1}{2})] \times [N+\frac{1}{2}]}{n}$$

8K	3K	Sample	n, 10^{11} cm^{-2}
3·5 ± 1	5·2 ± 2	6311a	3·0
4·0 ± 1	-	6311b	3·6
3·9 ± 1	5·6 ± 1	6311c	4·1

This shows that, at least within the rather large experimental errors, α_{xx} scales with the electron concentration for the GaAs - GaAlAs heterojunction. For the superlattice MB44, the ratio F at 8K and at 3K is 3·5 ± 0·5 and 4·3 ± 1 respectively, with $n = 14{\cdot}2 \times 10^{11}$ cm^{-2}. These values are in fair agreement with those of the GaAs - GaAlAs heterojunctions.

For the GaInAs - InP and GaInAs - InAlAs heterojunctions, the ratio F is

	8K	3K	Sample	n, 10^{11} cm^{-2}
	0·7 ± 0·15	2·2 ± 0·5	135	3·3
F =	0·9 ± 0·4	2·6 ± 0·8	58	3·8
	0·45 ± 0·1	1·6 ± 0·2	68	5·3
	0·7 ± 0·1	3·2 ± 0·7	168	6·9

The values of F at 8K are approximately constant but those at 3K differ quite widely. Thus, in contrast to the GaAs - GaAlAs system, it is not certain that α_{xx} scales with n in these two heterostructure systems. Furthermore, α_{xx} in these systems increases strongly with decreasing temperature, and obeys a power law dependence, T^c, over the whole temperature range. This is in contrast to the GaAs - GaAlAs system which gives a constant value of α_{xx}, except at very low temperature for the heterojunctions. This temperature-dependence of the GaAs - GaAlAs heterojunction may be caused by the same mechanism which gives rise to the proportionality between α_{xx} and n in this system.

Considering the zero field results, it is seen from table 5·3 that $\alpha(B=0)$ for the superlattice is much larger than for the heterojunctions. It is in fact larger than the predicted value α_o for the diffusion thermopower at low temperature. In contrast, the heterojunctions' values are lower than the predictions for the whole

temperature range. The ratio of $\alpha(B=0)/n$, denoted by F', has the following values

$$F' = \frac{\alpha(B=0)}{n}$$

10K	3K	Sample	n, 10^{11} cm^{-2}
0·36 ± 0·1	1·3 ± 0·6	135	3·3
0·63 ± 0·1	1·05 ± 0·3	58	3·8
0·1 ± 0·01	0·2 ± 0·06	68	5·3
0·1 ± 0·01	0·2 ± 0·04	168	6·9
0·7 ± 0·2	0·7 ± 0·2	6311a	3·0
0·6 ± 0·2	"	6311b	3·6
0·6 ± 0·1	0·6 ± 0·2	6311c	4·1
1·3 ± 0·3	1·3 ± 0·4	MB44	14·2

The ratio of F' is approximately constant for the samples 6311a, b, and c. However, F' for the superlattice is twice this value, and values of F' for the other heterojunctions differ widely, showing no systematic dependence on n. This is perhaps not surprising, as the value of $\alpha(B=0)$ is predicted to depend on the scattering rate which is sample-dependent.

The $\alpha(B=0)$ results also show a qualitative difference between the GaAs - GaAlAs heterojunctions and the heterojunctions of the other two systems, with the former remaining constant in temperature while the latter varies as T^{-1}.

The T^{-1} behaviour of α for the GaInAs - InP and GaInAs - InAlAs heterojunctions may be due to the phonon-drag contribution. From equation (6·26), this contribution has the correct temperature dependence but is smaller than the observed values by approximately a factor of 5. As discussed previously, equation (6·26) is only expected to give values of α_{drag} to the correct order of magnitude. Thus, it is

possible that $\alpha(B=0)$ for these two heterostructure systems is due to the phonon-drag contribution. The expected, large diffusion thermopower, α_0, seems to be suppressed, as in the case of the magnetic field results.

The T^0 behaviour of α for the GaAs - GaAlAs heterostructures may be due to the term α_1 which is proportional to $\frac{dE_F}{dT}$. In the bulk semiconductor, the Fermi level has the form $(E_D + O(kT))$ at low temperature for an n-type material, and $(E_A + O(kT))$ for a p-type material, where E_D and E_A are the donor and acceptor levels (Blakemore 1962). Therefore, $(\frac{dE_F}{dT})_{bulk}$ is independent of temperature for all cases, although its magnitude and sign depend on both the doping and the compensation ratio. For a heterojunction, variations of $(E_F)_{bulk}$ are reflected in the Fermi energy of the 2DEG. Although the relationship is not one-to-one because of the dependence of the band-bending on all the charge concentrations, this effect still gives rise to a temperature-independent thermopower in the 2DEG via the condition of constant chemical potential (equation (4·6)). For the superlattice, changes in the ionisation in the well or in the barrier layer with temperature could also lead to a temperature dependence of E_F, and hence a contribution α_1 to the thermopower. This change in the ionisation could come from the deep donors in the barrier, which are responsible for the persistent photoconductivity effect.

The flaw in this argument lies in the large value of α observed for the superlattice compared with the value for the heterojunctions. The contribution α_1 in the superlattice can only come from changes in the ionisation, but in the heterojunctions another contribution is $(\frac{dE_F}{dT})_{bulk}$ of the bulk layers which are not depleted. It is known that the number of ionised deep donors is greatly increased by the illumination on sample 6311. Thus, if α_1 is due mainly to the presence

of deep donors, large changes in $\alpha(B=0)$ are expected between samples 6311a, b, and c. This is not observed. At present, though, the α_1 contribution appears to be the only effect which can lead to a T^0 behaviour in zero magnetic field for a system of degenerate carriers.

6.4 Conclusion

In this, one of the first experimental works on the thermopower of semiconductor heterostructures, measurements have been made of the thermopower α for the GaInAs – InP, GaInAs – InAlAs, and GaAs – GaAlAs systems. In a magnetic field, for all samples, the diagonal component α_{xx} accurately follows the density of states as has been predicted by theory, even in the presence of spin–splitting and of two–subband occupation. Again as predicted by theory, the peak values are observed to scale with the inverse of the filling factor.

The magnitude and temperature dependence of α_{xx} for the superlattice sample are in agreement with the predictions for a 2DEG. In contrast, all the heterojunctions show serious disagreement with theory over the magnitude and temperature dependence of α_{xx}, even when level broadening is taken into account. Several possible causes for this disagreement were examined. None can explain the deviations from theory of α_{xx} in the heterojunctions. Empirically, it is found that α_{xx} is roughly proportional to the electron concentration, n, for the GaAs – GaAlAs system, although it is not certain that this is the case for the other two systems. It is thus possible that the suppression of the diffusion thermopower predicted by theory is greater for small values of n. Given that the diffusion thermopower is largely suppressed, the temperature dependence of α_{xx} for the GaInAs – InP and the GaInAs – InAlAs heterojunctions may be due in part to a phonon-drag contribution.

The zero–field thermopower α of the heterojunctions also shows a suppression of the predicted diffusion thermopower, which is expected to vary as T^{+1}. At the time of writing, the only available explanations for the T^{0} and T^{-1} dependences observed in these systems

are, respectively, the variation of the Fermi level with temperature, and the phonon drag contribution.

In conclusion, this exploratory study verifies some of the theoretical predictions for the new heterostructure systems first studied here. However, most of the experimental results cannot be explained quantitatively on the basis of present theories. As in the case of metals, the behaviour of the thermopower proves to be more complicated than has been expected. Theoretical calculations on the heterostructure as a whole rather than on the 2DEG alone are needed. Calculations of the effect of electron-phonon interaction on the thermopower are also required. It is hoped that this will lead to a greater understanding of the heterostructures.

CHAPTER 7

A study of the thermally ⁻ induced stress in thin film PbTe

7·1 Introduction

Lead Telluride and its alloys have been extensively studied because of their actual, and potential, commercial applications. The high degree of symmetry between the conduction band and the valence band, and the possibility of continuously varying the band gap by changing the pressure or the alloy composition makes them particularly suitable for devices such as photodetectors and solid-state lasers in the infra-red range (Dimmock et al. 1966, Walpole et al. 1976). However, optical studies of these materials, particularly those involving absorption, are difficult because of the high concentration of degenerate carriers even in the best grown materials (~ 10^{17} cm^{-3}). Furthermore, the reststrahl band is large in these polar materials (~ 14 - 114 cm^{-1} for PbTe). To counteract the first disadvantage, experiments are often performed on thin films of the compound grown on transparent substrates such as NaCl or BaF_2. These films can be grown to a high degree of perfection by the hot wall technique. Such films have been used in many studies of PbTe material. The review paper by Lopez-Otero (1978) which discusses this growth technique is of special interest here as the sample studied in this work was grown by Lopez-Otero.

For such a system, stress on the film may be caused by either the lattice mismatch between the film and substrate or by the difference in their thermal contraction once the sample is cooled from growth, or both. An early paper by Frank and van der Merwe (1949) predicted that for a lattice mismatch $\lesssim$ 9%, a monolayer film will be under strain (it will have the same lattice spacing as the crystalline substrate), but no dislocations will be produced. Later studies (Matthews and Kokholm 1972, Matthews and Blakeslee 1974) for films of finite thickness give a critical value for the thickness, which depends on the lattice

mismatch, below which the film is under elastic strain, and above which misfits start to be formed. This general theory for stress caused by lattice mismatch is not applicable to PbTe films, however. Asch et al. (1974) found that for PbTe and PbSe films grown on both BaF_2 and NaCl, a small compressive stress exists at room temperature on cooling from 400 °C, whatever the magnitude and sign of the lattice mismatch of the particular film-and-substrate combination involved.

From other observations, Asch et al. concluded that the lattice mismatch is of minor importance. For PbTe, the small compressive stress in the film is due to slips in the immediate vicinity of the interface, caused by the difference in thermal contraction of BaF_2 and the film on cooling from growth. If this thin layer of defects did not exist, the values of the thermal contractions from growth temperature (~ 400 °C) would lead one to expect a tensile, not compressive stress as was observed. Fantner et al. (1984) also found from X-ray measurements on superlattices of IV-VI semiconductors that the lattice mismatch is almost completely accommodated by misfit strain, while Zemel et al. (1965) observed that there was no significant strain at room temperature for PbTe films grown on rocksalt substrates, although unlike the other studies they postulated that this was due to dislocation in the substrate. It can thus be concluded that at room temperature, PbTe films on either BaF_2 or rocksalt substrates are under very little compressive stress. This results from a thin layer of defects at the interface, which takes up the lattice mismatch.

On cooling from room temperature, further stress is induced in the film because of the difference in the thermal contractions of substrate and film. This effect is greater for NaCl substrates than for BaF_2: the latter has been chosen as a substrate partly because of its thermal expansion compatibility with PbTe. Even for BaF_2 however, the small difference in the thermal expansion coefficient ($\Delta\alpha \sim 2\times10^{-6}\ K^{-1}$ at

300K - Asch et al. 1974) gives rise to values of stress in the film sufficient to induce significant changes in the band structure of PbTe. This effect has been experimentally observed as a change in the band gap (Mitchell et al. 1964). For samples grown on BaF_2 where the growth direction is <111>, the stress on cooling has the further effect of lowering the energy of the [111] ellipsoid with respect to the $\langle\bar{1}11\rangle$ ellipsoids, so that the carrier concentration of the former is increased at the expense of the latter. This has been observed in Shubnikov ⁋ de Haas experiments (Burke and Carver 1978, Carver et al. 1979, Ramage et al. 1977) and deduced from optical experiments (Gungor and Drew 1982). The stress also induces strain in the lattice which can be detected by X-ray diffraction (Fantner et al. 1984, Hearn 1977).

In this work, the relative shift in energy, $\Delta E(111)$, between the [111] ellipsoid and the $\langle\bar{1}11\rangle$ ellipsoids is measured from Shubnikov ⁋ de Haas and F.I.R. transmission experiments, for a sample of n ⁋ PbTe grown on BaF_2. This information when combined with values of the strain induced, which can be obtained from X-ray measurements, enables an accurate value of the deformation potential to be calculated. The deformation potential is still largely undetermined, and is needed in the sort of thorough investigation of PbTe which has been carried out.

Asch et al. (1974) also noted a work-hardening of the PbTe film after repeated thermal cycling to 77K, so that the value of the stress at room temperature was larger than the initial value after growth. In this work, it is assumed that the sample studied has had sufficient thermal cycling so that its stress has a constant value.

This work was carried out in conjunction with the interband magneto-optics study of Singleton (1985) on the same sample. Information on the Landau levels which were used here were calculated by Singleton from the interband transitions, using the six-band model of Mitchell and Wallis (1966) for the band structure of PbTe. In

section 7·2 the six-band model is referred to briefly, and the relationship between the stress and the deformation potential is formally derived. Section 7·3 gives the results of the Shubnikov ⁂ de Haas measurements. Section 7·4 presents the data of the F.I.R. transmission experiment, and analyses these by fitting the traces to computer simulations obtained from a model which is described. The conclusion is given in section 7·5.

7·2 Effect of stress on the band structure of PbTe

Lead Telluride has a cubic crystal structure and the conduction and valence bands, which are both at the L point, are highly symmetric. Each band consists of 4 constant energy surfaces which are ellipsoidal with major axes in the <111> directions and an eccentricity of ~ 10. The spin-orbit splitting is important compared with the small band gap, and determines the band ordering, as shown in figure 7·1.

Mitchell and Wallis (1966) showed that band structure calculations for the lead salts must take into account all six bands (depicted in figure 7·1). The interaction between the lowest conduction and highest valence bands is treated accurately while the other bands are included to order k^2 in their $\underline{k}.\underline{p}$ model. The spin-orbit mixing is treated explicitly. This is necessary to explain the fact that PbS's bands are almost spherical while PbTe has highly anisotropic band. The ordering of the six bands was calculated by Martinez et al. (1975) and confirmed experimentally by Jedrzejczak (1978). Zawadzki (Bauer 1978) solved the case of $\underline{B}$ parallel to <111> exactly, giving the eigenenergy values for the conduction and valence bands, and the selection rules for interband and intraband transitions. For $k_B = 0$, where k_B is the wavector parallel to $\underline{B}$, with the usual notation of $m_{\ell}^{\pm}$, $m_{t}^{\pm}$, $g_{t}^{\pm}$ representing the far-band contributions to the transverse and longitudinal effective masses and g factor in the valence (+) and conduction (-) bands, and $\tilde{m}_{cv}$ being the contribution to the effective mass from the direct highest valence (L_{1+}^{6+}) - lowest conduction (L_{3-}^{6-}) band interaction, the eigenenergies are:

$$E_{v,n,\sigma=-1}^{c,n,\sigma=+1} = \tfrac{1}{2}(a_n + b_n) \pm \tfrac{1}{2}\left[(a_n - b_n)^2 + 4E_g\, \hbar\tilde{\omega}_{cv}\,(n+1)\right]^{\frac{1}{2}}$$

$$E_{v,n,\sigma=+1}^{c,n,\sigma=-1} = \tfrac{1}{2}(c_n + d_n) \pm \tfrac{1}{2}\left[(c_n - d_n)^2 + 4E_g\, \hbar\tilde{\omega}_{cv}\,(n+1)\right]^{\frac{1}{2}}$$

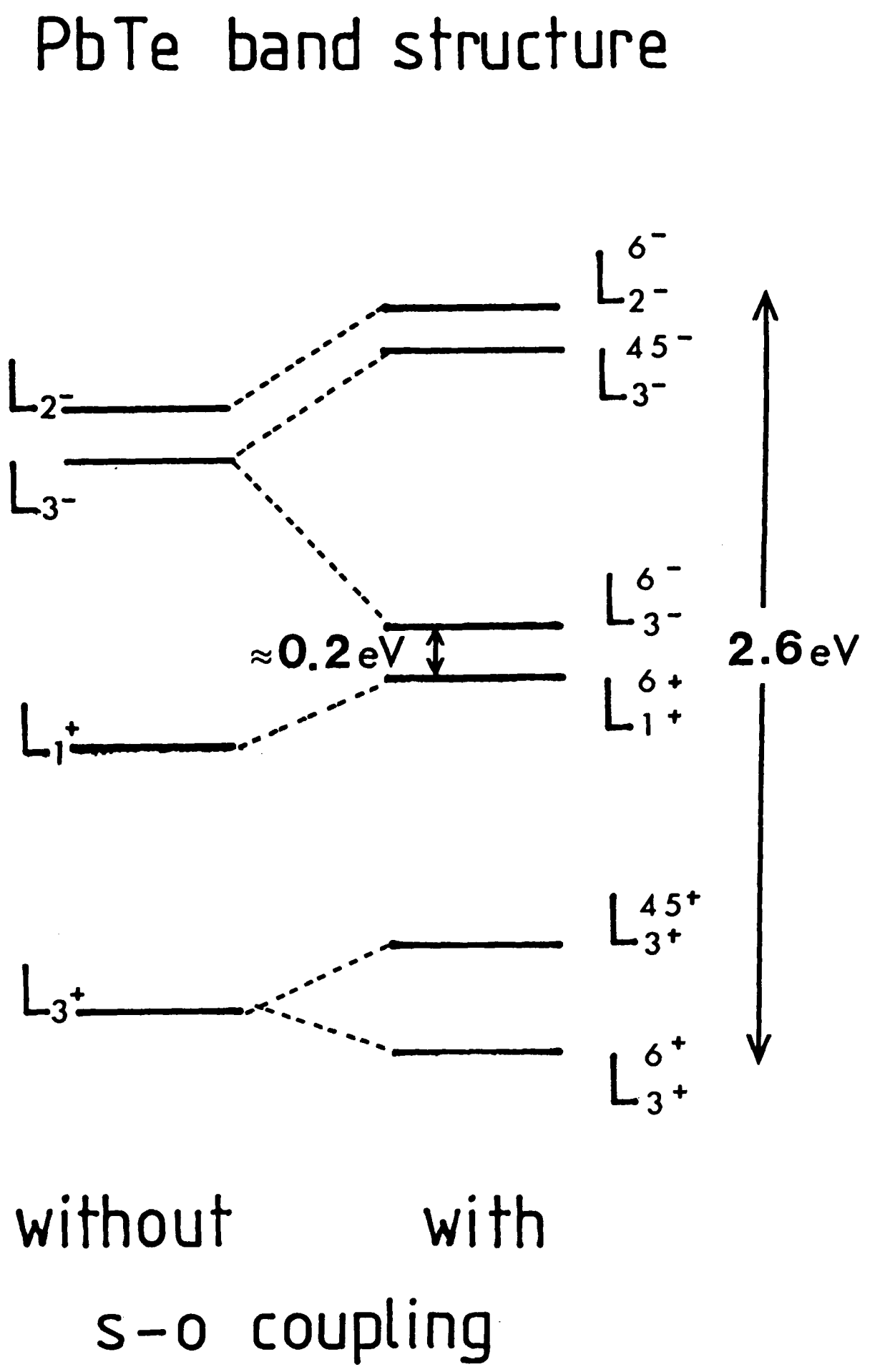


Figure 7·1

The importance of spin-orbit coupling in the band structure of PbTe.

where the indices are c for conduction band, v for valence band, n is the Landau level quantum number, $n \geq -1$ for $\sigma = -1$ and $n \geq 0$ for $\sigma = +1$, $\sigma = \pm 1$ for spin up or down, and

$$a_n = \frac{E_g}{2} + \hbar\omega_\ell^- (n + {}^1/_2) + \tfrac{1}{2} g_\ell^- \mu_B B$$

$$b_n = -\frac{E_g}{2} + \hbar\omega_\ell^+ (n + {}^3/_2) - \tfrac{1}{2} g_\ell^+ \mu_B B$$

$$c_n = \frac{E_g}{2} + \hbar\omega_\ell^- (n + {}^3/_2) - \tfrac{1}{2} g_\ell^- \mu_B B$$

$$d_n = -\frac{E_g}{2} + \hbar\omega_\ell^+ (n + {}^1/_2) + \tfrac{1}{2} g_\ell^+ \mu_B B$$

and

$$\omega_\ell^\pm = \frac{eB}{m_t^\pm} \quad , \quad \tilde{\omega}_{cv} = \frac{eB}{\tilde{m}_{cv}}$$

$\tilde{m}_{cv}/m_o = E_g m_o / 2P_\perp^2$ with $P_\perp$ being a direct interband momentum matrix element (appropriate to the component of momentum perpendicular to the magnetic field).

According to the above notation, the spin-split Landau levels are labelled (n+1) $|+\rangle$ and n $|-\rangle$. Zawadzki proposed a more physical notation, which is used subsequently, of increasing the value of n by +1 for the $\sigma = -1$ state, and giving an effective spin to the $|\pm\rangle$ states.

Equation 7·1 (with the new Zawadzki notation) was used by Singleton (1985) to calculate the Landau levels from interband magneto-optics data. The values of these Landau levels are then used in this work to calculate ΔE.

The second part of this section gives the relationship between the difference in the shifts in energy for valleys [111], $\Delta E(111)$, and the stress tensor.

Since the film of PbTe has a thickness of several microns compared with several millimeters of the areal dimensions, the thin film approximation is appropriate, and the strain should be uniform across the film, except at the edges (Asch et al. 1974). In addition, it is assumed that the substrate is negligibly deformed by the film.

In the co-ordinate system with axes along the film's crystal directions <110>, <112> and <111>, the stress, $\underline{\sigma}$, and strain, $\underline{\varepsilon}$, tensors are diagonal. With the boundary condition that there is no stress perpendicular to the film, we also have $\sigma_{33} = 0$, for films grown on BaF_2 substrates, i.e., those with interfaces in the (111) plane. The stress and strain are related by

$$\sigma_{ij} = C_{ijkl}\,\varepsilon_{kl} \tag{7·2}$$

where C_{ijkl} is the elastic stiffness tensor (defined for the appropriate axis system).

In the system with axes in the directions of the cubic crystal's edges, denoted in this work by the superscript cu, the elastic stiffness tensor is given simply by

$$C^{cu}_{ijkl} = \begin{cases} C^{cu}_{11} & i = j = k = l \\ C^{cu}_{12} & i = j \neq k = l \\ C^{cu}_{44} & i = l \neq j = k \\ 0 & \text{otherwise} \end{cases} \tag{7·3}$$

Transforming this to the axis system with 3rd axis parallel to <111>, and solving equation (7·2) for ε_{33} with $\sigma_{33} = 0$, gives

$$\varepsilon_{33} = \frac{-2(C^{cu}_{11} + 2C^{cu}_{12} - 2C^{cu}_{44})}{(C^{cu}_{11} + 2C^{cu}_{12} + 4C^{cu}_{44})}\,\varepsilon_{11} \tag{7·4}$$

The energy level of the k^{th} band in the ℓ^{th} valley is altered by the strain as

$$\delta E^{(lk)} = \sum_{ij} D_{ij}^{(lk)} \varepsilon_{ij}^{cu} \tag{7·5}$$

where $D_{ij}^{(lk)}$ is the deformation potential, which when defined in the cubic axes system is given by

$$D_{ij}^{(lk)} = D_{\alpha}^{(k)} \delta_{ij} + D_{u}^{(k)} U_{i}^{(l)} U_{j}^{(l)} \tag{7·6}$$

$D_{\alpha}^{(k)}$ and $D_{u}^{(k)}$ are the dilational and uniaxial deformation potential constants for the k^{th} band, and the $U_{i}^{(l)}$ are the cosines of the angles the l^{th} ellipsoid's major axis makes with the x_i cubic crystal axis.

The strain tensor in cubic axes is

$$\varepsilon_{ij}^{cu} = \begin{cases} \frac{1}{3}\left(2\varepsilon_{11} + \varepsilon_{33}\right) & i = j \\ \frac{1}{3}\left(\varepsilon_{33} - \varepsilon_{11}\right) & i \neq j \end{cases} \tag{7·7}$$

Therefore, the shift in energy for the [111] valley (for a BaF_2 substrate) is:

$$\delta E^{(k)} = \left(D_{\alpha}^{(k)} + \tfrac{1}{3} D_{u}^{(k)}\right)\left(2\varepsilon_{11} + \varepsilon_{33}\right) + \tfrac{2}{3} D_{u}^{(k)}\left(-\varepsilon_{11} + \varepsilon_{33}\right) \tag{7·8}$$

The shift for the $\langle\bar{1}11\rangle$ valleys is

$$\delta E^{(k)} = \left(D_{\alpha}^{(k)} + \tfrac{1}{3} D_{u}^{(k)}\right)\left(2\varepsilon_{11} + \varepsilon_{33}\right) - \tfrac{2}{9} D_{u}^{(k)}\left(-\varepsilon_{11} + \varepsilon_{33}\right) \tag{7·9}$$

Thus, the <u>relative</u> shift in energy between the [111] valley, which moves down, with respect to the other three valleys is

$$\Delta E(111) = -\tfrac{8}{9} D_{u}^{(k)}\left(-\varepsilon_{11} + \varepsilon_{33}\right) \tag{7·10}$$

It is ΔE (111) which is measured in this work.

7·3 Shubnikov – de Haas measurements

Shubnikov – de Haas (S-dH) measurements are a good method of determining the energy difference between the [111] ellipsoid and the $\langle\bar{1}11\rangle$ ellipsoids, since the fundamental frequencies of the oscillations are directly related to the carrier concentration of each ellipsoid. The contributions of the different ellipsoids can be identified by their variation with the angle which $\underline{B}$ makes with the crystal axes. $\Delta E(111)$ can then be obtained from the inequality in the carrier distribution between the four ellipsoids. Burke and Carver (1978) measured the S-dH oscillations and Hall coefficient of a sample of n-PbTe film on BaF_2 grown at White Oak. Their results showed that the shift in energy was so great that all the carriers were transferred to the [111] ellipsoid. They estimated this shift to be ~ 30 meV. A later study by Carver et al. (1979) on both White Oak and Linz – grown samples showed the strain to be unobservable for the Linz sample, while the White Oak samples still showed considerable carrier transfer to the [111] ellipsoid.

The sample used in this work, called 145·1, was grown in Linz by Lopez-Otero using the hot-wall epitaxy technique (Lopez-Otero 1978). The epitaxial layer of n-type PbTe is 6·48 μm thick and was grown along the <111> direction on a BaF_2 substrate. The characteristics at room temperature are

resistivity, $\rho = 4{\cdot}35 \times 10^{-2}\ \Omega\ cm$

mobility, $\mu = 1010\ cm^2\ V^{-1}\ s^{-1}$

carrier concentration, $n = 1{\cdot}42 \times 10^{17}\ cm^{-3}$

The Shubnikov – de Haas experiment was performed at 2K, at which temperature the high mobility and large carrier concentration give a sample resistance which is smaller than the resistance of the leads to the sample. The 4-contact voltage V was measured for a constant

current of 8·5 mA as the magnetic field was swept from 0T to 9T. Figures 7·2 and 7·3 show V versus resistivity and $-(d^2V/dB^2)$ against B respectively, for $\underline{B}$ parallel to <111>. Up to 1·8T, the oscillations which are best seen in the differentiated signal behave in the usual manner. At high fields, the quantum limit is reached.

Low field oscillations in $-(d^2V/dB^2)$ were measured for $\underline{B}$ at angles θ between 0° and 65° to the <111> direction (at θ = 90°, $\underline{B}$ is parallel to the film-substrate interface).

Some typical examples are shown in figure 7·4. These low field results are Fourier analysed to give the fundamental frequencies $F(\theta)$. The angular variation of F is given theoretically (Jensen et al. 1978) as

$$F = 31{\cdot}5\ (n/10^{18})^{2/3}\ K^{1/6}\ [1 + (K-1)\cos^2\phi]^{-1/2}$$

where

n = carrier concentration per cm^{-3} of the ellipsoid concerned

K = (maximum cross-section of the ellipsoid/ minimum cross-section)

ϕ = angle between $\underline{B}$ and the major axis of the ellipsoid.

In terms of $F_{min} \equiv F(\phi=0)$

$$F = F_{min}\ K^{1/2}[1 + (K-1)\cos^2\phi]^{-1/2}$$

and

$$F_{min} = 31{\cdot}5\ (n/10^{18})^{2/3}\ K^{-1/3} \qquad (7{\cdot}11)$$

Theoretical curves for $F(\theta)$ for the different ellipsoids were calculated with K = 9·8 (Singleton 1985). These are fitted to the experimental value of $F(\theta)$ with F_{min} as the unique variable parameter. The angular dependence of the set of strongest peaks in the Fourier transforms is well fitted by the theoretical calculations for $F(\theta)$ for the <111> ellipsoid, with F_{min} = 1·96T ± 0·2T. This is shown in figure 7·5.

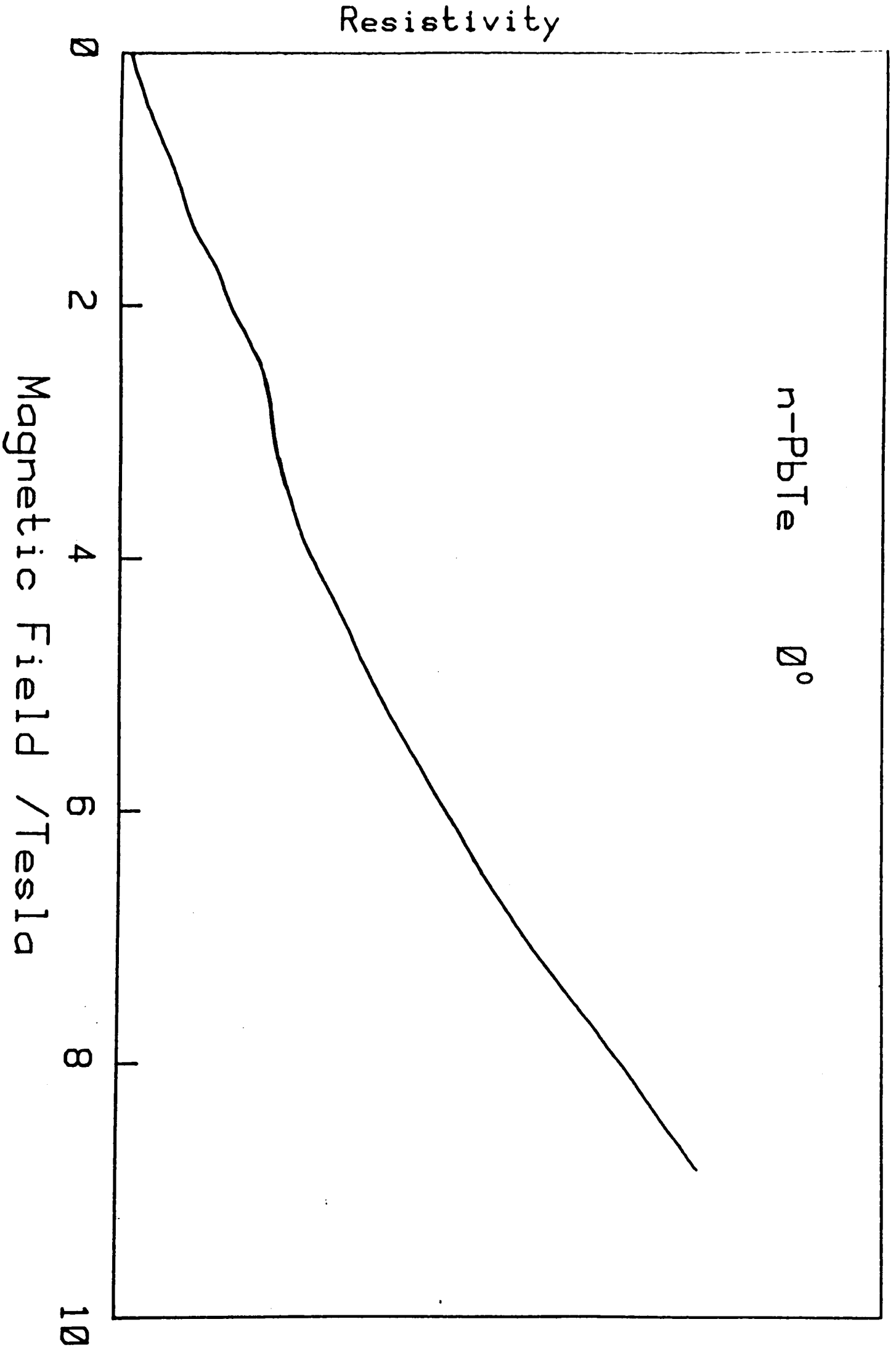


Figure 7·2

Magnetoresistance of n - PbTe at 2K, $\underline{B}$ || <111>.

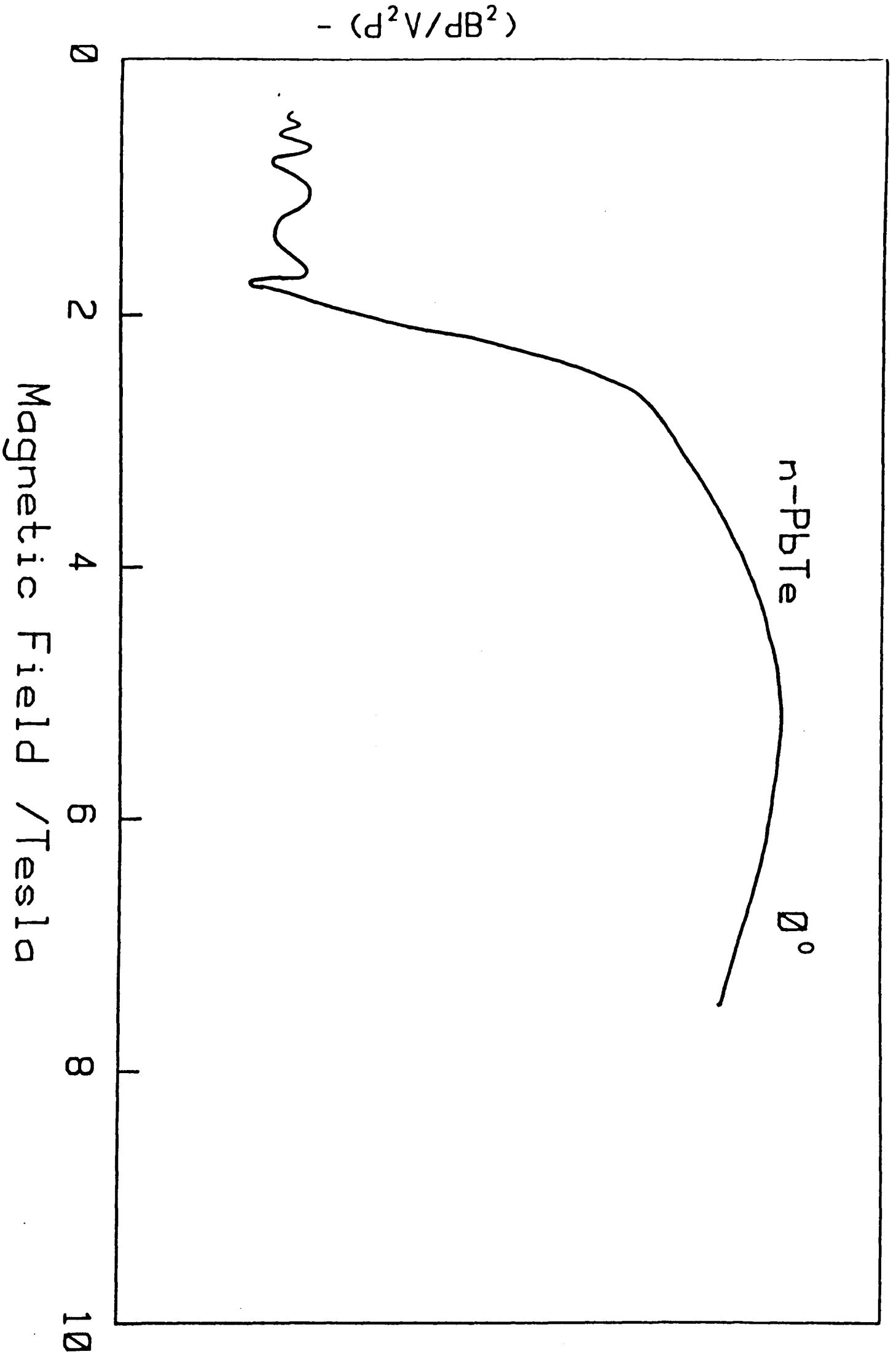


Figure 7·3

$-(d^2V/dB^2)$ versus B for n - PbTe at 2K, $\underline{B}$ || <111>.

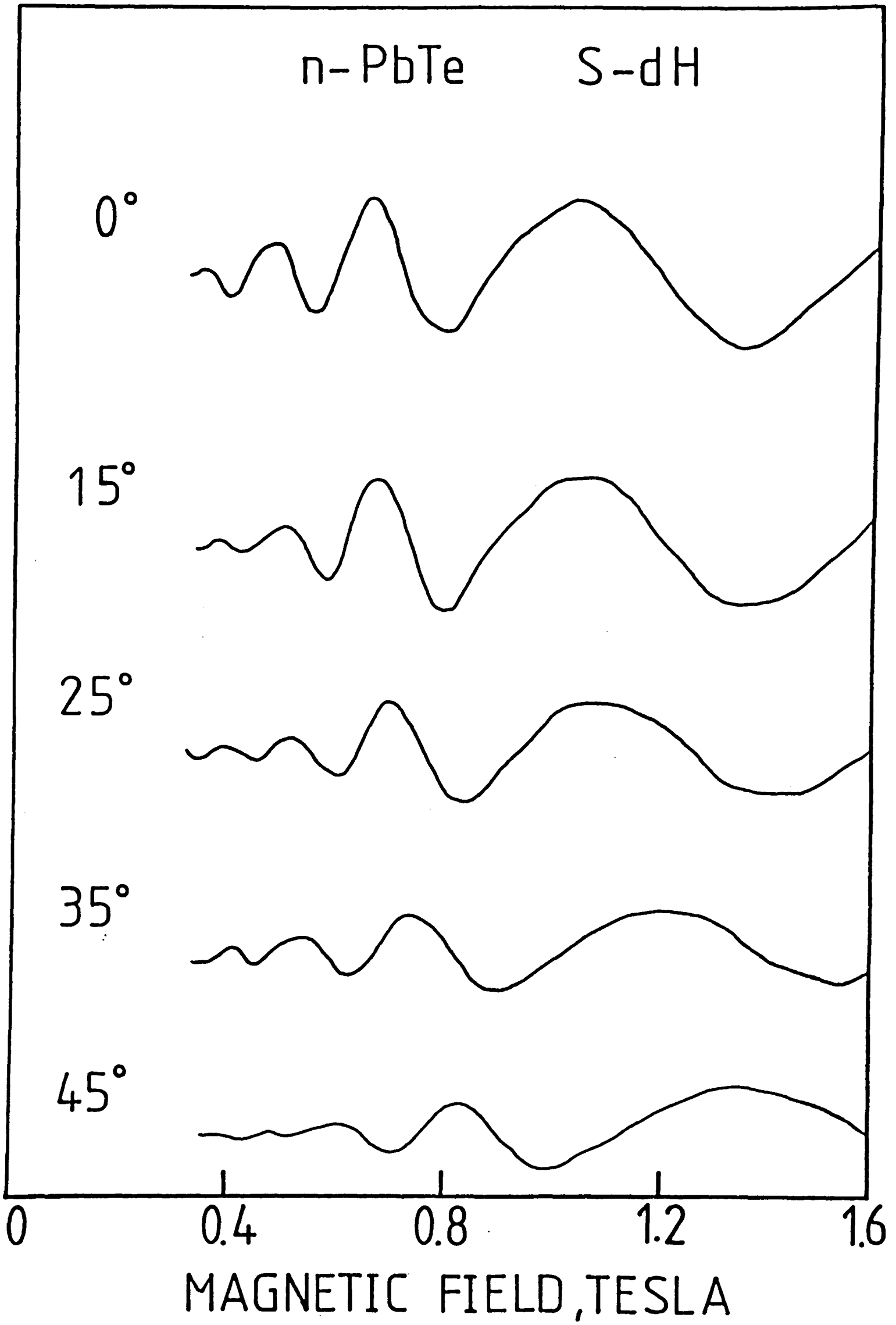


Figure 7·4

Low field oscillations in $-(d^2V/dB^2)$ for n - PbTe at 2K, for $\underline{B}$ at various angles to <111>.

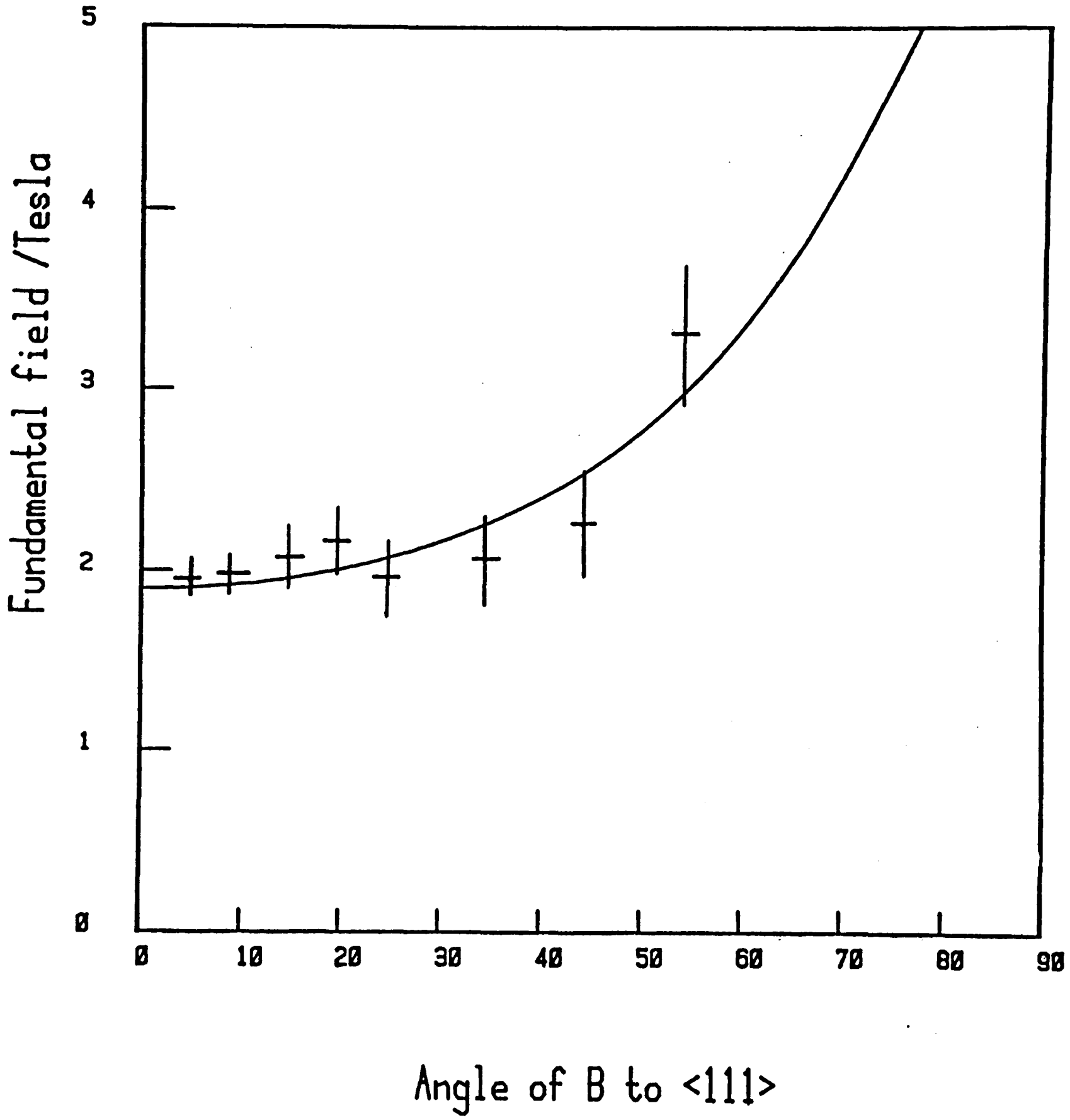


Figure 7·5

Fundamental frequency F(θ) versus angle of B to <111> θ.

Theoretical fit gives $F_{min} \equiv F(0)$ as 1·96 ± 0·2T.

There is a set of peaks lower in frequency than those of the [111] ellipsoid which has an angular dependence roughly that expected of the other three $\langle\bar{1}11\rangle$ ellipsoids. However, the experimental errors on these peaks, due to them being weak and also of low frequencies so that $\Delta F/F$ is large, mean that no accurate value for F_{min} could be determined for them. Nonetheless, it is clear that they are of lower frequencies than the [111] ellipsoid's peaks, implying that the other ellipsoids have smaller carrier concentrations as can be expected with stress in the film lowering the energy of the [111] valley.

In conclusion, the Shubnikov ⇔ de Haas results unfortunately were not clear enough for $\Delta E(111)$ to be calculated. However, it can be observed that some shift of the ellipsoid's energy levels is present from the redistribution of the carriers. Furthermore, the carrier concentration in the [111] ellipsoid was determined to be $4{\cdot}8 \times 10^{16}$ cm^{-3} ± 3%. This result is utilised in the interpretation of the F.I.R. transmission experiments, from which $\Delta E(111)$ was obtained. It may be noted that since there are some carriers left in the $(\bar{1}11)$ ellipsoids, the sample studied here must be under less stress than that used by Burke and Carver (1978) which showed total depopulation of these ellipsoids. Hence, it is expected that $\Delta E(111)$ for this sample is smaller than the 30 meV reported by Burke and Carver, in accordance with their later study (Carver et al. 1979).

7·4 F.I.R. magneto-optic experiment

(a) Experimental results

The transmission traces of sample 145·1 for F.I.R. of wavelengths 119 μm (H_2O laser), 192 μm (DCN laser) and 337 μm (HCN laser) were recorded for magnetic field up to 9 Tesla and temperatures varying from 17K to 50K. The apparatus used is described in chapter 1.

As the wavelengths concerned fall into the restrahl region of PbTe over most of the magnetic field range, the transmittivity is very low over most of the range and care was taken to eliminate all stray radiation. For instance, the thick edges of the transparent substrate, which could transmit the radiation, were covered with aluminium foil.

Some typical transmission traces are shown in figures 7·6a, 7·6b, 7·7a, 7·7b, 7·8a, and 7·8b. At low temperatures, the traces for all three wavelengths show two peaks in the transmission. Over the non-transmitting region, the real part of the dielectric constant ε is negative and the transmission peak at lower field is associated with the cyclotron resonance which changes the sign of ε to positive. The second peak at higher field is due to the dielectric anomaly which corresponds with the zero-crossing of ε (e.g., Ramage et al. 1977). As the temperature is increased, the features of the traces remain qualitatively the same for transmission of 119 μm and 172 μm. For 337 μm, it can be seen from figure 7·8b that the sharp peaks are changed to shallow troughs. The peak positions for the three wavelengths at various temperatures are given in table 7·1.

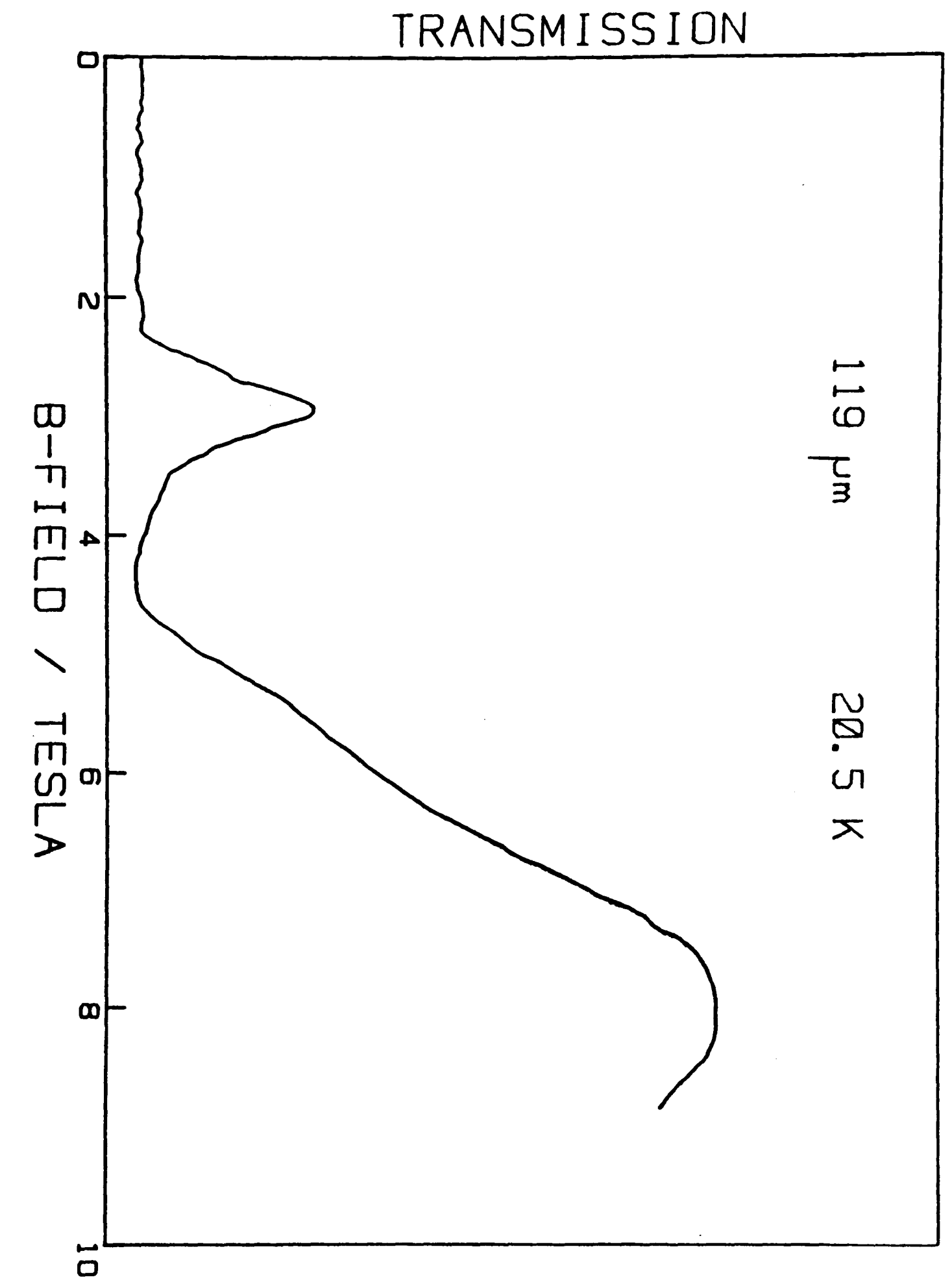


Figure 7·6a

Experimental recording of the transmission of 119 μm at 20·5K versus B.

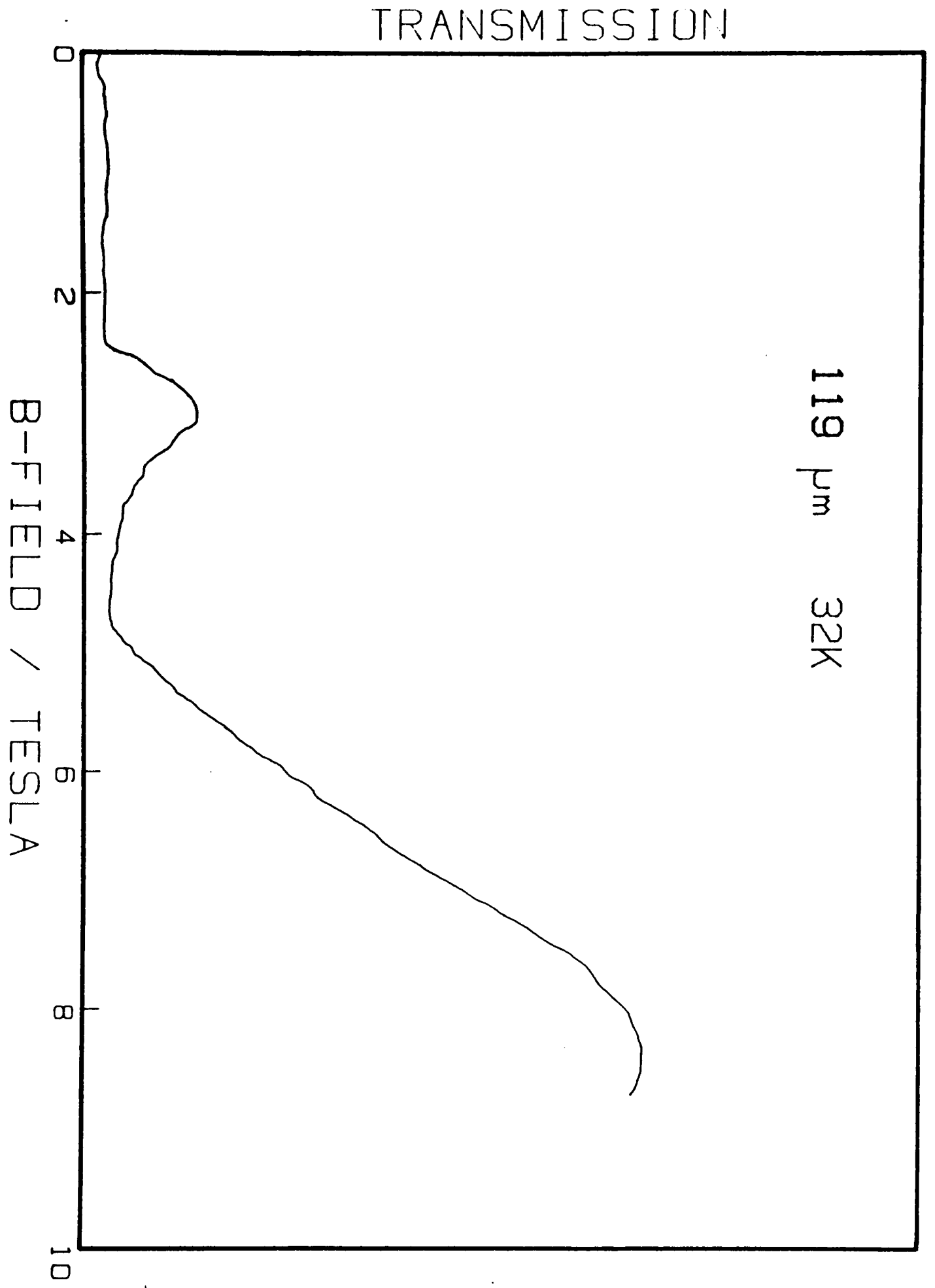


Figure 7·6b

Experimental recording of the transmission of 119 μm at 32K versus B.

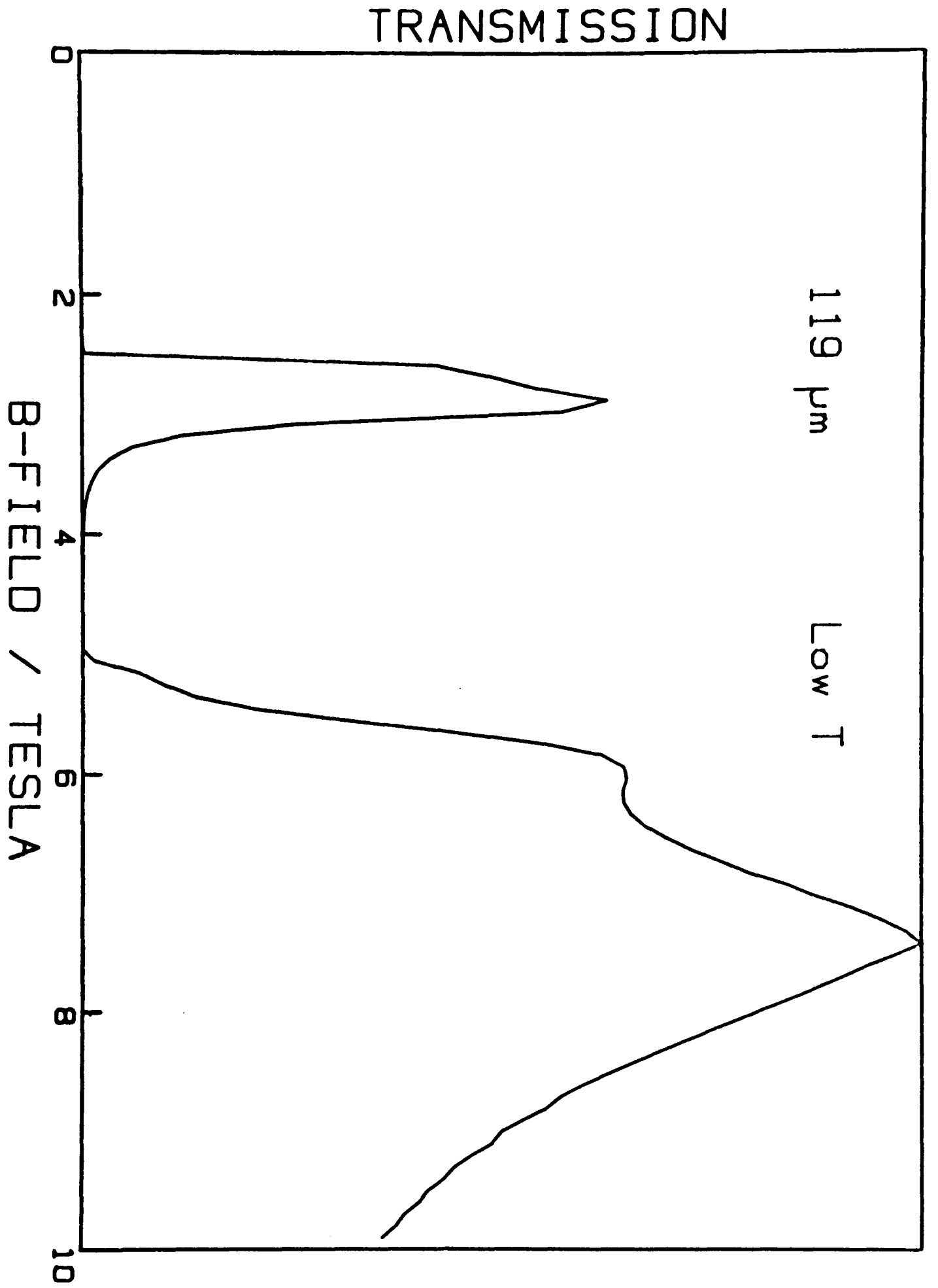


Figure 7·6c

Theoretical predictions of the transmission of 119 μm versus B.

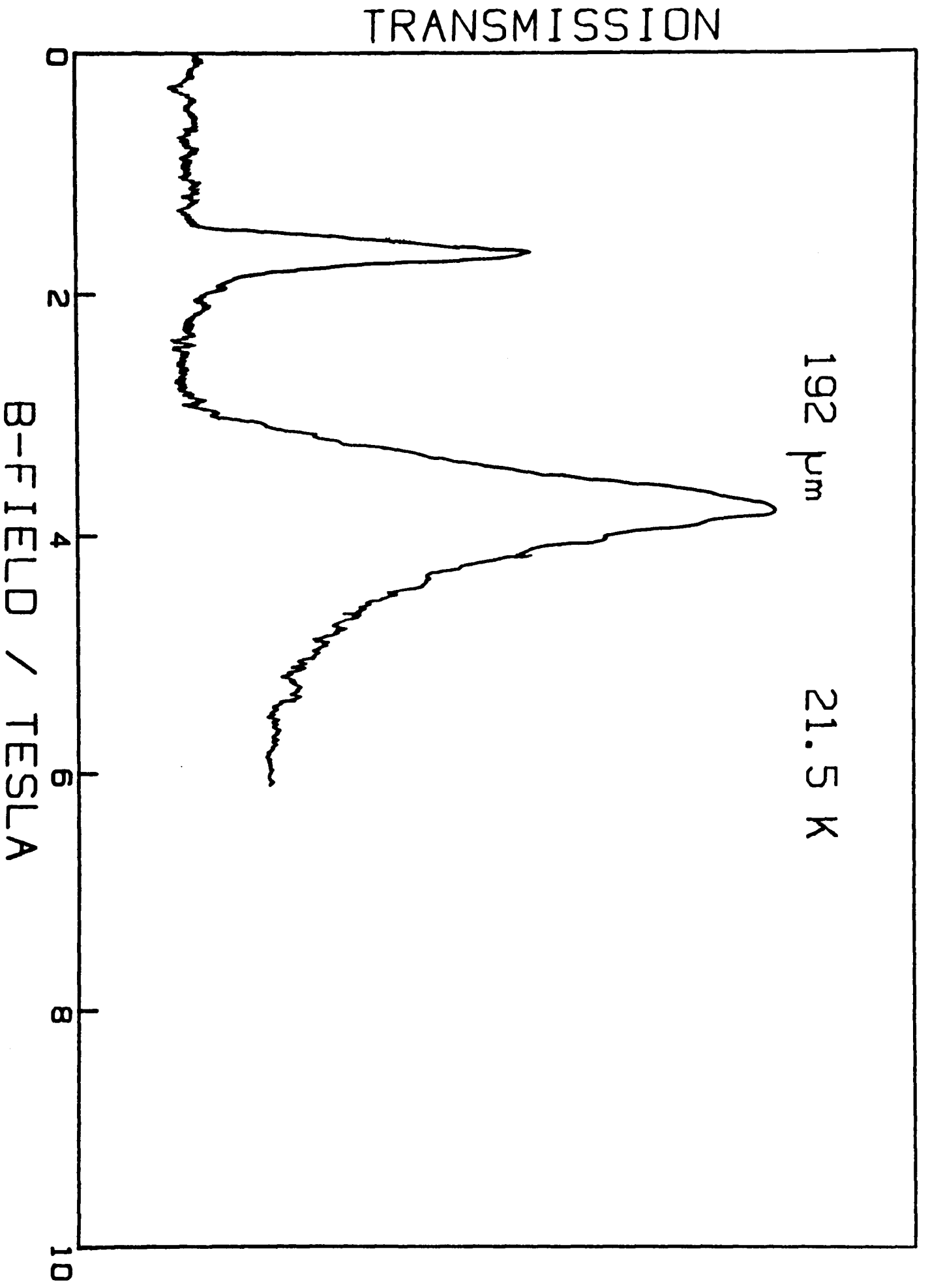


Figure 7·7a

Experimental recording of the transmission of 192 μm at 21·5K versus B.

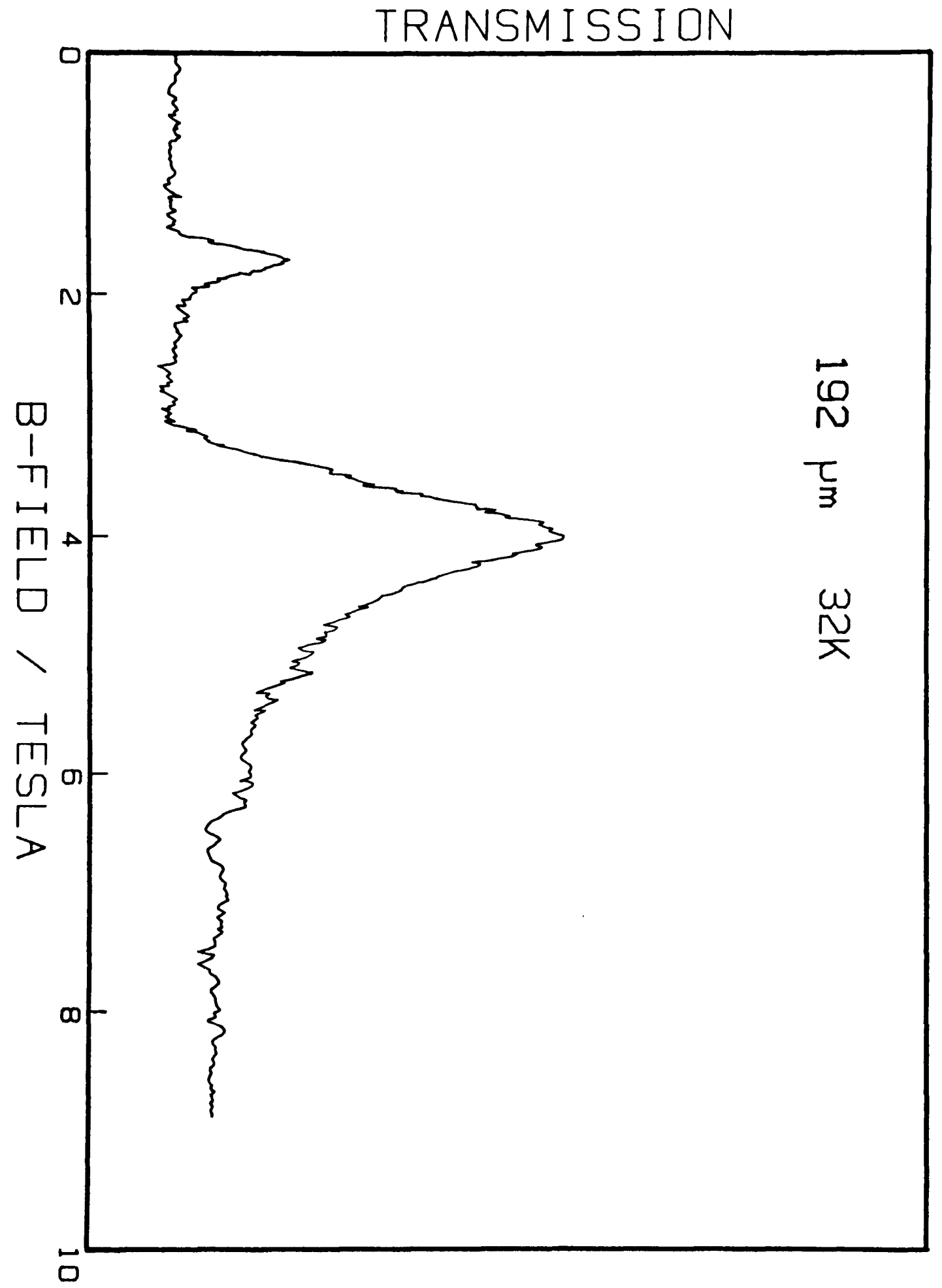


Figure 7·7b

Experimental recording of the transmission of 192 μm at 32K versus B.

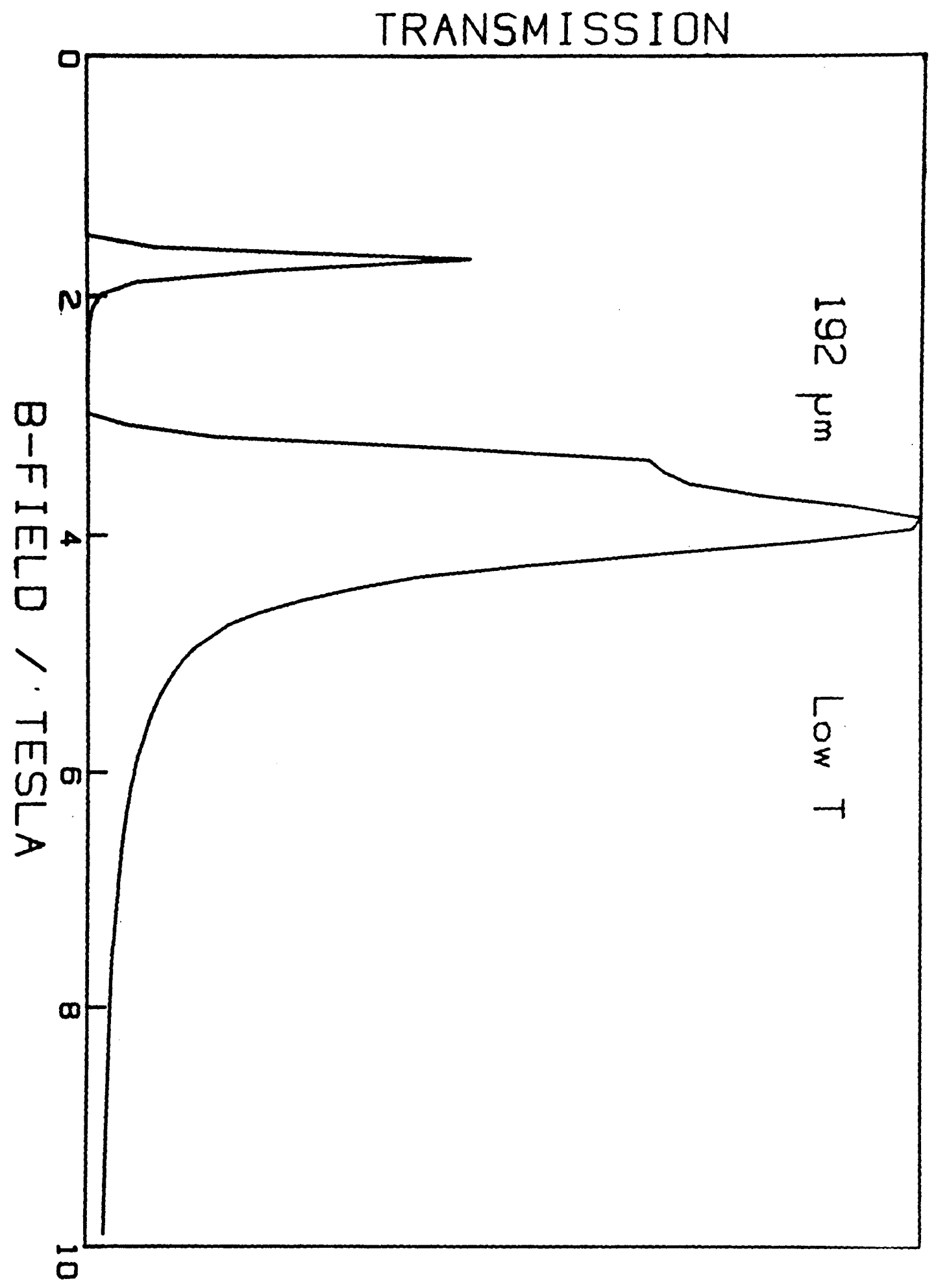


Figure 7·7c

Theoretical prediction of the transmission of 192 μm versus B.

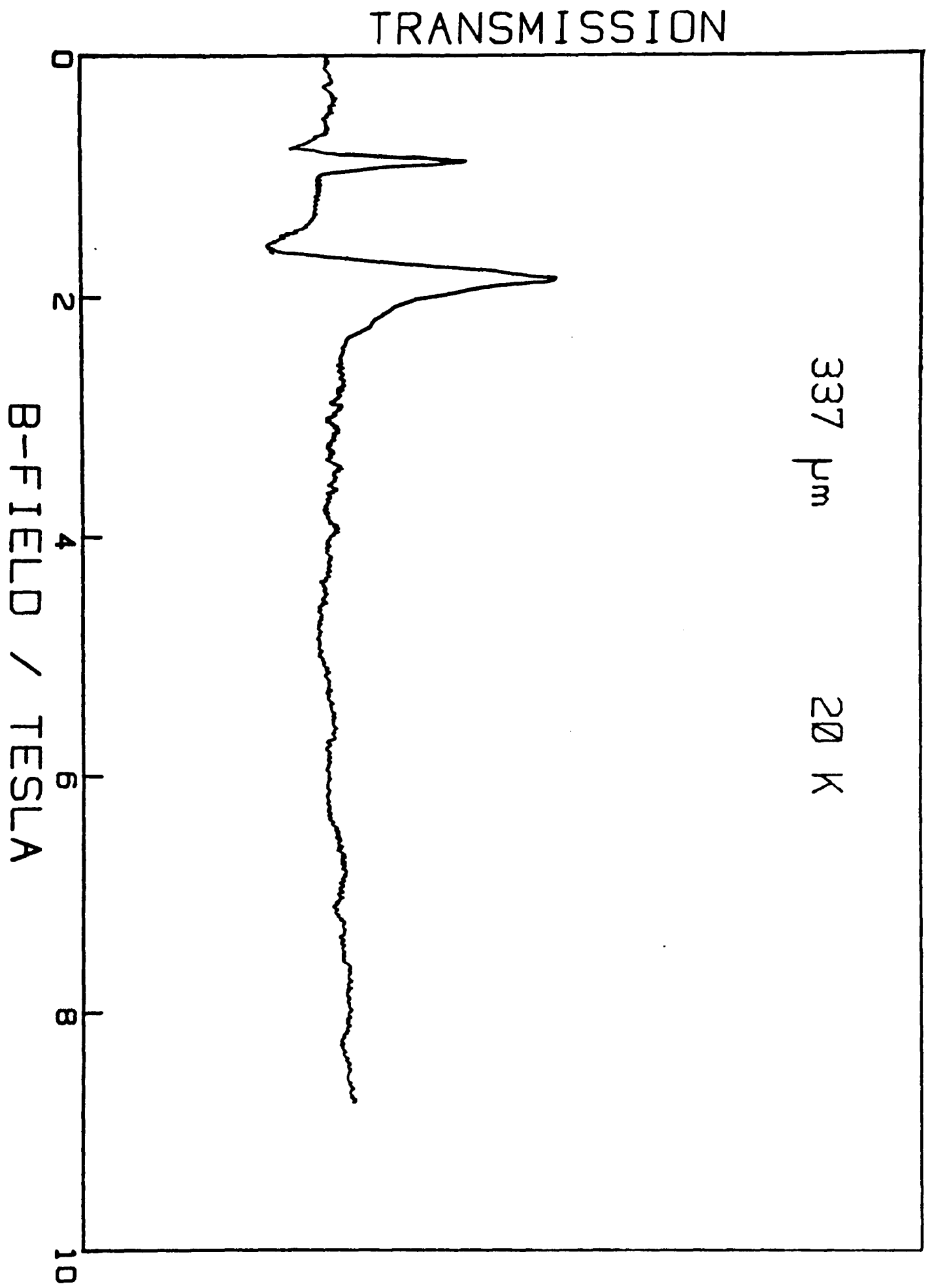


Figure 7·8a

Experimental recording of the transmission of 337 μm at 20K versus B.

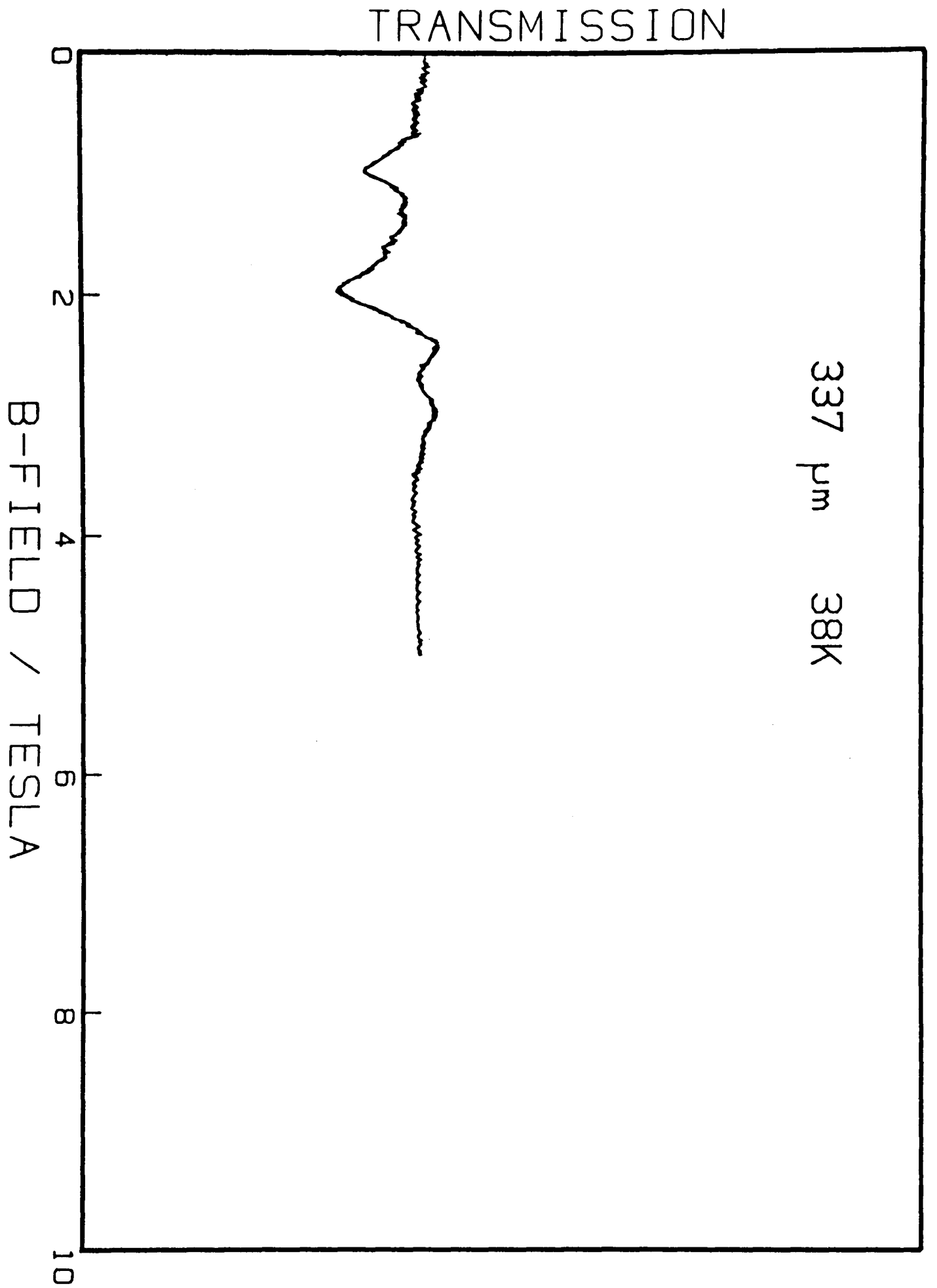


Figure 7·8b

Experimental recording of the transmission of 337 μm at 38K versus B.

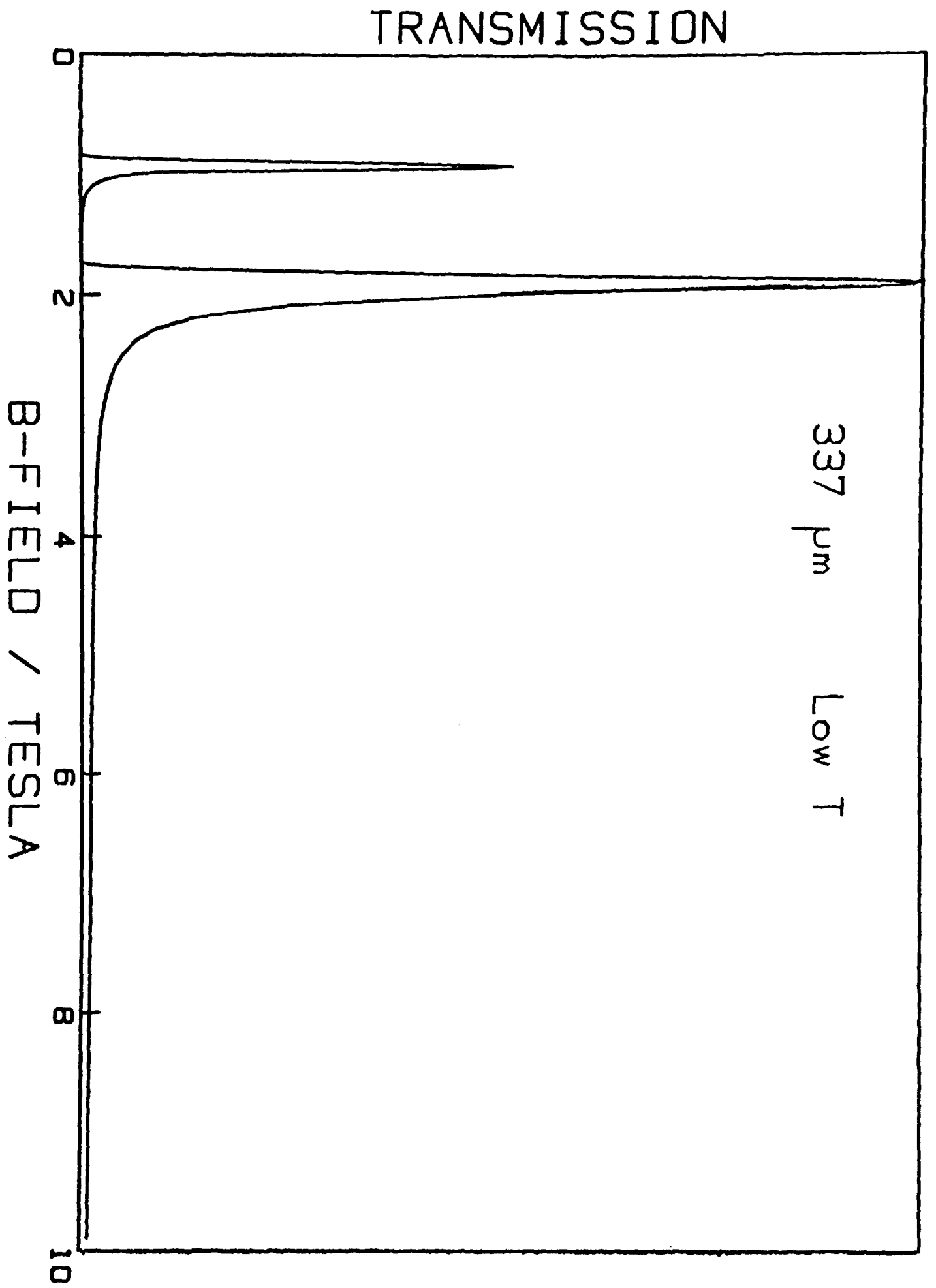


Figure 7·8c

Theoretical prediction of the transmission of 337 μm versus B.

Table 7·1

(a) For 119 μm (H_2O laser)

Temperature /K	Peak 1 /T	Peak 2 /T
18 ± 0·5	3·00 ± 0·05	7·9 ± 0·1
20 ± 0·5	3·02 ± 0·05	8·0 ± 0·1
24 ± 0·5	3·00 ± 0·05	8·2 ± 0·1
27 ± 1	3·00 ± 0·05	8·35 ± 0·1
33 ± 1	3·00 ± 0·05	8·6 ± 0·1
37 ± 2	2·98 ± 0·05	8·6 ± 0·1
59 ± 2	3·11 ± 0·1	*

* outside B-field range

(b) For 192 μm (DCN laser)

Temperature /K	Peak 1 /T	Peak 2 /T
19 ± 0·5	1·70 ± 0·03	3·7 ± 0·1
21 ± 0·5	1·70 ± 0·03	3·7 ± 0·1
24 ± 0·5	1·76 ± 0·03	4·0 ± 0·1
27 ± 1	1·72 ± 0·03	4·0 ± 0·1
29 ± 1	1·68 ± 0·03	4·0 ± 0·1
30 ± 1	1·72 ± 0·03	4·0 ± 0·1
32 ± 1	1·72 ± 0·03	4·0 ± 0·1
38 ± 2	1·70 ± 0·05	4·1 ± 0·1
43 ± 2	1·70 ± 0·05	4·1 ± 0·1
48 ± 2	†	4·3 ± 0·1

† intensity too low to be measured.

(c) For 337 μm (HCN)

Temperature /K	Peak 1 /T	Peak 2 /T
17 ± 0·5	0·91 ± 0·03	1·91 ± 0·03
20 ± 0·5	0·92 ± 0·03	1·94 ± 0·03
21 ± 0·5	0·93 ± 0·03	1·96 ± 0·03
22 ± 0·5	0·93 ± 0·03	1·96 ± 0·03
25 ± 1	0·94 ± 0·03	1·98 ± 0·05
27·5 ± 1	0·95 ± 0·05	2·01 ± 0·05

(b) Theoretical model

In PbTe, the interplay between the dielectric constant, the carrier concentration, and appropriate effective masses in a varying magnetic field is complicated and magneto-optic results can only be understood when the complex dielectric constant is calculated for each field value. Many attempts of such calculations have been made (Bauer 1978, Burkhard et al. 1976 (1), 1976 (2), 1977 (1), 1977 (2), 1979, Ramage et al. 1977, 1978, Nishi et al. 1980, Ichiguchi et al. 1980, Tennant 1976, Gungor and Drew 1982).

There are two main parts to this type of calculation. The first part is the statistics of the carriers and the values of the Landau levels in varying magnetic field. This is non-trivial because of the large non-parabolicity of PbTe which is experienced by the large concentration of degenerate carriers. Furthermore, even without the effect of stress due to the substrate, for $\underline{B}$ parallel to <111> the cyclotron mass and hence the Landau levels for the [111] ellipsoid are different from the other three ellipsoids. This leads to a continuous redistribution of the carriers amongst the two sets of inequivalent ellipsoids as the magnetic field is being continuously varied. The second part of the calculations is the model for the dielectric constant. Most authors use the semi-classical Wallace model which is found to be adequate. The alternative is the linear response model which is more complicated than the Wallace model but gives better agreement to the details of complicated spectra, such as reflectivity results. Bauer (1978) compares the two models.

In this work, variable parameters are replaced wherever possible by experimentally determined values. From interband transition data previously obtained on the same sample, the positions of the Landau levels were determined by fitting to the six band model (Singleton 1985). These levels are then directly used in this work, that is, the

band parameters which were determined from the interband transitions are used in the combination which fitted the experimental results, rather than separately. The levels are utilised firstly in the calculations of the population distribution of the carriers, and secondly in giving the cyclotron resonance energies at the appropriate B - field value in the theoretical fits. Thus parameters normally required to calculate Landau levels, such as the spin factor and the C.R. effective mass with their contributions from the direct and far band interactions, do not have to be entered separately in this work. As these parameters are energy-dependent - and therefore vary with the applied magnetic field - they could have represented a source of large errors. In eliminating them as variable parameters, the value of the shift in energy ΔE (111) due to the stress from the substrate can be obtained more accurately from the fits to the transmission traces. The theoretical calculations which produce these fits are divided into three parts:

(i) Distribution of the carriers amongst the four ellipsoids at each B-field value

Steps of 0·1 Tesla are used which are two times less accurate than the experimental resolution. The two criteria used are firstly that the total concentration of carriers, n, remains constant as the magnetic field is varied within 1%. Secondly, n is such that at 1 Tesla the carrier concentration in the [111] ellipsoid is $4{\cdot}8 \times 10^{16}$ cm^{-3} ± 2% (i.e., within the experimental error of the value obtained from Shubnikov - de Haas results). The value of 1 Tesla was chosen arbitrarily as a low field value, since the carrier concentration was determined from oscillations for B < 1·8 Tesla. The use of the value of [111] ellipsoid's concentration which was obtained at 2K for theoretical calculation to fit results at ~ 20K is an acceptable

approximation: the total carrier concentration remains constant in this range (Gibson (1952) found the Hall coefficient to be largely independent of temperature up to 600K). Any significant changes in the [111] ellipsoid's carrier concentration would come from a change in $\Delta E(111)$. However, as shown in figure 7·9, the thermal expansion coefficient which is responsible for $\Delta E(111)$ is a strong function of temperature and decreases to zero as $T \to 0K$. Therefore, the additional stress caused by cooling from 20K to 2K is negligible compared with the total stress caused by cooling from 300K to 2K.

For a given value of $\Delta E(111)$, the calculations give firstly the values at each B-field of the carrier concentrations in the [111] ellipsoid and that in the other three (assumed to be equivalent here and in the rest of this work). Secondly, they give the quantum numbers of the highest filled Landau levels for the two sets of ellipsoids, hereafter referred to by subscript 1 for the [111] ellipsoid, and 2 for the others. Let these numbers be M1 and M2 in later discussion.

(ii) The dielectric constant for PbTe

The Wallace model for the dielectric constant ε was used. For the case of the Faraday configuration, the two normal modes of propagation are the circularly polarised modes (subscripts + and -) for which the dielectric function is a simple sum of the contributions from the background lattice, the lattice vibrations and the free carriers (Palik and Furdyna 1970). In this case the dielectric constant for the two normal modes is given by

$$\varepsilon_{\pm}(w) = \varepsilon_{\ell}\left[1 + \frac{w_L^2 - w_T^2}{w_T^2 - w^2 - i\Gamma w} + \frac{i}{w}\sum_j \frac{w_{pj}^2}{\nu_j - i(w \pm w_{cj})}\right] \qquad (7\cdot12)$$

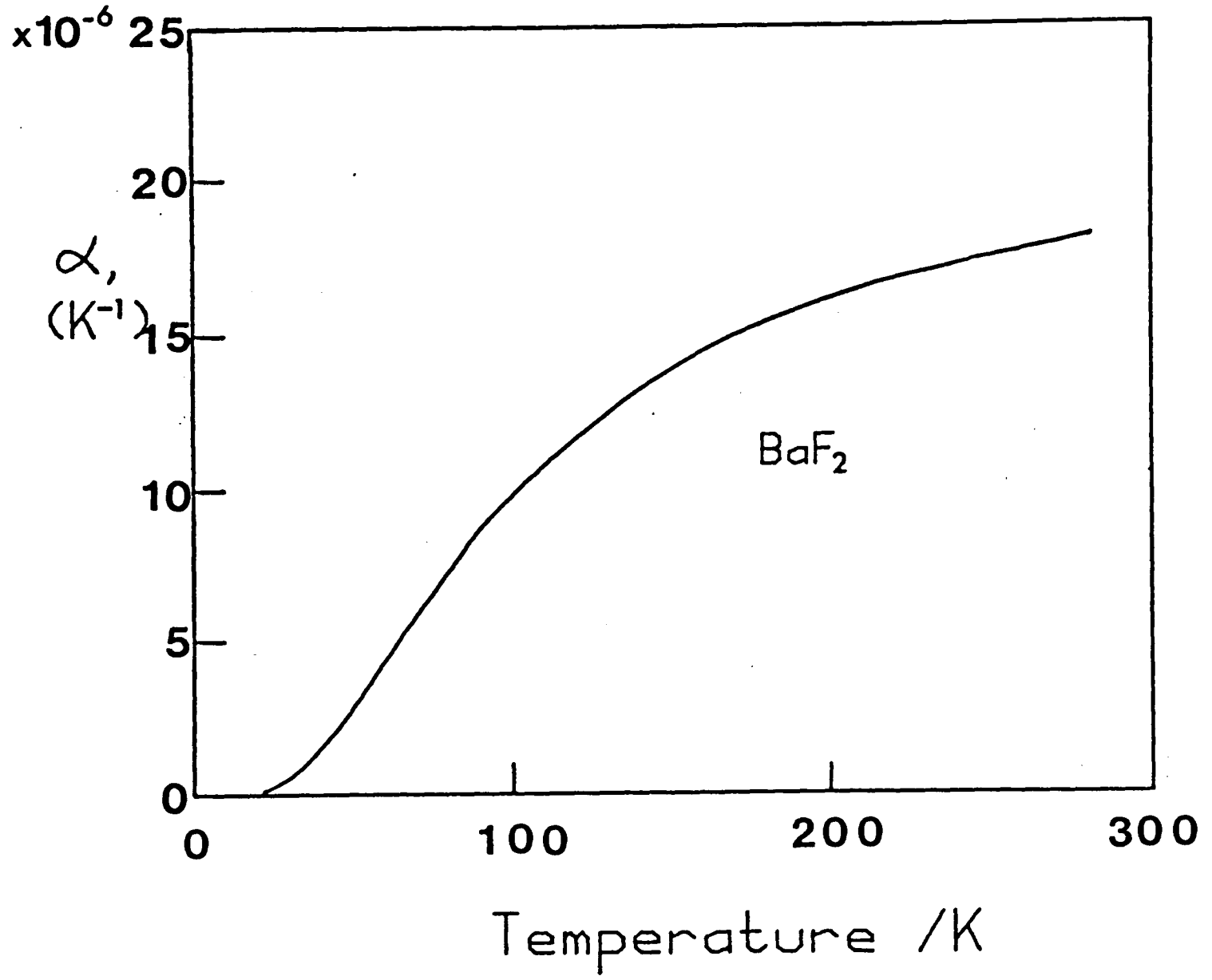


Figure 7·9

The temperature dependence of the linear expansion coefficient for BaF_2 (Bailey and Yates 1967).

where

ε_ℓ = high frequency dielectric constant

w_L = LO phonon angular frequency

w_T = TO phonon angular frequency

Γ = lattice damping constant

w = angular frequency of (laser) radiation

w_{pj} = plasma frequency of the j^{th} group of carriers

ν_j = damping constant of the j^{th} group of carriers

w_{cj} = cyclotron frequency of the j^{th} group of carriers.

Thus, if two groups of carriers j and j' have $\nu_j = \nu_{j'}$ and $w_{cj} = w_{cj'}$, then whether they are considered as two groups or as one gives the same result for $\varepsilon_{\pm}(w)$ since

$$w_{pj}^2 \propto n_j \quad \rightarrow \quad w_{p\ \text{total}}^2 = w_{pj}^2 + w_{pj'}^2$$

Therefore, the contributions of the three $(\bar{1}11)$ ellipsoids to $\varepsilon_{\pm}(w)$ are the same, and their sum is

$$3\varepsilon_\ell \frac{i}{w} \frac{w_{p_2}^2}{\nu_2 - i(w \pm w_{c_2})}$$

where

$$w_{p_2}^2 = n_2\, e^2/m_2^* \varepsilon_0 \varepsilon_\ell$$

$$w_{c_2} = \frac{1}{\hbar} \times \left[E_2(M_2+1) - E_2(M_2)\right]$$

$$m_2^* = \frac{eB}{w_{c_2}}, \quad \text{the cyclotron mass}$$

$E_2(M)$ = energy of Landau level of quantum number M, for ellipsoid 2.

Similarly, the contribution from the [111] ellipsoid is

$$\varepsilon_\ell \frac{i}{w} \frac{w_{p_1}^2}{\nu_1 - i(w \pm w_{c_1})}$$

where

$$w_{p_1}^2 = n_1 e^2 / m^*_1 \varepsilon_o \varepsilon_\ell$$

$$w_{c_1}^2 = \frac{1}{\hbar} \left[E_1 (M_1+1) - E_1(M) \right]$$

$$m^*_1 = \frac{eB}{w_{c_1}}$$

It is assumed that $\nu_1 = \nu_2 = \nu$. They are not expected to be very different and, furthermore, it was observed that varying ν_2 by 30% from ν_1 has negligible effect on the final result.

It is known (chapter 3) that the laser radiation is nearly linearly polarised. The initial fittings were made with the polarisation ratio as one of the variable parameters. However, for the carrier concentration involved here, it was found that the only effect of the C.R.I. mode is to add a small constant background to the theoretical plot of transmission vs B-field. It does not modify either the positions of the structures of the plot or their relative intensities. Thus, in later plots, the dielectric function and transmission of the C.R.A. mode alone are considered.

(iii) Transmission through a thin film and substrate

Using the boundary conditions for $\underline{E}$ and $\underline{H}$ at the two boundaries between air and film, and film and substrate, thus including the effect of multiple reflections and interference in the thin film automatically, a straight forward derivation gives the transmittance T as

$$T = \frac{\left[(1 + g)^2 + h_b^2\right] \times \left[(1+ g_c)^2 + h_c^2\right]}{\exp 2\alpha + C \cos 2\gamma - D \sin 2\gamma + (g_b^2 + h_b^2)(g_c^2 + h_c^2) \exp -2\alpha} \qquad (7\cdot13)$$

where subscripts b and c denote quantities appropriate to the film and the substrate,

$$\gamma = \frac{w}{c} d\, n_b \qquad \text{and } n_b = \mathrm{Re}\,(\tilde{n}_b)$$

$$\alpha = \frac{w}{c} d\, k_b \qquad \text{and } k_b = \mathrm{Im}\,(\tilde{n}_b)$$

$$d = \text{film thickness}$$

g's and h's are the real and imaginary parts of the Fresnel coefficients, i.e.

$$g_b + ih_b = \frac{n_a - (n_b + ik_b)}{n_a + (n_b + ik_b)}$$

$$g_c + ih = \frac{(n_b + ik_b) - n_c}{(n_b + ik_b) + n_c}$$

and

$$C = 2\,(g_b g_c - h_b h_c)$$

$$D = 2\,(g_b h_c + g_c h_b)$$

Equation 7·13 was used to calculate the transmission at different B-fields, taking values of $\tilde{n}_b = (n_b + ik_b) = \sqrt{\varepsilon}$, where ε is the dielectric function calculated in the way described above.

(c) Results of fits to experimental data

The values of the parameters used to simulate the F.I.R. transmission of PbTe film on BaF_2 in a varying magnetic field are given in table 7·2, together with references to the works from which the values were taken. Only the last three parameters, namely the T.O. phonon frequency w_T, the carrier damping constant ν, and the lattice damping parameter Γ, were varied within the range specified in table 7·2. The other parameters were fixed at their accepted values for the simulations. The reason for varying these three parameters was that w_T depends on the temperature and carrier concentration involved, because

Table 7·2

Parameters used for F.I.R. transmission fits for PbTe

Parameter	Value/range of values	References
w_L	114 cm^{-1}	Ramage et al. 1977 Burkhard et al. 1979
ε_∞	34	Ichiguchi et al. 1980 Bauer 1978 Burkhard et al. 1976 (1) and (2) 1977 (1) and (2)
w_T	18 cm^{-1} - 23 cm^{-1}	Tennant 1976 Burkhard et al. 1976 (2), 1977 (2), 1979 Kinch and Buss 1972
Γ	0·5 cm^{-1} - 5 cm^{-1}	Burkhard et al. 1976 (1) and (2), 1977 (1) and (2), 1979 Tennant 1976
ν	0·5 cm^{-1} - 3 cm^{-1}	Burkhard et al. 1977 (1) and (2)

the T.O. phonon softens as $q \to 0$ (Tennant 1976, Kawamura et al. 1975, Burkhard et al. 1976(2), 1977(2), 1979), while ν and Γ are sample-dependent.

For the set of parameters in Table 7·2, simulations for different values of $\Delta E(111)$ were obtained. It was found that ΔE = 9, 10, 11 meV were the only values to give the correct simulations for all three laser wavelengths, using the same parameters for all three, except for parameter ν. The carrier damping ν was taken to be magnetic field dependent, and was varied for different wavelengths so that its value was smaller for the larger wavelength, i.e., the carriers are assumed to be less localised at smaller values of B-field, which is reasonable. Figures 7·6c, 7·7c and 7·8c show the theoretical calculations for the three laser wavelengths, for $\Delta E(111)$ = 10 meV and w_T = 23 cm^{-1}, Γ = 3 cm^{-1} and

$$\nu = \begin{cases} 0{\cdot}8\ cm^{-1} \text{ for } 337\ \mu m \\ 1{\cdot}0\ cm^{-1} \text{ for } 192\ \mu m \\ 1{\cdot}1\ cm^{-1} \text{ for } 119\ \mu m. \end{cases}$$

By comparing these theoretical predictions with the low temperature (~ 20K) results given in figures 7·6a, 7·7a and 7·8a, it can be seen that the positions and, to some extent, the relative intensities of the transmission peaks are well reproduced. The feature on the low-field side of the second transmission peak in the theoretical simulations for λ = 119 μm and 192 μm (figures 5·6c and 5·7c) is caused by interference within the thin film (Ramage et al. 1977). This feature is not observed experimentally, probably because of the imperfections near the film-substrate interface, due to the thin layer of defects present there (see section 7·1).

As the temperature is raised, the experimental data show a small shift of the peak due to the dielectric anomaly (the peak at higher magnetic field) to higher B-field, while both peaks broaden out, with

the ratio of the intensities of the C.R. to the D.A. peak decreasing. These features can be simulated by increasing the carrier and phonon damping in the theoretical calculations, which is reasonable. However, the model is unable to reproduce the minima in the transmission of 337 μm at high temperature. The cause of this is not known.

7·5 Conclusion

In this work, the effect of the relative shift in energy between the conduction band's four ellipsoids, $\Delta E(111)$, due to stress induced by the different expansion coefficients of substrate and film, was taken into account when calculating the redistribution of the electrons in an applied magnetic field. From this calculation, by combining the F.I.R. transmission traces for three laser wavelengths and the carrier concentration value obtained from Shubnikov - de Haas measurements, a value for $\Delta E(111)$ was determined. This is 10 meV ± 1 meV for an n-type PbTe film grown on BaF_2, for temperatures around 18K. To my knowledge, only two other values of $\Delta E(111)$ have been obtained. Burke and Carver (1978) estimated $\Delta E(111)$ = 30 meV which is a much larger value than that obtained here. However, it is in agreement with other observations which compare the two samples, as was discussed in section 7·3. On the other hand, Gungor and Drew (1982) found a value of 1·8 meV for the energy split by fits to F.I.R. transmission and photoresponse. Their theoretical model is similar (though not identical) to the present one. However, in contrast to their results, it was observed in this work that the value of $\Delta E(111)$ controls primarily the position of the first peak in transmission (associated with C.R.) while the relative amplitudes of the peaks are mainly influenced by the carrier mobility and lattice damping parameter. A direct comparison of the values of $\Delta E(111)$ is unfortunately not possible, as the sample used by Gungor and Drew was not grown by Linz and thus may have very different strain characteristics, as noted by Carver et al. (1979).

Once the strain in the same film is measured by X-ray experiment, the value of $\Delta E(111)$ may be used to calculate the deformation potential of PbTe. This work is being carried out (Singleton 1985).

REFERENCES

References

Abrikosov A.A. (1972) 'Introduction to the theory of normal metals', Solid State Physics Supplement 12, pub. Academic Press.

Ando T. (1982) (a) J. Phys. Soc. Japan 51, 3893 (b) J. Phys. Soc. Japan 51, 3900.

Ando T., Fowler A.B. and Stern F. (1982) Rev. Mod. Phys. 54, 437.

Asch A.E., Gorski D.A., Hohnke D.K., Holloway K., Hurley M.D., Hutcheson E.T., Kaiser S.W., Rao P.V.S. and Varga A.J. (1974) Ford Motor Company 'Lead Telluride Photodiodes for operation at 170K', NTIS Report, AD 784 328.

Appel J. (1961) Phys. Rev. 122, 1760.

Armistead C.J., Najda S.P., Makado P.A., Stradling R.A., Colter P.C. and Stillman G.E. (1984) Solid State Commun. 48, 51.

Arora V.K. and Spector H.N. (1979) Phys. Status Solidi b94, 701.

Bagguley D.M.S., Stradling R.A. and Whiting J.S.S. (1961) Proc. Roy. Soc. A262, 340.

Bailey A.C. and Yates B. (1967) Proc. Phys. Soc. 91, 390.

Bastard G. (1983) Appl. Phys. Lett. 43, 591.

Bastard G. (1984) Surf. Sci. 142, 284.

Bauer G. (1978) Proc. 4th Int. Conf. on the Application of High Mag. Fields in Semiconductor Physics (Oxford: Clarendon Lab.) p.153.

Berman R. and Kopp J. (1971) J. Phys. F1, 457.

Bhatt R.N. and Rice T.M. (1980) Phil. Mag. B42, 859.

Blakemore J.S. (1962) Semiconductor Statistics (Pergamon Press) p.137.

Brummell M.A., Nicholas R.J., Brunel L.C., Huant S., Baj M., Portal J.C., Razeghi M., DiForte-Poisson M.A., Cheng K.-Y. and Cho A.Y. (1984) Surf. Sci 142, 368.

Burke J.R. and Carver G.P. (1978) Phys. Rev. B17, 2719.

Burkhard H., Bauer G., Grosse P. and Lopez-Otero A. (1976(1)) Phys. Stat. Sol. b76, 259.

Burkhard H., Bauer G. and Lopez-Otero A. (1976(2)) Sol. Stat. Commun. 18, 773.

Burkhard H., Bauer G., Grosse P. and Lopez-Otero A. (1977(1)) Physica 89B, 22.

Burkhard H., Bauer G. and Lopez-Otero A. (1977(2)) J. Opt. Soc. Am. 67, 943.

Burkhard H., Bauer G. and Zawadski W. (1979) Phys. Rev. B19, 5149.

Carver G.P., Houston Bland and Burke J.R. (1979) Sol. Stat. Commun. 30, 461.

Chamberlain J.M., Ergun H.B., Gehring K.A. and Stradling R.A. (1971) Sol. Stat. Commun. 9, 1563.

Chamberlain J.M., Simmonds P.E. Stradling R.A. and Bradley C.C. (1972) Proc. 11th Int. Conf. on Physics of Semiconductors (Warsaw: Polish Scientific Pub.) p.1016.

Chamberlain J.M. and Stradling R.A. (1969) Sol. Stat. Commun. 7, 1275.

Chattopadhya D. and Queisser H.J. (1981) Rev. Mod. Phys. 53, 745.

Cohen M.H. and Jortner J. (1973) Phys,. Rev. Lett 30, 696.

Cutler M. and Mott N.F. (1969) Phys. Rev. 181, 1336.

Dakhno A.N., Emal'yanenko O.V., Lagunova T.S. and Staroseltseva S.P. (1979) Sov. Phys. Semicond. 13, 1039.

Davis E.A. and Compton W.D. (1965) Phys. Rev. A140, 2183.

Delescluse P., Laviron M., Chaplart J., Delagebeaudeuf D. and Nguyen T. Linh (1981) Electron. Letters 17, 342.

Dimmock J.O., Melngailis I. an Strauss A.J. (1966) Phys. Rev. Lett. 16, 1193.

Drummond T.J., Morkoc H., Cho A.Y. (1981) J. Appl. Phys. 52, 1380.

Dyakonov M.I., Efros A.L. and Mitchell D.L. (1969) Phys. Rev. 180, 813.

Fang F.F. and Stiles P.J. (1968) Phys. Rev. 174, 823.

Fantner E.J., Clemens H. and Bauer G. (1984) Adv. X-ray Analysis 27, 171.

Frank F.C. and van der Merwe J.H. (1949) Proc. Roy. Soc. A198, 205 and 216.

Fritzsche H. (1958) J. Phys. Chem. Solids 6, 69, (1978) 'The Metal Non-metal Transition in Disordered Systems', ed. Tunstall D.P. and Friedman L.R. (Edinburgh: SUSSP Pub.) p.193.

Fujita S. and Lodder A. (1976) Physica 83B, 117.

Gibson A.F. (1952) Proc. Phys. Soc. B65, 378.

Gibbings C.J. and Pepper M. (1985) Proc. 17th Int. Conf. Phys. Semiconductors (San Francisco: Springer-Verlag) to be published.

Girvin S.M. and Jonson M. (1982) J. Phys. C15, L1147.

Gossick B.R. (1959) J. Appl. Phys. 30, 1214.

Gungor A. and Drew H.D. (1982) Sol. Stat. Commun. 44, 701.

Hearn E.W. (1977) Adv. X-ray analysis 20, 273.

Herring C. (1960) J. Appl. Phys. 31, 1939.

Hersee S.D., Hirtz J.P., Baldy M. and Duchemin J.P. (1982) Electron. Letters 18, 1076.

Hiyamizu S., Saito J., Nanbu K. and Ishikawa T. (1983) Japan J. Appl. Phys. 22, L609.

Hudson P.A. (1972) Proc. 4th Int. Conf. on Magnet Technology (Brookhaven: USAEC) p.444.

Hudson P.A., Jones H. and Whitworth H.M. (1984) J. de Physique Colloque 45, C1-55.

Ichiguchi T., Drew H.D. and Furdyna J.K. (1983) Phys. Rev. Lett. 50, 612.

Ichiguchi T., Nishikawa S. and Murase K. (1980) Sol. Stat. Commun. 34, 309.

Jedrzejczak A., Guillot D. and Martinez G. (1978) Phys. Rev. B17, 829.

Jensen J.D., Houstron Bland and Burke J.R. (1978) Phys. Rev. B18, 5567.

Jonson M. and Girvin S.M. (1984) Phys. Rev. B29, 1939.

Juretschke H.J., Landauer R. and Swanson J.A. (1956) J. Appl. Phys. 27, 838.

Kane E.O. (1963) Phys. Rev. 131, 79.

Kaufman L.A. and Neuringer L.J. (1970) Phys. Rev. B2, 1840.

Kawamura H., Saji H., Fukai M., Epido K. and Imai I. (1964) J. Phys. Soc. Japan 19, 288.

Keldysh L.V. and Proshko G.P. (1964) Sov. Phys. Solid State 5, 2481.

Kinch M.A. and Buss D.D. (1972) Sol. Stat. Commun. 11, 319.

Kubo R., Miyake S.J. and Hashitsume N. (1965) Solid State Phys. (Academic Press: New York) 17, 269.

Landolt-Börnstein (1982) 'Semiconductors: Physics of Group IV Elements and III-V Compounds', volume III/17a, pub. Springer-Verlag.

Larsen D.M., (1979) Phys. Rev. Lett. 42, 742.

Lawaetz P. (1971) Phys. Rev. B4, 3460.

Lee H.J., Basinski J., Juravel L.Y. and Woolley J.C. (1980) Can. J. of Phys. 58, 923.

Lee N., Larsen D.M. and Lax B. (1973) J. Phys. Chem. Solids 34, 1059.

Lin B.J.F., Tsui D.C., Paalanen M.A. and Gossard A.C. (1984) Appl. Phys. Lett. 45, 695.

Lopez-Otero A. (1978) Thin Solid Films 49, 3.

Mansfield R. and Ahmad I. (1970) J. Phys. C3, 423.

Martinez G., Schlüter M. and Cohen M.L (1975) Phys. Rev. B11, 651 and 660.

Matthews J.W. and Blakeslee A.E. (1974) J. Cryst. Growth 27, 117.

Matthews J.W. and Kokholm E. (1972) Mater. Res. Bull. 7, 213.

Mears A.L. and Stradling R.A. (1969) Sol. Stat. Commun. 7, 1267.

Mitchell D.L., Pakik E.D. and Zemel J.N. (1964) Proc. 7th Int. Conf. Phys. Semiconductors (Paris: Academic Press) p.725.

Mitchell D.L. and Wallis R.F. (1966) Phys. Rev. 151, 581.

Mott N.F. and Davis E.A. (1971) 'Electronic Processes in Non-Crystalline Materials' pub. Clarendon, Oxford.

Nag B.R. (1980) 'Electron Transport in Compound Semiconductors' pub. Springer-Verlag.

Narita S. and Kobayashi M. (1980) Phil. Mag. B42, 895.

Narita S., Shinbashi T. and Kobayashi M. (1982) J. Phys. Soc. Japan 51, 2186.

Nicholas R.J., Brummell M.A., Portal J.C., Cheng K.Y., Cho A.Y. Pearsall T.P. (1983) Sol. Stat. Commun. 45, 911.

Nicholas R.J. and Sarkar C.K. (1982) Sol. Stat. Commun. 41, 943.

Nicholas R.J., Vuong T.H.H., Brummell M.A. Portal J.C. and Razeghi M. (1985) Proc. 17th Int. Conf. Phys. Semiconductors (San Franciso: Springer-Verlag) to be published.

Nishi S., Kawamura H. and Murase K. (1980) Phys. Status Solidi b97, 581.

Norton P. (1976) Phys. Rev. Lett. 37, 164.

Obloh H., von Klitzing K. and Ploog K. (1984) Surf. Sci. 142, 236.

Oji H. (1984) (a) Phys. Rev. B39, 3148, (b) J. Phys. C17, 3059, (c) Sol. Stat. Commun. 49, 451.

Palik E.D. and Furdyna J.K. (1970) Rep. Prog. Phys. 33, 1193.

Palik E.D., Picus G.S., Teitler S. and Wallis R.F. (1961a) Phys. Rev. 122, 475.

Palik E.D. and Wallis R.F. (1961b) Phys. Rev. 123, 131.

Pistoulet B., Abdalla S. and Roche F.M. (1985) Proc. 17th Int. Conf. Phys. Semiconductors (San Francisco: Springer-Verlag) to be published.

Portal J.C., Nicholas R.J., Brummell M.A., Cho A.Y., Cheng K.Y. and Pearsall T.P. (1982) Sol. Stat. Commun. 43, 907.

Ramage J.C., Kuchar F., Stradling R.A. and Lopez-Otero A. (1977) J. Phys. C10, 5089.

Ramage J.C. (1978) Proc. 4th Int. Conf. on the Application of High Mag. Fields in Semiconductor Physics (Oxford: Clarendon Lab.) p.370.

Rochon P. and Fortin E. (1975) Phys. Rev. B12, 5803.

Schlesinger Z., Hwang J.C.M. and Allen S.J. (1984) Surf. Sci. 142, 423.

Shantharama L.G., Adams A.R., Ahmad C.N. and Nicholas R.J. (1984) J. Phys. C25, 4429.

Shklovskii B.I. and Efros A.L. (1971) Sov Phys. JETP 33, 468.

Shklovskii B.I. and Efros A.L. (1980) Sov Phys. Semicond. 14, 487.

Shklovskii B.I. and Efros A.L. (1971) 'Electronics Properties of Doped Semiconductors' pub. Springer-Verlag, chapter 3.

Singleton J. (1985) to be published.

Srinivas T.K., Chaudhury S. and Fujita S. (1981) Sol. Stat. Commun. 37, 919.

Stern F. (1972) Phys. Rev. B5, 4891.

Stern F. and Howard W.E. (1967) Phys. Rev. 163, 816.

Störmer H.L., Gossard A.C., Wiegmann W. and Baldwin K. (1981) Appl. Phys. Lett. 39, 912.

Streda P. (1983) J. Phys. C16, L369.

Streda P. (1984) Phys. Status Solidi b125, 849.

Streda P. and Oji H. (1984) Phys. Letts. 102A, 201.

Tennant W.E. (1976) Sol. Stat. Commun. 20, 613.

Thouless D.J. (1984) Surf. Sci. 142, 147.

Ting C.S., Houghton A. and Senna J.R. (1982) Phys. Rev. B25, 1439.

Tsui D.C. and Allen S.J. (1981) Phys. Rev. B24, 4082.

van der Pauw L.J. (1958) Philips Res. Repts. 13, 1.

von Klitzing K., Dorda G. and Pepper M. (1980) Phys. Rev. Lett. 45, 495.

von Klitzing K. and Ebert G. (1984) 'Two-Dimensional Systems, Heterostructures, and Superlattices' pub. Springer-Verlag, p.242.

Vuong T.H.H. and Nicholas R.J. (1985) to be published.

Walpole J.N., Calawa A.R., Harman T.C. and Groves S.H. (1976) Appl. Phys. Lett. 28, 552.

Walukiewicz W., Ruda H.E., Lagowski J. and Gatos H.C. (1984) Phys. Rev. B30, 4571.

Weisberg L.R. (1962) J. Appl. Phys. 33, 1817.

Wolfe C.M. anmd Stillman G.E. (1971) Appl. Phys. Lett. 18, 205.

Zawadzki W. and Lassnig R. (1984) Surf. Sci. 142, 225.

Zelenin S.P., Kondrat'ev A.S. and Kuchma A.E. (1982) Sov. Phys. Semicond. 16, 355.

Zemel J.N., Jensen J.D. and Schoolar R.B. (1965) Phys. Rev. A140, 330.